~~30~~
(1+2b)

SECOND CAMBRIDGE WORKSHOP ON COOL STARS, STELLAR SYSTEMS, AND THE SUN

Edited by M. S. GIAMPAPA and L. GOLUB

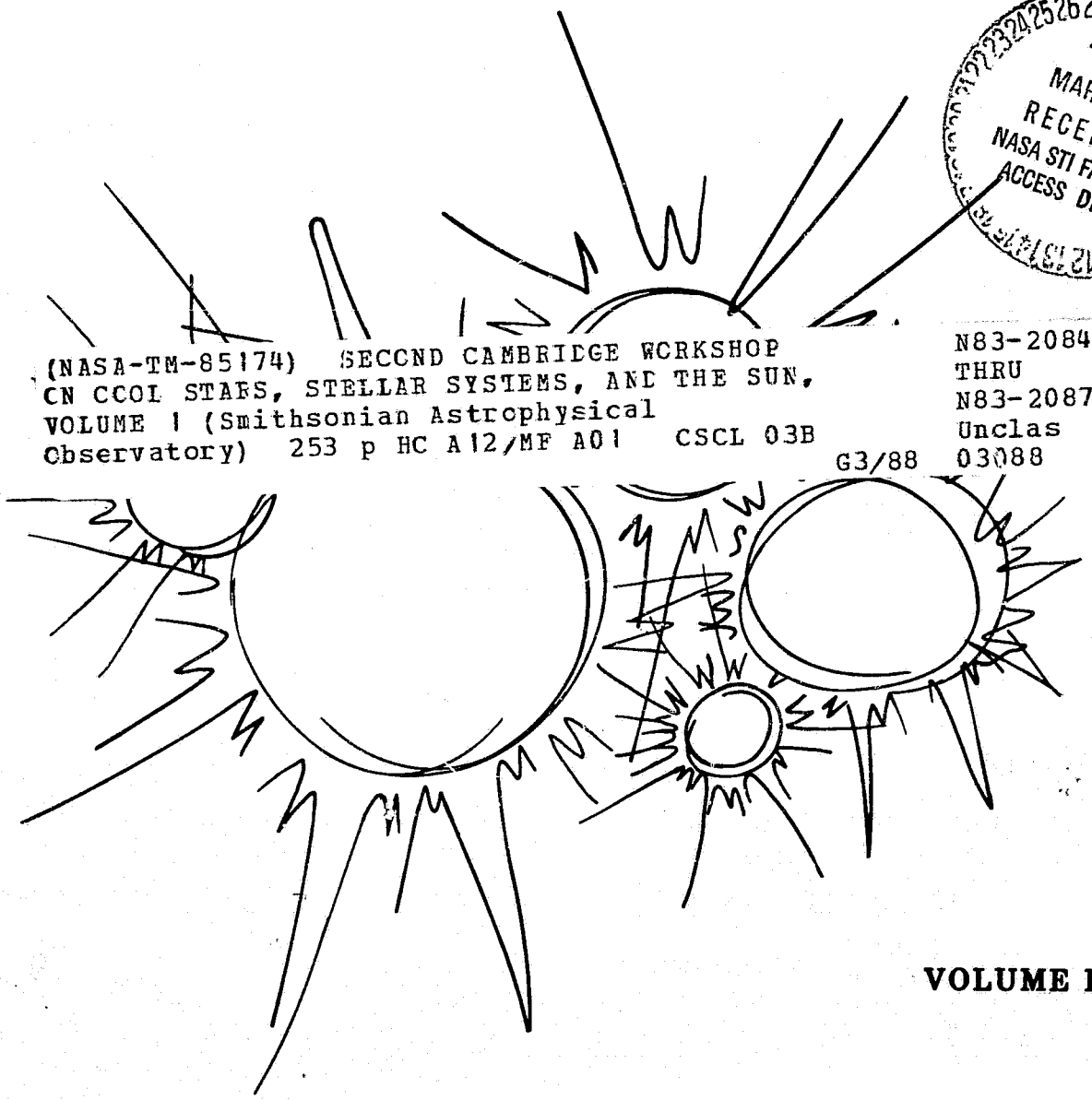

VOLUME I

Smithsonian Astrophysical Observatory
SPECIAL REPORT 392

Research in Space Science
SAO Special Report No. 392

SECOND CAMBRIDGE WORKSHOP ON

COOL STARS, STELLAR SYSTEMS, AND THE SUN

21–23 October 1981
Harvard-Smithsonian Center for Astrophysics
Cambridge, MA 02138

edited by

M.S. Giampapa and L. Golub

VOLUME I

AMERICAN INSTITUTE OF AERONAUTICS & ASTRONAUTICS, INC.
TECHNICAL INFORMATION SERVICE
555 WEST 57th STREET • NEW YORK, N.Y. 10019

A meeting supported in part by the James Arthur Fund and the Langley-Abbot Program of the Smithsonian Institution, the National Aeronautics and Space Administration, and the Harvard-Smithsonian Center for Astrophysics.

Organizing Committee

S.L. Baliunas
A.K. Dupree, Chairman
M.S. Giampapa
L. Golub
L. Hartmann
R. Levine

TABLE OF CONTENTS

TABLE OF CONTENTS (Cont.)

TABLE OF CONTENTS (Cont.)

TABLE OF CONTENTS (Cont.)

TABLE OF CONTENTS (Cont.)

PREFACE

In October 1981 the Second Cambridge Workshop on the general topic of "Cool Stars, Stellar Systems and the Sun" was held at the Harvard-Smithsonian Center for Astrophysics. Over 100 scientists assembled to present and discuss some of the most recent advances in the burgeoning field of cool star outer atmospheres.

With the advent of high sensitivity soft X-ray observations provided by the Einstein Observatory as well as the continued successful operation of the International Ultraviolet Explorer satellite, there has been an explosive growth in the investigation of cool stars. In fact we may say that cool stars have become the hot topic in astrophysics today!

A comparison of these proceedings with those of the first workshop (held in January 1980) will readily reveal the tremendous progress that has been realized in a relatively short time. In particular, the data base that has been established clearly illustrates the similarity between solar activity and stellar activity. The extension of these observations to stars characterized by significantly different fundamental physical properties, such as gravity, effective temperature and rotation rate, will provide the range in parameter space that is required to test various theoretical models that seek to explain stellar and solar atmospheric phenomena.

The workshop was made possible through support of the Harvard-Smithsonian Center for Astrophysics, the James Arthur Fund of the Smithsonian Institution, the Langley-Abbot Program of the Smithsonian Institution, and the National Aeronautics and Space Administration. We would like to thank the other members of the organizing committee: Andrea Dupree (Chairman), Sallie Baliunas, Lee Hartmann and Randolph Levine; we are also indebted to Sara Yorke and Stephanie Deeley for their invaluable assistance; and to Anne Omundsen and the SAO Publications staff for their help with this volume.

Mark Giampapa
Leon Golub
Cambridge, Massachusetts
February 17, 1982

I. ATMOSPHERIC STRUCTURE

D1

Chromospheric Structure in Relation to Radiation Losses

R. Grant Athay

High Altitude Observatory/National Center for Atmospheric Research[1]

Abstract

Under the assumptions that cool star chromospheres are heated by mechanical energy dissipation that depends quasi-linearly on density and cooled by radiation loss, it is shown that the basic properties of chromospheres are determined by the ionization of hydrogen. In particular, it is hydrogen ionization that provides the freedom for chromospheres to adjust their radiation losses to balance the prescribed heat input. The result of such an adjustment is an extended region of low temperature gradient.

Chromospheric radiation losses in cool stars occur mainly in the strongest spectral lines at wavelengths greater than about 2000 A and for which an appreciable fraction of the chromosphere is effectively thin. The most important lines include Ca II H and K and the infrared triplet and Mg II h and k. The strong lines of other abundant species, such as He, C, N, O and Si are less important because their high excitation energies reduce the collisional excitation rates.

Lyman-α losses are important because of the overwhelming abundance of hydrogen. However, the inability of chromospheres to adjust their Lyman-α losses limits the geometrical thickness of the effectively thin region in Lyman-α and, hence, limits the total Lyman-α flux.

I. Essential Properties of Chromospheres

For purposes of this discussion a cool star chromosphere is defined as a region at $\tau_c << 1$ (τ_c = continuum optical depth) in which the temperature, T, is raised above its radiative equilibrium value, T_r, by mechanical heating but remains below 5×10^4 K. This value of the upper limit is rather arbitrary and unimportant. It is intended to be high enough to include the majority of the Lyman-α radiation.

An atmosphere in quasisteady state must have gas pressure decreasing outwards. In certain temperature regimes, however, the temperature may increase outwards at such a rapid rate that the gas pressure remains virtually constant through a wide temperature range, as is the case in the solar chromosphere-corona transition region.

If a chromosphere is to be detected through current spectroscopic means, the chromosphere must be sufficiently optically thick in such ions as Ca II and Mg II to impose an easily recognizable signature on the stellar spectrum. This requires that such ions be abundant relative to the total hydrogen density, n_H, throughout a region where the gas pressure drops appreciably. This, in turn, requires that some region of the chromosphere has a small or moderate temperature gradient. Since the condition of constant gas pressure corresponds to $H\, d\ln T/dz = 1$, where $H = -dz/d\ln n_H$ is the density scale height, the requirement for a chromosphere to be readily observable may be stated as $H\, d\ln T/dz << 1$ for some range of T where singly ionized metals are abundant.

[1]The National Center for Atmospheric Research is sponsored by the National Science Foundation.

An alternative statement to the two conditions $T>T_r$ and $H\,d\ln T/dz<<1$ for some range of T is simply that enough mechanical energy be dissipated in an atmosphere constituted mainly of neutral hydrogen. As we shall demonstrate, the presence of neutral hydrogen insures that the condition $H\,d\ln T/dz<<1$ will very probably occur. Conversely, in the absence of neutral hydrogen there will be much less tendency for this condition to be fulfilled.

In order to demonstrate the assertion that the presence of neutral hydrogen will lead to an extended region of low temperature gradient, we assume that the heat energy input, Q, is removed from the chromosphere by an increased radiation loss, R. Thus, at each depth in the chromosphere, we require

$$Q = R, \tag{1}$$

where the units on Q and R are ergs $cm^{-3}\,s^{-1}$. In making the assumption expressed by equation (1), we are implicitly assuming that energy transport by thermal conduction and fluid motions are negligible. The requirement that $H\,d\ln T/dz<<1$ together with the relatively low values of T in the chromosphere insures that thermal conduction is small. The neglect of fluid motions is a valid approximation for the solar chromosphere and is most likely valid for stars with more or less normal emission components in Ca II and Mg II lines. There may be cases, however, in which fluid motions are important in the energy balance.

Although we know relatively little about the form of the heat input, Q, we know a considerable amount about the form of the radiation loss, R. In particular, it can be shown that under the conditions expected in cool star chromosphere R has such a distinctive dependence on temperature that certain features of the chromospheric temperature structure are expected to occur almost independently of Q. Looked at from another point of view, Q determines the magnitude of R, but the radiation mechanism itself determines the characteristic form of R. The form of R, in turn, determines the essentials of the temperature structure. (Of course, the form of R may influence somewhat the run of Q with height through the influence of R on the temperature and density structure.)

It is readily shown from the equation of radiative transfer that a general form for R is given by

$$R = \sum_i \rho_i \int \kappa_{\nu i} S_{\nu i}\, d\nu, \tag{2}$$

where the subscript i denotes a particular spectral feature, $\kappa_{\nu i}$ is the absorption coefficient, $S_{\nu i}$ is the source function and ρ_i is the escape coefficient (sometimes called net radiative bracket) defined by

$$\rho_i = 1 - \frac{\int \kappa_{\nu i} J_\nu\, d\nu}{\int \kappa_{\nu i} S_{\nu i}\, d\nu} \tag{3}$$

and J_ν is the mean intensity of radiation. An exact evaluation of R requires an evaluation of ρ_i, $\kappa_{\nu i}$, and $S_{\nu i}$ by solution of the coupled radiative transfer and statistical equilibrium equations and for each of the relevant transitions for a valid model atmosphere. Recent examples of such computations are provided by Vernazza, Avrett and Loeser (1981) and by Lites and Skumanich (1981).

There are certain conditions under which R can be approximated without solving the transfer equation. The required conditions are that $\kappa_{\nu i}$ be known, that the frequency dependence of $S_{\nu i}$ be known and that the optical depth be small enough that the overlying atmosphere is effectively thin. Since R tends to be relatively large for effectively thin conditions and to be very small for effectively thick conditions, the

approximation of R involves identifying the strongest spectral lines for which a substantial fraction of the chromosphere is effectively thin. One then obtains a reasonable approximation for the contribution to R by spectral lines by assuming that S is independent of frequency and that κ_ν is gaussian. For continuum transitions, S_ν is a Planck function and κ_ν is generally of a known form.

When the preceding conditions are satisfied the quantity $\rho_i S_{\nu i}$ is given by the photon creation rate. The creation rate, in turn, can often be expressed as a known function of temperature and density. For collisionally excited transitions and for two-body radiative recombinations (such as H^-), the resultant expression for R has the familiar form

$$R_i \alpha n_e n_i f_i(T), \tag{4}$$

where n_e is the electron density, n_i is the ion or atom density giving rising to the transition, and $f_i(T)$ is a function of temperature whose form depends on the parent ion or atom and gives the ionization/excitation state of the radiator.

The approximation for R expressed by equation (4) works reasonably well in the solar chromosphere (Athay, 1981a) provided one uses accurate solutions of the coupled transfer and statistical equilibrium equations to identify the appropriate transitions. For such cases as the resonance lines of Ca II and Mg II, the approximation is acceptable. However, there are pitfalls. In the case of the subordinate hydrogen transitions, which appear superficially to satisfy all of the necessary requirements for the approximations to be valid (Athay, 1976), the values of $\rho_i S_{\nu i}$ for individual transitions are large, but are negative for some transitions. This leads to strong cancellations with the result that the summation in equation (2) for the subordinate transitions in hydrogen has a small net value. The exact nature of the cancellations is not yet clear. Vernazza *et al.* (1981), for example, report that the energy loss in the Balmer-α line is cancelled by an energy gain in the Balmer continuum. Lites and Skumanich (1981), on the other hand, find cancellation between Balmer-α and Balmer-β. Such details are difficult to evaluate precisely even when the radiative transfer and statistical equilibrium equations are solved numerically.

The subordinate hydrogen transitions illustrate one example of a pitfall in the use of equation (4). There are probably others as well. On the other hand, equation (4) appears to work well for such transitions as the hydrogen Lyman-series, Ca II H and K doublet and the strong infrared triplet, and the Mg II h and k doublet.

To emphasize the role of hydrogen ionization, we rewrite equation (4) in the form

$$R_i \alpha n_H^2 \gamma(T,n_H) f_i(T), \tag{5}$$

where n_H is the hydrogen density (neutral plus ionized), $\gamma(T,n_H) = n_e/n_H$, and where we have assumed that n_i/n_H is constant. Thus, $\gamma(T,n_H)$ represents the fractional ionization of hydrogen when the ionization is sufficient that $n_e \approx n_p$ (n_p = proton density). The assumption that n_i/n_H is constant is a sufficiently good approximation for our purposes in the temperature region where n_i/n_H is near its maximum value. Although γ is a function of both T and n_H we are primarily concerned with the T dependence. Hereafter, we write $\gamma = \gamma(T)$.

The heat input, Q, will normally be determined by physical processes that are independent of R except to the extent that R influences the local density. Also, Q is expected to vary with geometrical height and to exhibit spatial and temporal fluctuations. If R were narrowly restricted in the range of values it could assume, equation (1) would require a similarly narrow restriction on Q. Such a situation seems unlikely on physical grounds. We insist rather that Q be allowed to take on whatever values are dictated by the heating mechanism. If equation (1) is to be satisfied, therefore, R

must be able to adjust to a reasonable range of values of Q. Since Q is expected to change "locally", the responsive changes in R must be local as well.

Of the parameters in equation (5) only $\gamma(T)$ and $f_i(T)$ are locally responsive. The chromosphere presumedly is near hydrostatic equilibrium, which means that n_H is determined primarily by the underlying atmosphere and is not subject to marked change in response to local changes in Q. In cool stars most of the chromospheric radiation loss is expected to arise from sources whose excitation energies are less than the ionization energy of hydrogen. This has the consequence that $\gamma(T)$ is a stronger function of temperature than is $f_i(T)$. It follows that most of the freedom to satisfy equation (1), so long as hydrogen is mainly neutral, resides in the quantity $\gamma(T)$.

It is possible to solve equations (1) and (5) for $H\,d\ln T/dz$ using approximate forms for $\gamma(T)$ and $f_i(T)$. The solution for $d\ln T/dz$ is (Athay, 1981b)

$$\frac{d\ln T}{dz} = \frac{T}{1.16\times10^4(X_2 + 2X_u)}\left[2\frac{d\ln Q}{dz} - 3\frac{d\ln n_H}{dz} - \frac{d\ln(1-\gamma)}{dz}\right], \tag{6}$$

which yields

$$H\frac{d\ln T}{dz} = \frac{T}{1.16\times10^4(X_2 + 2X_u)}\left[3 - 2\frac{d\ln(Q)}{d\ln n_H} + \frac{d\ln(1-\gamma)}{d\ln n_H}\right]. \tag{7}$$

X_2 is the excitation energy of the second principal quantum level in hydrogen (in eV) and X_u is the excitation energy of the upper quantum level of the transition producing the dominant radiation loss. Since $\gamma(T)$ is a strong function of T, equation (6) is not a full solution for $d\ln T/dz$. However, this solution is satisfactory for illustrating the following arguments. Equation (7) is valid only in the range where electrons come mainly from hydrogen so that $n_e \approx n_p$.

It is clear from equation (7) that $H\,d\ln T/dz << 1$ for $T \lesssim 10^4\,K$ and $\left|-2\frac{d\ln Q}{d\ln n_H} + \frac{d\ln(1-\gamma)}{d\ln n_H}\right| \lesssim 10$. The term $\frac{d\ln(1-\gamma)}{d\ln n_H}$ is small for $\gamma << 1$ and becomes large when γ approaches unity, i.e., when $\gamma(T)$ is no longer a strong function of T. The term $d\ln Q/d\ln n_H$ is unknown, but we assume that it is of order unity. In the solar chromosphere, for example, between the temperatures 6000 and 7000 K, $d\ln(1-\gamma)/d\ln n_H \approx 0$, $d\ln Q/d\ln n_H \approx 0.7$ and $H\frac{d\ln T}{dz} \approx .03$ (Vernazza *et al.*, 1981). (The value of $d\ln Q/d\ln n_H$ is estimated from equation (1) and the radiation loss curve given by Vernazza *et al.*, 1981.) Within this same temperature range $\gamma(T)$ increases by approximately a factor of 60 whereas $f_i(T)$ for the dominant radiation loss (Ca II lines, Vernazza *et al.*, 1981) increases by a factor of only 2.4.

This solar example is discussed in more detail by Athay (1981b) and illustrates vividly the strong influence of hydrogen ionization on the temperature gradient in the chromosphere. Further illustration is given in Figure 1, which indicates the levels in the mean chromospheric model of Vernazza *et al.* (1981) where hydrogen ionization controls the electron density, viz., $10^{-4} \lesssim \gamma \lesssim .5$. Throughout this entire range the temperature gradient remains small, and just outside this range the temperature gradient increases dramatically. On the high temperature side the increase in $d\ln T/dz$ is due to the $1-\gamma$ term in equation (6), and on the low temperature side it is due to insufficient hydrogen ionization, in which case the electrons come mainly from ionization of metals.

These properties of the temperature curve are not dependent upon any phenomena peculiar to the solar atmosphere. There is good reason to suppose,

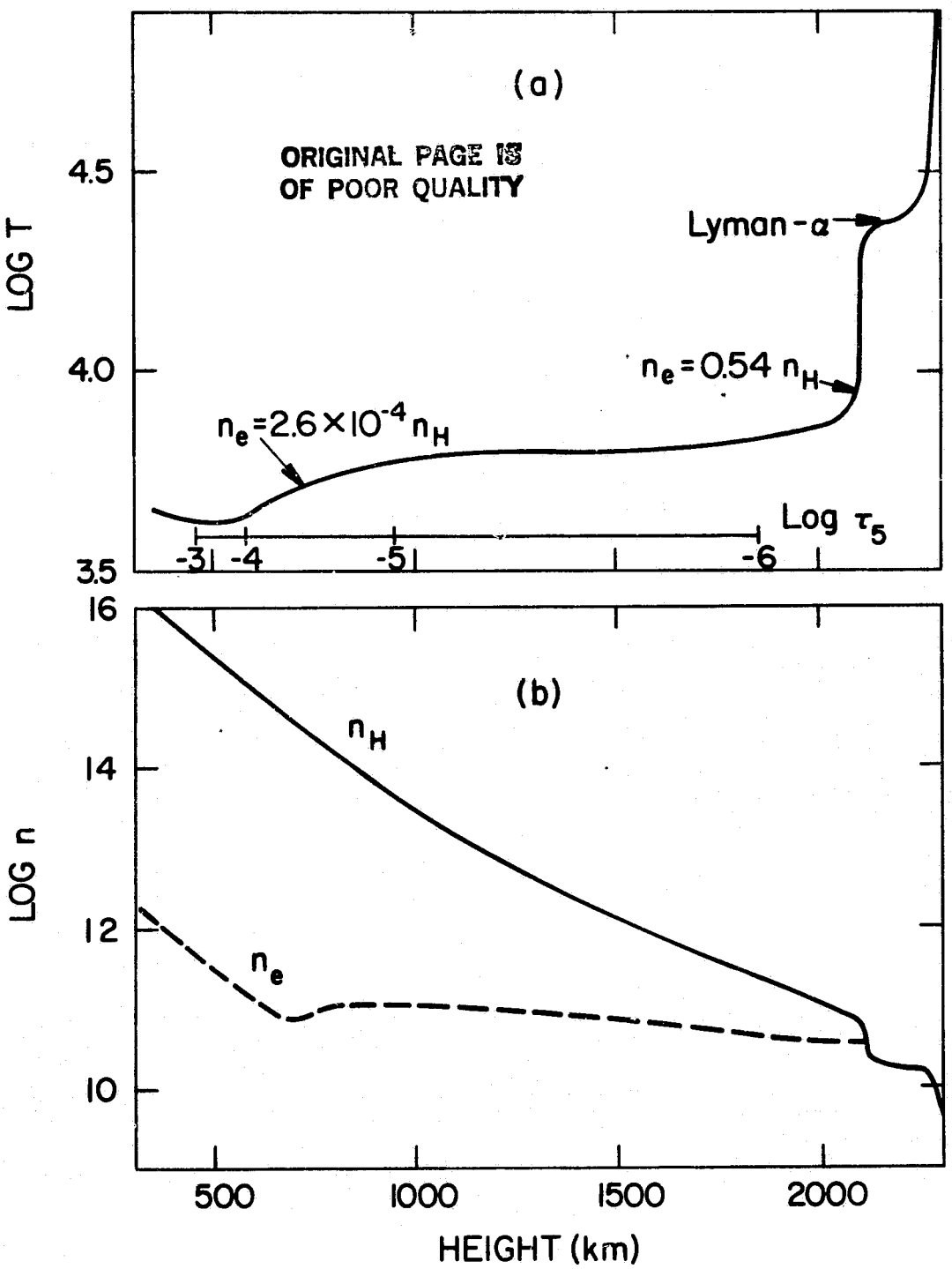

Figure 1. Plots of T, n_e and n_H as functions of height for the recent Vernazza, Avrett, Loeser (1981) model of the solar chromosphere. The points $n_e = 2.6\times10^{-4} n_H$ and $n_e = 0.54 n_H$ indicated on the temperature curve represent, respectively, the points where $n_e \approx n_p$ and $\gamma(T) \approx .5$. The third arrow indicates the primary region of Lyman-α losses.

therefore, that they will be quite common properties of cool star chromospheres. In particular, we expect ionization to produce a substantial region in which $H\, d\ln T/dz << 1$. Furthermore, once $\gamma(T)$ approaches unity the ability to adjust R_i is very limited and it is unlikely that an extended region of low temperature gradient will occur.

II. Spectral Characteristics

A. The Hydrogen Ionization Plateau. In the preceding discussion and in the discussion immediately following, we are considering only the chromospheric temperature plateau due to hydrogen ionization. This includes the regions where many strong chromospheric lines, such as Ca II, Mg II and Si II, are formed. However, it does not include the region in which Lyman-α is formed. Most of the Lyman-α radiation from stellar atmospheres arises in regions for which $\gamma(T)$ is very close to unity, which places it beyond the upper border of the hydrogen ionization plateau. The question of Lyman-α radiation is discussed in paragraph B of this section.

The total radiation loss per unit area from a chromosphere may be represented as

$$RL = \sum_i R_i L_i, \tag{8}$$

where the L_i's are characteristic scale lengths for the chromospheric thickness. Most of the loss is expected to occur in regions for which $d\ln T/dz$ is small. We emphasize that for the dominant radiation loss both R_i and L_i are fixed by Q. Since the combined quantity $\gamma(T)f_i(T)$ in equation (5) can vary by more than four orders of magnitude, cool star chromospheres can readily adjust to provide a balance between R and Q through a wide range of values of Q. Thus, it is not particularly surprising to find a large range in emission line fluxes from stellar chromospheres.

A rough estimate for RL is obtained by integrating the photon creation rate through the effectively thin region of the chromosphere. Thus, we approximate RL by

$$\frac{1}{4\pi} RL \approx \pi^{1/2}\Delta\nu \int_0^{\tau_{ch}} \varepsilon B_\nu d\tau_0, \quad \tau_{ch} \lesssim \varepsilon^{-1}, \tag{9}$$

where $\Delta\nu$ is the Doppler width of the absorption profile, ε is the thermalization probability, B_ν is the Planck function, τ_0 is the optical depth at line center and τ_{ch} is the characteristic chromospheric optical thickness for the transition under consideration. The quantity εB_ν is the creation rate in units of $ergs/\mathrm{cm}^{-2}\, d\nu^{-1}\, ster^{-1}$, and the factor $\pi^{1/2}\Delta\nu$ comes from integrating the absorption profile over frequency. To integrate equation (9), we assume that εB_ν is constant. Also, we set $\varepsilon = \tau_{th}^{-1}$, where τ_{th} is the thermalization depth. The result is

$$\frac{1}{4\pi} RL \approx \pi^{1/2}\Delta\nu \frac{\tau_{ch}}{\tau_{th}} B_\nu, \quad \tau_{ch} \lesssim \tau_{th} \tag{10}$$

If τ_{ch} exceeds τ_{th}, i.e., if the chromosphere is effectively thick, equation (10) becomes

$$\frac{1}{4\pi} RL \approx \pi^{1/2}\Delta\nu B_\nu, \quad \tau_{ch} > \tau_{th}. \tag{11}$$

This results from setting ρS_ν in equation (2) to εB_ν for $\tau_{ch} \lesssim \varepsilon^{-1}$ and $\rho S_\nu \doteq 0$ for $\tau_{ch} > \varepsilon^{-1}$.

It is clear from equations (10) and (11) that most of the radiation loss will occur in lines for which τ_{ch}/τ_{th} is relatively large and for which B_ν is relatively large. Also, two or more effectively thick lines at nearby wavelengths will have approximately equal fluxes.

All abundant ionic species would produce large chromospheric energy losses if their resonance lines were strongly excited in the region of low temperature gradient, i.e., if they occurred in spectral regions where B_ν is relatively large. Of the astrophysically abundant elements, the most important contributors to energy loss from the temperature plateau formed by hydrogen ionization are Ca II and Mg II. Other abundant species such as He, C, N, O and Si have resonance lines of the populous ions at very short wavelengths where B_ν is small. Lyman-α losses are important because of the overwhelming abundance of hydrogen. However, these losses occur above the main temperature plateau and require special treatment.

In regions of the spectrum where the photospheric lines are weak or absent, as in the EUV, the chromospheric flux appears as free-bound continua or emission lines (often self-reversed) above the background continuum. However, in spectral regions where the photospheric absorption lines are strong, chromospheric flux appears as additional radiation near line center. Whether this additional radiation flux produces a recognizable emission component in a particular spectral line depends upon the ratio

$$\frac{I_{ch}}{I_{min}} = 1 + \left(\frac{B_{ch}}{B_{min}} - 1 \right) \left(\frac{N_{ch}}{N_{th}} \right)^{1/2} \zeta \left(\frac{\Delta\nu_{ch}}{\Delta\nu_{min}}, \; V_{macro} \right) \qquad (12)$$

where subscripts *ch* and min refer, respectively, to the chromosphere near the beginning of the lower temperature gradient produced by hydrogen ionization and the temperature minimum region; I is the specific intensity; B is the planck function at the wavelength of the line; V_{macro} is the macroturbulent velocity; N is the scattering depth (cf. Athay, 1981a); N_{th} is the thermalization depth in scattering steps. To a sufficiently good approximation $N_{ch}/N_{th} = \tau_{ch}/\tau_{th}$. The exact form of the function ζ has not been determined, but, in general, ζ decreases as either $\Delta\nu_{ch}/\Delta\nu_{min}$ or V_{macro} increases. Since we expect $\Delta\nu_{ch}/\Delta\nu_{min}>1$ and $V_{macro}>0$, we expect $\zeta<1$. The influence of ζ can be quite pronounced, as it is in the case of the sun.

As is evident from equation (12), the appearance of an emission feature is favored by shorter wavelength (increased B_{ch}/B_{min}) and by increased optical depth (increased N_{ch}). Thus, the emission features in Mg II are relatively enhanced over those in Ca II and those in the Ca II H and K lines are enhanced over those in the infrared triplet of Ca II.

The absence of an emission feature in a spectral line does not imply an absence of chromospheric emission. Whenever the second term on the right hand side of equation (12) is much less than unity the chromospheric emission will merely raise the observed flux, i.e., fill in the line core. Since ζ and $(N_{ch}/N_{th})^{1/2}$ may each be small compared to unity, even a large ratio B_{ch}/B_{min} does not necessarily produce an emission feature.

In the case of the sun, all lines on the wing portion of the curve-of-growth have a chromospheric component. This includes such examples as Na D lines, Mg b lines, the Ca I resonance line and many strong lines of Fe I and Fe II. In addition, the high excitation lines, such as hydrogen Balmer lines and He I lines have strong chromospheric components. None of these lines has observed emission components because τ_{ch}/τ_{th} is very small. Thus, the chromospheric flux is small. Collectively, however, these lines may be important. No proper assessment of the combined contribution of such lines to the radiation loss has been carried out, except for the Balmer lines.

Since the contrast between photospheric and chromospheric emission is proportional to $B_{ch}/B_{min} - 1$, the contrast should disappear when B_{ch}/B_{min} is of order unity. We expect a tendency for this to occur in early type stars where B_{min} is high enough that $n_e \approx n_p$ at the temperature minimum. In this case, the temperature gradient

should tend to remain small in the lower chromosphere. The condition $n_e \approx n_p$ at the temperature minimum is expected for all stars earlier than spectral type F1, which is where Ca II emission normally disappears (Linsky, 1981). Exceptions to this rule will occur in cases where Q is large enough in the low chromosphere to force $\gamma(T) >> 10^{-4}$.

The hydrogen ionization plateau is expected to persist in all stars that have mainly neutral hydrogen at the temperature minimum. This includes stars up to early B spectral classes. Thus, most of spectral type B and later type stars are capable of producing chromospheres with extended regions of low temperature gradient. Given a source of mechanical heating, Q, such stars should have strong chromospheric emission. However, in spectral types B and A conspicuous emission features should be less prevalent.

In O type stars without appreciable neutral hydrogen, it is difficult to find a mechanism that would produce extended regions of low temperature gradient at chromospheric temperatures. Thus, stars of this class are expected to have very different types of chromospheres from later type stars with abundant neutral hydrogen.

B. Lyman-α. Lyman-α radiation from stellar chromospheres presents an intriguing puzzle. In the region in which Lyman-α photons escape readily, the quantity $\gamma(T) f_i(T)$ in equation (5) is essentially constant (Thomas and Athay, 1961). The equivalent statement with regard to equation (9) is that $B_\nu d\tau_0$ is essentially independent of temperature. This means that R is determined basically by the value of n_H^2. Since the transition from the top of the hydrogen ionization plateau where $\gamma \approx .5$ to the region where Lyman-α photons escape readily occurs with a steep temperature gradient, the gas pressure in the Lyman-α region is fixed by the gas pressure at the depth where $\gamma \approx .5$. Thus, we may set

$$n_{H.5} T_{.5} \approx N_{H\alpha} T_\alpha, \tag{10}$$

or

$$\frac{n_{H\alpha}}{n_{H.5}} = \frac{T_{.5}}{T_\alpha} \tag{11}$$

where α refers to the base of the Lyman-α region and .5 refers to the depth where $\gamma = .5$.

In any given star, the ratio $T_{.5}/T_\alpha$ is fixed solely by the ionization properties of hydrogen. It follows from equation (11) that $n_{H\alpha}/n_{H.5}$ is fixed and, hence, from equation (5) that $R_\alpha/R_{.5}$ is fixed. Furthermore, the ratio $R_\alpha/R_{.5}$ is large compared to unity. This latter result is demonstrated in Figure 2, which shows a plot of $R/n_e n_H T^2$ versus temperature (Summers and McWhirter, 1979; Athay, 1981b). The maximum in the plot in Figure 2 occurs in the Lyman-α region. At a temperature of 8000° K, which is characteristic of the $\gamma = .5$ region, R is below the maximum in the solid curve by about a factor of 20.

It appears from the preceding arguments that there is no way to avoid a large jump in R between the $\gamma = .5$ and Lyman-α regions if, indeed, the Lyman-α photons escape readily. This, in turn, appears to impose an arbitrary requirement on Q, which seems physically unacceptable.

In stars with an insufficient value of Q in excess of that dissipated in the main body of the chromosphere, the potential for increased Lyman-α loss simply limits the temperature to a value somewhat below T_α. This will provide a smooth continuity in R by reducing the escape of Lyman-α photons. Such stars, if they exist, are expected to have chromospheres but no coronae.

In stars that have a corona overlying the chromospheres, it is inescapable that some region is effectively thin in Lyman-α, and, hence, that large Lyman-α losses will

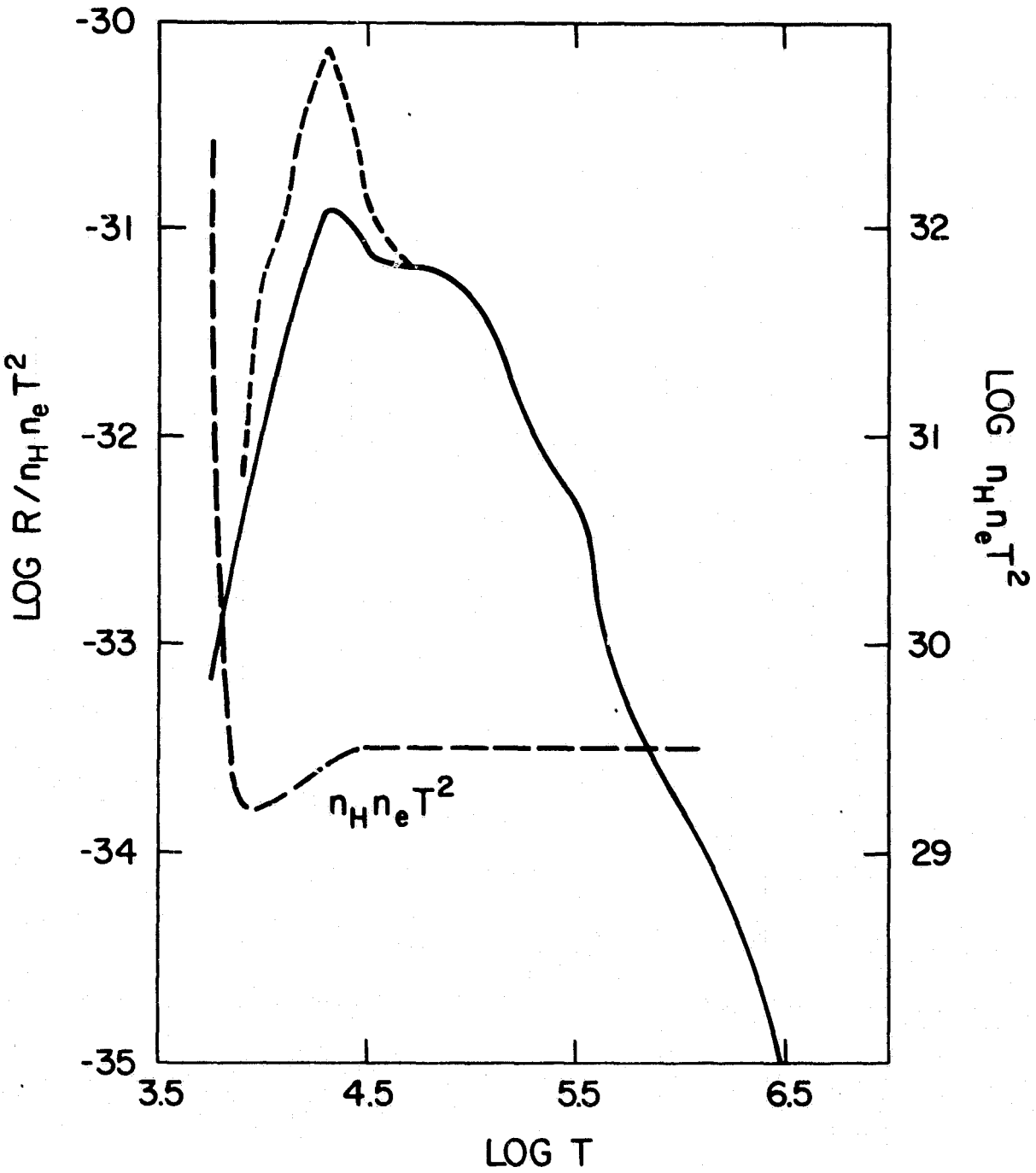

Figure 2. A plot of the radiation loss rate $R/n_H n_e T^2$ versus temperature for the effectively thin condition. The dashed curve for $\log T<4.6$ and the solid curve for $\log T>4.6$ are from Summers and McWhirter (1979). The solid curve below $\log T = 4.6$ is based on a different collisional excitation cross-section for Lyman-α (Athay, 1981b) than that used by Summers and McWhirter (1979) and includes Ca II, Mg II and Lyman-α losses.

occur. As a result a large jump in R will occur in the transition from $\gamma = .5$ to the Lyman-α region. It is equally inescapable that this seemingly places an arbitrary requirement on Q. This difficulty is well illustrated in the case of the sun. At $\gamma = .5$, $R \approx 10^{-3}$ and in the Lyman-α region $R \approx 2\times10^{-2}$ (Vernazza *et al.*, 1981; Athay, 1981b). Thus, there is, indeed, a large jump in R. In the region of low temperature gradient below $\gamma = .5$, $R \propto n_H^{0.7}$, which implies $Q \propto n_H^{0.7}$. Why then does Q suddenly jump by a factor of 20 when n_H decreases by approximately a factor 2.5 in the Lyman-α region? One answer to this question is simply that the Lyman-α region may be fed by an energy source that is physically distinct from that which is operative in the lower chromosphere. This point will be discussed further in Section III.

A second interesting feature of the Lyman-α region is that although R is relatively large there appears to be no mechanism for forming an extended temperature plateau. Since $R \propto n_H^2$ any variation of Q with height, other than a fortuitous proportionality to n_H^2, means that R and Q cannot be in balance except in a very limited range of n_H. This situation manifests itself in the solar chromosphere by a slight pause in the temperature gradient near $T = 2\times10^4$ K, as shown in Figure 1. The region of low $d\ln T/dz$ is much less than one density scale height at this temperature so that n_H is essentially constant across the narrow plateau.

III. Radiation Losses

A reliable determination of chromospheric radiation losses is difficult to obtain. In the case of EUV emission lines, such as Lyman-α, the total line flux is a good measure of the chromospheric losses in these lines. Unfortunately, most of the radiation losses are in Fraunhofer lines, and there is no obvious way of identifying the chromospheric contribution to the emergent flux. The practice of simply taking all of the flux in the Ca II and Mg II line cores between the minima outside of the emission components provides a crude estimate for the losses in these particular lines. However, such estimates are not likely to be accurate to more than a factor two or three, and they completely ignore the many lines with chromospheric components but without identifiable emission features.

The most detailed computation of energy losses in the strong Fraunhofer lines of hydrogen, Ca II and Mg II is due to Vernazza *et al.* (1981). Their tabulation of energy losses from Ca II and Mg II is repeated in Table I. Lyman-α contributes an additional 3×10^5 ergs cm^{-2} s^{-1}. The total loss from these sources is 4.6×10^6 ergs cm^{-2} s^{-1}. Most of the loss occurs in the low chromosphere with an indicated maximum near a temperature of 5500 K and $\gamma \approx 10^{-3}$. Above the maximum, the radiation loss is given approximately by

$$R \approx 1\times10^{-11} n_H^{0.7}. \qquad (15)$$

This form remains valid up to the top of the first temperature plateau. Within the Lyman-α plateau R is numerically equal to $10^{-12} n_H$ or to $10^{-9} n_H^{0.7}$, but there is not enough height range to determine the exponent on n_H.

Computed energy losses of the type tabulated in Table I are quite sensitive to the model atmosphere and to atomic cross-sections that in many cases are not accurately known. Thus, they are not to be taken too literally. The exponent on n_H in equation (12), for example, could lie anywhere within the range 0.5 to 1. The total chromospheric loses from the lines considered are probably accurate to within a factor of two.

The biggest uncertainty in the total chromospheric radiation loss is in the neglect of many lines that contribute to energy loss in the low chromosphere and temperature minimum region. The low chromosphere maximum shown in the radiation loss tabulation of Vernazza *et al.* (1981) may be due entirely to this neglect.

Table I

Chromospheric Radiation Losses from Hydrogen Ionization Plateau in Units of 10^5 ergs cm^{-2} s^{-1} (Vernazza et al., 1981)

	Ca II					Mg II		H^-
Line	K	H	8542	8498	8662	k	h	cont.
Radiation loss	7	5	7	6	5	5	4	4

The temperature rise in the low chromosphere is not necessarily indicative of the onset of mechanical heating. In fact, it can be shown that a temperature rise will occur even when Q is decreasing with geometrical height through the temperature minimum and low chromosphere (Athay, 1981a).

A striking feature of the results in Table I is the near equality of the radiation losses in different lines. For a given ion, the near equality results from the strong coupling between the lines. In Ca II, for example, the H and K doublet and the infrared triplet share common upper levels, and scattering photons move freely from one line to another. The equality between lines of Ca II and Mg II is less obvious. However, the ratio of Ca II K to Mg II k intensities predicted by equation (11) is approximately 4 at 6000 K and 2 at 8000 K. The closer equality indicated by Table I probably results from the multiple sharing among the 5 Ca II lines and the fact that the chromosphere is not effectively thick in the infrared lines.

The Lyman-α flux of 3×10^5 ergs cm^{-2} s^{-1} is not a major fraction of the chromospheric energy loss. However, as noted in Section II, the loss rate, R, increases markedly and abruptly in the Lyman-α region. This suggests the possibility that the heating process in the Lyman-α region is different from that in the middle chromosphere where Ca II and Mg II losses predominate. Further suggestion that this may be the case comes from considerations of the energy balance in the transition region to the corona.

Observed emission measures at temperatures near 10^6 K suggest a downward conduction flux of about 6×10^6 ergs cm^{-2} s^{-1} (Gabriel, 1976). Thus, one expects to see at least this amount of radiation flux from the transition region. However, when the emission line fluxes in EUV and XUV regions that are of transition region origin are combined they amount to only about 3×10^5 ergs cm^{-2} s^{-1}. The deficit between this value and the conduction flux is just sufficient to provide the observed Lyman-α flux. Hence, one is tempted to assign the energy source for the Lyman-α flux to thermal conduction from the corona. This provides an apparent energy balance, but it raises other problems.

No physical model of the transition region has been developed that successfully carries energy from the corona into the Lyman-α region in sufficient quantity to even approximate the observed Lyman-α flux (cf. Athay, 1981c; Gabriel, 1976). The basic problem is that for a temperature of, say, 5×10^4 K the value of dT/dh required to give a conduction flux of 3×10^5 ergs cm^{-2} s^{-1}, as required by Lyman-α, is about 0.6 K cm^{-1}. Observed emission measures, on the other hand, require a value of dT/dh approximately 100 times smaller. Also, an enthalpy flux of this magnitude at 5×10^4 K and an average hydrogen density of 10^{10} cm^{-3} would require an average downflow velocity of 75 km s^{-1}, which is unacceptably large. Thus, while the suggestion that thermal conduction from the corona is somehow connected to Lyman-α radiation is attractive, it remains for someone to discover an energy transport process that transports coronal energy effectively into the temperature region where Lyman-α is formed.

The author is indebted to A. Skumanich for helpful comments on the manuscript.

References

Athay, R.G. 1976, "The Chromosphere and Corona: Quiet Sun" (Dordrecht: Reidel)

Athay, R.G. 1981a, "The Sun as a Star", Chap. 4, ed. S. Jordan (Washington, D.C.: NASA SP 450).

Athay, R.G. 1981b, Ap. J., Nov. 15, in press.

Athay, 1981c, Ap. J., 249, 340.

Gabriel, A.H. 1976, Phil. Trans. R. Soc. Lond. A., *281*, 339.

Linsky, J.L. 1981, "Solar Phenomena in Stars and Stellar Systems", Eds. R.M. Bonnet and A.K. Dupree (Dordrecht: Reidel)

Lites, B.W. and A. Skumanich 1981, *Ap. J.*, submitted for publication.

Summers, H.P. and R.W.P. McWhirter 1979, J. Phys. B, *14*, 2387.

Thomas, R.N. and R.G. Athay 1961, "Physics of the Solar Chromosphere", Chap. 4 (New York: Interscience)

Vernazza, J.E., E.H. Avrett and R. Loeser 1981, Ap. J. Supp., *45*, 635.

Models of Transition Region and Coronal Plasma in Solar "Loop" Structures

J. C. Raymond and R. Rosner

Harvard-Smithsonian Center for Astrophysics

The theory of coronal loops has been extensively developed in the last few years. We will discuss comparisons between the simple version of the theory and observations before turning to more recent theoretical work.

A. Comparison of Equilibrium Models with Observations.

The theory of static, magnetically confined coronal loops (e.g., Landini & Monsignori-Fossi 1975; Craig, McClymont & Underwood 1978; Rosner, Tucker & Vaiana 1978; Vesecky, Antiochos & Underwood 1979; Levine & Pye 1980; Jordan 1980) makes two very general, fairly testable predictions. The models assume local energy balance; the sum of the non-radiative heating (mechanical or electromagnetic), the radiative energy losses, and the divergence of the conductive flux must be zero. The heating rate is generally taken to be some simple function of the distance along the loop, or of density, and constant pressure or hydrostatic equilibrium is assumed. The models are quite insensitive to the details of the heating, and reflect mainly the balance between thermal conduction and radiative losses. The prediction responsible for much of the recent interest in loop models is the scaling law (Rosner, Tucker & Vaiana 1978)

$$T_{max} = 1400(pL)^{1/3}.$$

Differing assumptions, most notably the shape of the cooling curve, lead to slightly different relations (e.g., Craig, McClymont & Underwood 1978).

This scaling relation has been discussed by Pallavicini *et al.* (1981) using Skylab S054 data. While compact flare loops do not fit the relation, in the sense that the lengths predicted from the temperature and pressure are much larger than the observed lengths, this is not surprising, since such loops last too short a time to be considered static. All other features, ranging from compact high pressure active region loops to long, low pressure loops connecting different active regions, fit the scaling prediction extremely well. In fact, the scatter in the plot of predicted length versus measured length is only about what would be expected from the uncertainty inherent in the temperature determination alone.

The small scatter is remarkable, because none of the measured quantities is obviously equivalent to the theoretical quantity in the scaling law. The theoretical relation uses the maximum temperature in the loop, while the measured temperature is a mean over the actual temperature range, weighted by the emissivities in the observed wavelength bands. Since the temperature gradient goes to zero at T_{max}, the emission measure does peak there, and the measured temperature should be only slightly lower than T_{max}. The simple model does not predict the temperature structure perpendicular to the loop axis. It is potentially nonuniform, since each field line is effectively isolated from the others, and it

may be quite interesting to explore this possibility, because some heating mechanisms predict energy deposition in a narrow sheath. However, if the scaling law holds for each field line, and all are the same length, then the pressure is proportional to T^3 and the volume emissivity to T^4, so that the emission is very heavily weighted toward the highest temperatures. This is convenient for providing an easy test of the scaling law, but unfortunate for attempts to make observations which discriminate among the various heating theories.

The small scatter is also surprising in view of the fact that the length which enters the theory is the length along the field lines. If the loop is twisted, this will be greater than the length measured on an X-ray image. Evidently, the twist is not very great. Finally, the pressures used to predict the lenghts from the scaling law are based on the assumption that the hot plasma uniformly fills the observed emitting region. It is not otherwise obvious that the loop is not a bundle of fine, high pressure filaments, but apparently it is not.

Altogether then, the remarkable agreement between the scaling law and the observations yields some support for the accuracy of classical thermal conductivity and the standard radiative cooling curves, though it doesn't say much about the heating mechanism. This is not without value, since the rather large mean free paths of the faster electrons could potentially change the thermal conductivity (e.g. Scudder and Olbert 1979), and thermal diffusion (e.g. Rousel-Dupre 1980) or time-dependent ionization could distort the cooling curve beyond recognition.

A second observational test is the emission measure distribution. The simple loop model below 10^6 K is a plane-parallel atmosphere in which the divergence of the thermal conductive flux balances radiative losses. If the pressure is constant and the radiative cooling coefficient is propotional to $T^{-1/2}$ (applicable between 10^5 and 10^7 K), the emission measure distribution is proportional to T. No emission measure curve is available for a single hot loop, but active regions, at least above 10^5 K, ought to be superpositions of many loops. If one averages over an entire active region, different structures are likely to dominate the average at different temperatures. However, if all loops have an emission measure distribution proportional to T between 10^5 and 10^6 K, the sum of their emission measures must be no steeper than that in this temperature range. Levine and Pye (1980) have attempted to place limits on the distribution of loop parameters based on X-ray and EUV observations of an active region, and Pallavicini *et al.* (1981) have derived equivalent loop structures to match the average of an active region. The Vernazza and Reeves (1978) averaged active region EUV spectrum can be fit with an emission measure curve (Doyle and Raymond 1981). It turns out to be much steeper than predicted by the thermal conduction theory. Most of the hot plasma in that particular active region is not connected to the chromosphere through a plane-parallel, static transition region dominated by thermal conduction. The easiest modifications to the simple loop theory which would accommodate the observations are divergence of the magnetic field or mass flows.

Spectroheliograms from the SO82A instrument aboard Skylab suggest that there are two separate populations of loops; high temperature hydrostatic ones and cooler, nonstatic loops (e.g. Dere 1981; Cheng, Smith, and Tandberg-Hanssen 1980). The latter loops have been extensively studied by Foukal (1976; 1978). They are sometimes asso-

ciated with sunspots, and seem to have cool cores surrounded by hotter material. The temperature gradients along the loop axes are so low that thermal conduction is much too small to balance radiative losses. Even loops selected on the basis of visibility in the high temperature lines of Mg X or Si XII show detectable associated cool gas. Though there has been a great deal of theoretical investigation of loop instabilities recently, there is no neat theoretical interpretation of the difference between hot and cool loops.

It is also interesting to consider in detail the distribution of material at one point along the length of a loop (Raymond and Foukal 1981). Three loops for which spectral scans were obtained at a known position in the loop above the limb were selected from raster scans of the Harvard Skylab spectroheliometer. Two were cool loops of the sort studied by Foukal, and the third was a hot, X-ray emitting loop. Offlimb spectra were chosen to avoid confusion with background tranistion region emission and to make it possible to use weak lines normally buried by the Lyman continuum emission. An emission measure curve was constructed based on about 50 lines. We made the usual assumption of ionization equilibrium, then looked for discrepancies indicative of departures from equilibrium. Such departures were found in the highest quality loop spectra. Line ratios of O III, O IV, and Ne VII showed that these lines were formed at temperatures below their equilibrium temperatures. This means that the gas was rapidly cooling, presumably radiatively. The emission measure curves show the presence of gas throughout the temperature range to which the instrument was sensitive, 2×10^4 to 4×10^6 K. The low temperature gas is too high above the surface of the Sun to be in hydrostatic equilibrium. The highest temperatures, as indicated by the [Fe XVIII] and S XIV lines, are present with about a tenth the emission measure of the $\approx 2\times10^6$ K peak of the emission measure curve.

The high temperature gas should not be there. The height above the surface is known, since the distance above the limb is measured from the raster scans. The pressure is known from line ratios and from emission measure - volume analysis. Static loop models predict that the thermal conduction flux at any height can be at most what can be radiated away by the layers below. While the pressure, height and temperature (2×10^6 K) of the peak of the emission measure curve satisfy this prediction, the hottest gas observed produces an order of magnitude too much conductive flux. One possible explanation would involve high temperature loops with high pressures and very small filling factor along the line of sight. An intriguing alternative speculation is that this gas is directly connected with the heating process. Most theories of energy deposition in active region loops rely upon heating which is localized in very small volumes. The energy is then distributed by conduction or advection. The existence of a rather small amount of gas at temperatures significantly above the typical temperature of a given loop is a natural consequence of such theories. The theories are not yet able to make detailed predictions of how much or how hot it should be, however.

B. Existence and Stability of Equilibrium Loop Atmospheres.

Within the past several years, the existence and stability of equilibrium solutions to the hydrostatic equations of motion for magnetically-confined "loop" structures on the solar surface have been extensively studied (Antiochos 1979; Habbal & Rosner 1979; Hood & Priest 1979; Priest 1980). As will be discussed further below, the temporal behavior of the confined atmosphere is not at all straightforward to predict, particularly because it is difficult to realistically simulate the appropriate boundary conditions at the "loop" foot-

points (i.e., at the base of the transition region) in analytic calculations. However, by the end of the Skylab/ATM Active Region Workshop, the consensus view held that unless the conductive flux at the loop base was "large", instability was inevitable, and that the loop atmosphere was then unlikely to be in a state approximating hydrostatic conditions (Priest 1980). Under these circumstances, the extent to which the predictions based on simple loop models match the data is even more remarkable than just discussed above.

Existence of Equilibrium Solutions. The question of *existence* of hydrostatic equilibrium solutions to the "loop" equations of motion arose soon after the initial discussions of such solution. For example, Hood & Priest (1979) focussed on the problem of finding solutions in the case that the temperature at the transition region boundary was specified, and showed that (for fixed loop length and local heating rate) the equilibrium equations do not always yield a continuum of solutions as the loop pressure is allowed to vary as a free parameter. We shall not review this earlier work (cf. Priest 1980), but instead discuss a somewhat different calculation, which may have some relevance to recent observations of coronal emission from very active late-type stars. Rosner *et al.* (1982) have recently reexamined the equilibrium analysis for confined coronal plasma, and in particular have extended the analysis to higher coronal temperatures. Three regimes turn out to be of importance as the coronal heating rate is increased: (i) classical thermal conduction prevails in the transition region and line cooling dominates the coronal radiative losses; (ii) classical thermal conduction prevails in the transition region and bremsstrahlung dominates the coronal radiative losses; and (iii) heat flux-saturated thermal conduction prevails in the transition region and bremsstrahlung dominates the coronal radiative losses.

It is quite straightforward to solve the hydrostatic equations of motion in these three regimes. The basic new physical effect which enters into the analysis is the fact that (for fixed loop length) for temperatures log $T < 7.3$ [the exact value of T depending on the radiative equilibrium calculations used], the maximum classical thermal conductive flux in the transition region scales exactly the same way with the coronal temperature as the critical threshold value of the thermal flux necessary to initiate heat flux saturation (which scales as the product of the sound velocity and the pressure); but for log $T > 7.3$, the scaling behavior of the critical flux changes, and heat flux saturation becomes possible. The consequence of this behavior is best appreciated if one plots the maximum loop temperature versus the input heating flux (in erg $cm^{-2}sec^{-1}$; see Fig. 1). It is evident that a rather curious phenomenon takes place: for heating rates above some critical value, there exist *two* solutions to the equilibrium equations, *neither* of which is stable! The lack of stability is easily demonstrated. Consider the upper branch first: these solutions have coronal temperatures above the critical value at which heat flux saturation takes place, yet are based on the assumption of classical thermal conduction; such solutions are therefore internally inconsistent, and one would expect heat flux saturation to initiate. Now consider the lower branch: here the coronal temperature is *below* that required for heat flux saturation, yet the model assumes saturated heat conduction in the transition region; again, the model is internally inconsistent, and one would expect the heat flux saturation process to shut off. Thus, neither solution can be in steady state. It is indeed tempting to associate the highly variable high-temperature components of active late-type stars with such a process, but more study (particularly, detailed simulation of the non-linear development of the instability in this regime) is clearly called for.

The particular example just discussed may well serve as an apt caution that obtaining solutions to the equilibrium equations of motion (static or not) is quite insufficient. Not only

may one not always obtain equilibrium solutions, but even if such solutions can be found, such solutions may be totally unstable (either because they are internally inconsistent, as here, or because of other time-dependent processes which the equilibrium equations ignore on *a priori* grounds; see below).

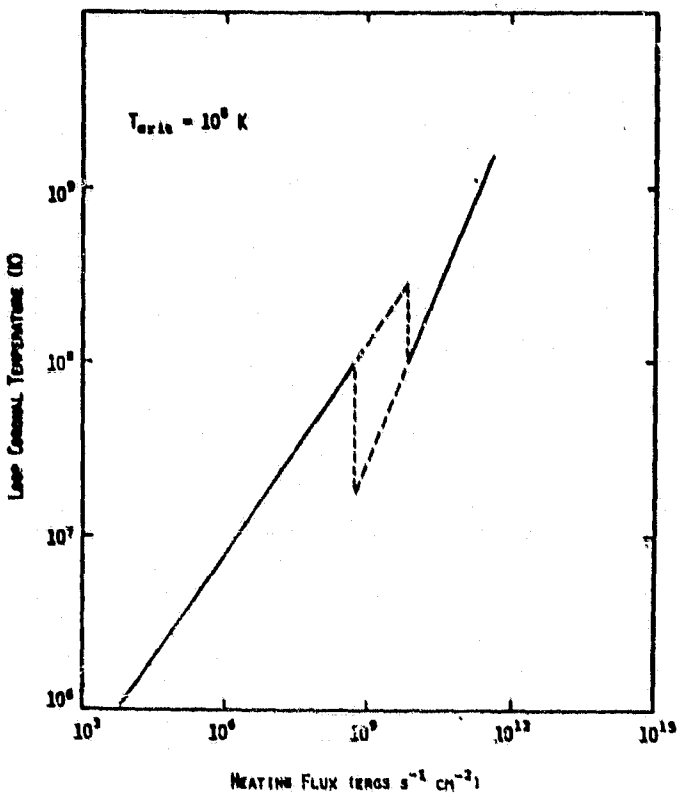

Figure 1: Variation of the maximum coronal temperature with the imposed "mechanical" heating flux for a simple hydrostatic "loop" model (from Rosner, Golub, & Vaiana 1982); the assumed transition temperature marking changeover to the heat flux-saturated regime is 10^8 K. The domain of heat input for which no consistent equilibrium models exist is shown in dashed lines.

Stability of Equilibrium Solutions. The early work on stability focussed on two distinct issues: first, are the equilibrium solutions stable to isobaric perturbations if the *base temperature* is held fixed, or, second, if the *base conductive flux* is held fixed (Antiochos 1979; Habbal & Rosner 1979; Hood & Priest 1980). The first case (A) would seem to be appropriate if the base is located sufficiently deep in the atmosphere so that coronal (or transition region) perturbations do not disturb local energy balance; the second case (B) is more appropriate if the base of the loop is chosen to lie in regions where radiative processes can control the temperature rise (cf. Basri *et al.* 1979), and is more difficult to treat because the base may take on the character of a free surface whose *spatial location may vary*. The results of Antiochos (1979) and Hood & Priest (1980) for case A (which assumes fixed conditions in the underlying chromospheric plasma) showed instability was inevitable for small base conductive fluxes, but with growth rates sensitively dependent on the ratio of base to peak temperature.

The issue for case B is more complex, and depends on whether one chooses to fix the base conductive flux at fixed location (so that the base temperature is free to vary; Antiochos 1979; Hood & Priest 1979), or at fixed temperature (so that the base location is free to vary; Habbal & Rosner 1979); it is not clear which alternative is realized in nature (see however Basri *et al.* 1979). Previous predictions of loop instability in the first case have been recently shown to be in error by Craig & McClymont (1981), who demonstrate that for a realistic radiative loss function at low temperatures, the instability time scales for the most unstable modes of Antiochos or Hood & Priest for the "thermally-isolated" case far exceed typical observed lifetimes of the loop structures in question; we therefore conclude that for this case, instability of hydrostatic equilibrium solutions is irrelevant for modelling of all but the longest-lived loop structures. For the case of fixed conductive flux at fixed temperature, Habbal & Rosner (1979) showed that the stability of hydrostatic equilibrium solutions depended on (i) the ability of the loop base to adjust to coronal (or transition region) perturbations; and (ii) the response of the local heating process to imposed perturbations. For a particularly simple class of perturbations (which correspond to uniformly increasing the loop temperature, and 'pushing' the transition region downwards), Habbal & Rosner demonstrated stability for all the heating processes they considered. This result is not conclusive: there may exist classes of perturbations which *do* lead to instability; and their relatively simple parametrization of the various coronal heating processes may not properly take account of the fully-nonlinear response of such heating mechanisms. Because of the difficulty of proceeding any further by analytical means in this case, Peres *et al.* (1981) chose to attack the problem by numerical simulation. This approach also avoids the problem of choosing the appropriate boundary conditions at the nominal base of the loop; rather than adopting essentially *ad hoc* boundary conditions at, for example, the base of the transition region (which may or may not be based justified on physical grounds), simulation allows one to *calculate* the response of the underlying atmosphere. Using a time-dependent, 1-D, single fluid hydrodynamic code, variable spacing, and allowing for upper chromospheric response, Peres *et al.* showed that hydrostatic equilibrium solutions are quite robust: even large amplitude perturbations did not result in catastrophic instability; loop evolution appeared to be largely governed by mass exchange across the transition region, resulting in loop behavior which strongly resembled that of the 'evaporative' time-dependent model of Krall & Antiochos (1980), in which the response of the atmosphere lying below the loop base was assumed as an *ad hoc* boundary condition (Fig. 2). It is notable, however, that these calculations did not take into account the response of the "mechanical" heating process to the perturbation; some effort in this direction is currently underway (Ferrari *et al.* 1982). Similar results showing the great stability of the corona and transition region to even substantial perturbations, but based on a rather different 1-D, two-fluid time-dependent hydro code, have been recently obtained by Boris, Mariska, Oran, and coworkers at NRL (cf. Boris & Mariska, this volume, and references therein; see also An, McClymont, & Canfield 1980). Their work in fact argues that the corona-transition region structure is the unavoidable *end product* of the nonlinear evolution of an initially-uniform state (as related calculations for thermal instability of the interstellar medium suggested earlier; see also Craig 1980). The simulations thus show that (i) earlier concerns that hydrostatic models may be unavoidably unstable were unfounded; (ii) the loop base does appear to act as a free surface in the simulations.

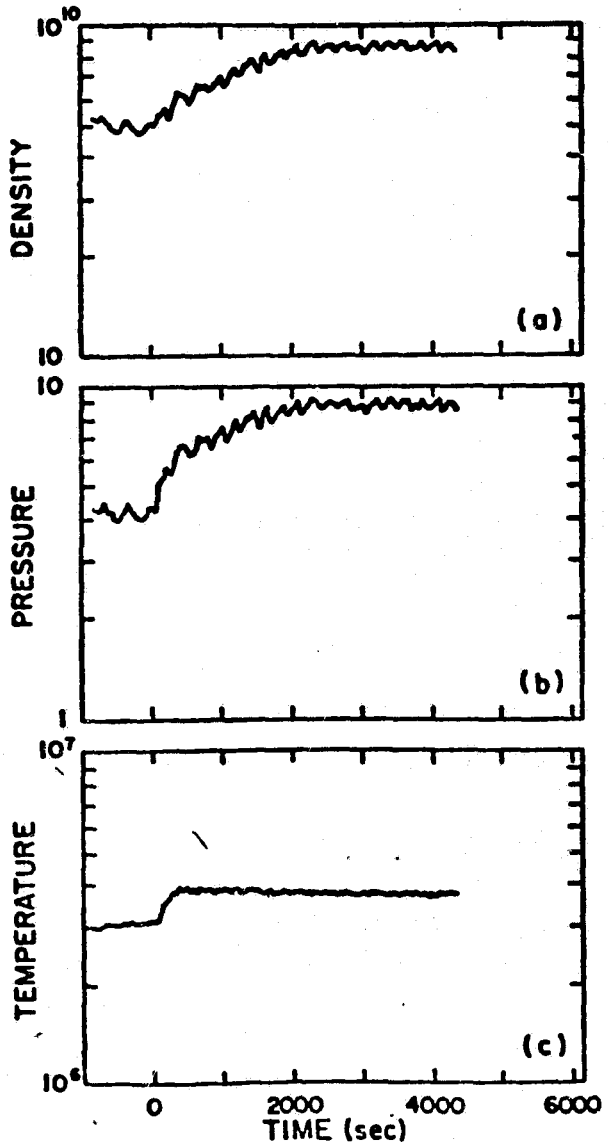

Figure 2: Response of an initially hydrostatic loop atmosphere to a perturbation in heating rate for typical active region conditions (from Peres *et al.* 1981); the calculation is meant to simulate the evolution of active region structures (as opposed to flaring behavior). Note that the model calculation shows evidence for "evaporation", e.g., mass exchange across the chromosphere/transition region boundary, in response to the perturbation.

C. Conclusions.

From both the observational and the theoretical perspective, it now appears that the gross properties of the confined corona can be understood by considering simple hydrostatic equilibrium models, although the reasons for this are quite complex and, in some cases, still not well-understood; the difficulty of matching the observed steep differential emission measure profiles in spatially-unresolved data stands as a particularly vexing problem. When one however looks at the corona in some detail, the simplicity dissolves, and it

is apparent that hydrostatic models are seriously inadequate. Observations of intensity fluctuations, of persistent up and down flows, of relatively cool matter residing at coronal heights, of apparent spatial comingling of hot plasmas at quite different temperatures, all call for more sophisticated modeling. The new plasma simulations have appeared at an opportune time.

This work was supported by NASA contract NAS 5-3949 and the Langley-Abbot Program of the Smithsonian Institution (JR) and by the NASA Solar-Terrestrial Theory Program at the Harvard-Smithsonian Center for Astrophysics (RR).

References

An, C.-H., McClymont, A. N., and Canfield, R. C. 1980, *BAAS*, **12**, 913.
Antiochos, S. K. 1979, *Ap. J. (Letters)*, **232**, L125.
Basri, G. *et al.* 1979, *Ap. J.*, **230**, 924.
Cheng, C.-C., Smith, Jr., J. B., and Tandberg-Hanssen, E. A. 1980, *Solar Phys.*, **67**, 259.
Craig, I. J. D. 1980, in **Solar Flare Magnetohydrodynamics** ed. E.R. Priest, Gordon and Breach.
Craig, I. J. D., and McClymont, A. N. 1981, *Nature* (in press).
Craig, I. J. D., McClymont, A. N., and Underwood, J. H. 1978, *Astron. Ap.*, **70**, 1.
Dere, K. P. 1981, in preparation.
Doyle, J. G., and Raymond, J. C. 1981, in preparation.
Foukal, P. F. 1976, *Ap. J.*, **210**, 575.
Foukal, P. F. 1978, *Ap. J.*, **223**, 1046.
Ferrari, A., Rosner, R., & Vaiana, G. S. 1982, in preparation.
Habbal, S. R., and Rosner, R. 1979, *Ap. J.*, **234**, 1113.
Hood, A. W., and Priest, E. R. 1979, *Astron. Ap.*, **77**, 233.
Jordan, C. 1980, *Astron. Ap.*, **86**, 355.
Krall, K. R., and Antiochos, S. K. 1980, *Ap. J.*, **242**, 324.
Landini, M., and Monsignori-Fossi, B. C. 1975, *Astron. Ap.*, **42**, 213.
Levine, R. H., and Pye, J. P. 1980, *Solar Phys.*, **66**, 39.
Morrison, P., and Ionson, J. A. 1981, preprint.
Pallavicini, R., Peres, G., Serio, S., Vaiana, G. S., Golub, L., and Rosner, R. 1981, *Ap. J.*, **247**, 692.
Peres, G., Rosner, R., Serio, S., and Vaiana, G. S. 1981, *Ap. J.* (in press).
Priest, E. 1980, ch. 8 of *Skylab Active Region Workshop*, ed. F. Q. Orrall.
Raymond, J. C., and Foukal, P. F. 1981, *Ap. J.*, in press.
Rosner, R., Golub, L., and Vaiana, G. S. 1982, in preparation.
Rosner, R., Tucker, W. H., and Vaiana, G. S. 1978, *Ap. J.*, **220**, 643.
Rousel-Dupre, R. A. 1980, *Ap. J.*, **241** 402.
Scudder, J. D., and Olbert, S. 1979, *J. G. R.*, **84**, 2755.
Vernazza, J. E., and Reeves, E. M. 1978, *Ap. J. Suppl.*, **37**, 485.
Vesecky, J. F., Antiochos, S. K. and Underwood, J. H. 1979, *Ap. J.*, **233**, 987.

D3

N83 20849

CHROMOSPHERIC AND CORONAL HEATING MECHANISMS

John Leibacher
Lockheed Palo Alto Research Laboratory
Palo Alto, CA 94304

Robert F. Stein
Department of Physics and Astronomy
Michigan State University
East Lansing, MI 48824

INTRODUCTION

We have recently reviewed this general subject (Leibacher and Stein, 1980; Stein and Leibacher, 1980) and several other good reviews have also appeared during the last year: "The Sun as a Star" (Jordan, 1981), "Solar Phenomena in Stars and Stellar Systems" (Bonnet and Dupree, 1981), and "On the Theory of Coronal Heating Mechanisms" (Kuperus, Ionson and Spicer, 1981). We shall not attempt to duplicate this work, but will rather outline the problem and comment on some recent investigations. The bibliography extends beyond the actual references cited here, to guide the reader to the recent literature.

What are the problems? We grew up with texts such as Unsold and Aller and the paradigm that the atmospheres of stars were in radiative equilibrium. The existence of higher temperature outer atmospheres violates this picture, and is incompatible with a structure controlled by thermal energy transport. The problem is that we have a heat flux from a cool region of the star to a hot region of the star, which violates the second law of thermodynamics. Something is required to make that occur, namely a non-thermal energy flux. While convection transports the thermal flux, a very small percentage is converted into a nonthermal flux. The major part of the outgoing convective energy is turned back into the radiation field which gets decoupled from the star when the star becomes transparent and the radiant energy escapes to space. The small non-thermal flux (10^{-3} - 10^{-4} of the thermal flux) is transmitted upwards and becomes the dominant energy flux still coupled to the star.

Any proposed non-thermal heating mechanism must address four issues. First, the radiative losses from the chromosphere and corona are observed, and any mechanism must generate at least that much non-thermal energy. Unfortunately, that is all too easy to do. Almost any process can generate enough flux from the convection zone, because the amount needed is such a small fraction of the thermal flux. So this is a good place to start. If the mechanism doesn't provide this threshold you might as well forget about it. Second, and much more challenging, is the vertical distribution of temperature and dissipation. Acoustic waves provide a lot of energy, but can they get it up to the corona? (It is worth recalling that the losses from the non-thermal flux in the photosphere far far exceed the losses in the chromosphere, which in turn far exceed the losses in the corona.) This has lead people to turn to Alfven waves which are capable of propagating energy to great heights. That is all

well and good, but they may provide only 0.1% of the energy losses in the chromosphere, which remains an outstanding problem when discussing Alfven waves. Third, the variation of the observed radiative losses across the HR diagram, their dependence upon surface gravity and effective temperature, has proved to be a very fruitful discriminator. EINSTEIN and IUE observations have served to unblock a situation that existed in solar physics for a long time. The acoustic heating hypothesis has been judged and found deficient. There are probably several mechanisms at work simultaneously, both within one star as a function of altitude between the chromosphere and corona, and across the HR diagram. Finally, there is the issue of spatial and temporal inhomogeneity of the heating. How does it vary across the surface of the star, and how does it vary in time? Is the heating steady state or is it impulsive, is it associated with open and closed structures and hence modulated by rotation, or is it uniform as for acoustic waves generated by convection?

We shall discuss the acoustic wave and magnetic field associated mechanisms separately. The two points we would like to make are: First, that while the mood is shifting away from the acoustic wave hypothesis to currents and magnetic waves dissipating in the corona, you should not throw the baby out with the bath water. Even though magnetic, current heating mechanisms are appropriate for the corona, acoustic waves appear to be appropriate for the temperature minimum, and in terms of the total energy budget they represent a substantial loss to the solar atmosphere. So don't believe everything bad you hear about acoustic waves. Secondly, the whole heterogeneous class of mechanisms associated with "currents", that is currents induced in pre-existing magnetic structures, while very, very promising and popular, are based upon a number of very uncertain elements. The theory of stellar rotation cannot yet describe the sense of the differential rotation that lies at the base of possible dynamos. Dynamo theory has not yet advanced to the point where the observed periodicities in the magnetic field arise naturally, nor can it can predict the fraction of surface area covered by strong fields, nor the rate of emergence of new flux. The spectrum of convective motions, which stresses the magnetic fields, is assumed to resemble that of homogeneous turbulence, which we know should be a poor approximation for the spatial scales involved.

ACOUSTIC WAVE MECHANISM

What are some of the arguments used against non-magnetic waves? First, there is Athay and White's (1978) and Bruner's (1978, 1981) OSO-8 observations that with the measured kinetic energy density in the chromosphere (from line widths and shifts), propagating at the sound speed, you can't get enough energy up into the corona. This is not true for the temperature minimum and the low chromosphere. The balance between observed radiative losses and observed kinetic energy density times sound speed occurs in the upper chromosphere. Secondly, the observed regions of large energy losses are very inhomogeneous compared to the homogeneous source. If turbulent convection were the source, we would expect it to be more or less uniform over the solar surface, but we see loops and active regions which have enormously larger loss rates than their surroundings. Third, Linsky and collaborators, using IUE data, showed that the chromospheric radiation losses do not have the inverse dependence upon surface gravity that acoustic emission predicts,

$$F_{AC} \propto g^{-1} T_{eff} \quad (10\text{-}15)$$

(see Bohn, these proceedings). The observed dependence of the magnesium line flux on the surface gravity is insignificant. In addition, the observed dependence on the effective temperature is also much smaller than predicted. Just as the observed radiative losses vary over the HR diagram, they also vary at one point on the HR diagram. For a given total luminosity and temperature, substantial differences in the losses from the outer atmosphere are observed. This contradicts another paradigm - the Russell-Vogt theorem - that the structure of a star depends only upon its mass and chemical composition. What we are seeing is evidence for a third dimension to the HR diagram, possibly rotation. This is incompatible with the basic concept of the acoustic wave mechanism, that convective generation is a function of g and T_{eff} only. Finally the dissipation lengths are off. A lot of energy is generated, but the vertical distribution of the dissipation doesn't match up with the observations. Figure 1 shows that most of the wave energy is dissipated near the temperature minimum and doesn't produce a corona (Fig. 2). This calculation started with a radiative equilibrium atmosphere with a boundary temperature of 4500 K. An acoustic wave flux of 4×10^7 ergscm^{-2}s^{-1} was fed into the bottom of the atmosphere by a piston, and the atmosphere heated up, until a quasi-steady state was established. We see that as the waves reach the visible surface they suffer radiative losses, and the flux drops enormously. This is characteristic of radiative damping. For most waves that have some compressibility, as soon as the fluctuations can see outer space most of the wave's energy gets radiated away. Here 80% of the energy is lost by radiative damping. For other stars it could be 99%. There is a very strong filter function between the predictions of acoustic flux generation below the visible surface and what arrives in the chromosphere and corona. Most of the energy is lost in the photosphere. (It is interesting to consider what effect all of this mechanical energy loss below the temperature minimum will have on radiative equilibrium models.) The second drop in the flux further out is due to the formation of shocks and the onset of dissipation, which forms the temperature minimum. Short period, short wavelength waves dissipate their energy about 3-400 km. above $\tau = 1$. The important point is that after these waves have traveled up another 4-5 scale heights all their energy is dissipated. Very little of the energy reaches the corona. Another way of seeing this is by looking at the temperature structure (Figure 2). Depending on the opacity, a temperature rise to 5-7000 K is obtained. Note that the chromospheric structure is very sensitive to the radiative losses. Hence we may be able to calculate accurate chromospheric models, even with an uncertain energy input. Again we see that all the energy has been dissipated at chromospheric temperatures. There is no corona. Thus the acoustic heating mechanism (or equivalently slow magnetic waves) can account for the structure of the low chromosphere, but not the corona.

MAGNETIC MECHANISMS

How does the magnetic field influence the heating of structures on the sun? Consider the flow of energy through the sun, illustrated in Figure 3. A thermal flux carries the energy from the interior nuclear energy source to the surface. It is a radiative flux in the interior and becomes a convective flux in the outer third of the sun. The presence of a magnetic field in the turbulent convective zone provides a restoring force against which the convective motions can do work; they can store some of their energy in the field. Two very different scales of motion play a role: giant cells, with sizes comparable with the depth of the convection zone, drive the dynamo giving rise to the surface magnetic fields, while small scale motions (shear turbulence)

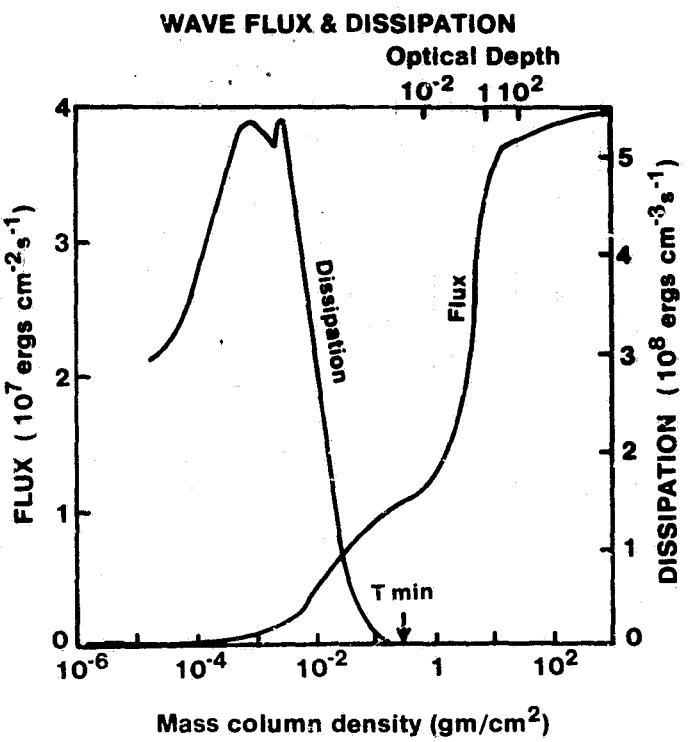

Figure 1. Acoustic wave flux and dissipation as a function of mass column density (Stein, unpublished). An initial atmosphere in radiative equilibrium above $\tau = 1$ and adiabatic below is heated by 30s period acoustic waves and cooled by gray LTE radiation, until a quasi-stationary state is reached.

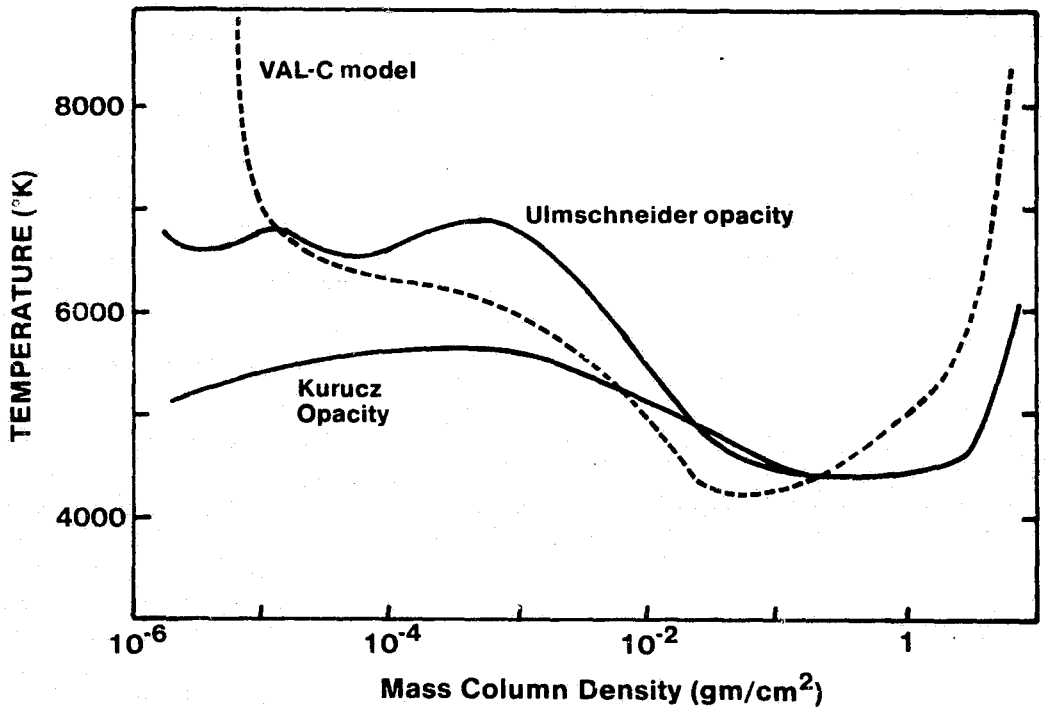

Figure 2. Temperature as a function of mass column density. Calculations, similar to figure 1, were performed using two different opacities, one a table calculated by Kurucz (private communication) and the other a power law fit by Ulmschneider et al. (1978). Also shown is the empirical model of Vernazza, Avrett and Loeser (1981). These results are similar to those of Ulmschneider et al. (1978).

stress the surface fields to generate a non-thermal flux that is transmitted along them. The dependence of magnetic heating mechanisms upon the vagaries of a dynamo involving both convective motions and rotation to generate the basic restoring force contrasts with the acoustic wave mechanism, which depends only upon convection. We suspect that magnetic mechanisms may possess some of the stochastic properties of the large scale solar magnetic field -cycles on the order of tens of years and variations on the order of tens of cycles -to which some of the dispersion in observed chromospheric and coronal properties at a given position on the HR diagram may be attributed. In addition, the dynamo will vary as rotation varies, on a time scale possibly short compared to evolution.

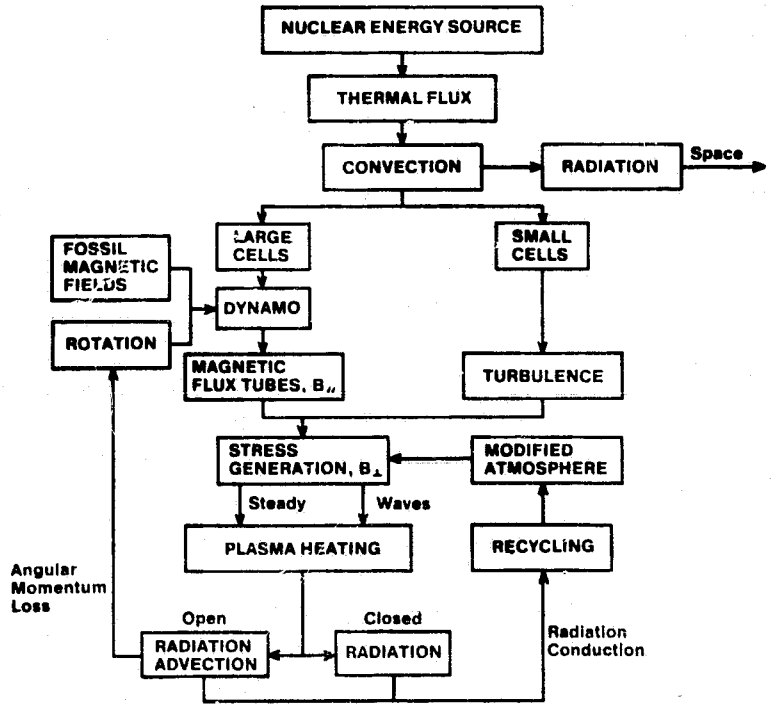

Figure 3. Flow chart of energy transport through the sun and other cool stars (after Rosner, previous workshop).

The magnetic field can do two things: First, as a flux tube rises because of the buoyancy associated with its magnetic energy density, it will be subjected to the turbulent stresses of the convection zone through which it passes. The tube rises up into the corona, where the magnetic pressure dominates the gas pressure, so that any unbalanced magnetic forces cannot be resisted, and, after an agitated beginning, a loop relaxes to a potential configuration (Galloway and Weiss 1981, Golub et al. 1980, Golub et al. 1981). Its stresses are relieved by work done against the surrounding corona (Book, 1980) and by dissipation of the currents associated with the helicity of the magnetic field. It now appears that magnetic flux is continuously appearing all over the sun, and that upward advection of stressed fields could make a substantial contribution to coronal heating. Second, the turbulent convective motions can shake the flux tube, twist it and induce currents to flow along it. As the energy is being transmitted out very little is dissipated on route. However, when it gets up to a region where the gas pressure is very low compared to the magnetic pressure, the magnetic field once again is important– in dissipating the non-thermal flux. There are

a number of dissipation mechanisms that astronomers are familiar with primarily in the context of solar flare theory. These mechanisms involve either very high current densities, filamentation of the currents so that the current density in a very small area goes up and becomes unstable, or shearing of the magnetic field, which also leads to instability. Once the non-thermal flux is dissipated, the energy can either escape to space by radiation or via the solar wind if it is in an open structure, a coronal hole, or it can be recycled, that is, conducted back down, changing the structure of the lower atmosphere. Again the magnetic field plays a role in channeling this flux, which can be a source of energy to a number of secondary processes, such as spicules. This energy can be recycled and transmitted through many many processes before it finally escapes. Hence we must be careful that we don't become simplistic looking for a one-shot mechanism throughout the entire atmosphere. That is the big picture and now we shall discuss the individual components.

(i) Generation

The magnetic fields coming through the visible surface have a huge magnetic energy, but often they are sitting there in a loop, a potential configuration. There is a large energy density, but there is no way of using it, because it is in its lowest energy state. There is no magnetic free energy. The potential field, those nice loops we see, don't have any free energy. Magnetic flux coming up through the convection zone is subject to a lot of stresses. When it emerges it is in a stressed configuration. It can relax into a potential field and get rid of those stresses. Alternatively, once this flux tube linking the convection zone with the corona exists, the convective motions can agitate it, shake it around, because the kinetic energy density is greater than the magnetic energy density. Consider a flux tube of length $\ell_{//}$, which is twisted a small distance $\ell_{\perp}$. This will produce a perpendicular magnetic field of the order of

$$\delta B \approx B(\ell_{\perp}/\ell_{//}),$$

where $\ell_{\perp}/\ell_{//}$ is the tangent of the angle through which the magnetic field lines were twisted. The energy density is

$$\frac{B^2}{4\pi}(\ell_{\perp}/\ell_{//})^2.$$

If the magnetic tube is twisted by the length $\ell_{\perp}$ every correlation time τ, by for example granules or super granules, then the rate of energy generation is

$$E = \frac{B^2}{4\pi}\left(\frac{\ell_{\perp}}{\ell_{//}}\right)^2 \tau^{-1}.$$

If the driving velocity is u, then

$$\ell_{\perp} \approx u\tau.$$

If the flux tube is twisted slowly, the non-thermal energy flux is

$$F_{DC} \approx (B^2/4\pi)(u^2\tau/\ell_{//}), \qquad \tau > \ell_{//}/a$$

(Sakurai and Levine, 1981, Sturrock and Uchida, 1981) where $a = B/\sqrt{4\pi\rho}$ is the Alfven speed. If the agitation is rapid, that is on a time scale less than the Alfven propagation time along the loop, then $\ell_{//}$ becomes the distance the disturbance can propagate in a correlation time,

$$F_A = \frac{B^2}{4\pi} u = \rho u^2 a. \qquad \tau < \ell_{//}/a$$

We get something which looks very familiar, the kinetic energy density times the Alfven speed. If the flux tube is twisted slowly enough a DC current is produced, if rapidly enough Alfven waves are produced. Note, these waves are actually tube modes (Spruit, 1981a,b), because of the loop structure of the magnetic field.

Both currents and waves are extremes of a very similar situation. Twisting a flux tube generates a ∇xB, a current. If the loop is capable of dissipating the energy more rapidly than it is fed in, then a steady DC current along the loop is generated. If the bottom of the loop is twisted rapidly, with a coherence time of the motion less the Alfven propagation time along the loop, then waves are generated. These waves have currents associated with them, which can be dissipated in much the same manner as DC currents. There is, however, some difference in these two situations, since when the field is twisted at high frequency macroscopic motions are associated with the currents. Those macroscopic motions can be dissipated by all of the acoustic wave mechanisms, so there is another dissipation channel. Alfven waves are somewhat of an exception, in the sense that they are compressionless; they don't have a density fluctuation associated with them. Other magnetic waves, the fast and slow modes, have compressibility associated with the currents and that compressibility can lead to dissipation.

Let us note that Osterbrock had all these ideas way back in 1961. The problem was that magnetic fields in those days were thought to be smaller, so the dissipation of Alfven waves low down was very substantial, and the energy never got to the corona. That can still be a problem for some modes. Even when enough non-thermal energy is generated, it must propagate through the temperature minimum and be transmitted to the corona, not dissipated low down. Slow modes will be damped by radiation, similar to the acoustic waves we saw before. Mode coupling occurs whereby large amplitude Alfven waves form other waves which run away and damp much more efficiently. So the process of getting energy through the temperature minimum and up to the corona is still complicated.

The expression for the energy flux due to rapid twisting of the flux tube footpoints can be scaled to other stars (Stein, 1981). In an equipartition surface field, the flux generated as Alfven and slow mode waves is comparable,

$$\frac{F_A}{\sigma T_{eff}^4} \approx \frac{F_S}{\sigma T_{eff}^4} \approx 10^{-9} g^{-0.2} T_{eff}^{2.2} .$$

Slow modes are just acoustic waves travelling along the flux tube. Note that the dependence on both surface gravity and effective temperature is much weaker than for acoustic waves in non-magnetic regions, in much better accord with the MgII observations. This leads us to think that slow mode (acoustic) waves heat the lower atmosphere, the temperature minimum and low chromosphere, while Alfven waves, which dissipate further up, heat the corona.

(ii) Transmission

Recently, an interesting way of looking at the transmission of this magnetic free energy through the temperature minimum up into the corona has been proposed by Ionson (1980) and Spicer (1981). Instead of looking at the transmission of waves along the loop waveguide, the loop can be viewed as part of a complete current circuit (Figure 4). A single loop can be viewed as a circuit with an emf, a distributed resistance, inductance and capacitance. Or the circuit instead of closing from one footpoint to the other, can close within the same footpoint, and the loop contain antiparallel currents. How these circuits close in or below the photosphere is a major uncertainty. Finally, in an open field line, the circuit is closed at infinity. We can consider the circuit as made up of parallel or coaxial wires. The inductance of the circuit is of order

$$L \sim \ell_{//}/c^2 ,$$

where $\ell_{//}$ is the length of the circuit, and we have neglected the logarithm of the ratio of the wire separation to their size. The capacitance of the circuit is

$$C \sim \varepsilon \ell_{//} \sim \ell_{//} c^2/a^2 ,$$

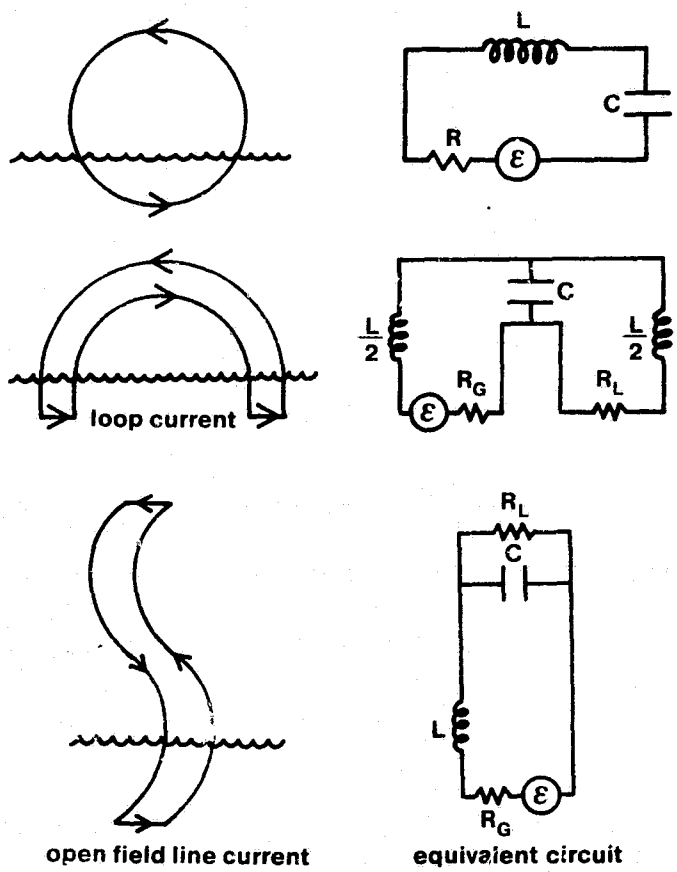

Figure 4. Equivalent circuits for open and closed magnetic field configurations. See also Ionson (1980) and Spicer (1981).

where ε is the dielectric constant of the plasma. The resistance of the circuit is

$$R = \eta \ell_{//}/A,$$

where $\eta = \sigma^{-1} = 4\nu_{eff}/\omega_{pe}^2$ is the resistivity, ν_{eff} is the effective collision frequency of the electrons with each other, with ions or with clumped charges due to instabilities and waves in the plasma, ω_{pe} is the electron plasma frequency, and A is the cross sectional area through which the current flows. Although we treat the equivalent circuit as a linear system, in reality the resistance is a function of the current, because the effective collision frequency and area through which the current flows are determined by non-linear processes.

If we think of the circuit as a transmission line, then when the resistance and leakage are small, it will propagate waves at the Alfven speed

$$V = \left[\left(\frac{L}{\ell_{//}}\right)\left(\frac{C}{\ell_{//}}\right)\right]^{-1/2} = a .$$

Small but finite resistance and leakage reduce this velocity. It is thus reasonable that a LRC circuit with small resistance has a resonant frequency

$$\omega_o = (LC)^{-1/2} = a/\ell_{//} ,$$

where L and C are the lumped values for the entire circuit. This resonant frequency implies global oscillations of the entire loop (Ionson, 1980). The time constant of the circuit (which also holds in the limit of large resistance and no oscillations) is

$$\tau_M \approx L/R \approx A/\eta c^2.$$

This is also the magnetic field diffusion time or resistive skin time. The Joule heating time scale in the corona is, however, much shorter, since the thermal energy density is much less than the magnetic energy density,

$$\tau_{JH} \approx \beta \tau_M$$

(Spicer, 1981), where $\beta = 8\pi P/B^2$ is the ratio of thermal to magnetic energy densities.

The transition region produces reflections in the transmission line because of the impedance mismatch across it, just as it produces reflections of waves because of the sudden change in propagation speed. At the transition region the abrupt change in Alfven speed produces an abrupt change in the capacitance, while the abrupt change in density produces an abrupt change in resistance. Spreading of the loop also occurs and reduces the resistance and to a lesser extent modifies both the inductance and capacitance.

(iii) Dissipation

Whether one thinks of the energy as transported by Alfven waves or currents, it must be dissipated. Unless very small scale structures are somehow continually generated, the damping lengths will be large compared with the lengths of coronal

loops, and the dissipation rate will be very small. In terms of the circuit model, the problem can be viewed as follows: If the resistance in the circuit is small, the circuit will have a well defined resonant period and a high Q value. Such a resonant circuit will dissipate only the energy fed into it in the band width

$$\Delta\omega/\omega_o = Q^{-1} = R\sqrt{C/L} = (\omega_o \tau_M)^{-1}$$

about the resonant frequency. Even though all the energy produced by the driver in this spectral range is dissipated, for a large Q this may be an insignificant fraction of the total power in the driving photosperic velocity field. For significant heating, Q must be near 1, or in the wave picture, the damping length must be comparable to the length of the loop.

There are two processes that are treated more naturally in the wave picture: The first is damping of waves by radiative transfer, which applies primarily to the slow mode acoustic-gravity waves in the photosphere. The second is non-linear coupling between wave modes. Coupling from Alfven to compressive slow or fast waves is especially important for damping.

Whichever model of energy transmission one uses - either waveguide or circuits - dissipation occurs because collisions transfer momentum and energy, in a way that randomizes kinetic energy of directed motions into thermal kinetic energy. This occurs via two processes: viscosity and resistivity. Viscosity leads to energy and momentum transfer between different portions of fluid in relative macroscopic motion. It is significant only where fluid parcels a mean free path apart are in relative motion. Resistivity transfers energy from the drifting electrons in an electric current to the thermal plasma. It leads to Joule heating and magnetic field reconnection. Classically, the collisions involved in both processes are binary collisions between individual particles. However, in a plasma, collective effects (modes of the plasma) can clump the charges, thereby increasing the effective charge of a scattering center enormously and hence greatly increasing the effective coulomb collision rate, which produces "anomolous transport" of energy and momentum.

The energy dissipated by currents or waves is ultimately either (1) radiated away, (2) recycled back down to the chromosphere, or (3) on open field lines given to the stellar wind. On open field lines the wind is a bottomless pit - absorbing all the energy and momentum fed into it. Indeed, as others at this meeting have stressed, energy and momentum transfer from Alfven waves is crucial in producing cool winds in giant stars.

CONCLUSION

In conclusion, acoustic waves are not everything they were cracked up to be, but let us not overreact and forget them entirely. They are probably the dominant mechanism at the temperature minimum. Magnetic fields are really not the scary things we thought they were, although the ingredients of the magnetic controlled mechanisms are not as well understood as the Lighthill mechanism for generating acoustic waves. This is the canonical way to end a talk, saying that there remains lots of good stuff still to do. Dynamos require a lot more study. The rate of emergence of flux tubes and the fraction of the surface area covered by them is very important, and is still very uncertain. We have a very good mechanism for coupling the convection

zone to the corona, but a very small fraction of the convection zone is actually permeated by these flux tubes and how that varies from star to star is very important. The spectrum of energy generation is poorly understood. The whole question of resonant circuits is exciting, but needs more development. Again we would like to emphasize that waves and currents are largely two ways of looking at the same thing. For dissipation processes we can fall back on what we have learned in solar flares. In spite of the difficulty of that subject, we have learned a lot about the dissipation mechanisms in the last several years. Finally, we shouldn't forget how important the recycling of energy via advection and conduction is.

ACKNOWLEDGEMENTS

JWL would like to thank the organizers for their hospitality and acknowledges support by NASA contract NAS5-23758 and the Lockheed Independent Research Program. RFS acknowledges support by NSF grant AST 79-19465 and NASA grant NSG 7293.

BIBLIOGRAPHY

Note that we have included relevant references that have appeared since the previous meeting, even though not cited in the text.

Alvarez, M. 1980, Astrophys. J. 240, 322: Energy Balance from the Chromosphere-Corona Transition Region.

Arcoragi, J.-P. and Fontaine, G. 1980, Astrophys. J. 242, 1208: Acoustic Fluxes in White Dwarfs.

Athay, R. G. and White, O. R. 1978, Astrophys. J. 226, 1135-1139: Chromospheric and Coronal Heating by Sound Waves.

Ayres, T. R. 1980, Solar Phys. 68, 125-134, Does H^- Truly Cool the Solar Chromosphere?

_____. 1981, Astrophys. J. 244, 1064-1071: Thermal Bifurcation in the Solar Outer Atmosphere.

Ayres, T. R. and Linsky, J. L. 1980, Astrophys. J. 241, 279: Outer Atmospheres of Cool Stars, V. IUE Observations of Capella. The Rotation-Activity Connection.

Baliunas, S. L., Hartmann, L., Vaughan, A. H., Liller, W. and Dupree, A. K. 1981, Astrophys. J. 245, 473-483: Short Time Scale Variability of Chromospheric Ca II in Late-Type Stars.

Barry, D. C., Cromwell, R. H., Hege, K. and Schoolman, S. A. 1981, Astrophys. J. 247, 210-221: Chromospheric Decay and the Ages of Solar Type Stars.

Bohm-Vitense, E. and Dettmann, T. 1980, Astrophys. J. 236, 560-566: The Boundary Line in the H-R Diagram for Stellar Chromospheres and the Theory of Convection.

Bonnet, R. H. and Dupree, A. K. 1981, "Solar Phenomena in Stars and Stellar Systems" (Editors) (Dordrecht: Reidel).

Book, D. L. 1980, NRL Memo. Rpt. 4408: A Mechanism for Heating the Solar Corona.

Bruner, E. C. 1978, Astrophys. J. 226, 1140-1146: Dynamics of the Solar Transition Region.

_____. 1981, Astrophys. J. 247, 317-324: OSO 8 Observational Limits to the Acoustic Coronal Heating Mechanism.

Cargill, P. J. and Priest, E. R. 1980, Solar Phys. 65, 251-269: Siphon Flows in Coronal Loops. I. Adiabatic Flow.

Chapman, R. D. 1980, (Editor), "The Universe at Ultraviolet Wavelengths", NASA CP-2171.

Chiuderi, C. and Einaudi, G. 1981, Solar Phys. 73, 97-114: The Dynamic Formation of Quasi-Static Active Region Loops.

Cox, D. P. 1981, Astrophys. J. 245, 534-551: Mechanical Heating of the Interstellar Medium. II. The Phase Properties and Structural Control.

Craig, I. J. D. and McClymont, A. N. 1981, Solar Phys. 70, 97-114: The Dynamic Formation of Quasi-Static Active Region Loops.

Durney, B. 1981, Astrophys. J. 244, 678-694: On a Model of a Slowly Rotating Convective Zone.

Fontaine, G., Villeneuve, S. and Wilson, J. 1981, Astrophys. J. 244, 550-556: On the Acoustic Flux of Sirius A.

Foukal, P. and Smart, M. 1981, Solar Phys. 69, 15-26: Propagation of Magnetically Guided Acoustic Shocks in The Solar Chromosphere.

Galeev, A. A., Rosner, R., Serio, S. and Vaiana, G. S. 1981, Astrophys. J. 243, 301-308: Dynamics of Coronal Structures-Magnetic Field Related Heating and Loop Energy Balance.

Galloway, D. J. and Weiss, N. O. 1981, Astrophys. J. 243, 945-953: Convection and Magnetic Fields in Stars.

Glencross, W. M. 1980, Astron. Astrophys. 83, 65: Plasma Flows Along Sheared Magnetic Arches within the Solar Corona.

_____. 1981, Solar Phys. 73, 67-80: Role of Plasma Flow in Determining Structure of the Chromosphere-Corona Transition Zone of the Sun.

Golub, L., Maxson, C., Rosner, R., Serio, S. and Vaiana, G. S. 1980, Astrophys. J. 238, 343: Magnetic Fields and Coronal Heating.

Golub, L., Rosner, R., Vaiana, G. S., and Weiss, N. O. 1981, Astrophys. J. 243, 309-316: Solar Magnetic Fields: The Generation of Emerging Flux.

Haisch, B. M., Linsky, J. L. and Basri, G. S. 1980, Astrophys. J. 25, 519: Outer Atmospheres of Cool Stars. IV. A Discussion of Cool Stellar Wind Models.

Hallam, K. L. and Wolff, C. L. 1981, Astrophys. J. 248, L73-76: Rotation of Dwarf Star Chromospheres in the Ultraviolet.

Hartmann, L., Dupree, A. K. and Raymond, J. C. 1981, Astrophys. J. 246, 193-202: On The Relationship Between Coronae and Mass Loss in Late-Type Stars.

Hartmann, L. and MacGregor, K. B. 1980, Astrophys. J. 242, 260: Momentum and Energy Deposition in Late-Type Stellar Atmospheres and Winds.

Hasan, S. S. and Venkatakrishman, P. 1981, Solar Phys. 73, 45-58: A Time Dependent Model for Spicule Flow.

Hinata, S. 1980, Astrophys. J. 235, 250: Electrostatic Ion-Cyclotron Heating of Solar Atmosphere.

_____. 1981, Astrophys. J. 246, 532-537: Stability of Coronal Loops Heated by Direct Current Dissipation.

Hollweg, J. V. 1981, Solar Phys. 70, 25-26: Alfven Waves in the Solar Atmosphere. II. Open and Closed Magnetic Flux Tubes.

Ionson, J. A. 1980, NASA Technical Memo 82065: Resonant Electrodynamic Heating of Stellar Coronal Loops: An LRC Circuit Analogue.

Jordan, C. 1980, Highlights of Astronomy (P. A. Wayman, Ed.) 5: Chromospheres, Coronae and Mass Loss in Solar and Late Type Stars.

Jordan, S. D. 1981, (Editor), "The Sun as a Star", NASA SP 450.

Knobloch, E. 1981, Astrophys. J. 247, L93-96: Solar Surface Magnetic Fields. A Model.

Knobloch, E. and Rosner, R. 1981, Astrophys. J. 247, 300-311: On the Spectrum of Turbulent Magnetic Fields.

Krall, K. R. and Antiochos, S. K. 1980, Astrophys. J. 242, 374: The Evolution of Active-Region Loop Plasma.

Kuperus, M., Ionson, J. and Spicer, D. 1981, Ann. Rev. Astron. Astrophys, 19, 7-40: On the Theory of Coronal Heating Mechanisms.

Lee, M. A. 1980, Astrophys. J. 240, 693: Comments on the Dissipation of Hydromagnetic Surface Waves.

Leibacher, J. W. and Stein, R. F. 1980, Highlights of Astronomy (P. A. Wayman, Ed.) 5, 581-590: Small-Scale Dissipative Processes in Stellar Atmospheres.

Lindsey, C. A. 1981, Astrophys. J. 244, 659-677: Heating of the Solar Chromosphere by Ionization Pumping.

Linsky, J. L. 1980, Ann. Rev. Astron. Astrophys. 18, 439-488: Stellar Chromospheres.

Mercier, C. and Heyvaerts, J. 1980, Solar Phys. 68, 151-176: Energy Balance in Current Sheets. From Petschek to Gravity Driven Reconnection?

Nagai, F. 1980, Solar Phys. 68, 351-380: A Model of Hot Loops Associated With Solar Flares. I. Gasdynamics in Loops.

Noci, G. 1981, Solar Phys. 69, 63-76: Siphon Flows in the Solar Corona.

Osterbrock, D. E. 1961, Astrophys. J. 134, 347: The Heating of the Solar Chromosphere, Plages, and Corona by Magnetohydrodynamic Waves.

Pallavicini, R., Golub, L., Rosner, R., Vaiana, G. S., Ayres, T. and Linsky, J. L. 1981, Astrophys. J. 248, 279-290: Relations Among Stellar X-ray Emission Observed from Einstein, Stellar Rotation and Bolometric Luminosity.

Pallavicini, R., Peres, G., Serio, S., Vaiana, G. S., Golub, L., and Rosner, R. 1981, Astrophys. J. 247, 692-706: Closed Coronal Structures. III. Comparison of Static Models With X-ray, EUV, and Radio Observations.

Parker, E. N. 1981a, Astrophys. J. 244, 631-643: The Dissipation of Inhomogeneous Magnetic Fields and the Problem of Coronae. I. Dislocation and Flattening of Flux Tubes.

_____. 1981b, Astrophys. J. 244, 644-652: The Dissipation of Inhomogeneous Magnetic Fields and the Problem of Coronae. II. The Dynamics of Dislocated Flux.

Peterson, R. C. 1981, Astrophys. J. L31-34: Circumstellar Winds in Globular Cluster Giants.

Piddington, J. H. 1981, Astrophys. J. 247, 293-299: Turbulent Diffusion of Magnetic Fields in Astrophysical Plasmas.

Poletto, G. 1980a, Astrophys. J. 240, L69: Hot Downflow Above Supergranular Boundaries.

_____. 1980b, Solar Phys. 66, 323-334: Common Origin for UV and Radio Fluctuations.

_____. 1981, Solar Phys. 73, 233-256: Mass Motions in the Transition Region.

Rabin, D. and Moore, R. L. 1980, Astrophys. J. 241, 394: Coronal Holes, the Height of the Chromosphere, and the Origin of Spicules.

Roberts, B. 1981a, Solar Phys. 69, 27-38: Wave Propagation in a Magnetically Structured Atmosphere. I. Surface Waves at a Magnetic Interface.

_____. 1981b, Solar Phys. 69, 39: Wave Propagation in a Magnetically Structured Atmosphere. II. Waves in a Magnetic Slab.

Roberts, B. and Frankenthal, S. 1980, Solar Phys. 68, 103-110: The Thermal Statics of Coronal Loops.

Sakurai, T. and Levine, R. H. 1981, Astrophys. J. 248, 817-829: Generation of Coronal Electric Currents Due to Convective Motions on the Photosphere.

Schmitz, F. and Ulmschneider, P. 1981, Astron. Astrophys. 93, 178-188: The Stellar Chromospheres of Late Typ Stars. V. Temperature Minima in the Gray LTE Approach.

Serio, S., Peres, G., Vaiana, G. S., Golub, L. and Rosner, R. 1981, Astrophys. J. 243, 288-300: Closed Coronal Structures. II. Generalized Hydrostatic Model.

Sillen, R. M. J. and Kattenberg, A. 1980, Solar Phys. 67, 47-56: A Low Beta Coronal Loop Model. I. Kink Instabilities the Beta O Limit.

Spicer, D. S. 1981a, NRL Memorandum Report 4550: Magnetic Energy Storage and Conversion in the Solar Atmosphere.

_____. 1981b, Solar Physics, 70, 149-172: Loop Models of Solar Flares--Revisions andComparisons.

Spruit, H. C. 1981a, Astron. Astrophys. 98, 155-160: Motions of Magnetic Flux Tubes in the Solar Convection Zone and Chromosphere.

_____. 1981b, Bonnet and Dupree eds., "Solar Phenomena in Stars and Stellar Systems" (Reidel), 289-300: Magnetohydrodynamics of Thin Flux Tubes.

_____. 1981c, Solar Physics, 71, 115-124: First Phase Heating and Particle Acceleration During Solar Flares by Fast Traveling Modes.

Stein, R. F. 1981, Astrophys. J. 246, 966-971: Stellar Chromospheric and Coronal Heating by Magnetohydrodynamic Waves.

Stein, R. F. and Leibacher, J. W. 1980, I.A.U. Coll. No. 51, Stellar Turbulence, eds., D. F. Gray and J. L. Linsky: (Springer, Heidelberg), 225-247: Mechanical Energy Transport.

Stencel, R. E. and Mullan, D. J. 1980, Astrophys. J. 238, 221 (Addendum 240, 718): Detection of Mass Loss in Stellar Chromospheres.

Sturrock, P. A. and Uchida, Y. 1981, Astrophys. J. 246, 331-336: Coronal Heating by Stochastic Magnetic Pumping.

Swank, P. A., White, N. E., Holt, S. S. and Becker, R. H. 1981, Astrophys. J. 246, 208-214: Two-Component X-Ray Emission from RS Canum Venaticorum Binaries.

Tavakol, R. K. and Tworkowski, A. S. 1981, Solar Phys. 71, 203-214: Redistribution of Energy by Vertical Oscillations in the Solar Atmosphere.

Ulmschneider, P., Schmitz, F., Kalkofen, W. and Bohn, H. U. 1978, Astron. Astrophys. 70, 487-500: Acoustic Waves in the Solar Atmosphere. V. On the Chromospheric Temperature Rise.

Ulmschneider, P. and Bohn, H. U. 1981, Astron. Astrophys. 99, 173-176: Comments on the Acoustic Heating of Stellar Coronae.

Vaiana, G. S. et al. 1981, Astrophys. J. 244, 163-182: Results from an Extensive Einstein Stellar Survey.

Van Tend, W. 1980a, Solar Phys. 66, 21-28: The Importance of Photospheric Magnetic Field Complexity for Coronal Energy Storage.

_____. 1980b, Solar Phys. 66, 29-38: Coronal Heating by Prominence Turbulence.

Vardavas, I. M. and Hearn, A. G. 1981, Astron. Astrophys. 98, 241-245: Models for Stellar Coronae. Comparison with Minimum Flux Corona Theory.

Vernazza, J., Avrett, E. and Loeser, R. 1981, Astrophys. J. Suppl. 45, 635.

Wallenhorst, S. G. 1980, Astrophys. J. 241, 229: Spicular Downflows and the Transition to High Mass-Loss Rates in G and K Giants.

Walter, F. M. 1981, Astrophys. J. 245, 677-681: On the Coronae of Rapidly Rotating Stars. II. A Period-Activity Relation in G Stars.

Walter, F. M. and Bowyer, S. 1981, Astrophys. J. 245, 671-676: On the Coronae of Rapidly Rotating Stars. I. The Relation Between Rotation and Coronal Activity in RS CVn Systems.

Webb, A. R. and Roberts, B. 1980a, Solar Phys. 68, 71-86: Vertical Motions in an Intense Magnetic Flux Tube. IV. Radiative Relaxation in a Uniform Medium.

_____. 1980b, Solar Phys. 68, 87-102: Vertical Motions in an Intense Magnetic Flux Tube. V. Radiative Relaxation in a Stratified Medium.
Wilson, P. R. 1980, Astrophys. J. 237, 108B: The Interaction of Acoustic Waves With Flux Tubes.
Wragg, M. A. and Priest, E. R. 1981, Solar Phys. 70, 293-314: The Temperature-Density Structure of Coronal Loops in Hydrostatic Equilibrium.
Zweibel, E. 1980, Solar Phys. 66, 305-321: Thermal Stability of a Corona Heated by Fast Mode Waves.

SOLAR ACTIVITY — THE SUN AS AN X-RAY STAR

Leon Golub

Smithsonian Astrophysical Observatory

ABSTRACT

The existence and constant activity of the Sun's outer atmosphere are now thought to be due to the continual emergence of magnetic fields from the Solar interior and the stressing of these fields at or near the surface layers of the Sun. The structure and activity of the corona are thus symptomatic of the underlying magnetic dynamo and the existence of an outer turbulent convective zone on the Sun. On this view, a sufficient condition for the existence of coronal activity on other stars would be the existence of a magnetic dynamo and an outer convective zone. However, theoretical estimates of the level of activity to be expected on other stars are extremely uncertain at this time, so that tracers of activity and their scaling relations must be sought. The theoretical relationship between magnetic fields and coronal activity can be tested in detail by Solar observations, for which the individual loop structures can be resolved. However, a number of parameters which enter into the alternative theoretical formulations remain fixed in all Solar observations. In order to determine whether these are truly parameters of the theory we need to extend our observations to nearby stars on which suitable conditions may occur.

1. Introduction

A substantial fraction of the papers presented at this conference are being devoted to the subject of how Solar observations can be used to help stellar studies. I feel it appropriate in the present contribution to address the specific question, how can stellar observations help us to understand the formation and heating of the Sun's corona? This is clearly an area which could be the subject of a meeting itself.

In the following I will select only a single well-defined topic, namely observational testing of magnetic field-related Solar coronal heating theories and discuss in some detail the ways in which stellar observations may be helpful in testing the correctness of such, theories proposed within the context of Solar coronal observations. I will then discuss some of the complications which we know to exist in the case of the Solar corona, the ways in which these complications may make interpretation of stellar data more difficult and some possibilities for simplification which may allow us to use stellar data in testing Solar-derived theories.

2. Magnetic Fields and Coronal Structure

Certainly the most important advance in our understanding of the Solar corona in the last twenty years has been the close association found between the location on the Solar surface of strong magnetic field regions and the enhanced x-ray emission above those locations. The fact that loops of hot plasma were located above active regions was known many years ago (Billings 1966). However, it has been the ability to observe the corona *on the disk* without line of sight integration effects, which has allowed us to determine the precise nature of the interaction between the magnetic fields and the coronal x-ray emitting plasma.

The connection between bipolar surface fields and coronal x-ray loops is illustrated in figure 1. This figure shows four different exposures of an active region, chosen to show the inner core loops and the larger, fainter loops connecting more widely separated portions of the active region. The magnetogram, which is coaligned and to the same scale as the x-ray images, shows that the x-ray loops do indeed connect opposite polarity areas, as expected.

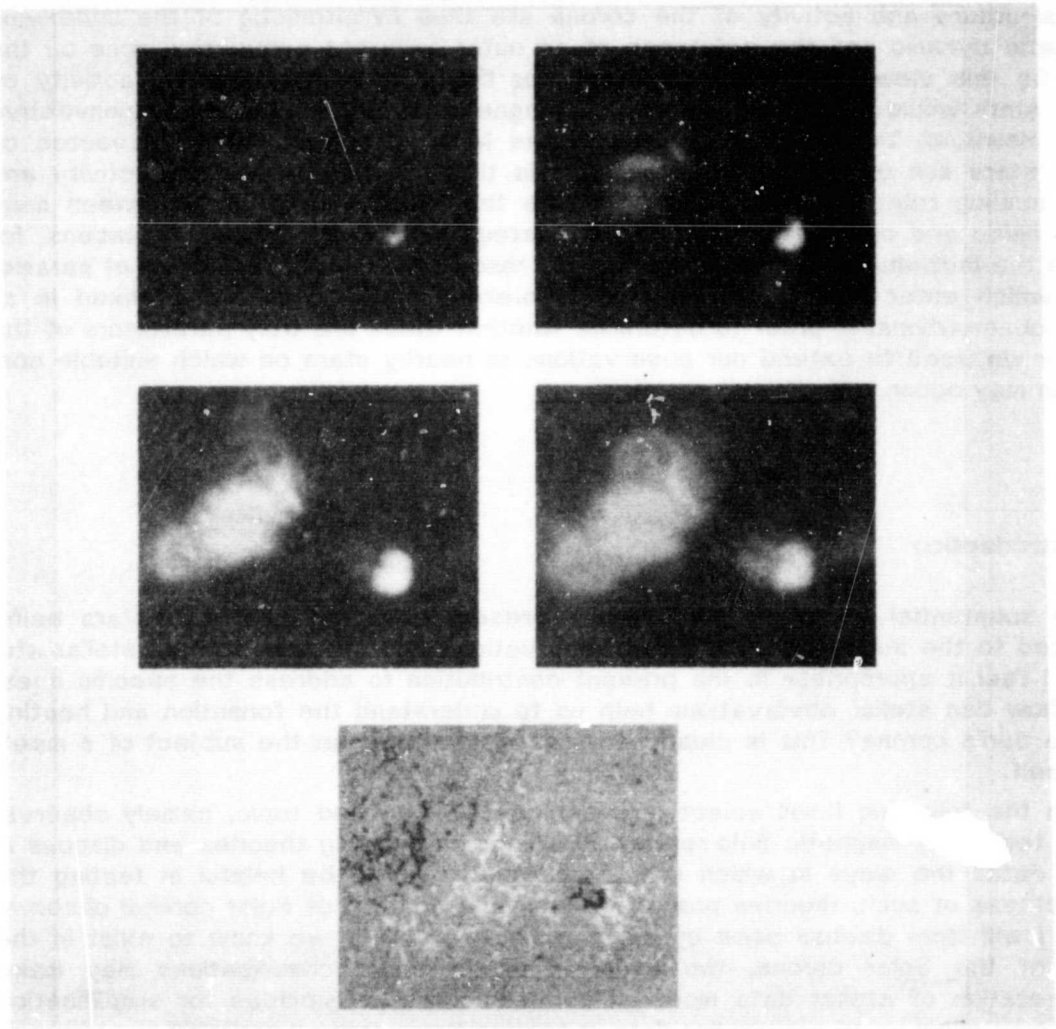

Fig. 1. Four x-ray images of an active region, showing inner core loops and larger, weaker outer loops interconnecting regions of opposite magnetic polarity,as shown by the bottom magnetogram (from Rosner et al. 1978a).

The rapid evolution and possible complexity of these coronal loops structures is shown in figure 2. The four images cover two days in the history of three active regions; one of them is large and well-developed at the start of the observing sequence, while two small regions emerge during the observation. We see that the large region develops a series of complex loops, some of which interconnect to nearby surface areas on the Sun. The smaller active regions grow rapidly and one of them flares early in its development (top right). The large range of scale sizes for coronal loops and the even larger range of surface brightness values encountered in the Solar corona is evident even from this example.

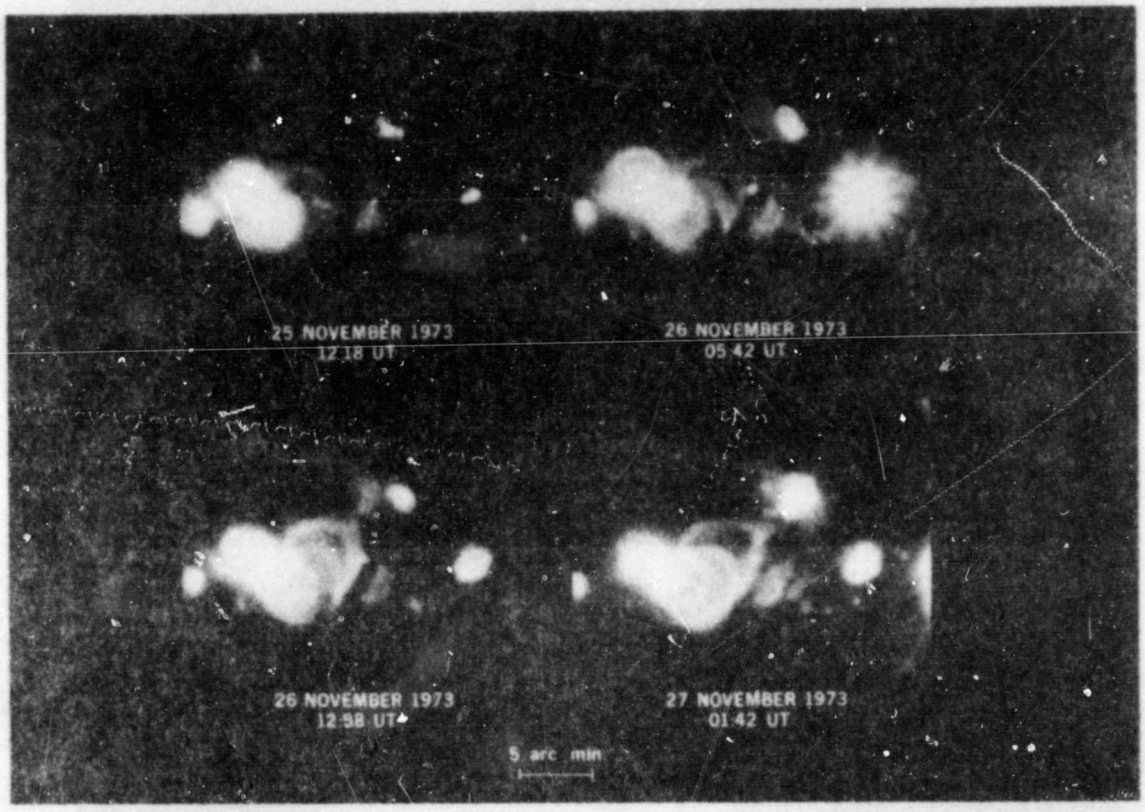

Fig. 2. Two days in the evolution of an active region and two emerging flux regions. Note the rapid and complex development of the x-ray loops, the flare in the young emerging region and the development of interconnecting loops between the regions. (Photo courtesy of G. S. Vaiana)

Figure 3 is a full disk view of the x-ray corona and illustrates most of the major (non-flare) features seen on the Sun. The bright, overexposed areas are active regions such as those shown in figures 1 and 2. The larger scale, more

diffuse emission is the evolved state of such large active regions and is often called quiet corona, although *no* part of the corona is truly quiet in x-rays. The elongated dark north-south region is a *coronal hole*. It is a large region on the surface dominated by a single magnetic polarity, so that the magnetic field becomes open to interplanetary space. Coronal holes are thus associated with high speed streams in the Solar wind, recurrent geomagnetic substorms and other terrestrial disturbances (Krieger, Timothy and Roelof 1973).

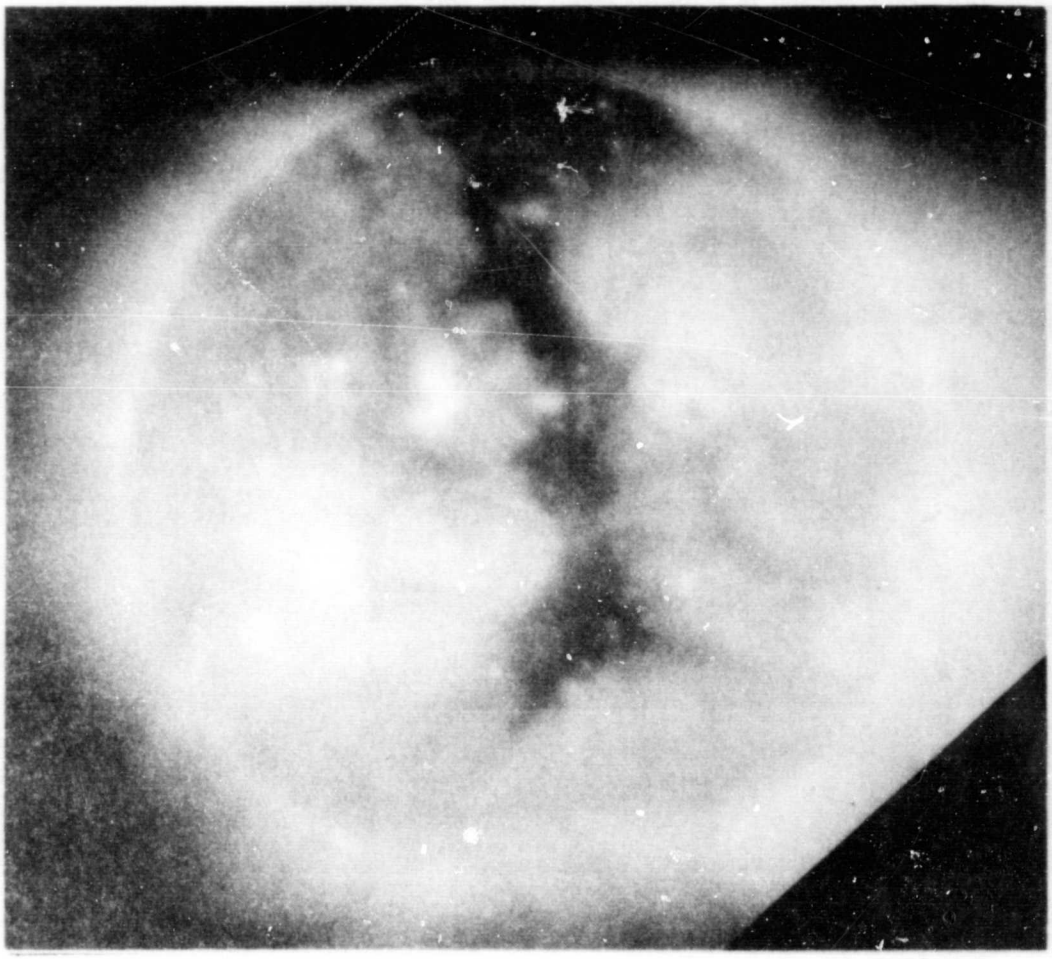

Fig. 3. X-ray image of the Solar corona, obtained from the S-054 x-ray telescope on Skylab, 1 June 1973. Most of the major non-flare features of the Solar atmosphere can be seen, including active regions, bright points, coronal holes and large-scale (quiet corona) structures. (Photo courtesy G. S. Vaiana)

The numerous small bright features throughout the corona are the so-called x-ray bright points. These are now known to be small bits of emerging magnetic flux, just as are the larger active regions (Golub *et al.* 1977). They form a continuous spectrum of scale sizes with active regions so that the distinction between them and the larger regions is somewhat arbitrary. However, the shape of the size distribution is such that the small regions account for most of the emerging magnetic flux on the Sun, except near times of maximum sunspot number. Equally surprising, there is an anticorrelation observed between the large and small regions (Golub, Davis and Krieger 1979), so that the emergence of magnetic fields on the Sun throughout the Solar cycle is more an oscillation of the *wavenumber* distribution of the emerging fields than a variation in the total quantity of flux emerging.

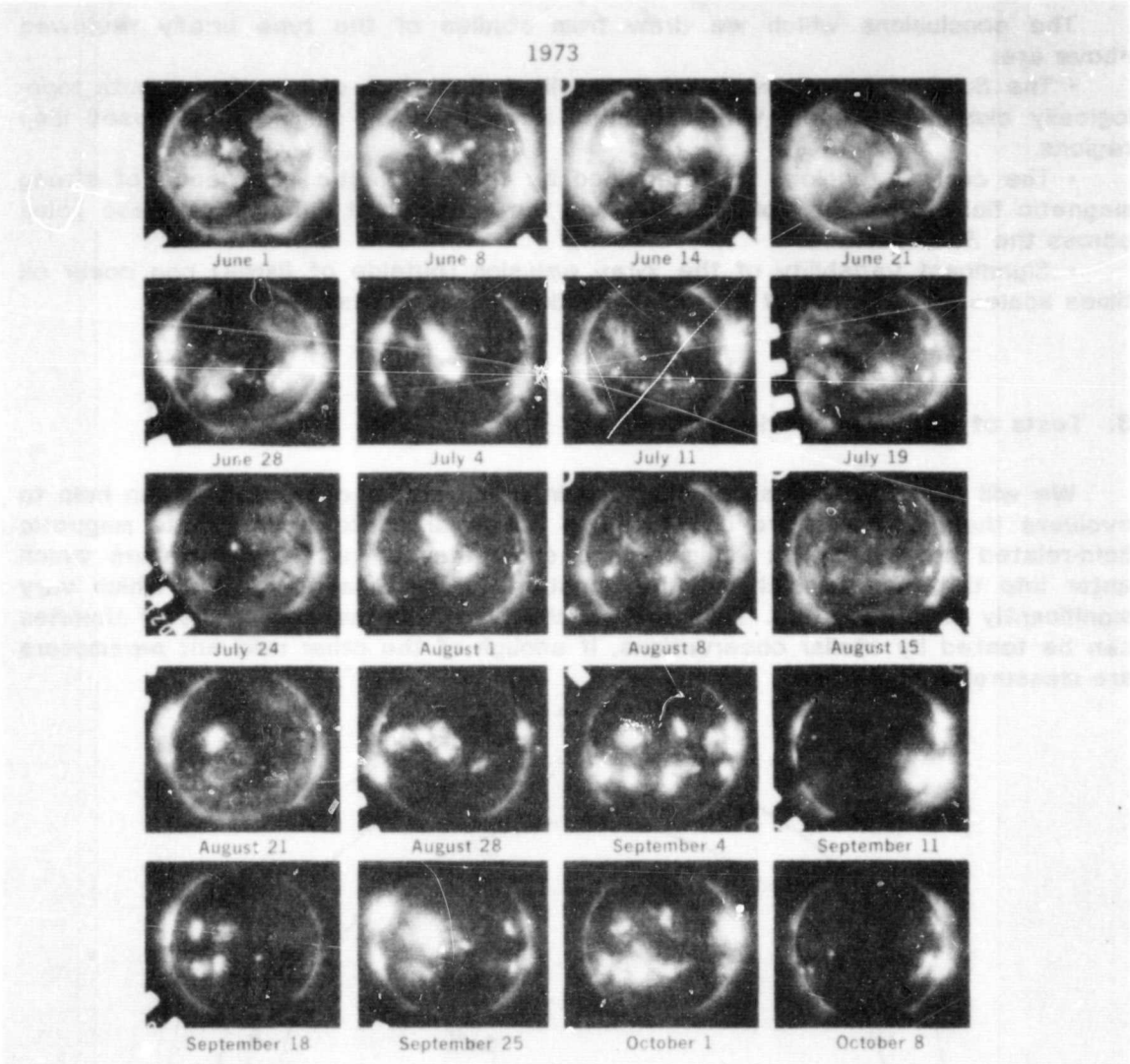

Fig. 4. Five Solar rotations of the x-ray corona as seen from Skylab. Columns are arranged to show the same quadrant on successive rotations. Note the eruption of a complex of activity in early September and the very low level of activity in the corona at 90° longitude separation.

If we ask the question, what does the typical Solar corona look like in x-rays?, the answer will depend on exactly when you look. This is illustrated clearly in figure 4, which shows five Solar rotations observed from *Skylab* image across is ~90° separated from the adjacent images. Thus each of the vertical columns show the evolution of the same Solar longitude during the five rotations. It is clear from examining these data, that the corona is highly variable, even during the relatively brief duration of the *Skylab* mission. The rapid variability is particularly evident during the fourth and fifth rotations, in which a large complex of activity emerged on one side of the Sun while there was a marked absence of activity on the other hemisphere. Thus the corona was observed to vary from a Solar maximum type to a Solar minimum type configuration during a period of only seven days.

The conclusions which we draw from studies of the type briefly reviewed above are:

- The Solar corona consists of a complicated mixture of structures, both topologically closed and open, with enhanced x-ray emission coming from closed loop regions.
- The coronal topology is determined by the stochastic emergence of strong magnetic fields from the Solar interior and the subsequent diffusion of these fields across the Solar surface.
- Significant variability of the x-ray emission (outside of flares) can occur on times scales of the order of the Solar rotation period, or less.

3. Tests of Heating Theories

We will now briefly examine the way in which stellar observations can help to evaluate theories which are developed in the Solar context. We chose magnetic field-related heating as an example and show that there are parameters which enter into the theory which may be constant for all Solar loops, but which vary significantly on other stars. Thus the possibility exists that this class of theories can be tested by stellar observations, if enough of the other relevant parameters are measurable quantities.

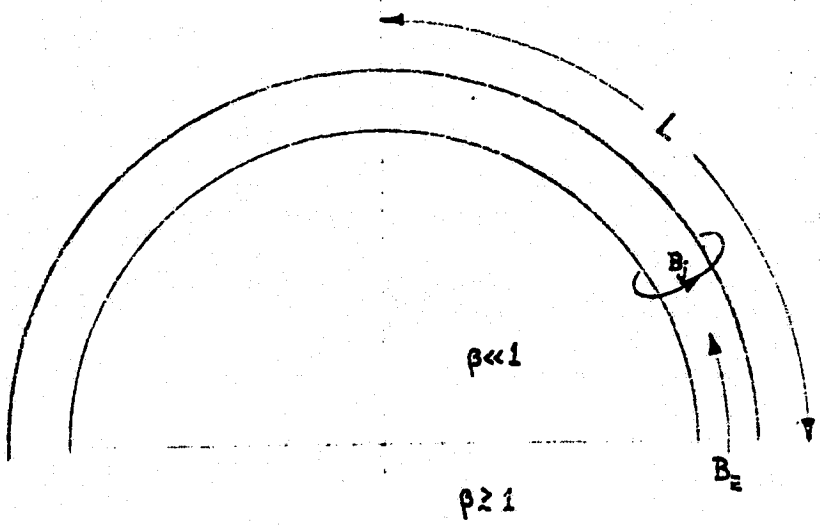

Fig. 5. Parameters of loop model.

The simplified model consists of a single loop of magnetic field, as shown in figure 5. We assume the following (see Golub *et al.* 1980 for a more detailed discussion):

- The energy necessary for confinement and heating of the plasma derives from shear at the base of the loop,
- The potential field, labelled B_z, does no heating or confinement,
- above is done by the current-related azimuthal field B_j.

The energy available for heating is

$$W_m = B_j^2 V/8\pi \tag{3.1}$$

and

$$dB_j/dt = B_z \, \partial v_\phi/\partial z \quad . \tag{3.2}$$

The energy balance in the loop is obtained by assuming that all of the energy generated in the shearing process is dissipated in the corona:

$$dW_m/dt = E_H \tag{3.3}$$

where

$$E_H = 10^5 \, p^{7/6} \, L^{-5/6} \tag{3.4}$$

is the heating function obtained by Rosner et al. (1978b) and assumed in the following to apply to the full range of loops discussed in that paper.

Combining all of the above relations, we obtain the following general relation, which does not depend on a particular heating mechanism provided that eq. 3.3 holds:

$$p = 2.6 \, (B_j \, B_z \, v_\phi)^{6/7} \, L^{-1/7} \, . \tag{3.5}$$

For the Solar case, eq. 3.5 involves some quantities which are measurable, namely the coronal plasma pressure p, the loop length L and the longitudinal magnetic field B_z at the base of the corona, i.e., in the upper chromosphere. The quantity v_ϕ is the "effective twisting velocity" (Tucker 1973) and may not be directly observable; however, it should be related to the fluid velocity at the $\beta \sim 1$ level.

The quantity B_j is not at the present time directly measurable in the corona and theory does not provide definitive limits on the range of values which it can assume. In Golub *et al.* 1980 we assumed arbitrarily that B_j is a constant fraction of the longitudinal field B_z for all loops:

$$B_j = \alpha \, B_z \quad . \tag{3.6}$$

Subsequently, Galeev *et al.* (1981) showed that, for a broad class of heating mechanisms the azimuthal field is related to the coronal plasma pressure:

$$B_j = 8.8 \, p^{1/4} \quad . \tag{3.7}$$

The latter relation leads to

$$p = 63 \, B_z^{3/2} \, L^{-1/4} \, v_\phi^{6/7} \quad . \tag{3.8}$$

This equation may be integrated over an entire bipolar region to yield an integral relation among observable quantities:

$$U_T = 42\ \Phi_T^{3/2}\ L^{-1/4}\ v_\phi^{6/7}, \qquad (3.9)$$

where the quantity U_T is the total thermal energy content in the corona:

$$U_T = \int \epsilon\ dV = \int 3p/2\ dV \quad . \qquad (3.10)$$

We note that the relation between U_T and the total magnetic flux Φ_T is dominated by the trivial dependence between area and volume, since the respective integrations involved those quantities. However, the fact that the loop pressure p and the longitudinal magnetic field B_z in eq 3.8 are related by the 3/2 power is specific to the heating mechanism assumed and does contain true physical content. Comparison of eq. 3.8 with the previous relation 3.5 is sufficient to demonstrate this point.

It is at present not possible to test the question whether v_ϕ is truly a parameter in coronal heating. Even if it were *in principle* possible to observe the direct interaction between the fluid flows which provide the energy for heating and their interaction with the magnetic field in producing a shear, it appears at the present time that such processes occur at a spatial scale which is below the best resolution limit achieved to date in Solar observations. Moreover, it is likely that the process of interest occurs at a depth in the Solar atmosphere which is not directly observable by any known means.

Thus, we are forced to consider other means of testing the model. The obvious method, which now seems to be within reach, is to observe other Solar-type stars with coronal emission and for which the relevant parameter, in this case v_ϕ, is very different from the Solar value. The attempt appears feasible, since the quantity U_T has now been measured on a large number of stars of spectral type dG through dM (Vaiana *et al.* 1981; Pallavicini *et al.*, this volume) and it now appears that Φ_T may be measureable on at least some of these stars (see contributions in these proceedings). At the same time, the level of surface turbulence in late-type stars varies by an order of magnitude, which may be enough to decide the question.

4. Are Attempts at Modelling Unresolved Coronae Realistic?

(i) The Division into "Active" vs. "Quiet" Regions

When we consider the extremely complicated mixture of loop structures which are formed in the Solar corona, it seems reasonable to ask whether unresolved stellar observations which necessarily average over the entire ensemble of structures in the stellar atmosphere can really be of any use in explicating the properties of the Solar corona. In the following, we will examine some of the limited information available and assess the feasibility of such work. In particular, we will find that within certain limits there is still a good possibility that unresolved stellar observations can answer some Solar questions and that continued close interaction between the two fields will be fruitful.

The usual way in which structure is introduced into unresolved observations of the emission in a particular line or radiative passband is to arbitrarily assign the total emission to two atmospheric components, "active" and "quiet" (see, e.g. Giampapa 1980). The question whether such a division is reasonable in the Solar atmo-

sphere has specifically been examined by Cook *et al.* (1980), in the wavelength region 1175-2100 A. They used Skylab data from the S-082B instrument and calrocket data, to cover the period 1973-79. Thus the study examined the usefulness of the active/quiet division both at a single point in the cycle and as a function of the cycle.

For our purposes, the major result of the study was that the integrated full disk flux can reasonably well be represented by:

$$F_\lambda \cong \pi \langle I_Q \rangle_{disk} [\, f C_\lambda + (1-f)] \quad , \qquad (4.1)$$

where C_λ is a wavelength-dependent contrast factor I_{active}/I_{quiet} and f is the fraction of the disk occupied by plage. As a byproduct of the investigation, Cook *et al.* used data from Sheeley (1967) to relate the fraction f to another activity indicator, the Zurich relative sunspot number R_z:

$$f \cong 6.3 \times 10^{-4} R_z \quad . \qquad (4.2)$$

A study of more direct relevance for XUV and x-ray observations was performed by Pallavicini *et al.* (1981), using Skylab S-054 and S-055 x-ray and XUV data. A typical set of XUV rasters of an active region is shown in figure 6, which

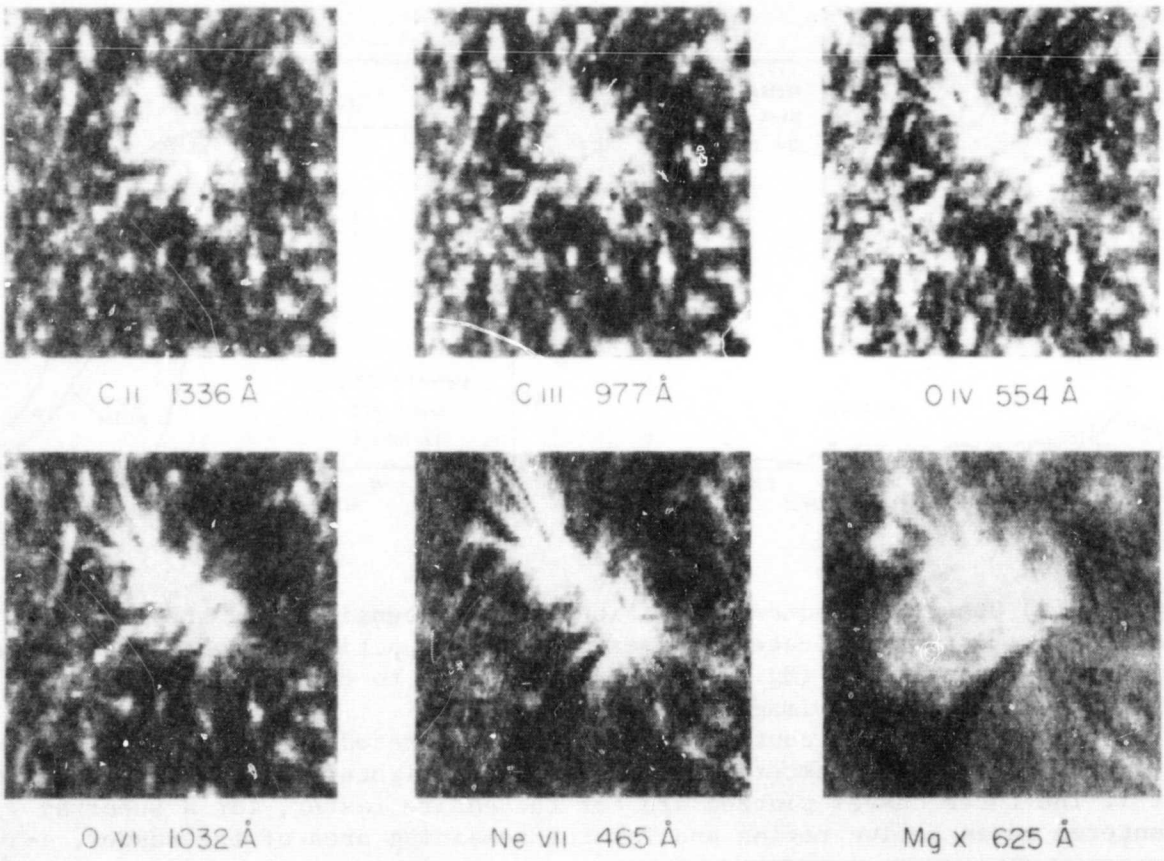

Fig. 6. Spectroheliograms of a Solar active region in XUV lines observed by the HCO S-055 experiment on Skylab. (from Pallavicini et al. 1981)

illustrates the appearance of a plage region in lines ranging in temperature from chromospheric (C II) to coronal (Mg X); the x-ray appearance of such regions has been illustrated in figures 1-3 above. In this study we examined the question whether there exist intensity values of coronal emission, such as x-rays or Mg X, which can be used as cuts to separate active vs. quiet areas in the underlying transition region and chromosphere. Such a procedure is clearly a necessary step in attempting to interpret unresolved stellar observations and the success of this effort is necessary if we are to proceed with the analysis of the stellar data.

The findings of the study are illustrated in figure 7; we have chosen the line of O VI at λ1032, but the result is similar for the other lines as well. We find that the very high contrast in the corona between active and quiet regions on the Solar surface is translated down throughout the entire transition region and into the chromosphere. That is, a spatial mask made by applying an intensity cut to a coronal emission line serves nearly as well in defining a spatial mask for the lower temperature emission. The procedure allows us to not only divide the XUV integrated emission into active and quiet contributions, but also determines automatically the appropriate value of the intensity value to be used as a cut in each line and the values of the ratio I_{active}/I_{quiet}.

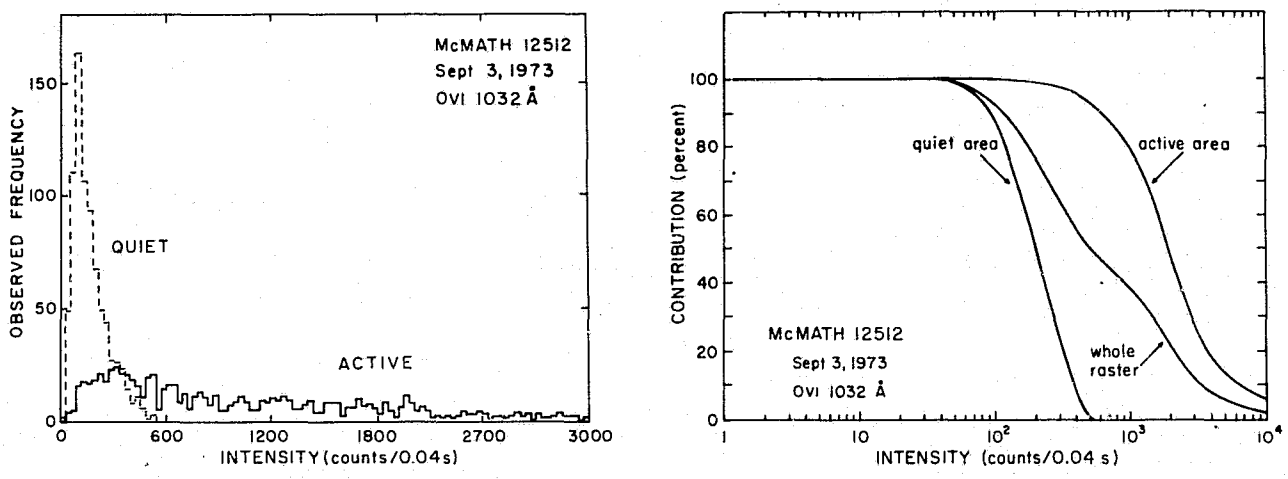

Fig. 7. (left) Observed frequency distribution of intensities in the line of O VI at 1032 A. "Active indicates an area centered on active region structures as seen in a coronal line (Mg X) and "quiet" refers to the remaining picture elements in the raster image.

(right) Percentage contribution to the integrated intensity over selected areas of the XUV raster, from data points brighter than I as a function of I. The three curves plotted are for the entire raster, for a subarray centered on an active region and for the remaining area of the raster.

(from Pallavicini et al. 1981)

(ii) Atmospheric Components and Their Variation Throughout the Activity Cycle

We have so far examined the question, whether coronal emission from unresolved observations can be represented reasonably well by two-component models. More precisely, we are asking whether it is possible by unresolved observations to determine the values of parameters which are of interest in testing Solar-derived theories for the formation and heating of the corona. To this point it appears that the approach is a promising one if we are seeking to differentiate a particular type of Solar feature, such as a large active region, from the weaker and more diffuse large scale structure generally referred to as "quiet corona".

Unfortunately, we must now face another complication. The Solar atmosphere does not form itself neatly into just two types of structures. As pointed out in §2, there are many different types of magnetic structures in the corona, both large and small, open and closed and with substantially different temperatures, densities and evolutionary timescales. A skeleton outline of the range of different atmospheric constituents found on the Sun is shown in Table 1:

Table 1

Major Components of the Solar Atmospheric Emission

Feature	Size (10^9cm)	Lifetime (sec)	Magn. Φ (Mx)	Distrib.	Flux Contrib. (%) at min	at max
XBP	1	$<3\times10^4$	$<10^{19}$	Uniform	70	20
ER	2-5	$<10^5$	$<10^{20}$	Peaked	20	20
AR	10	$>10^5$	$>10^{20}$	Peaked	10	40
AR Compl.	20-50	$>10^7$	$>10^{22}$	Peaked	0	20

This table lists the atmospheric components which are important in terms of the amount of magnetic flux which they bring to the Solar surface. We note that the relevant quantity is the *flux per unit time*, denoted above as "flux contribution". If we consider the effect on coronal structure of the emerged flux, then it is necessary to consider the lifetimes of the various emerging features; thus, the longterm structure of the large scale corona is controlled by the largest active regions, even though they account for only a small percentage of the total emerging magnetic flux.

- During the ascending and descending phases of the Solar cycle, a single loop size/single temperature model is not adequate to characterize the emission properties of the corona, except within the limits noted above.

- Even at Solar maximum and minimum, there is significant short term variability, on time scales from seconds to days (see figure 4).

In order to produce an overall representation of coronal emission in terms of the various known atmospheric components, we need to consider the evolutionary histories of the different types of emerging field regions, including their lifetimes, temperatures, surface distribution patterns and their interaction with nearby atmospheric components. In addition, it is necessary to consider the Solar cycle variation of all of these quantities, since the relative importance of, e.g., large vs. small active regions is known to be a strong function of phase in the cycle. Moreover, the fraction of the, Solar surface area covered by coronal holes is strongly dependent on the cycle, as is the scale size of the quiet corona since this depends on the properties of the active regions which are feeding the large scale structure.

A first rough attempt at modelling all of these complications is shown in Table 2. We have listed not only the emerging field regions from Table 1, but also the structures into which they evolve, namely large scale structure from active regions and complexes of activity, coronal holes from large active regions, and XBP remnants representing the equivalent of the large scale structure at Solar minimum (fig. 8).

Table 2

Properties of Atmospheric Components vs. Solar Cycle

Feature	Luminosity Contrib.(%) at min	at max	Phase wrt Cycle	T (10^6K)	$\int n_e^2 dl$ (cm^{-5})
XBP	2	0	180°	1.8	10^{28}
ER	2	1	none	2.0	$2X10^{28}$
AR	5	40	0°	2.4	$2X10^{29}$
AR Comp.	0	30	0°	2.4-4.0	10^{30}
XBP Remn.	20	3	180°	1.6	$2X10^{27}$
LSS	70	25	0°	1.8	$3X10^{27}$
CH	1	1	±90°	1.3	$3X10^{26}$

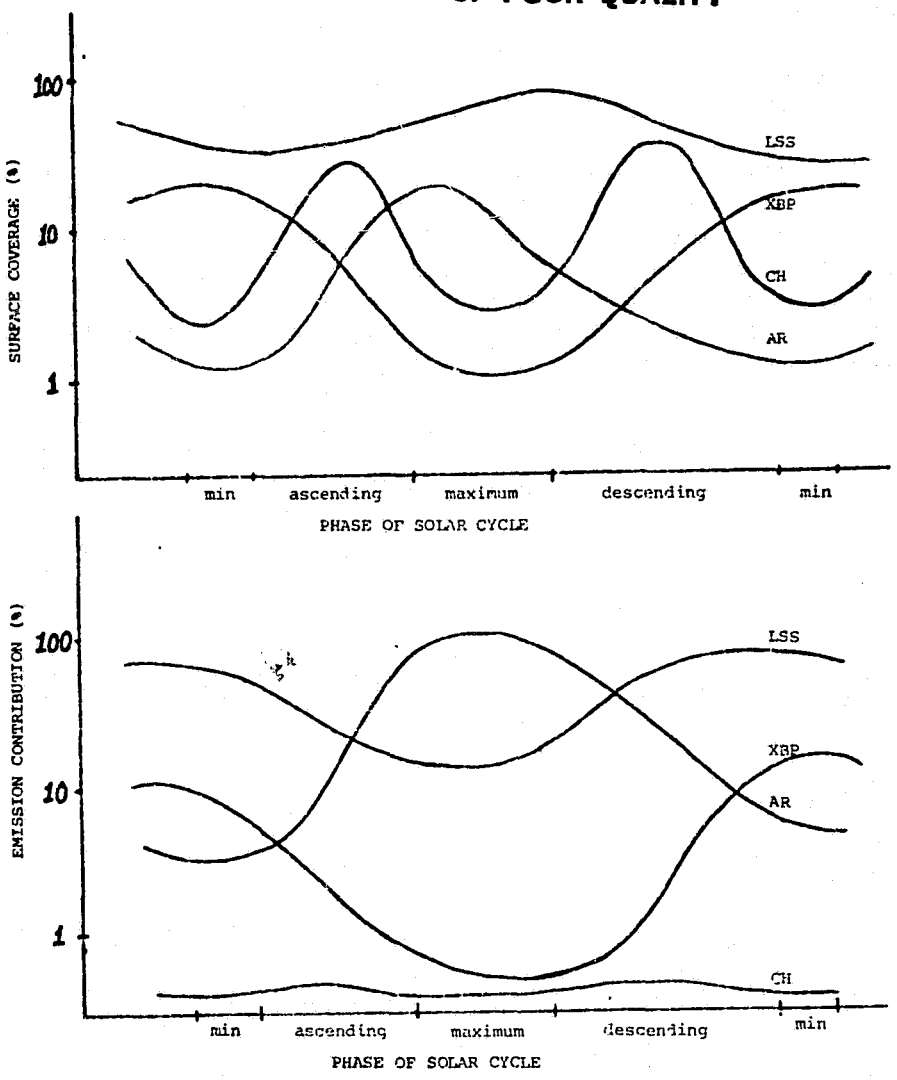

Fig. 8. Solar cycle variations of the major components of the Solar corona. Top curves show the variation throughout a cycle of the percentage area coverage for the largest atmospheric features.
Bottom curves indicate the relative percentage contribution to the total integrated Solar coronal emission for the features indicated above and their evolved forms, where applicable.

From examination of this "composite corona" model, we may draw the following preliminary conclusions:

• The *average* Solar corona is dominated by a single type of structure approximately 50% of the time.

At Solar maximum, we may characterize the entire coronal emission by the properties of large active regions, with $T \sim 3X10^6$ K and emission measure $\sim 10^{50.5}$.

At times of Solar minimum, the corona is characterized by $T \sim 1.8X10^6$ and $EM \sim 10^{49}$.

5. Conclusions

In answer to the question we have posed, namely are attempts at modelling unresolved coronae realistic?, the answer with caution seems to be, yes there is hope. This implies that there is also hope for the larger question, whether stellar observations can be of use in helping us to understand the physical processes involved in the formation and heating of the Solar corona. The parameters involved in testing Solar coronal theories - such as magnetic flux, X-ray and XUV emission, rotation rates, optical, EUV and x-ray spectral features, surface turbulent velocities - *can* be measured, at least on some stars. It is therefore not only legitimate, but imperative, that Solar physics make use of the vast new opportunities now opening in the stellar area as a means of advancing our understanding of the Sun's outer atmosphere.

This work was supported by NASA under grant NASW-112.

6. References

Billings, D. E. 1966, "A Guide to the Solar Corona", Academic Press, New York

Cook, J.W., Brueckner, G.E. and Van Hoosier, M.E. 1980, J.G.R. 85, 2257.

Galeev, A. A., Rosner, R., Serio, S. and Vaiana, G. S. 1981 *Ap. J.* **243**, 288.

Giampapa, M. S. 1980, Ph. D. Thesis, U. of Arizona, Tucson.

Golub, L., Davis, J. M. and Krieger, A. S. 1979, *Ap. J. (Letters)* **229**, L145.

Golub, L., Harvey, J. W., Krieger, A. S. and Vaiana, G. S. 1977 *Sol. Phys.* **53**, 111.

Golub, L., Maxson, C. W., Rosner, R., Serio, S. and Vaiana, G. S. 1980 *Ap. J.* **238**, 343.

Krieger, A. S., Timothy, A. F. and Roelof, E. C. 1973 *Sol. Phys.* **29**, 505.

Pallavicini, R., Peres, G., Serio, S., Vaiana, G. S., Golub, L. and Rosner, R. 1981, *Ap. J.*, **247**, 692.

Rosner, R., Golub, L., Coppi, B. and Vaiana, G. S. 1978a, *Ap. J.*, **222**, 317.

Rosner, R., Tucker, W. H. and Vaiana, G. S. 1978b, *Ap. J.*, **220**, 643.

Sheeley, N. R., Jr. 1967 *Ap. J.*, **147**, 1106.

Tucker, W. H. 1973 *Ap. J.*,**186**, 285.

Vaiana, G. S., *et al.* 1981, *Ap. J.*, **245**, 163.

DYNAMIC PHENOMENA IN CORONAL FLUX TUBES

J.T. Mariska and J.P. Boris

E.O. Hulburt Center for Space Research and
Laboratory for Computational Physics
Naval Research Laboratory, Washington, D.C. 20375

INTRODUCTION

One of the major unsolved problems in the study of stellar atmospheres is the determination of specific physical mechanisms, geometries, and magnetic structures by which coronae are maintained. Ultraviolet and soft X-ray components observed in the radiative output of cool stars and the sun require counter-entropic temperature gradients for their explanation. The existence of a hot corona has long been recognized as resulting from mechanical or fluid dynamic effects and more recently the fact that the magnetic field plays an important role in this heating has come to be accepted. Thus magnetohydrodynamic energy release associated with the emergence of magnetic flux through the chromosphere and its dynamic readjustment in the corona are major counter-entropic phenomena which must be considered as primary candidates for coronal heating.

The medium in which these phenomena take place, a hot, magnetically-confined low-pressure plasma, has itself numerous non-intuitive properties which must be untangled and understood separately before observations of transient and spatially localized heating phenomena in this medium can be interpreted. It is the purpose of this paper to discuss results obtained using the recently-developed Dynamic Flux Tube Model to simulate and quantify some of these coronal plasma properties in magnetic flux tube configurations representing the chromospheric-coronal transition region, complete coronal loops, plasma jets, and flares. Results of these studies show that the strong dynamic interplay between thermal conduction and radiation gives the plasma a stressed, non-local behavior which makes non-monotonic and shocked profiles difficult to achieve. Nonlinear condensations can and do appear but their acceleration to sonic velocity and higher indicates magnetic forces. Numerical simulations show acceleration and flows generated by local heating to be a highly inefficient way of generating kinetic energy because enthalpy fluxes at flow rates of 5 - 10 km s^{-1} in coronal plasma are large enough to redirect energy being deposited at a rate adequate to maintain the corona.

DISCUSSION

To perform these calculations a new computational model has been developed to describe convective, wave, and heat transfer phenomena in the outer layers of the solar atmosphere. In this model a locally axisymmetric magnetic flux tube is represented by the complete nonlinear MHD equations fully resolved in the axial direction but integrated over an assumed but time varying similarity-like radial profile. To facilitate comparison with observations, a time-dependent description of the nonequilibrium ionization of oxygen has been included which is calculated along with the evolving MHD flow. Special techniques have been devised to permit accurate resolution of the dynamically important phenomena which take place in the thin transition region. Many aspects of the model have been described in previous publications (Oran, Mariska, and Boris 1982; Mariska et al. 1982). Here we concentrate on two aspects which have stimulated the most questions: our treatment of the chromosphere and our resolution of the transition region.

Although the coronal plasma has properties which make some aspects of its behavior difficult to understand, it is an open book compared to the complex interactions and processes in the chromosphere. Because of these complexities, there has been a natural tendency to solve problems which treat the transition region as a lower boundary to the corona (e.g., Krall and Antiochos 1980). We have found, time and again, that the chromosphere responds dynamically to changes in the coronal heat flux and pressure in a way which cannot be modeled as a boundary condition. The chromosphere behaves much like a loaded spring with the overlying layers providing most of the loading. Thus, changes in the pressure, such as might be caused by heating rate changes in the overlying layers, will cause the chromosphere and overlying transition region to rise and fall in response. This coupled system response requires inclusion of at least two scale heights of chromosphere within the computational region. A chromospheric region is also required in order to calculate evaporation of chromospheric material into the corona or condensation of coronal material back into the chromosphere.

Our computational treatment of the chromosphere avoids most of the usual radiation transport, opacity, and atomic physics difficulties by assuming the fluid to be an extension of the coronal plasma to higher density without large energy input from below or correspondingly large energy loss from radiation and transport. When the material exceeds 10^4 K, it radiates the excess heat away according to the Cox-Tucker-Raymond optically thin plasma law. This radiation includes L-alpha components from $1 - 3 \times 10^4$ K but this loss is zero when the plasma temperature drops below 10^4 K. The "chromospheric material" in this approach moves, evaporates, condenses, compresses, etc. in a realistic way to properly support the transition region and corona. When compressed to temperatures above 10^4 K, the dense chromosphere radiates the excess energy away. Thus, our chromosphere is essentially

isothermal and we do not have to be concerned with large energy depositions from below and corresponding large radiative losses from the chromosphere.

A number of calculations have been performed looking at the steady state transition region structure as a function of improving computational resolution. These calculations were designed to address two questions: the existence of a steady state and the necessary spatial grid size to resolve the transition region accurately. Another paper at this conference (Rosner 1982) has addressed the issue of whether or not the equilibrium transition region is hydrodynamically stable or unstable. The conclusion there, as in our papers, is that the combined corona-transition region-chromosphere system is stable. Reports of instability in earlier works are traced to improper boundary conditions and/or application of functionally unstable heating functions. This means that the observed fluctuations in the transition region plasma have to be attributed to external driving effects like changes in the heating rate or magnetic flux tube geometry. They appear not to result from any inherent turbulent tendency in the transition region structure itself. The uniformity and repeatability of laser-plasma experiments, where the thin ablation layer is closely analogous to the transition region, supports this theoretical conclusion indirectly.

In the transition region the temperature and hence the electron thermal conductivity decrease rapidly requiring very short temperature gradient scale lengths to maintain the downward directed heat flux. At the typical quiet sun coronal pressures of about 0.2 dynes cm^{-2}, temperature scale heights $h < 1$ km are required in the $1 - 5 \times 10^4$ K region. An important part of the downward directed heat flux high in the corona goes into the dense but thin transition region plasma at temperatures between $\sim 10^4$ K and $\sim 3 \times 10^4$ K which radiates L-alpha. Thus, our model automatically allows for this significant energy leakage from the corona.

The leakage also means the lower transition region is constantly "stressed" or connected by a significant heat flux well down into material normally considered chromospheric. The profiles of temperature, density, and hence radiation output in the hotter $3 - 15 \times 10^4$ K plasma just above are correspondingly altered to steeper gradients which transport the additional downward directed heat flux that is required to feed L-alpha. This already moving heat flux connects separated regions in the transition region and lower corona by a communication mechanism, electron thermal conduction, which moves faster than sound and therefore tends to stabilize purely fluid effects. The presence of steeper gradients also means that other models may underestimate the resolution required for convergence.

A number of calculations were performed of the same physical conditions for a typical quiet sun loop varying the spatial resolution from 20 km down to 1 km. While the structure of the low temperature transition region clearly reflects the resolution changes, the total

radiated power from the whole layer ~1 - ~5 x 10^4 K was remarkably insensitive (~10 - 20% variations) to whether the temperature varies by a factor of two per computational cell or changes by only 10% per cell (Mariska et al. 1982).

When an excess of downward heat flux beyond that needed for the L-alpha radiation readjustment is supplied, the temperature rises in an energy conserving way until the heat flux to lower layers plus the increased radiation from higher temperatures can handle the increased input. This channeling of heat flux to lower layers and increased radiation in the vicinity of our L-alpha peak seems to be governed by integral conservation constraints of mass, momentum, and energy flow and hence is very insensitive to the local resolution. The success of the method with 5 - 10 km resolution can be traced to this relatively fortunate algorithm based insensitivity.

Several misconceptions exist in the literature concerning the systematic flow of plasma from one end of a coronal flux-tube to the other (e.g., Cargill and Priest 1980). Therefore, we have performed a number of detailed simulations to study these issues. We find that a pressure difference along the flux tube from the transition region at one end to the transition region at the other cannot be sustained by the complete chromosphere-corona-chromosphere system. The hot corona in a low-lying loop effectively equalizes the pressure when a continual source of coronal heat is present. Thus, the major flow is an expansion of the chromosphere at the high pressure end of the loop and a corresponding compression at the low pressure end until the two pressures have essentially equalized. The transition regions and corona readjust quickly and smoothly to follow the damped acoustic oscillations of the two chromospheres.

In the steady-state which eventually ensues (with or without systematic flow) there can be no net pressure difference without a corresponding acceleration of fluid from one end of the loop to the other. Since there is no net momentum increase in the overall system, the pressure difference at a given altitude can only arise from masses of overlying material. Since the coronal density is very low, the transition region pressures are essentially equal.

We do not see supersonic flows over the top of the loop at any time during these calculations, nor have we been able to generate standing shocks as postulated in the literature. The usual models for flow in closed loops generally also neglect the smoothing, stabilizing effects of thermal conduction. We have found, however, that systematic flows result quite naturally from asymmetric coronal heating. In general the flow direction is away from regions of excess heat deposition and in such a direction as to equalize radiative losses from the two transition regions.

These flows are saturated in the sense that the flow is as fast as it can be without actually over balancing the energy distribution in the opposite direction to the nonphysical case where more energy is being dissipated on the side of the loop farthest from the heat source. Once the asymmetry becomes appreciable the velocity saturates at about 5 km s^{-1}. This is the velocity necessary to redistribute the energy evenly via the enthalpy flux.

CONCLUSIONS

The work summarized here for the cool stars meeting includes as well the efforts of our colleagues D. Book, C.-C. Cheng, G.A. Doschek, J. Karpen, E. Oran and T. Young. From these investigations, referenced below, the following conclusions, in the form of declarative sentences arose.

- The nonlinear evolution of the condensational instability leads in the presence of volumetric heating to a two-phase state in which a cool, dense plasma is surrounded by a hot, tenuous plasma.
- Once formed, these condensations will last a long time. In fact, such phenomena are observed.
- Once formed, a condensation may be accelerated by forces in the plasma such as those arising from gravity, differential heating, or magnetic fields.
- Shocks generated by transition region mass ejections are a possible coronal heating mechanism and these masses may be a possible source of coronal mass.
- The transition region is a dynamically stable structure which resembles the state resulting from the nonlinear evolution of the condensational instability.
- The thin laminar structure of the transition region is insensitive to changes in the heating function.
- The heating and cooling of small loops results in relative ionic abundances which can differ substantially from equilibrium values.
- Systematic flows in coronal flux tubes result from asymmetric heating.
- Doppler velocity measurements of downflows in the network suggest heating is concentrated elsewhere.
- Systematic flows can exist without substantial chromospheric pressure differences.

- Dynamic chromospheric-coronal coupling is required for meaningful calculations of dynamic phenomena in coronal flux tubes.

REFERENCES

Cargill, P.J., and Priest, E.R. 1980, Solar Phys., 65, 251.

Krall, K.R., and Antiochos, S.K. 1980, Ap. J., 242, 374.

Mariska, J.T., Boris, J.P., Oran, E.S., Young, T.R., and Doschek, G.A. 1982, Ap. J., in press.

Oran, E.S., Mariska, J.T., and Boris, J.P. 1982, Ap. J., in press.

Rosner, R. 1982, these proceedings.

D6

IS ENERGY CONSERVED AT THE FOOT OF THE SOLAR CHROMOSPHERE?

Wolfgang Kalkofen

Harvard-Smithsonian Center for Astrophysics

ABSTRACT

Current empirical models of the solar atmosphere have kinetic temperatures that are too low at the temperature minimum to balance radiative heating and cooling. If there is additional energy input from the dissipation of hydrodynamic waves the apparent imbalance is aggravated.

It is suggested that the problem lies in the assumption of a static upper photosphere. It is proposed that the mechanical waves, which further out cause the chromospheric temperature rise, traverse the temperature minimum region with large amplitude and produce the apparent non-conservation of energy as well as other difficulties of the empirical models through non-linear, time-dependent effects.

I. INTRODUCTION

Most of the non-radiative energy that heats the solar chromosphere and corona is dissipated at the base of the chromosphere. Thus the radiation emitted from these layers plays a crucial role in empirical estimates of the energy supplied to the medium and places tight constraints on any theory of the generation of non-thermal energy in the hydrogen convection zone. The structure of the atmosphere at the temperature minimum and in the low chromosphere is therefore well studied and several empirical models have been constructed. But, instead of agreeing with one another within the uncertainties of the observations, these models differ from one another systematically, depending on the observed spectral feature on which the model is based; and they have in common that energy appears not to be conserved. In addition, the limb darkening of radiation originating in the temperature minimum region is steeper than the models predict. This paper suggests that these problems may be related and it ascribes them to the use of static models; time-dependent models are proposed as the solution. Section II describes the inconsistencies of the empirical models with each other, with the energy conservation law in a static atmosphere, and with the observed limb darkening; Section III discusses Ayres' proposal to solve the energy problem and Section IV, the wave model; Section V draws some conclusions.

II. STATEMENT OF THE PROBLEM

There are three unresolved problems associated with the empirical temperature structure of the transition region between photosphere and chromosphere:

1) The kinetic temperature at the foot of the chromosphere in semi-empirical models of the quiet sun (Gingerich et al. 1971, hereafter HSRA; Vernazza et al. 1976, hereafter VAL) is too low to conserve energy in radiative equilibrium (Avrett 1981; Ayres 1981). Because of the low temperature, less radiation is emitted than absorbed; if any mechanical energy dissipation is admitted, the difficulties are aggravated since the imbalance of heating over cooling is increased.

2) The minimum temperature obtained from the analysis of different spectral features shows a systematic trend with wavelength: The infra-red continuum near 0.1mm yields the low temperature of 4170K of the HSRA, which agrees with the value of 4150K of the VAL model, obtained from the same IR continuum and from the Si continuum near 0.15μm. The lines of singly ionized Ca (Shine et al. 1975) and Mg (Ayres and Linsky 1976) require higher temperatures for the part of the lines (K1 and k1, resp.) that is formed in the temperature minimum region; for the Ca II line at 3934A the minimum temperature is 4450K, and for the Mg II line at the shorter wavelength of 2796A, it has the higher value of 4500K.

3) The limb brightening observed at 1400A of continuum radiation originating in the layers on the chromospheric side of the temperature minimum as well as the limb darkening observed at 1664A of radiation from the photospheric side of the temperature minimum (Samain 1979) are both steeper than the center-to-limb variation calculated from present models (Vernazza et al. 1981).

III. AYRES' BIFURCATED SOLAR MODEL

The most important source of opacity at the temperature minimum is the H^- ion. At the kinetic temperatures of the empirical models, heating due to the absorption of radiation by H^- exceeds cooling due to photorecombination. Since the medium is optically thin, with the optical depth at 5000A between 10^{-4} and 10^{-3}, the bound-free heating rate per H^- ion due to the absorption of photospheric radiation is fixed; but the corresponding cooling rate at 4000K, e.g., depends on temperature as $T^{4.6}$ (Kalkofen and Ulmschneider 1979). Therefore, with increasing temperature, the H^- cooling rate increases rapidly. Energy balance by H^- alone can then be achieved at the much higher temperature of 4900K (Ayres 1981).

In the theoretical model of Kurucz (1974), energy balance at an optical depth that corresponds to the location of the temperature minimum in the empirical models is found with the much lower gas temperature of 4300K. In this radiative equilibrium model, the deficient cooling by H^- is compensated by numerous metal lines, which are assumed to be formed in local thermodynamic

equilibrium (LTE).

Ayres has criticized the LTE treatment by Kurucz, pointing out that the local net heating rate in a particular transition which in LTE is proportional to J-B, where J and B are the integrated mean intensity and Planck function, is reduced by the effect of scattering to $\varepsilon(J-S)$ where ε is the well-known collision parameter and S the source function. For a typical metal line at the temperature minimum the coefficient ε may be as small as 10^{-3} or 10^{-4} (Avrett, private communication). Thus, for a given net transition rate J-S, the net heating rate $\varepsilon(J-S)$ is very low. This led Ayres to conclude that the metals are unable to compensate the excessive heating rate due to photodissociation of H^- and to suggest that the temperature is either very much higher, where H^- alone can balance the energy, or very much lower, where the carbon monoxide molecule becomes a very efficient coolant and hence CO and H^- together can achieve energy balance. He thus proposed a solar model in which the atmosphere is bifurcated into two distinct thermal zones; in the hotter zone the temperature is near 4900K, and in the cooler one it is below 4000K and may be as low as 2900K.

The reasoning by which Ayres rejected the metal lines as effective coolants is fallacious: While it is true that for given mean integrated intensity and source function the scattering of photons reduces the local net cooling rate very significantly, the scattering also partly compensates for the local reduction by increasing the effective distance a photon travels before being truly absorbed and by allowing the migration of photons into the line wings where escape is facilitated by the lower opacity. The latter effect is inhibited in regions of dense line blanketing but the former is fully effective.

The consequences of scattering for the total cooling by a line can easily be demonstrated in the idealized case of coherent scattering in a one-dimensional medium, where the thermalization distance is only of order $1/\sqrt{\varepsilon}$ rather than the full value of $1/\varepsilon$ as for a Doppler broadened line with complete redistribution. The source function is given by (cf. Kalkofen 1974)

$$S(\tau) = B\,[1-(1-\sqrt{\varepsilon})\,e^{-\sqrt{\varepsilon}\,\tau}] \quad , \tag{1}$$

where the true emission fraction ε and the Planck function B are assumed constant. The local net cooling rate is therefore proportional to

$$S - J = B\,\frac{\varepsilon}{1+\sqrt{\varepsilon}}\,e^{-\sqrt{\varepsilon}\,\tau} \quad , \tag{2}$$

and the total net cooling due to the line is proportional to

$$H(o) = \frac{\sqrt{\varepsilon}}{1+\sqrt{\varepsilon}}\,B \quad . \tag{3}$$

Thus, for coherent scattering, the line cooling is reduced only by the factor $\sqrt{\varepsilon}$.

For a strong, thermally broadened line formed with completely non-

coherent scattering in a static medium, the main effect of the scattering is to distribute the energy loss over a larger region of the atmosphere; the total cooling is not very different from that of a line formed in LTE. If the atmosphere has motions, the cooling effect of the line with scattering might well be larger than that of a line computed in LTE for a static medium.

The case against the LTE treatment of Kurucz is much weaker than appears from Ayres' discussion. However, the observational basis of high temperatures as seen in the UV metal lines and of cool temperatures as found for the molecular lines in the infra-red (Ayres and Testerman 1981) remains strong. But, instead of further analyzing Ayres' proposed model I will discuss a time-dependent model in which temporal averages, rather than spatial averages, give rise to the variety of observed and inferred temperatures.

IV. THE WAVE MODEL

It is generally accepted that the solar chromosphere is heated by some form of hydrodynamic wave. The waves are expected to be pure acoustic waves in regions of the quiet sun with very weak magnetic field, and slow mode waves in magnetic regions (Ulmschneider and Stein 1981). These waves are generated near the top of the hydrogen convection zone and propagate outward into layers of density decreasing exponentially with height. Their velocity therefore grows nearly exponentially - except for radiation damping which is largest in the dense layers of the photosphere, where most of the energy is lost from the waves, and is negligible at the temperature minimum. Eventually the acoustic waves turn into shocks, dissipating their energy and heating the medium. The site of shock formation is the chromosphere. Below the region of strong dissipation the waves reach large amplitude (Ulmschneider and Kalkofen 1977) but gradients of the state variables of the gas are sufficiently small to be insignificant for mechanical dissipation. The cooling time of the gas of ca. 8min. (Giovanelli 1978) is long compared to typical wave periods of 1/2 min. (Ulmschneider 1970, 1974; Athay and White 1978). Therefore the waves travel essentially adiabatically through those layers, where the atmosphere reaches its lowest temperature.

Throughout the photosphere and the low chromosphere, the dominant terms in the energy balance are the radiative and the mechanical energy fluxes. Their time average must be constant, and the gradients satisfy the conservation equation (Ulmschneider et al. 1978)

$$\overline{d\,F_{mech}/d\tau} = 4\pi \int_0^\infty d\nu\, \kappa_\nu \quad (J_\nu - B_\nu) \quad , \qquad (4)$$

where F_{mech} is the wave flux, h the height measured outward, and κ_ν the monochromatic opacity per cm^3, with the bar indicating time averaging. At the temperature minimum, because of the near adiabaticity of the waves, the mechanical flux gradient is very small and hence the radiative terms alone must satisfy the energy equation, which is similar to the radiative equilibrium equation except that the time average heating must balance the time average cooling.

Since the compressive waves reach large amplitude in the temperature minimum region, they cause a variety of non-linear effects, depending on the quantity that is averaged. The most interesting quantity at the temperature minimum is the minimum temperature. Its inferred value depends strongly on the observational criterion, i.e., whether it is defined by the degree of excitation or degrees of ionization or dissociation, for example.

Consider the average temperature: The opacity and the Planck function depend strongly on temperature. For bound-free transitions of H^-, e.g. the cooling rate in LTE between 3500K and 4500K depends on temperatures as $T^{4.9}$ or $T^{4.4}$, resp.; for the (grey) opacity provided by Kurucz, the fit by Ulmschneider et al. (1978) gives the temperature dependence of $T^{5.7}$. While the precise value of the exponent of T in the opacity and the emissivity may be quite uncertain, the observation that the value is well in excess of unity is not subject to serious doubt. An immediate consequence of this temperature dependence, especially of the cooling term in the energy equation, is that the excess of emission in the compressive phase of the wave can be balanced by the deficit in the expansive phase only if the temperature increase above the ambient temperature during compression is smaller than the decrease during expansion. Therefore, the time averaged temperature at a fixed (Lagrangian) position in the gas will fall below the temperature in the undisturbed atmosphere.

An observation of the average temperature itself would determine a value that is lower than that of the undisturbed, static atmosphere in radiative equilibrium. In the calculations of Ulmschneider et al. (1978) the temperature depression is found to be between 200K and 500K, depending on opacity and wave energy and period. However, a measurement of brightness temperature in the far infra-red continuum does not isolate the effect of the wave on the temperature. The density, ρ, is modified as well, with ρ proportional to $T^{3/2}$ for adiabatic compression. Neglecting changes in metal ionization, the variations of the emissivity caused by the wave is as $T^{7/2}$. Since this dependence is weaker than that of the cooling term in the energy equation (4), the inferred temperature in the IR may still be depressed, but by less than the time averaged temperature.

The center-to-limb variation of radiation formed in the transition region between photosphere and chromosphere depends on the run of the source function. The source function, in turn, is coupled to the Planck function via the collision parameter ε, which is proportional to the electron density. Now, if the compressive waves increased the effective electron density over its value in the static atmosphere, the coupling between source function and Planck function would be increased, forcing the source function to have a stronger depth gradient and the emergent radiation to have a steeper center-to-limb variation, as required by observations. The effect of the waves on metal ionization therefore holds considerable interest.

We can easily analyze the result of the wave on metal ionization if we assume, for the present, that the gas is in LTE. The temperature increase of the gas during the compressive phase favors ionization; the concomitant

pressure increase weakens it. The net result of the adiabatic compression is an increase in the electron density. The opposite happens during the adiabatic expansion. The balance, i.e., the time averaged electron density, is higher than the electron density of the static atmosphere, provided the metals are either very highly ionized or nearly neutral at both the highest and lowest temperatures reached during the passage of the wave, assumed to have a symmetric temperature profile. Now, at the solar temperature minimum, the temperature and density are such that the degree of ionization, α, is strongly affected by the wave, with α much more sensitive at the lower temperature, resulting in a time averaged electron density that is lower than that of the undisturbed medium.

The actual state of the gas depends on the ratio of the time scale for metal ionization relative to that of the wave, which is expected to have a period of about 1/2min. The time scale for collisional ionization by neutral atom impact is long compared to the hydrodynamic time scale but the photoionization time is short compared to the wave period. We may therefore expect that the ionized state is populated mainly by means of radiative transitions. Now, the ionizing radiation field represents a source function average over a region of space and is therefore less subject to the instantaneous, local temperature variations. The radiative recombination rate, on the other hand, is fully affected by it, both from the temperature change itself and from the density change. It is therefore likely that, during the compressive phase, the radiative recombination rate exceeds the photoionization rate; and the opposite is true during expansion. It is conceivable, therefore, that the electron density during the compression is lower than in the static atmosphere. Even if it should be increased on account of the general density increase during compression, the change in n_e is not likely to be large enough to have a significant effect on the limb darkening. But the problem is certainly very complicated as it involves radiative transfer in a strongly time-dependent medium.

The low temperature reached during the expansion phase of the wave promotes the formation of the carbon monoxide molecule by three-body association involving C, O, and H atoms. Given a rate coefficient of 10^{-32} cm^5 s^{-1} (as an estimate of an upper limit; for a general review of such reactions, cf. Kaufman 1969), the time-scale for forming CO, about one week, is comfortably long compared to the wave period. The CO density, therefore, assumes a value given by the time average of the degree of dissociation, $<n_{CO}>$. The temperature corresponding to $<n_{CO}>$ in the undisturbed atmosphere, $T(<n_{CO}>)$, is lower than the temperature in the static atmosphere, T_o, and the density is higher. For a symmetric wave with an amplitude of 500K travelling in an atmosphere with T_o=4300K, the equilibrium density of CO varies by a factor of 20. The actual, i.e., time averaged density, however, is only by a factor of about two larger than the density in the undisturbed atmosphere, and corresponds to a temperature by about 100K lower than T_o. Since at the lowest temperatures of the waves the carbon and oxygen atoms are nearly completely associated, an asymmetric wave with a larger downward excursion in temperature increases the CO density by only an insignificant amount.

The effect of the compressive waves on the CO molecule is thus to increase the density to a value corresponding to a lower temperature than that of the static atmosphere. The populations of CO in the vibrational and rotational states follow the temperature and density fluctuations of the waves practically instantaneously, hence observations of the vibration-rotation bands should reveal their presence.

The largest observational effect of the waves may be expected in lines at wavelengths that are short compared to the wavelength at which the Planck function at the temperature minimum reaches its maximum, because of the strong amplification of temperature changes by the Wien function, which for the K-line of Ca II is a factor of 9 and for the k-line of Mg II, a factor of 12. If we consider again a symmetric wave with an amplitude of 500K about T_c=4300K, the time-average of the Planck functions at the highest and lowest temperatures corresponds to a Planck function at a temperature of 4470K for the Ca II resonance line and to 4530K for the Mg II resonance line. For an asymmetric wave with a larger downward excursion, the apparent temperatures are reduced very little because of the high weight in the Wien function of the temperature peak. Thus, the temperatures typical of those encountered in the numerical simulations of acoustic waves lead, qualitatively, to the increases in the Planck function that are required by the atmospheric models based on the UV lines. Whether the proposed mechanism can bring agreement with the observations depends on line transfer with partial redistribution in a time-dependent, moving medium; the trend of the apparent temperatures suggests that it may.

V. CONCLUSIONS

The attractive feature of the hydrodynamic waves for the explanation of the discrepant temperatures in the empirical models is that they were not invoked specifically to solve the problems of the models. Rather, the compressive waves are required in any event to explain the outward increase of the temperature into the chromosphere. As a natural by-product, they produce the apparent high temperatures observed in UV lines and the low apparent temperatures seen in molecular lines. The high and low temperatures postulated by Ayres are reached in the time-dependent model during the compressive and expansive phases of the waves. In addition, as indicated by time-dependent simulations of wave propagation, the time-averaged temperature falls well below the temperature of the undisturbed, static atmosphere, leading to a low apparent temperature, which may result in energy conservation without bifurcation. Whether the wave model can reproduce the steep observed center-to-limb variation of radiation originating in the temperature minimum region without inhomogeneities will depend on the result of radiative transfer calculations. Of course, apart from the effect on time-averaged quantities, the time-dependent behavior of the waves should be observable in transitions reaching unit optical depth at the temperature minimum. The best candidates may be the vibration-rotation bands of carbon monoxide. Since these lines are formed in LTE, the temperature and density fluctuations should leave a distinct signature. Observations of these transitions would establish whether the many

different phenomena seen at the temperature minimum are caused by compressive waves with the properties postulated to explain the phenomena as well as to produce the temperature structure of the low chromosphere.

ACKNOWLEDGEMENTS

It is a pleasure to acknowledge useful and stimulating discussions with E. H. Avrett, J. Black, A. Dalgarno, R. W. Noyes, P. Ulmschneider, and G. Victor. This work has been supported in part by the Fluid Research Fund of the Smithsonian Institution and by the NASA grant NAGW-253.

REFERENCES

Athay, R. G. and White, O. R. 1978, Ap. J., 226, 1135.
Avrett, E. H. 1981, in Solar Phenomena in Stellar Systems. R. Bonnet and A. K. Dupree, eds. Reidel Publ. Co., Boston, USA.
Ayres, T. R. 1981, Ap. J., 244, 1064.
Ayres, T. R. and Linsky, J. L. 1976, Ap. J., 205, 874.
Ayres, T. R. and Testerman, L. 1981, Ap. J., 245, 1124.
Gingerich, O., Noyes, R. W., Kalkofen, W. and Cuny, Y. 1971, Sol. Phys., 18, 347 (HSRA).
Giovanelli, R. G. 1978, Sol. Phys., 59, 293.
Kalkofen, W. 1974, J.Q.S.R.T., 14, 309.
Kalkofen, W. and Ulmschneider, P. 1979, Ap. J., 227, 655.
Kaufman, F. 1969, Canad. J. of Chem., 47, 1917.
Kurucz, R. L. 1974, Sol. Phys., 34, 17.
Samain, D. 1979, Astron. Astrophys., 74, 225.
Shine, R. A., Milkey, R. W. and Mihalas, D. 1975, Ap. J., 199, 724.
Ulmschneider, P. 1970, Sol. Phys., 12, 403.
_____. 1974, Sol. Phys., 39, 327.
Ulmschneider, P. and Kalkofen, W. 1977, Astron. Astrophys., 57, 199.
Ulmschneider, P., Schmitz, F., Kalkofen, W. and Bohn, H. U. 1978, Astron. Astrophys., 70, 487.
Ulmschneider, P. and Stein, R. F. 1981, preprint.
Vernazza, J. E., Avrett, E. H. and Loeser, R. 1976, Ap. J. Suppl., 30, 1 (VAL).
_____. 1981, Ap. J. Suppl., 45, 635.

N83 20853

The Generation of Acoustic Energy from Stellar Convection Zones

H. U. Bohn
Institut f. Astron. u. Astrophys. Univ. Wurzburg, W.-Germany

I Introduction

The heating of stellar chromospheres and coronae by the dissipation of acoustic waves remains an important heating mechanism in spite of many contradicting arguments. It is only in the lower solar chromosphere that short period acoustic wave heating seems to be undisputed (Stein and Leibacher, 1979). The arguments leading to the rejection of the so-called "acoustic heating theory" (cf. Ulmschneider and Bohn, 1981) are derived mainly from comparisons of calculated acoustic energy fluxes with observational or theoretical requirements.

From the measurements of absolute Ca-II K line fluxes for main sequence stars (Blanco et al., 1974) it appeared relatively early that the theoretical acoustic fluxes of DeLoore (1970) for stars later than K0 were insufficient to account for the emission of this chromospheric line alone. In the same way it is shown by Vaiana et al. (1981) that the X-ray emission of main sequence stars is up to four orders of magnitude larger than the calculated acoustic fluxes by Renzini et al. (1977). For the construction of a theoretical chromosphere for the K0 V star 70 Oph A Schmitz and Ulmschneider (1980a) found that a factor of five more acoustic energy would be required for agreement with observations. This factor had to be raised to 140 in the case of the dK7e star EQ Vir (Schmitz and Ulmschneider, 1980b). However, before the acoustic heating theory is rejected, one should reexamine the boundary conditions of this theory, i.e. the amount of acoustic energy available for dissipation. In particular, modifications are necessary in the convection zone models and in the sound generation mechanism.

II Convection Zone Models

The amount of acoustic energy generated in a star depends sensitively on the structure of the convection zone. Therefore, the material equations used to supplement the usual stellar structure equations and the mixing length theory have to be evaluated as accurately as possible. In this respect there are two physical effects that have been neglected in the former models (Nariai, 1969; DeLoore, 1970; Landini and Monsignori-Fossi, 1973; Renzini et al., 1977; Fontaine et al., 1981) which are particularly important for later type stars. One is that absorption from molecules and dust is not taken into account in the opacity tables, and the second is the neglect of the dissociation of the H_2-molecule since Hydrogen is the most abundant element. A greater opacity shifts the upper boundary of the convection zone further out and results in higher convective velocities. The dissociation of H_2-molecules influences convection in the same way as any ionization process does, i.e., the adiabatic temperature gradient is brought down below the value of 0.4 which facilitates convective instability.

In this work the opacity tables of Alexander (1975) are used in addition to the usual tables by Cox and Tabor (1976) to take into account absorption by molecules and dust. This leads to an absorption coefficient for late M stars which is five orders of magnitude greater than when this molecular absorption is neglected.

For the calculation of the thermodynamical quantities a set of Saha-equations for particle densities is simultaneously solved with an equivalent equation for the H_2-dissociation. The partition function of the H_2-molecule is formed by summing over all possible energy terms of rotation and vibration, and at the same time the internal energy is calculated from temperature derivatives of the logarithms of these terms (Wehrse, 1977). This eliminates the need of a numerical differentiation in the calculation of the internal energy. All the other thermodynamic quantities, however, can be found from the internal energy by numerical differentiation in a straightforward way.

III Sound Generation

Almost all calculations of acoustic fluxes from stellar convection zones (Nariai, 1969; DeLoore, 1970; Landini and Monsignori-Fossi, 1973; Renzini et al., 1977; Fontaine et al., 1981) rely on the theory of turbulent sound generation by Lighthill (1952) and Proudman (1952). This theory assumes a homogeneous atmosphere without mechanical boundaries which implies a pure quadrupole source term in the inhomogeneous wave equation. It has been known for some time, however, that for gravitationally stratified stellar atmospheres dipole and monopole sound generation can also be expected (Unno, 1964).

The efficiency of acoustic energy generation depends on the multipole order and is largest for the monopole. The acoustic power is

$$N \propto \rho u^2 u / l \, (l/\lambda)^{2n+1},$$

where u is the mean convective velocity, l the diameter of a convective eddy, λ the wavelength of the emitted sound, and n = 0, 1, 2 for a monopole, dipole, and quadrupole source, respectively. In the convection zone the quantity l/λ may be replaced by u/c, where c is the velocity of sound, so the expression for the acoustic flux becomes (Stein and Leibacher, 1980)

$$F_m \propto \rho u^3 (u/c)^{2n+1}. \qquad (1)$$

Since $u \ll c$ it is obvious that the acoustic efficiency for n = 0 is at maximum.

Stein (1967) has extended Lighthill's theory to take into account density stratification due to the stellar gravitational field. With his theory it is possible to find a combined source term and to calculate the radiated power by solving the inhomogeneous wave equation after a multipole expansion of the source term. An application of his method to the sun (Stein, 1968) showed that, inspite of some power in the lower multipoles, the acoustic emission was dominated by quadrupole radiation and comparable in magnitude to previous results using the Lighthill theory.

However, considering the fact that the maximum convective mach number is about 0.25 in the sun and becomes much smaller for later type stars (< 0.05 at M5V) it is evident from relation (1) that for stars of later than solar type monopole and dipole radiation will be more important. Therefore, Stein's (1967) method is used to derive the acoustic emission in our models. His original code was modified to cut off the generation of g-modes and to calculate the sound generation from pure multipoles in addition to the total emission.

IV Acoustic Energy Fluxes

In the following, acoustic fluxes for stellar models of 2500 K $\leq T_{eff} \leq$ 9500 K and 0 $\leq$ log g $\leq$ 5 are presented. For all models the chemical composition by mass is chosen to be X : Y : Z = 0.68 : 0.30 : 0.02 to represent population I stars. The ratio of mixing length to pressure scale height is assumed to be one.

Figure 1 shows the three multipole fluxes in comparison with the total acoustic flux for log g = 4.5 stars. It is evident from this plot that the dipole and monopole sound generation becomes indeed increasingly important for stars of later than solar type as was expected from the discussion in section III. The monopole emission is even dominant for stars with T_{eff} < 4000 K and log g = 4.5 .

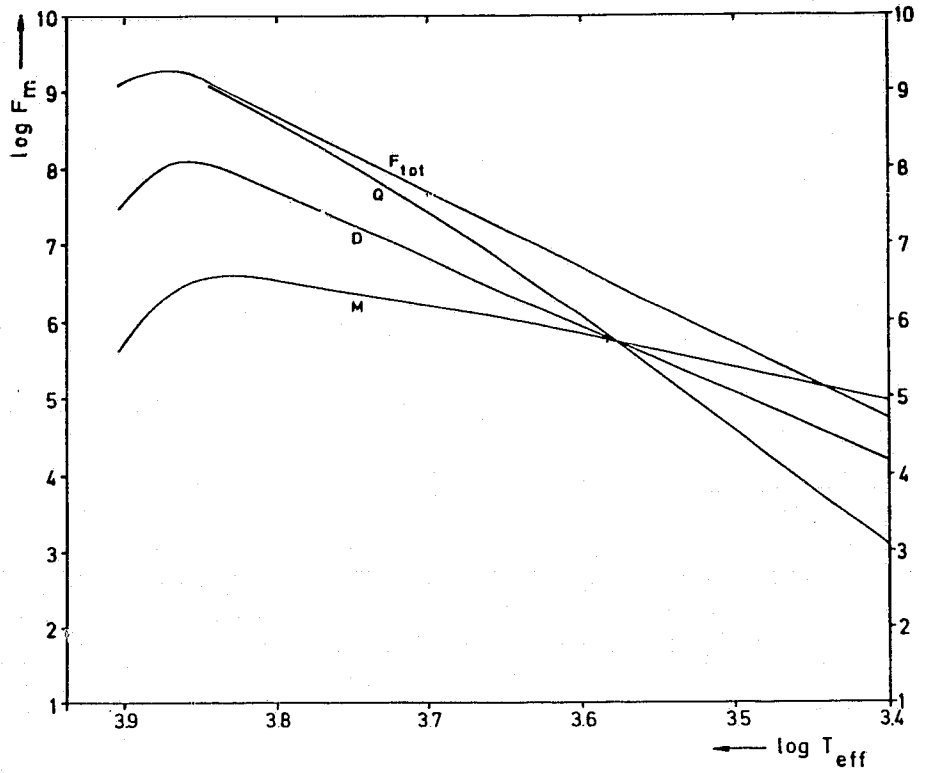

Figure 1. The total acoustic fluxes of log g = 4.5 stars in comparison to pure monopole (M), dipole (D), and quadrupole (Q) sound generation.

The total acoustic fluxes for all the calculated models are shown in Figure 2 with log g as a parameter. Here the influence of the three multipole contributions can be seen from the two thin lines separating different regions of T_{eff} and g in the diagram. Below the lower line acoustic energy generation is dominated by monopole emission. For a fixed stellar gravity, going from lower to higher T_{eff}, one finds, after crossing this line, a superposition of all three multipoles with dominant quadrupole emission. For the dependence of the total sound generation on stellar parameters one finds approximately

$$log\ F_m \sim -26.15 + 9.75 + \log T_{eff} - 0.5 \log g. \qquad (2)$$

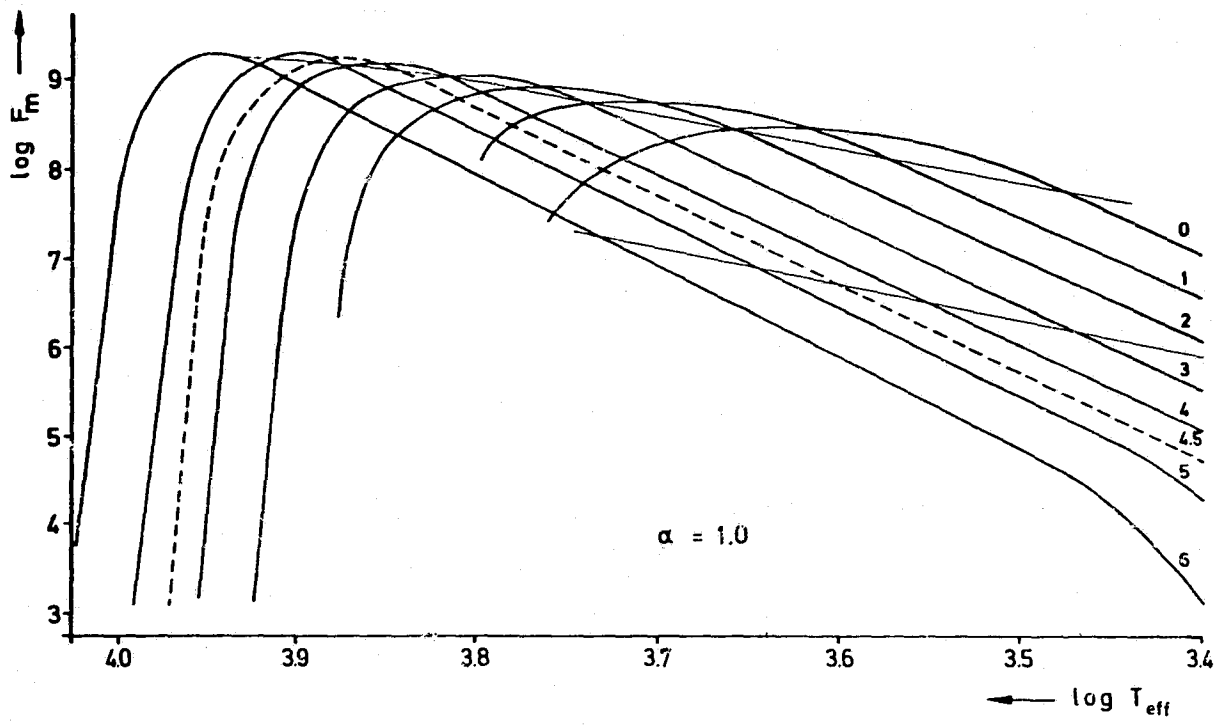

Figure 2. Acoustic fluxes from stellar convection zone models with log g as a parameter.

By comparison with the pure multipole emissions it is possible to calculate the constants of proportionality for monopole, dipole, and quadrupole sound generation from relation (1). The constant for quadrupole emission is found to be 35.7 in fairly good agreement with Proudman's (1952) analytical results. The corresponding values for dipole and monopole sound generation are 2.0 and 0.1, respectively.

Figure 3 shows the acoustic fluxes for log g = 4 and 4.5 stellar models compared to older calculations by Renzini et al. (1977) and X-ray luminosities from main sequence stars (Vaiana et al., 1981). The acoustic fluxes of this work are up to five orders of magnitude larger than the results of Renzini et al. (1977) for the latest type stars. It now becomes apparent that acoustic heating of stellar chromospheres and coronae cannot be rejected by a mere insufficiency of calculated

fluxes in comparison to observations. This is especially true in view of the conservative assumptions which led to the results of this paper. These assumptions are: the ratio of mixing length to pressure scale height of one is at the lower end of the usually assumed range, molecular opacities are still only partially known, and the assumption of isotropic turbulence for the turbulent energy spectrum (Stein, 1967) does not account for eventual enhancement of turbulent energy in the radial direction due to stellar gravity. Thus, the calculated fluxes represent lower bounds for possible acoustic emission from stellar convection zones.

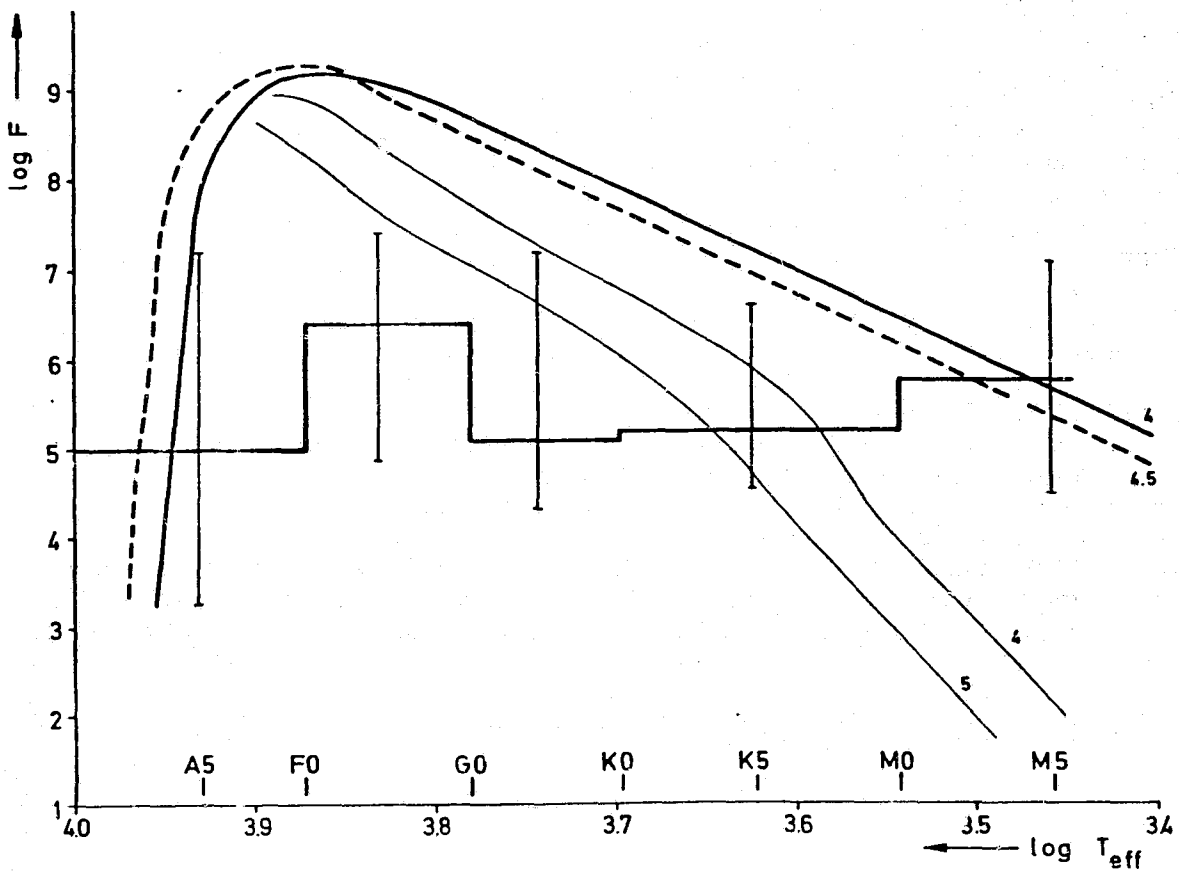

Figure 3. Acoustic fluxes of log g = 4 and 4.5 stars (thick lines) in comparison to Renzini's (1977) results (thin drawn lines) and the absolute X-ray fluxes of main sequence stars (fully drawn histogram; Vaiana et al., 1981). The vertical bars represent the range of observed X-ray emission within the various spectral types.

It also has to be pointed out that there are, in contradiction to Linsky's (1980) conclusions, arguments which support the acoustic heating theory. First, the observed minimum of the X-ray flux occurs at spectral type A5 where the acoustic energy vanishes due to decaying convection zones (Fig. 3). Secondly, the maximum of the X-ray scatter also happens at A5 where a small uncertainty in the stellar gravity would cause a large change in the acoustic output.

Acknowledgements

This work was supported by the German Science Foundation (DFG). I want to thank Prof. P. Ulmschneider for his guidance with acoustic heating, Prof. R. F. Stein for help with acoustic energy generation, and Dr. R. P. Stefanik for reading and improving the manuscript.

References

Alexander, D.R., 1975, Astrophys.J.Suppl.Ser. **29**, 363.
Blanco, C., Catalano, S., Marilli, E., Rodono, M., 1974, Astron.Astrophys. **33**, 257.
Cox, A.N., Tabor, J.E., 1976, Astrophys.J.Suppl.Ser. **31**, 271.
DeLoore, C., 1970, Astrophys.Space.Sci. **6**, 60.
Fontaine, G., Villeneuve, B., Wilson, J., 1981, Astrophys.J. **243**, 550.
Landini, M., Monsignori-Fossi, B.C., 1973, Astron.Astrophys. **25**, 9.
Lighthill, M.J., 1952, Proc.Roy.Soc. A **211**, 564.
Linsky, J.L., 1980, SAO Spec. Report **389**.
Proudman, J., 1952, Proc.Roy.Soc. A **214**, 119.
Renzini, A., Cacciari, C., Ulmschneider, P., Schmitz, F., 1977, Astron.Astrophys. **61**, 39.
Schmitz, F., Ulmschneider, P., 1980 a, Astron.Astrophys. **84**, 191.
Schmitz, F., Ulmschneider, P., 1980 b, Astron.Astrophys. **84**, 93.
Stein, R.F., 1968, Astrophys.J. **154**, 297.
Stein, R.F., 1967, Solar Phys. **2**, 385.
Stein, R.F., Leibacher, J.W., 1980, in: "Stellar Turbulence", Lecture Notes in Physics **114**, 225, D.F.Gray, J.L.Linsky eds., Springer.
Ulmschneider, P., Bohn, H.U., 1981, Astron.Astrophys. **99**, 173.
Unno, W., 1964, Transactions of the IAU XII, 555, J.C.Pecker, ed.
Vaiana, G.S., Cassinelli, J.P.,Fabbiano, G., Giacconi, R., Golub, L., Gorenstein, P., Haisch, B.M., Harnden, F.R.Jr., Johnson, H.M., Linsky, J.L., Maxson, C.W., Mewe, R., Rosner, R., Seward, F., Topka, K., Zwaan, C., 1981, Astrophys.J. **244**, 163.
Wehrse, R., 1977, Astron.Astrophys. **59**, 283.

A HEATING MECHANISM FOR THE CHROMOSPHERES OF M DWARF STARS

M. S. Giampapa, L. Golub, R. Rosner and G. S. Vaiana

Harvard-Smithsonian Center for Astrophysics

J. L. Linsky

Joint Institute for Laboratory Astrophysics, University of Colorado
and National Bureau of Standards

S. P. Worden

Department of Astronomy, University of California, Los Angeles

INTRODUCTION

The systematic, detailed observational and theoretical investigation of the atmospheric structure of the dwarf M stars is especially important to the general field of stellar chromospheres and coronae. More specifically, the M dwarf stars constitute a class of objects for which the discrepancy between the predictions of the acoustic wave chromospheric/coronal heating hypothesis and the observations is most vivid. Conversely, they must therefore represent a class of stars where alternative atmospheric heating mechanisms, presumably magnetically related, are most clearly manifested. We thus propose to ascertain the validity of a recently advanced hypothesis to account for the origin of the chromospheric and transition region line emission in M dwarf stars.

As a prelude to the discussion of the heating mechanism that may give rise to the chromospheric and transition region line emission in M dwarf stars, we will briefly summarize our recent ultraviolet, optical and X-ray observations of a sample of dMe and dM stars. In particular, we will delineate the similarities and differences in the observed chromospheric line spectra of dMe and dM stars, and discuss the relative importance to chromospheric radiative cooling of various spectral line features. Finally, we will perform a preliminary assessment of the role of coronal X-ray emission in the heating of M dwarf atmospheres.

DISCUSSION

A detailed description of the ultraviolet and optical spectrum of M dwarf stars is given by Linsky et al. (1981). We will briefly discuss a principal result of this investigation and, in conjunction with our X-ray data, demonstrate the importance of these results for theories that seek to describe the heating mechanisms that give rise to stellar chromospheres.

The far ultraviolet line spectra of several dM and dMe stars are shown in Figures 1 and 2. The brightest "high temperature" features tend to be C IV

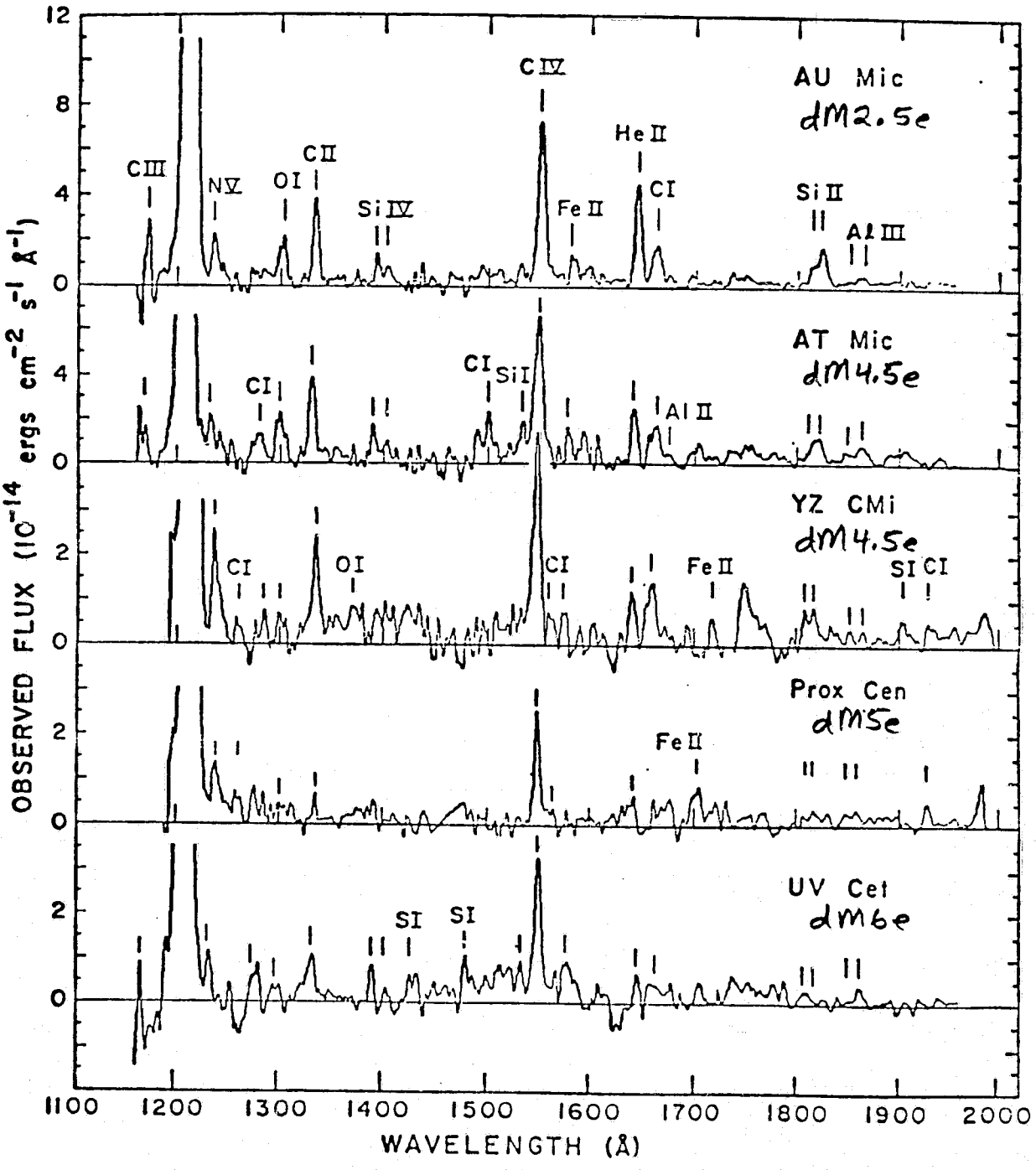

Fig. 1. Far ultraviolet observations of dMe stars.

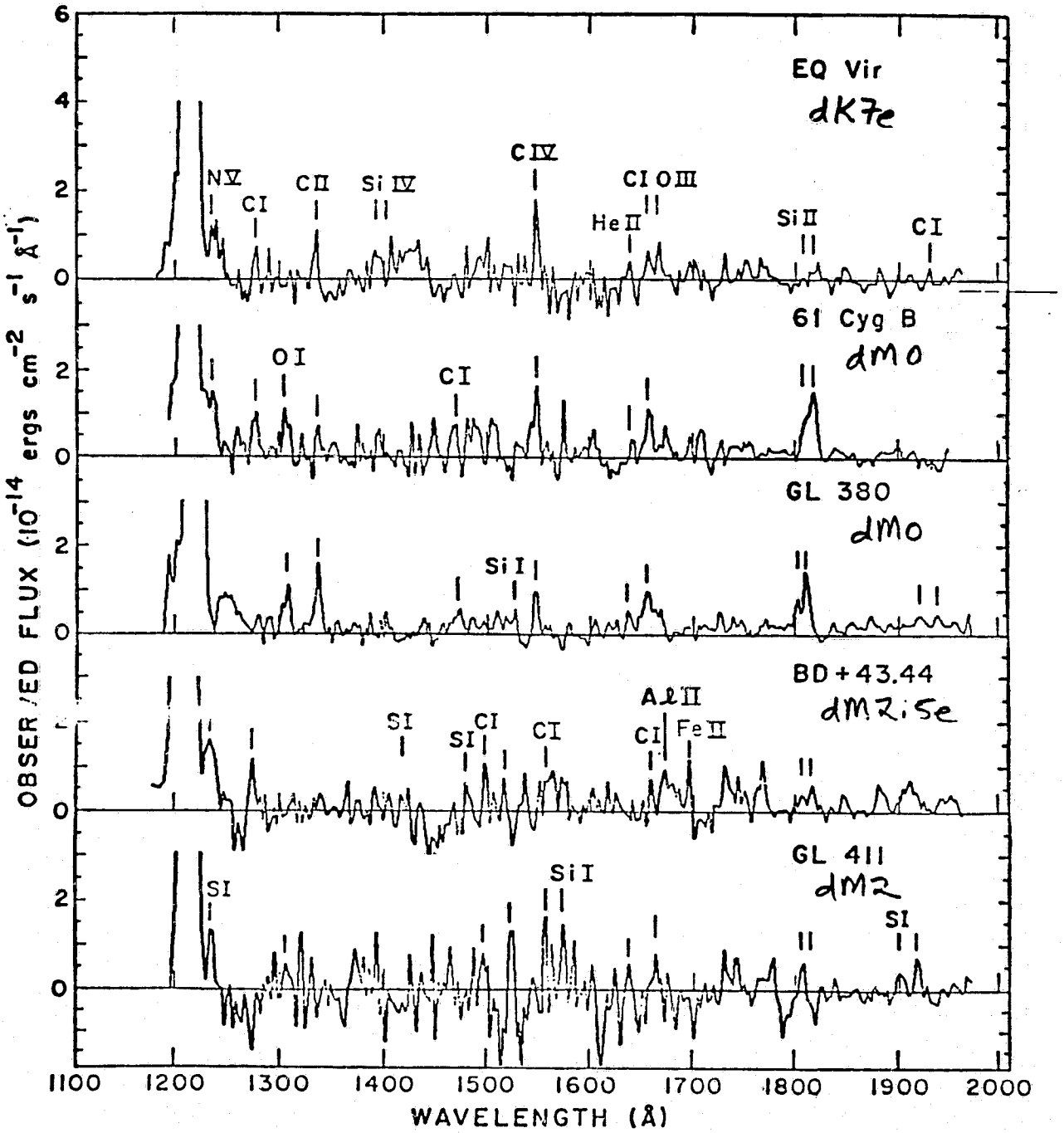

Fig. 2. Far ultraviolet spectra of dM and dMe stars.

λ1550, C II λ1335 and He II λ1640, although the He II line may be formed by recombination-cascade following photoionization by coronal X-rays. Hence its temperature of formation is somewhat ambiguous. We also note, parenthetically, that the C II λ1335 line arises in more nearly chromospheric ($T \sim 2 \times 10^4$ K) regions while the C IV doublet is purely a transition region diagnostic ($T \sim 10^5$ K). The transition region lines, such as C IV λ1550, are brighter than the relatively low temperature chromospheric lines (e.g. C I λ1657 and Si II λ1812) in the dMe stars while the reverse is true in the dM stars. Furthermore, the surface fluxes of the high temperature lines (N V, C IV, S IV, etc.) in the dMe stars are 10 - 100 times greater than the corresponding line surface fluxes for the quiet Sun. In contrast, the high temperature line surface fluxes for the dM stars are similar to or slightly less than those of the quiet Sun.

A significant new result of our optical and ultraviolet survey of M dwarf stars is the following: the Balmer lines are the most prominent chromospheric emission line features in the dMe stars (see Figure 3 herein and Worden et al. 1981 for examples of hydrogen line profiles in dMe spectra). The Balmer lines are, in total, 3 - 9 times as bright as the Mg II resonance lines and, consequently, emit more energy than all the other chromospheric lines combined. Thus the Balmer lines are the principal contributors to the net radiative cooling of the chromospheres of dMe stars. Utilizing the line surface flux data given by Linsky et al. (1981), we find that the largest integrated cooling rates for the dMe stars in order of decreasing importance are due to the Balmer lines, Fe II, the Mg II resonance lines, and the Ca II resonance lines (although the last 3 cooling rates are within factors of 2 or 3 of each other). Interestingly, this order of importance also follows the order of elemental abundance, with hydrogen the most abundant element and calcium the least abundant among the principal contributors to the chromospheric radiative cooling of dMe stellar atmospheres. This result is likely a consequence of the relative abundance of a particular atom or ion coupled with the collisional control of the source functions of the important line transitions. In contrast, Vernazza, Avrett and Loeser (1980) find for the average quiet Sun that the largest integrated cooling rates in order of decreasing importance are due to the Ca II infrared-triplet and resonance lines, the Mg II resonance lines, H^- and Lα.

The value of the previously described observations is significantly enhanced with the addition of recently acquired X-ray observations of these stars. Recent Einstein satellite observations have shown that the dMe stars are intense X-ray sources characterized by X-ray luminosities that can be as large as 10% of the visual luminosity of the star (Vaiana et al. 1981). In terms of bolometric luminosity, L_B, the fractional quiescent X-ray luminosity, L_X/L_B, can still be an order of magnitude greater than that for solar active regions and two orders of magnitude greater than L_X/L_B for the quiet Sun (Haisch and Linsky 1980). As a result, Cram (1981) has suggested that the atmospheric regions (i.e. chromospheres and transition regions) beneath the X-ray emitting coronae of these stars are illuminated by an intense flux of X-rays, and are consequently heated above the temperature that would exist in a pure radiative-convective equilibrium model. In particular, the major

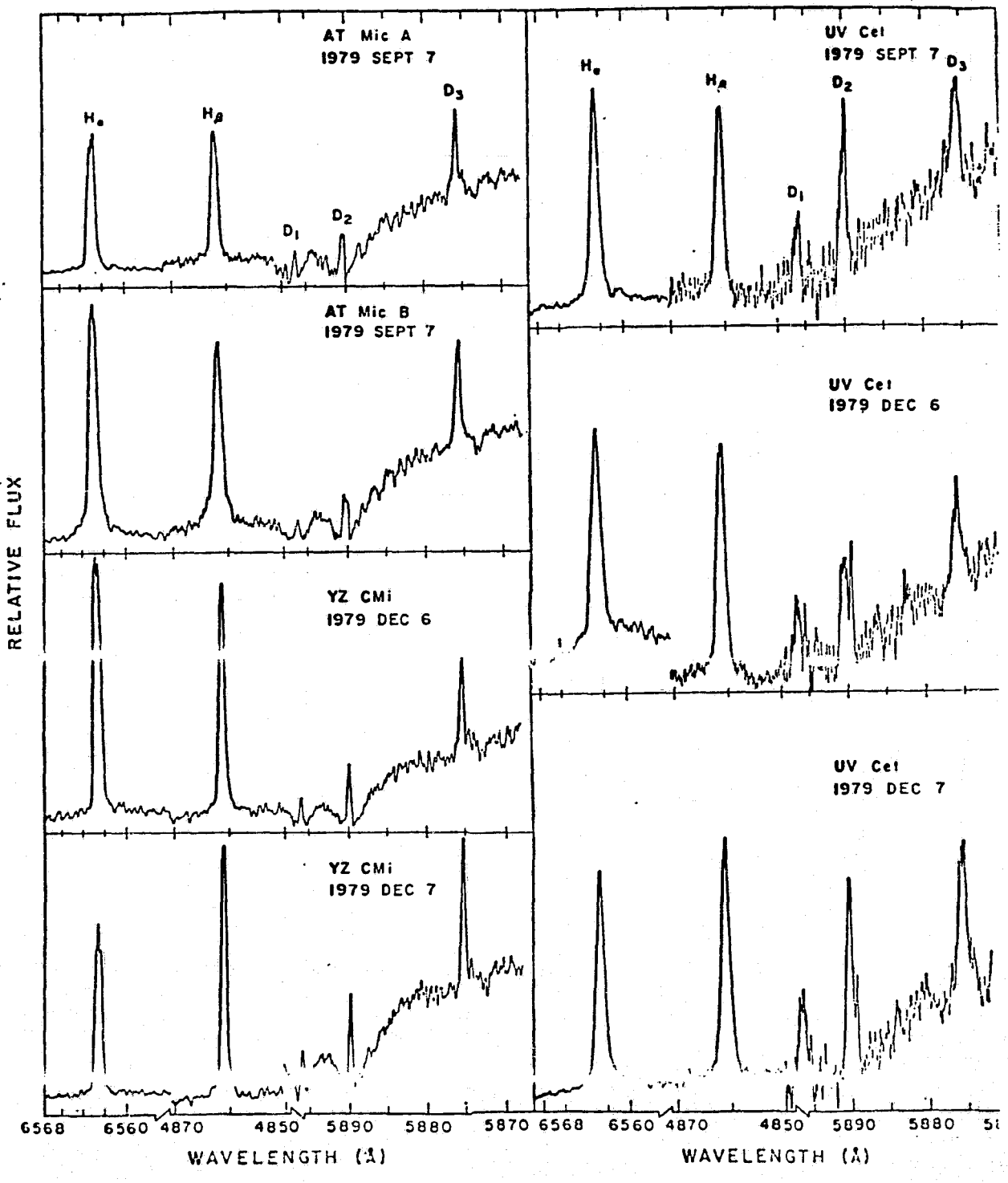

Fig. 3. Balmer line profiles for dMe stars.

portion of the downwardly directed X-ray flux will be absorbed by the underlying atmosphere, subsequently leading to photoionization. The resulting high energy photo-electrons will rapidly thermalize, thus converting the original X-ray radiative flux from the corona to thermal energy. This thermal energy is then emitted as transition region and chromospheric radiation.

If X-ray heating by an overlying corona is an important component in the energy balance of dwarf M chromospheres, then the observed quiescent X-ray flux from a dMe star should be similar to the total observed chromospheric-transition region radiation. We may therefore consider the viability of the hypothesis by comparing our recent optical, IUE and HEAO-B observations of M dwarf stars. The total chromospheric-transition region line luminosities and the X-ray luminosities, as taken from Linsky et al. (1981) and Vaiana et al. (1981), respectively, for a small sample of dwarf M stars are shown in Table 1.

Table 1. A comparison of chromospheric and X-ray luminosities in a small sample of M dwarf stars.

Object	Chromosphere L_c (erg s^{-1})	Corona L_x (erg s^{-1})	L_x/L_c
EQ Vir (dK7e)[1]	1.1 (29)	2.3 (29)	2.1
61 Cyg B (dM0)	1.3 (28)	3.2 (27)	0.2
EQ Peg (dM4.5e+dM3.5e)[1]	3.8 (27)	6.3 (28)	16.6
YZ CMi (dM4.5e)	3.0 (28)	2.5 (28)	0.83
Prox Cen (dM5e)	1.1 (27)	1.2 (27)	1.0
UV Ceti (dM6e)	4.9 (27)	3.5 (27)	0.71

[1] Estimate of chromospheric losses does not include radiative losses attributable to Balmer line emission.

Inspection of Table 1 reveals that the chromospheric-transition region luminosities, L_c, are comparable to the X-ray luminosities, L_x, in four of the six stars in this small sample. The fact that L_x/L_c is greater than 1 in some cases may be due, in part, to the lack of data for Balmer line emission strengths in the estimate of L_c. A further important caveat is that the UV and X-ray observations were not contemporaneous. Thus variability due to flare activity as well as variability intrinsic to stellar surface active regions, as recently demonstrated by Linsky et al. (1981), may also account for differences between L_c and L_x. The eventual acquisition of additional IUE data for these stars, as well as other M dwarf stars for which X-ray data are currently available, will enable us to more accurately define the mean quiescent level of chromospheric emission present and thus partially circumvent the problems introduced by variability.

CONCLUSIONS

Our preliminary investigation corroborates the suggestion by Cram (1981) that X-ray heating by an overlying corona is the dominant heating mechanism in dMe stellar chromospheres. Of course this does not entirely resolve the problem of the heating of M dwarf atmospheres since the question concerning the origin of the X-ray emission itself (i.e., coronal heating) still remains. Nevertheless, the identification of a dominant chromospheric heating mechanism for a particular class of stars is a significant advance for the understanding of the origin of stellar chromospheres. The importance of X-ray heating in other stellar types should be assessed by comparing the observed total chromospheric-transition region line luminosities with the observed X-ray luminosities for sets of "active" and "quiet" stars of various spectral types. Interestingly, X-ray heating appears important in that region of the H-R diagram where turbulent velocities are low. We therefore speculate that for earlier stellar types, characterized by higher turbulent velocities, direct heating of the stellar chromosphere by magneto-acoustic mechanisms (e.g., see Ulmschneider and Bohn 1981; Leibacher and Stein, this volume) becomes relatively more important than external heating by coronal X-rays.

REFERENCES

Cram, L. E. 1981, Ap. J., submitted.
Haisch, B. M. and Linsky, J. L. 1980, Ap. J. (Lett.), 236, L33.
Leibacher, J., and Stein, R. F. 1981, in Cool Stars, Stellar Systems, and the Sun, eds. M. S. Giampapa and L. Golub, SAO Special Report.
Linsky, J. L., Bornmann, P. L., Carpenter, K. G., Wing, R. F., Giampapa, M. S., Worden, S. P. and Hege, E. K. 1981, Ap. J., submitted.
Ulmschneider, P. and Bohn, H. U. 1981, Astron. Ap., 99, 173.
Vaiana, G. S., et al, 1981, Ap. J., 244, 163.
Vernazza, J. E., Avrett, E. H., and Loeser, R. 1981, Ap. J. (Suppl.), 45, 635.
Worden, S. P., Schneeberger, T. J. and Giampapa, M. S. 1981, Ap. J. (Suppl.), 46, 159.

II. ATMOSPHERIC STRUCTURE

N83 20855

MOMENTUM AND ENERGY BALANCE IN LATE-TYPE STELLAR WINDS

K. B. MacGregor
High Altitude Observatory/National Center for Atmospheric Research

I). Introduction

a). Overview

The results of a variety of recent observations at ultraviolet and X-ray wavelengths indicate that the classical picture of a static stellar atmosphere containing a radiative equilibrium temperature distribution is inapplicable to the majority of late-type stars. In fact, both mass loss and the presence of atmospheric regions characterized by gas temperatures in excess of the stellar effective temperature now appear to be almost ubiquitous throughout the HR diagram. In the present review, we briefly summarize the observational evidence pertaining to the thermal and dynamical structure of the outer envelopes of cool stars. These results are then compared with the predictions of several theoretical models which have been proposed to account for mass loss (in the form of a stellar wind) from late-type stars. Specifically, models in which the outflow is thermally-, radiatively-, or wave-driven are considered in an attempt to identify the physical processes responsible for the observed wind properties. In view of the observed variation of both the wind thermal and dynamical structure as one proceeds from the supergiant branch toward the main sequence in the cool portion of the HR diagram, consideration is given to potential mechanisms for heating and cooling the flow from low-gravity stars. In the particular case of a wind driven by the force due to outwardly propagating Alvén waves, the results of several qualitative energy balance calculations are presented.

The reader who is interested in a more detailed discussion of both the observational and theoretical aspects of mass loss from cool stars should consult the following recent review papers: Weymann (1978), Cassinelli (1979), Goldberg (1979), Dupree and Hartmann (1980), Hagen (1980), Holzer (1980), Castor (1981), Dupree (1981), Hartmann (1981), Linsky (1981), Cassinelli and MacGregor (1982).

b). Observational Indicators of Gas with T>Teff

In the present section, we enumerate a few of the spectroscopic indicators used to establish the existence of gas having temperatures T>Teff in the outer atmospheres of late-type stars. A detailed discussion of the temperature distribution throughout the solar atmosphere is given in the book by Athay (1976); the subject of stellar chromospheres, transition regions, and coronae is treated in the review papers by Wilson (1966), Mewe

(1979), Ulmschneider (1979), Linsky (1980), and Cassinelli and MacGregor (1982).

i). Chromospheres

The term chromosphere is taken to refer to an atmospheric layer whose morphology is similar to that of the middle solar chromosphere. In particular, for stars having 3000 $\lesssim$ Teff $\lesssim$ 6500 K, it is a region in which the balance between non-radiative heating and radiative cooling gives rise to gas temperatures T $\lesssim$ few X 10^4K, and in which T is a fairly slowly increasing function of height above the temperature minimum location. The presence of chromospheric gas is most frequently inferred from the detection of spectral lines whose formation requires temperatures and densities comparable to those of the solar chromosphere. Among the most commonly observed such lines are the CaII H(λ3968) and K(λ3934) lines, the MgII h(λ2803) and k(λ2796) lines, the Lα(1216) line of HI, the infrared triplet ($\lambda\lambda$8498, 8542, 8622) lines of CaII, as well as numerous ultraviolet lines due to species such as CI, CII, OI, SiII, SI, and FeII.

ii). Transition Regions

In the solar atmosphere, the transition region is a thin layer separating the chromosphere and corona, in which T increases abruptly from a value $\approx$ 3 X 10^4K to T ~ 10^6K. The most commonly used diagnostics of transition region gas are ultraviolet emission lines due to multiply-ionized elements, such as SiIV ($\lambda\lambda$1394, 1403) CIII ($\lambda\lambda$977, 1175, 1909) CIV ($\lambda\lambda$1548, 1551), NV ($\lambda\lambda$1239, 1243), OV (λ1371), and OVI ($\lambda\lambda$1032, 1038). We note that since the flux of ionizing radiation from stars with Teff $\lesssim$ 6500K is generally small, the detection of any of the lines listed above should indicate the presence of a collisionally-ionized plasma having a temperature somewhere in the range of 3 X 10^4 $\lesssim$ T $\lesssim$ 3 X 10^5K.

iii). Coronae

By analogy with the sun, the detection of transition region emission lines in a stellar spectrum constitutes indirect evidence for the presence of an overlying corona (T $\gtrsim$ 10^6K). The solar corona is directly studied through observations of emission lines (at X-ray, UV, and visible wavelength) due to highly-ionized species, continuum emission (at X-ray and radio wavelengths), and photospheric radiation scattered by coronal electrons. However, the weakness of coronal emission at visible and radio wavelengths, together with the fact that many of the characteristic UV lines have wavelengths (λ<1000A) outside the spectral region in which satellite-borne instruments are maximally sensitive, generally precludes the use of these indicators to detect hot gas in the atmospheres of stars other than the sun (see, however, Gary and Linsky 1981). Hence, efforts to observe coronal gas in late-type stars have centered on the use of experiments designed to measure emission at X-ray wavelengths (see, e.g., Vaiana et al. 1981; Ayres et al. 1981).

C-2

c). Observational Indicators of Mass Loss

i). Main-Sequence Stars

The prevalence of soft X-ray emission among late-type dwarf stars suggests that they possess coronae in which $T \gtrsim 10^6$K (cf. Vaiana et al. 1981). By analogy with the sun, it therfore seems likely that such stars undergo mass loss in the form of tenuous, hot stellar winds, driven primarily by the force due to the thermal pressure gradient in the outflowing material (for an extensive discussion of the physics of the solar wind, see the reviews by Holzer [1979, 1980]). Adopting the average quiet solar wind mass loss rate ($\dot{M} \sim 10^{-14}$ $M_\odot yr^{-1}$) and terminal velocity ($V_\infty \approx 400$-500 kms^{-1}) as representative of the outflows from late-type dwarfs in general, it is easily seen that the implied wind column density is too low to give rise to any observable spectroscopic effects. Hence, mass loss from cool, main-sequence stars is not directly detectable. Furthermore, for $M^* = M_\odot$, the time scale over which such stars lose an appreciable fraction of their mass is of order $\tau_M = M^*/\dot{M} \sim 10^{14}$ yrs, a value too long for noticeable evolutionary effects. However, in the solar case, the inclusion of the interplanetary magnetic field in the treatment of coronal expansion indicates that magnetic stresses enforce corotation of the outflow with the sun out to a distance significantly in excess of the solar radius (Weber and Davis 1967; Belcher and MacGregor 1976). As a result, the e-folding time for angular momentum loss, $\tau_J = J/\dot{J}$, is comparable to the main-sequence lifetime of the sun. Hence, observations indicating that the average surface rotation speed of main-sequence stars (1) decreases sharply for spectral types later than FS, and (2) is a decreasing function of age for stars like the sun (Skumanich 1972; Soderblom 1980, and references therein) provide indirect evidence that late-type dwarf stars lose both mass and angular momentum via magnetically-coupled winds originating in hot stellar coronae.

ii). Giants and Supergiants

Among late-type, low-gravity stars, mass loss apparently occurs at a rate sufficient to produce several characteristic emission and absorption features in the stellar spectrum. Frequently used indicators of appreciable, continuous mass loss from cool giants and supergiants include: blue-shifted absorption lines due to a variety of neutral and singly-ionized metals, arising from the absorption and scattering of stellar radiation by atoms and ions in the outflow (cf. Reimers 1975; Goldberg 1979; Hagen 1980; Castor 1981; Hartmann 1981); emission cores of chromospheric collision-dominated spectral lines (e.g. CaII H and K, MgII h and k) which are asymmetric in the sense that the intensity of the K_{2V} peak is less than that of the K_{2R} (or k_{2r}) peak (Stencel 1978; Weiler and Oegerle 1979; Stencel and Mullan 1980; Linsky 1980); 10 μm emission and infrared excesses, attributed to the absorption and subsequent re-emission of photospheric radiation by dust grains in an expanding circumstellar envelope (cf. Reimers 1975; Weymann 1978; Hagen 1980; Castor 1981, and references therein). Detailed analysis of each of the spectroscopic indicators listed above can, in principle, lead

to an estimate of the mass loss rate $\dot{M}$ for a given star (see Castor 1981 for an extensive discussion). In practice, however, incomplete understanding of the physical processes affecting the dynamical, thermal, and ionization state of the outflow gives rise to considerable uncertainty in the $\dot{M}$ values so determined, as is evidenced by the case of αOri (M2Iab), for which the following estimates of $\dot{M}$ have been derived: $\dot{M}(M_\odot yr^{-1}) = 5.0 \times 10^{-6}$ (Weymann 1962b), 7.0×10^{-7} (Gehrz and Woolf 1971), 1.0×10^{-6} (Reimers 1975) 1.7×10^{-7} (Sanner 1976) 3.0×10^{-5} (Bernat 1977), 1.5×10^{-7} (Hagen 1978), $4.0 \times 10^{-7} - 2.0 \times 10^{-6}$ (Knapp et al. 1980), 1.5×10^{-5} (Jura and Morris 1981). Despite the quantitatively unreliable nature of mass loss rate determinations for low-gravity stars, we conclude that the detection of any of the spectroscopic indicators listed above implies a wind column density corresponding to an $\dot{M}$ value significantly larger than those for the sun and dwarf stars.

d). Behavior in the HR Diagram

When the observational results described briefly in the preceding sections are considered together, the following schematic picture of the variation of wind thermal and dynamical properties in the cool portion of the HR diagram emerges. Main-sequence stars possess chromospheres, transition regions, and coronae, and probably undergo mass loss in the form of hot ($T \sim 10^6$K), tenuous ($\dot{M} \sim 10^{-14}$ $M_\odot$ yr^{-1}), and fairly high-velocity ($V_{oo} \sim$ several $\times 10^2$ km s^{-1}) stellar winds. Proceeding from the main sequence toward the giant and supergiant branches, both the thermal and dynamical structure of late-type stellar winds change. Transition region emission lines and coronal soft X-ray emission are not detected in the coolest and most luminous supergiant stars indicating the presence of little (if any) hot ($T \geq 10^4$K) gas. Circumstellar absorption lines and chromospheric emission line asymmetries are seen in the spectra of these stars, suggesting that mass loss occurs in the form of a cool, massive ($\dot{M} \sim 10^{-6}$ $M_\odot$ yr^{-1}) outflow. Moreover, the wind terminal velocities inferred from the observed blue-shifted absorption features are generally in the range $V_{oo} \sim 10$-100 km s^{-1}, well below the surface gravitational escape speed. Intermediate between the main-sequence and supergiant stars are the so-called hybrid stars (Hartmann, Dupree, and Raymond 1980; 1981), which show spectroscopic evidence for both the presence of gas at transition region temperatures and atmospheric expansion at relatively high velocities ($V_{oo} \sim 100$ km s^{-1}). However, these stars may be undergoing mass loss at rates significantly higher than those corresponding to the winds of dwarf stars.

II). Mass Loss Mechanisms

a). Overview

Complete understanding of mass loss from late-type stars necessarily requires detailed knowledge concerning the identity of the physical processes responsible for the observed outflows. Toward this end, we describe several mechanisms which have been proposed to account for mass loss from

cool stars. We assume that the winds of late-type dwarf stars are essentially thermally-driven, and restrict the following discussion to the massive outflows associated with giants and supergiants.

b). Thermally-Driven Winds

In the present section, we attempt to determine whether or not the winds from low-gravity stars can be driven by the force due to the thermal pressure gradient in an expanding stellar atmosphere. For this purpose, consider a steady, isothermal, spherically-symmetric flow emanating from a star of mass M_* and radius R_*. Under these conditions, the sonic point location (i.e., the distance r at which the flow speed is equal to the local speed of sound) is given by $r_s = (GM_*/2a^2)$, where, for a gas of temperature T and mean mass per particle μ, $a = (kT/\mu)^{\frac{1}{2}}$ is the isothermal sound speed (see, e.g., Parker 1963; Hundhausen 1972). It can likewise be shown that the energy per unit mass carried by the wind is a constant of the motion, from which an approximate expression for the initial velocity V_o of the flow can be derived. When $V_o << a$, the result is

$$V_o \approx a z_s^2 \exp\left(\frac{3}{2} - 2z_s\right) , \qquad (1)$$

(cf. Parker 1963). For illustration, adopt $M_* = 16\ M_\odot$, $R_* = 400\ R_\odot$; for cool supergiant stars, the apparent absence of coronal and transition region emission indicates $T \leq 10^4$K. Choosing $T = 10^4$K and $\mu = 0.667\ M_H$ (characteristic of a hydrogen and helium plasma with $N_e = N_H$, $N_{He}/N_H = 0.1$), it follows that $r_s \approx 31\ R_*$ and $V_o \approx 8 \times 10^{-18}$ cm s^{-1}. Since conservation of mass requires that $\dot{M} = 4\pi R_*^2 \mu N_o V_o$ (N_o is the total number density at the base of the wind), it would seem that (for reasonable values of N_o) the lack of hot gas in supergiant atmospheres rules out the possibility of thermally-driven mass loss at rates comparable to these inferred from observations.

An alternative approach to the same problem has been suggested by Weymann (1962a, 1978). For the stellar parameters given above, we assume $N_o = 10^{11}$cm^{-3} and determine T such that V_o yields a mass loss rate $\dot{M} = 10^{-6}\ M_\odot$ yr^{-1}. The temperature so obtained is $T = 68{,}724$K, a value incompatible with absence of transition region emission lines (e.g., those due to CIV) in the spectra of cool supergiants (see Weymann 1978 for further discussion).

c). Radiatively-Driven Winds

We consider the possibility that the winds from late-type, low-gravity stars can be driven by the force due to the absorption and scattering of radiation from the stellar photosphere by sources of opacity in the outflow. An immediate and fundamental difficulty with this suggestion has been pointed out by Goldberg (1979). Namely, for the physical conditions appropriate to the cool winds emanating from giants and supergiants, the abundant atoms and ions have resonance lines (expected to be among the strongest sources of opacity) situated in the visible and UV portions of the spectrum, while the photospheric continuum radiation field peaks in the red or near IR. To

date, there have been several proposals for circumventing this spectral mismatch, three of which are described briefly below.

1.) Maciel (1976, 1977) has suggested that the IR bands of molecular species such as Co, H_2O, and OH may contribute to the wind opacity. At present, it is not clear whether the rate at which momentum is gained by the flow due to this mechanism is sufficient to account for the observed wind mass loss rates. The attainment of supersonic velocities requires that at some point in the wind, the radiative and gravitational forces on the gas must be equal, e.g. $GM_*/r^2 \approx K_{mol} L_*/4\pi r_c^2$ (Phillips 1979). Adopting the estimate $K_{mol} \sim 0.005$ cm^2 gm^{-1} (Salpeter 1974) for the molecular opacity per unit mass of the wind material, it is seen that stellar luminosities $>10^6$ $L_\odot$ are needed to fulfill this constraint.

2.) Wilson (1959) and Haisch et al. (1980) have suggested that the force arising from the scattering of chromospheric Lyman α radiation by neutral hydrogen atoms in the flow could be responsible for the winds of cool giants and supergiants. Such a force is sensitively dependent upon both the degree of ionization of the wind and the Lα optical depth. To assess the plausibility of the mechanism, assume $\dot{M} \sim 10^{-6} M_\odot$ yr^{-1}, $V_\infty \sim 10$ km s^{-1}, corresponding to a wind momentum transport rate of order $\dot{M} V_\infty \sim 6 \times 10^{25}$ dyne. If the outflow results from the single scattering of Lα photons, the requisite Lα luminosity is $\dot{M} V_\infty c \sim 1.9 \times 10^{36}$ erg s^{-1}. For a star having $R_* = 400\ R_\odot$ and Teff = 3000-4000 K, this value amounts to a few $\times 10^{-2}$ L_*. For comparison, the solar Lα flux is approximately $F(L\alpha) \approx 3 \times 10^5$ erg cm^{-2} s^{-1}, implying $L(L\alpha)/L_\odot \approx 4.8 \times 10^{-6}$. If this value is representative of late-type stars in general, we conclude that Lα radiation pressure may affect the dynamical state of a small portion of the stellar chromosphere, but cannot by itself drive mass loss of the type observed.

3). The presence of 10 μm emission and infrared excesses in the long wavelength spectra of some cool stars and the interpretation of these features in terms of dust grains in a circumstellar shell has led several authors (cf. Gehrz and Woolf 1971) to propose that the grains themselves are responsible for mass loss. The condensation of grains and their subsequent outward acceleration by radiative forces can cause the entire circumstellar envelope to expand into a wind, provided that the collisional transfer of momentum from grains to the background gas is sufficiently strong (Gilman, 1972). Numerous models of such dust-driven winds have been constructed (cf. Salpeter 1974; Kwok 1975; Goldreich and Scoville 1976; Lucy 1976; Menietti and Fix 1978; Phillips 1979); while they differ in the extent to which they treat the details of grain formation, acceleration, destruction, and the transfer of radiation in the envelope, the models have in common the properties that the grain condensation radius R_c is located in the immediate vicinity of the flow sonic point, and that the calculated wind terminal velocity is approximately equal to the gravitational escape speed at $r = R_c$. This value is generally too high in comparison with observational results, unless provision is made for grain destruction by sputtering when the grains attain large drift velocities relative to the background gas (cf. Kwok 1975).

Note that in order to produce mass loss at rates $\gtrsim 10^{-7}$ $M_\odot$ yr^{-1}, it is necessary for grain condensation to occur fairly close to the stellar surface where the ambient gas density is high. There exist a variety of arguments (both theoretical and observational) which suggest that this is difficult to accomplish (see the reviews by Linsky 1981, and Cassinelli and MacGregor 1982 for detailed discussions). Dust formation is thought to require temperatures $\lesssim 10^3$ K; such values are unlikely to occur within several stellar radii of some stars which are observed to have both massive winds and relatively high effective temperatures (e.g., K giants and supergiants). Indeed, infrared observations of α Ori (Sutton et al. 1977) and the Mira variable IRc 10011 (Zappalla et al. 1974) suggest that most of the emitting dust surrounding these cool objects is located at distances >12 R_* and >3 R_* from the respective stars. Additional evidence supporting a subordinate dynamical role for dust grains comes from observations of chromospheric emission line asymmetries, extended chromospheres about red giant stars (Stencel 1982, this volume), and mass loss from hybrid stars, each of which indicates an outflow which originates or is underway in atmospheric layers having $T>10^3$ K. Moreover, Hagen (1978) has shown that mass loss rate estimates for M giants and supergiants are apparently insensitive to the dust-to-gas ratio in the wind, in contradiction to the behavior predicted by the dust-driven models. Finally, Castor (1981) has noted that the mass loss rate which can be produced by grains is approximately $\dot{M} \simeq \Delta L/CV_\infty$, where ΔL is the rate at which energy is radiated by the dust. Using measured values of ΔL for several M supergiants, he finds that the above estimate for $\dot{M}$ is generally less than the value derived from analysis of circumstellar absorption lines. On the basis of this and the foregoing results, we conclude that radiatively - accelerated dust grains appear to be unable to account for the observed properties of the winds from the majority of cool, low-gravity stars.

d). Shock Wave-Driven Winds

Observations of substantial mass loss from long-period (Mira) variable stars suggest that the outflow may be a consequence of stellar pulsation (Willson 1976; Slutz 1976; Wood 1979; Willson and Hill 1979). In this picture, the periodic compressional disturbances which are generated by the oscillation of the stellar surface propagate outward as shock waves. As noted by both Wood (1979) and Willson and Hill (1979), such discontinuities can give rise to mass ejection from atmospheric layers in which the gas density is sufficiently low that the propagating shocks behave adiabatically. An estimate of the mass loss rate attainable by this mechanism can thus be obtained by determining the density which characterizes the level at which adiabatic behavior begins (Willson and Hill 1979; Castor 1981). For this purpose, we adopt as an estimate of the flow time scale for the post-shock gas the time required to travel a distance equal to the local density scale height, $t_{flow} \sim a/g$, where a is the sound speed and g is the stellar gravity (it has been assumed that $V = a$ for the post-shock gas). Likewise, the cooling time is given by $t_{cool} \sim kT/N_H P_R(T)$, where $P_R(T)$ is the

radiative cooling coefficient. The onset of adiabatic behavior occurs when $t_{flow} \sim t_{cool}$, or when $N_H \sim gkT/aP_R(T)$. The resulting mass loss rate estimate is therefore

$$\dot{M} \sim 4\pi r^2 \mu N_H a \sim 4\pi GM_* \mu kT/P_R(T). \qquad (2)$$

Adopting $T = 10^4$K, $P_R(T) \approx 2.6 \times 10^{-24}$ erg cm^3 s^{-1} (Avrett and Hartmann 1982), it follows that $\dot{M} \sim 1.56 \times 10^{-11}$ (M/M$\odot$) M$\odot$ yr^{-1}. Although the estimate given above is somewhat low, it must be remembered that the results depend sensitively upon the magnitude of the cooling coefficient P_R, a quantity whose value in the present circumstances is poorly known. One as yet unsettled question concerning the mechanism is its applicability throughout the cool portion of the HR diagram, particularly for stars having lower luminosities and higher surface gravities than the Mira variables. Along these lines, Willson and Pierce (1982, this volume) have noted that in addition to directly accelerating atmospheric material, pulsationally-generated shock waves may also induce mass loss by supporting gas out to distances beyond which another mechanism (e.g., radiatively-accelerated dust grains; see also Jones et al. 1981) can initiate an outflow, or by heating the atmosphere to produce conditions under which thermally-driven mass loss can occur.

e). Alfvèn Wave-Driven Winds

The observation of large amplitude Alfvèn waves in the solar wind (Belcher and Davis 1971) suggests that such modes may also be present in the atmospheres of late-type stars having mechanically/magnetically heated chromospheres. Numerous authors have considered the dynamical consequences of the observed wave flux for solar coronal expansion (see, e.g., Belcher 1971; Jacques 1977, 1978), and it has been noted that undamped Alfvèn waves can drive a wind from stars having atmospheres too cool to undergo thermally-driven mass loss (Belcher 1971; Belcher and Olbert 1975).

The effect of an outwardly propagating flux of Alfvèn waves on the dynamics of winds from cool, low-gravity stars has been investigated by Hartmann and MacGregor (1980) (see also Haisch et al. 1980). For radial propagation in the absence of dissipation, it is found that the force due to waves is equal to the negative gradient of the wave energy density $\varepsilon = \delta B^2/8\pi$, where δB is the wave amplitude. In the limit that the wavelength of the disturbance is shorter than any of the scale heights in the background gas (i.e., the WKB limit), it can be shown that $\varepsilon \propto [M_A(1+M_A)^2]^{-1}$, where if $A = B/\sqrt{4\pi\rho}$ is the Alvèn speed, $M_A = V/A$ is the Alvènic Mach number (Parker 1965). For radially-directed magnetic field and flow, $M_A \propto \rho^{-\frac{1}{2}}$; as a result, ε is a decreasing function of distance from the star, and the waves exert an outward force on the gas. Physically, the outward decrease in ε (and the wave flux) appears locally as an increase in the streaming energy per unit mass of the flow, and results from the fact that the waves do work on the background medium (whose properties vary with distance) through which they propagate.

When thermal acceleration of the flow is negligible, critical point and energy conservation considerations can be used to approximately determine the initial and, terminal velocities, V_o and V_{oo}, of a wind driven by Alfvén waves. The results are

$$V_o \approx 2\left(\frac{r_o}{GM_*}\right)^{3/2}\left(\frac{\mathcal{E}_o}{\rho_o}\right)^2 , \qquad (3)$$

$$V_{oo} \approx \left[V_o^2 - \frac{2GM_*}{r_o} + \frac{2\mathcal{E}_o}{\rho_o}\left(\frac{3}{2} + \frac{1}{M_{Ao}}\right)\right]^{1/2} , \qquad (4)$$

in which r is the location of a reference level in the stellar atmosphere, and the subscript "o" denotes evaluation at r_o. For illustration, adopt the parameters $M_* = 16\ M_\odot$, $r_o = R_* = 400 R_\odot$, $N_o = 10^{11}\ cm^{-3}$, $\mu = 0.667\ M_H$, $B_o = 10$ G and $\delta B_o = B_o/\sqrt{10}$ (yielding an initial wave energy flux $\approx 3 \times 10^6$ erg cm^{-2} s^{-1}). Application of the above formulae yields $\dot{M} \approx 6.6 \times 10^{-7}\ M_\odot$ yr^{-1} and $V_{oo} = 379$ km s^{-1}. The results of detailed numerical calculations substantiate this result (cf. Hartmann and MacGregor 1980): namely, for energy fluxes $\sim 10^5 - 10^6$ erg cm^{-2} s^{-1}, Alfvén waves can initiate mass loss at rates $\gtrsim 10^{-8}\ M_\odot\ yr^{-1}$, but the resulting values of V_{oo} are significantly higher than observed.

One way to alleviate this difficulty is to include the effect of wave dissipation with a characteristic damping length $L \sim R_*$. Such a prescription causes most of the wave energy to be deposited near the base of the flow where the gas density is high. As a result, wind models calculated assuming $L = R_*$ exhibit reduced values of V_{oo}, but have mass loss rates which are nearly the same as these obtained in the case of undamped waves (cf. Hartmann and MacGregor 1980). While a number of plausible mechanisms for damping Alfvén waves in cool stellar winds exist, lack of knowledge concerning wave periods, propagating directions, and the strength and geometry of the stellar magnetic field precludes accurate determination of the dissipation length. However, the wave damping rates required to account for the observed wind properties imply that the flow is heated as well as accelerated; the effect of Alvén waves on the wind temperature distribution is considered in the following section.

III). Energy Balance in Wave-Driven Winds

a). Energy Equation

In the present section we consider the effect of Alvén wave dissipation on the thermal structure of winds from cool, low-gravity stars. The energy equation for a steady, spherically-symmetric outflow containing radially propagating Alfvén waves can be obtained by noting that the total energy flux (i.e., the sum of the wind, wave, conductive, and radiative

energy fluxes) is conserved. Neglecting thermal conduction, the resulting wind energy equation is (Hartmann and MacGregor 1982)

$$\frac{3}{2} NkV \frac{dT}{dr} = \Gamma - \Lambda - NkT \left(\frac{2V}{r} + \frac{dV}{dr} \right) , \qquad (5)$$

in which Γ and Λ are, respectively, the wave heating and radiative cooling rates (units: erg cm^{-3} s^{-1}). The quantity Γ is determined by noting that the rate at which thermal energy is added to the flow by wave dissipation is equal to the difference between the total rate of decrease of the wave energy flux and the rate at which the waves do work on the wind (Hollweg 1973). Using this prescription in the WKB limit, the time-averaged wave heating rate is found to be $\Gamma = \varepsilon(V+A)/L$, where ε is the wave energy density and L is the damping length. Note that by the discussion given above, $\Gamma = o$ in the absence of wave dissipation.

To complete the specification of the terms in the energy equation (5), we assume that the radiative cooling rate can be written in the form $\Lambda = N_H^2 P_R(T)$, where N_H is the total hydrogen number density and $P_R(T)$ is the radiative cooling coefficient. The quantity $P_R(T)$ is taken to be a function only of T, and is determined in the following way. For $T \lesssim 15{,}000K$, $P_R(T)$ is obtained by assessing the net radiative losses at different levels (corresponding to different temperatures) in model chromospheres computed for the star ε Gem (G8Ib) and the sun (Avrett and Hartmann 1982; see also Avrett 1981). At higher temperatures, the fit of Rosner et al. (1978) to the optically thin, collisional equilibrium cooling coefficient of Raymond is used.

b). Results

Using previously calculated dynamical solutions to determine V and dV/dr, the energy equation (5) has been integrated to obtain wind temperature distributions corresponding to several different values of the stellar surface gravity g. For each solution, $L = R_*$, $B_o = 3G$, $\delta B_o = B_o/\sqrt{10}$, and N_o is chosen such that the quantity $(\varepsilon o/L)/(\rho o GM_*/R_*^2)$ (a measure of the force ratio at the base of the flow) has the value 10^{-1}. The results for models having log g = -0.42, 0.75, and 1.79 are summarized in Table 1, which lists the initial Alfvén wave energy flux $F_o(\approx \varepsilon o Ao)$, the wind mass loss rate $\dot{M}$ and terminal velocity V_{oo}, and the maximum value of the temperature in the flow Tmax.

In order of increasing surface gravity, the solutions are characterized by the following values of $N_o(cm^{-3})$ and $T_o(K)$: $(N_o, T_o) = (1.69 \times 10^{10}, 5050)$, $(3.88 \times 10^9, 6250)$, $(3.51 \times 10^9, 7333)$.

The details of the energy balance throughout the wind are qualitatively the same for each of the models. Near the base of the flow, conditions appropriate to thermal equilibrium obtain, and T is determined by the local

balance between wave heating and radiative cooling, i.e., $\varepsilon(V+A)/L \approx N_H^2 P_R(T)$. The rapid acceleration of the wind in the immediate vicinity of the stellar surface causes N_H^2 to initially decrease outward faster than the wave energy flux $F \approx \varepsilon A$. Since $P_R(T)$ is an increasing function of T for $T \lesssim 10^5$K, the gas temperature at first increases with distance from the star. At larger, distances, however, the depletion of the wave energy flux due to the effect of dissipation causes T to decrease. Hence, the temperature distribution contains a maximum, which, for the models listed in Table 1 occurs at distances $\approx$ 2-3 R_*. As is apparent from the table, the value of Tmax increases with increasing g, a result due in large part to the assumed constancy of the wave dissipation length L. Ultimately, adiabatic cooling dominates the wind energy balance and $T \propto r^{-4/3}$. It is important to note, however, that this occurs quite far from the star; for the models listed above, the adiabatic cooling rate first exceeds the radiative cooling rate at distances $\approx$ 7-9 R_*. Heat conduction does not contribute significantly to the energy balance in any of the models, although the temperatures attained in the model having log g = 1.79 are sufficiently high that the thermal pressure gradient may become dynamically important.

Table 1. Wind Properties

M_* ($M_\odot$)	R_* ($R_\odot$)	Fo(erg cm^{-2} s^{-1})	$\dot{M}$ ($M_\odot$ yr^{-1})	V_∞ (km s^{-1})	Tmax (K)
7	707	2.23×10^5	6.96×10^{-7}	28	7,160
9	209	4.65×10^5	2.02×10^{-8}	66	19,430
1	21	4.89×10^5	1.99×10^{-10}	106	84,070

The results presented in Table 1 indicate that as the stellar surface gravity is increased, both V_∞ and Tmax increase while $\dot{M}$ decreases. We close this section by noting that: (i) this behavior is in qualitative agreement with the observed variation of wind thermal and dynamical properties in the cool portion of the HR diagram (cf. sec. I.); (ii) the heating which takes place as a consequence of requiring Alfvèn wave dissipation (cf. sec. III. e.) gives rise to wind temperature distributions which are consistent with recent observational evidence implying the existence of extended chromospheres surrounding late-type, low-gravity stars. The reader is referred to the papers by Hartmann and Avrett (1982) and Stencel (1982) (both contained in this volume) for further discussion of these points.

IV). Conclusion

In the preceding sections, we have briefly described a few of the mechanisms which have been suggested to account for winds from cool, low-gravity stars. Space limitations have prevented us from considering additional processes, such as winds driven by magnetic reconnection (Mullan

1980; Pneuman 1981) or the effects of spicular downflows on atmospheric energy balance and mass loss (Wallenhorst 1980, 1981). Where possible, the physical predictions of models based upon the proposed mechanisms have been compared with the results of observations. On the basis of this procedure, we conclude that although a number of suggestive agreements/disagreements exist between theory and observation, it is presently not possible to confidently identify a particular mechanism as being primarily responsible for mass loss from cool stars. Indeed, it may well be that the observed wind properties result from the combined effects of several of the processes considered above. Only continued theoretical and observational effort can reduce the number of quantitative uncertainties present in our current understanding of late-type stellar winds.

The author gratefully acknowledges numerous stimulating conversations concerning mass loss from stars with Drs. L. Hartmann, T. E. Holzer, A. J. Hundhausen, and E. N. Parker. The National Center for Atmospheric Research is sponsored by the National Science Foundation.

References

Athay, R. G. 1976, The Solar Chromosphere and Corona: Quiet Sun (Dordrecht: Reidel).

Avrett, E. H. 1981, in Solar Phenomena in Stars and Stellar Systems, ed. R. M. Bonnet and A. K. Dupree (Dordrecht: Reidel), p. 173.

Avrett, E. H., and Hartmann, L. 1982, in preparation.

Ayres, T. R., Linksky, J. L., Vaiana, G. S., Golub, L., and Rosner, R. 1981, Ap. J., 250, 293.

Belcher, J. W. 1971, Ap. J., 168, 509.

Belcher, J. W., and Davis, L. R. 1971, J. Geophys. Res., 76, 3534.

Belcher, J. W., and Olbert, S. 1975, Ap. J., 200, 369.

Belcher, J. W., and MacGregor, K. B. 1976, Ap. J., 210, 498.

Bernat, A. P. 1977, Ap. J., 213, 756.

Cassinelli, J. P., 1979, Ann. Rev. Astr. Ap., 17, 275.

Cassinelli, J. P., and MacGregor, K. B. 1982, to be published.

Castor, J. I. 1981, in Physical Processes in Red Giants, ed. I. Iben, Jr., and A. Renzini (Dordrecht: Reidel).

Dupree, A. K. 1981, in Proc. IAU Colloq. No. 59: Effects of Mass Loss on Stellar Evolution, ed. C. Chiosi and R. Stalio (Dordrecht: Reidel).

Dupree, A. K., and Hartmann, L. 1980, in Stellar Turbulence, IAU Colloq. No. 51, ed. D. F. Gray and J. L. Linsky (New York: Springer-Verlag), p. 279.

Gary, D. E., and Linsky, J. L. 1981, Ap. J., 250, 284.

Gehrz, R. D., and Woolf, N. J. 1971, Ap. J., 165, 285.

Gilman, R. C. 1972, Ap. J., 178, 423.

Goldberg, L. 1979, Quart. J. Roy. Astron. Soc., 20, 361.

Goldreich, P., and Scoville, N. 1976, Ap. J., 205, 144.

Hagen, W. 1978, Ap. J. Suppl. 38, 1.

_____ 1980, in Cool Stars, Stellar Systems and the Sun, ed. A. K. Dupree, Smithsonian Astrophysical Observatory Special Report No. 389, p. 143.

Haisch, B. M., Linsky, J. L., and Basri, G. S. 1980, Ap.J., 235, 519.

Hartmann, L. 1981, in Solar Phenomena in Stars and Stellar Systems, ed. R.M. Bonnet and A. K. Dupree (Dordrecht: Reidel), p. 331.

Hartmann, L., and MacGregor, K. B. 1980, Ap. J., 242, 260.

_____ 1982, in preparation.

Hartmann, L., Dupree, A. K., and Raymond, J. C. 1980, Ap. J. (Letters), 236, L143.

_____ 1981, preprint.

Hollweg, J. V. 1973, Ap. J., 181, 547.

Holzer, T. E. 1979, in Solar System Plasma Physics, ed. C. F. Kennel, L. J. Lanzerotti, and E. N. Parker (Amsterdam: North-Holland), p. 101.

_____ 1980, in Cool Stars, Stellar Systems, and the Sun, ed. A. K. Dupree, Smithsonian Astrophysical Observatory Special Report No. 389, p. 153.

Hundhausen, A. J. 1972, Coronal Expansion and Solar Wind (New York: Springer-Verlag).

Jacques, S. A. 1977, Ap. J., 215, 942.

_____ 1978, Ap. J., 226, 632.

Jones, T. W., Ney, E. P., and Stein, W. A. 1981, Ap. J., 250, 324.

Jura, M., and Morris, M. 1981, Ap. J., 251, 181.

Knapp, G. R., Phillips, T. G., and Huggens, P. J. 1980, Ap. J.(Letters), 242, L25.

Kwok, S. 1975, Ap. J., 198, 583.

Linsky, J. L. 1980, Ann. Rev. Astr. Ap., 18, 439.

_____ 1981, in Proc. IAU Collq. No. 59: Effects of Mass Loss on Stellar Evolution, ed. C. Chiosi and R. Stalio (Dordrecht: Reidel).

Lucy, L. B. 1976, Ap. J., 205, 482.

Maciel, W. J. 1976, Astro. Ap., 48, 27.

_____ 1977, Astr. Ap., 57, 273.

Menietti, J. D., and Fix, J. D. 1978, Ap. J., 224, 961.

Mewe, R. 1979, Space Sci. Rev., 24, 101.

Mullan, D. J. 1980, in Cool Stars, Stellar Systems and the Sun, ed. A. K. Dupree, Smithsonian Astrophysical Observatory Special Report No. 389, p. 189.

Parker, E. N. 1963, Interplanetary Dynamical Processes (New York: Interscience).

_____ 1965, Space Sci. Rev., 4, 666.

Phillips, J. P. 1979, Astr. Ap., 71, 115.

Pneuman, G. W. 1981, preprint.

Reimers, D. 1975, in Problems in Stellar Atmospheres and Envelopes, ed. B. Baschek, W. H. Kegel, and G. Traving (Berlin: Springer), p. 229.

Rosner, R., Tucker, W. H., and Vaiana, G. S. 1978, Ap. J., 220, 643.

Salpeter, E. E. 1974, Ap. J., 193, 585.

Sanner, F. 1976, Ap. J. Suppl., 32, 115.

Skumanich, A. 1972, Ap. J., 171, 565.

Slutz, S. 1976, Ap. J., 210, 750.

Soderblom, D. R. 1981, preprint.

Stencel, R. E. 1978, Ap. J.(Letters), 223, L37.

Stencel, R. E., and Mullan, D. J. 1980, Ap. J., 238, 221.

Sutton, E. C., Storey, J. W. V., Betz, A. L., Townes, C. H., and Spears, D. L. 1977, Ap. J.(Letters), 217, L97.

Ulmschneider, P. 1979, Space Sci. Rev., 24, 71.

Vaiana, G. S. et al., 1981, Ap. J., 245, 163.

Wallenhorst, S. G. 1980, Ap. J., 241, 229.

_____ 1981, Ap. J., 249, 176.

Weber, E. J., and Davis, L. 1967, Ap. J., 148, 217.

Weiler, E. J., and Oegerle, W. R. 1979, Ap. J. Suppl., 39, 537.

Weymann, R-1962a, Ap. J., 136, 476.

_____ 1962b, Ap. J., 136, 844.

_____ 1978, in Proc, IAU Colloq. No. 42, The Interaction of Variable Stars With Their Environment, ed. R. Kippenhahn, J. Rahe, and W. Stroheimer, Pub. Bamberg Obs., p. 577.

Willson, L. A. 1976, Ap. J., 205, 172.

Willson, L. A., and Hill, S. J. 1979, Ap. J., 228, 854.

Willson, O. C., 1959, Ap. J., 130, 499.

_____ 1966, Science, 151, 1487.

Wood, P. R. 1979, Ap. J., 227, 220.

Zappalla, P. R., Becklin, E. E., Matthews, K., and Neugebauer, G. 1974, Ap. J., 192, 109.

1980 ROCKET CORONAGRAPH MEASUREMENTS OF THE SOLAR WIND ACCELERATION REGION

George L. Withbroe and John L. Kohl
Harvard-Smithsonian Center for Astrophysics

Richard H. Munro
NCAR High Altitude Observatory

and

Heinz Weiser
Harvard-Smithsonian Center for Astrophysics

ABSTRACT

Spectroscopic measurements of temperatures, densities and flow velocities in the solar wind acceleration region provide critical empirical constraints on solar/stellar wind theory. Preliminary results of an analysis of H I Lyman-alpha and white light measurements made on 16 February 1980 in a polar coronal region are reported. The hydrogen kinetic temperatures in the observed region were found to be nearly constant with $T_{HI} \gtrsim 10^6$ K at heliocentric distances between 1.5 and 4 $R_\odot$. The outflow velocities were found to be subsonic indicating that the critical point in the observed region was located at $r \gtrsim 4\ R_\odot$.

1. INTRODUCTION

The solar corona provides a critical testing ground for theoretical models of stellar winds generated in hot coronal envelopes. The objective of the Center for Astrophysics/High Altitude Observatory coronagraphs program is to measure temperatures, densities and outflow velocities in the solar wind acceleration region. Measurements of these parameters place empirical constraints on mechanisms for plasma heating, solar wind acceleration and the transport of mass, momentum and energy in the solar corona and also provide empirical constraints on solar/stellar wind theory.

2. INSTRUMENTATION

The instruments consist of a pair of coronagraphs that are carried above the UV absorbing layers of the terrestrial atmosphere by a Black Brandt V sounding rocket. A white light coronagraph measures the intensity and polarization of the electron-scattered white light corona and thereby acquires information on coronal structures and electron densities. A UV coronagraph measures the intensity and profile of the resonantly scattered component of the H I Lyman-alpha coronal radiation. Even though only about one proton in 10^7 is in the form of neutral hydrogen at coronal temperatures, there are sufficient H I atoms to resonantly scatter a measurable amount of chromospheric

Lyman-alpha radiation. Coronal Lyman-alpha provide a direct measurement of the hydrogen velocity distribution (along the line of sight) which specifies the hydrogen kinetic temperature. The ratio of the Lyman-alpha intensity and white light intensity provides information on solar wind outflow velocities via Doppler dimming as described below.

The rocket coronagraphic instruments have been flown twice, on 13 April 1979 and on 16 February 1980. Results of the first flight have been reported by Kohl et al. 1980 and Withbroe et al. 1982. The present paper reports preliminary results of the 1980 flight. The primary objective on this flight was to observe, near solar maximum, a coronal hole located at the south solar pole. Coronal holes are thought to be a primary source of solar wind, particularly high speed solar wind streams (cf. Zirker 1981); consequently, coronagraphic determinations of plasma parameters of these features are of considerable importance.

3. TEMPERATURES

Figure 1 shows a profile measured at a distance $r = 1.8\ R_\odot$ from sun center in the southern polar region. The profile illustrates the high quality data that can be obtained with a UV coronagraphic instrument. The observations (solid line) can be fit very nicely with a Gaussian profile (dashed line) suggesting that the velocity distribution of the hydrogen atoms in the line of sight was nearly Maxwellian. The theoretical profile has lower intensities in the line wings, however, until a more detailed analysis of the data is completed, we will not know whether or not this is significant. It is important to note that thermalization times are long in the solar wind acceleration region. For example, the proton-proton thermalization time is 100 seconds at $r = 1.8\ R_\odot$ and 1000 sec at $r = 3.0\ R_\odot$. Consequently plasma heating or energy transport mechanisms that introduce non-thermal components in the particle velocity distribution can produce non-Gaussian profiles. Thus, measurements of spectral line profiles provide constraints on possible mechanisms operating in the solar wind acceleration region. How tight the constraints are depends on whether or not a given mechanism produces a significant non-Maxwellian component in the particle velocity distribution.

Profiles were measured at several positions ρ on a radius vector directed along the axis of a coronal hole that was centered on the south solar pole. The parameter ρ is the distance measured in solar radii from sun-center to the point where the line of sight intersects the plane of the solar disk. The profiles measured at $\rho = 1.5$, 2.5 and 3.0 $R_\odot$ had nearly identical widths implying that the hydrogen kinetic temperature was nearly constant ($T_{HI} \approx 10^6$) over the height range where the line profiles were formed $r = 1.5 - 4\ R_\odot$. The points in Figure 2 are the temperatures determined from the line profiles. These points are plotted at the radii ($r = 1.7$, 3.1 and 3.8 $R_\odot$) corresponding to the mean heights where the radiation observed at $\rho = 1.5$, 2.5 and 3.0 $R_\odot$ originated (see Withbroe et al. 1982). The magnitude of the error estimates given depend upon the uncertainties in fitting the profiles with a Gaussian curve and the uncertainties in the correction for the effects of geocoronal

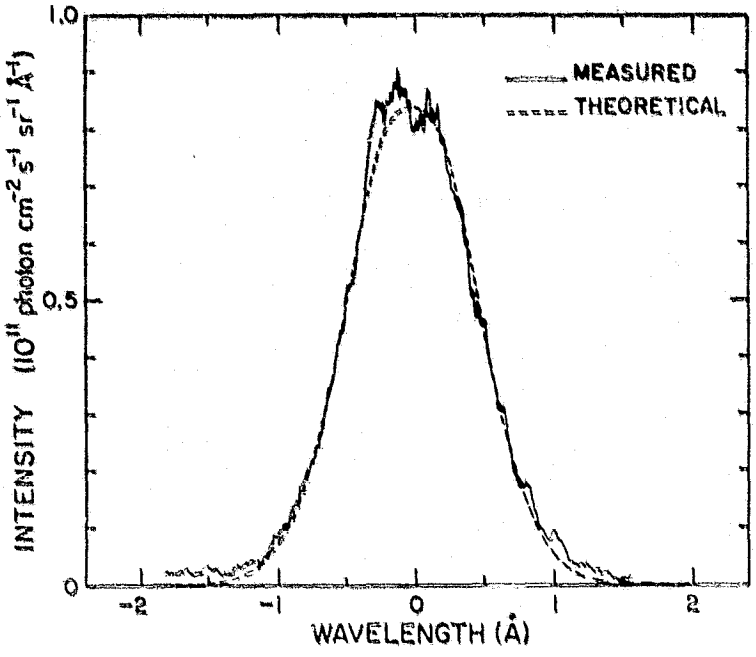

Figure 1. A comparison of empirical (solid line) and theoretical (dashed line) profiles of the resonantly scattered component of hydrogen Lyman-alpha. The theoretical profile has been convolved with the instrumental profile which has a FWHM = 0.35 A.

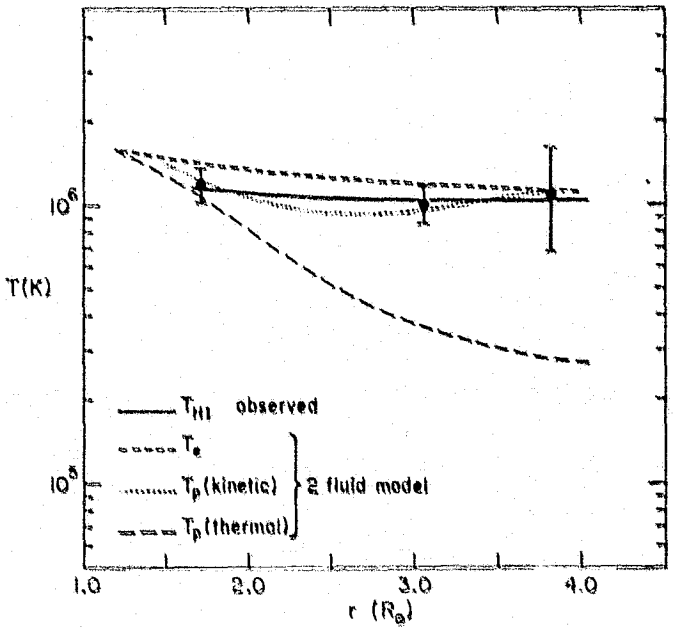

Figure 2. Temperature as a function of radius. The observed values (points) yield the variation with radius of the hydrogen kinetic temperature (solid line). Two fluid model results are: electron temperature (short dash line), proton thermal temperature (long dash line) and proton kinetic temperature (dotted line, see text).

emission/absorption near line center (cf. Withbroe et al. 1982). The solid line is the inferred run of temperature. It should be emphasized that this is a kinetic temperature and includes the effects of both thermal and non-thermal motions broadening the Lyman-alpha line profiles.

For comparison we have plotted temperatures predicted by a simple two fluid model with no plasma heating above the base of the corona (cf. Hartle and Sturrock 1968, Nerney and Barnes 1977, Hollweg 1978). The short dash line gives the run of electron temperature with radius, while the long dash line gives the predicted proton thermal temperatures. The electron and proton temperatures diverge with height due to the rapid decrease in electron-proton coupling with decreasing density. The electron temperature has a shallow temperature gradient due to the high thermal conductivity of electrons, while the proton temperature falls off nearly adiabatically. We obtained an estimate of the electron temperature from the ratio of the Lyman-alpha and white light intensities. This ratio depends on the ionization equilibrium of hydrogen which is a function of the electron temperature (see Gabriel 1971). The value obtained, 1.5×10^6 K for $r = 1.7\ R_\odot$, provides a boundary condition for the assumed two fluid model.

Because of the strong coupling between coronal hydrogen atoms and protons (due to charge exchange, see Holzer 1977) in the observed height range, one expects the hydrogen and proton kinetic temperatures to be equal. The lack of agreement between the observed coronal hydrogen kinetic temperatures and the calculated proton thermal temperatures indicates that the assumed model is inadequate. One way of bringing the calculated and observed temperatures into agreement is to increase the rms velocity of the protons. There are several ways of accomplishing this. One way is through extended proton heating in the region 1.5 to 4 $R_\odot$. Addition of thermal energy by a mechanism with an energy dissipation length of about 4 $R_\odot$ could explain the observations. A similar conclusion was obtained for observations of an unstructured "quiet" region of the solar corona acquired during the 1979 flight of the coronagraphs. See Withbroe et al. (1982) for details.

Energy carried by waves could also be contributing to the rms motions of the protons. Consider Alfven waves which have been suggested as a possible source of energy and momentum for plasma heating and/or solar wind acceleration in coronal holes (see review by Hollweg 1981). For non-dissipating Alfven waves Hollweg gives $N^{1/2} < v^2 >$ = constant where v is the rms velocity amplitude of the waves. If the rms velocity is specified at one height, then this relationship can be used to calculate the rms velocities at other heights from the measured variation of density N with height. The dotted line gives the predicted proton kinetic temperature obtained by assuming

$$T_p\ (\text{kinetic}) = T_p\ (\text{thermal}) + T_A$$

with

$$T_A = m\langle v^2 \rangle / 2k = m \times \text{constant}/2kN^{1/2}$$

where the constant was adjusted to give the best fit to the observations. The adopted value of the constant corresponds to $v_{rms} = 115$ km/sec at $r = 4\ R_\odot$.

The fit between the calculated and observed kinetic temperatures is sufficiently good to suggest that plasma motions due to Alfven waves may be contributing significantly to the broadening of the H I Lyman-alpha line. The shapes of the line profiles, which are nearly Gaussian, place a constraint on the spectrum of these Alfven waves, if they are present. It is important to note that there are other explanations for the nearly constant width of the Lyman-alpha line, such as the above mentioned extended proton heating. In order to distinguish between thermal and non-thermal line broadening mechanisms, additional empirical constraints are needed, such as measurements of spectral lines from ions with different masses (see Kohl and Withbroe 1982).

4. FLOW VELOCITIES

As indicated in the introduction the ratio of the intensities of the hydrogen Lyman-alpha line and the white light continuum provides an empirical constraint on possible values of the solar wind outflow velocities in the observed region. The intensity of the hydrogen Lyman-alpha line is due to resonant scattering of chromospheric Lyman-alpha radiation. In a static atmosphere the central frequency of the coronal scattering profile is identical to that of the chromospheric spectral line. However, in a region with solar wind flow, the coronal scattering profile is Doppler shifted with respect to the chromospheric profile, hence there is less optimum scattering resulting in a reduction in the intensity of the scattered radiation. This effect is known as Doppler dimming (see Beckers and Chipman 1974, Withbroe *et al.* 1981 and references cited therein). The measured ratio of the intensities of the Lyman-alpha line and the white light continuum was nearly independent of height. This indicates that the flow velocity of the plasma emitting the observed Lyman-alpha and white light radiation was less than about 150 km/sec, that is, the velocities were sufficiently low that the Lyman-alpha line was not significantly affected by Doppler-dimming (*cf.* Kohl and Withbroe 1982).

In order to define the limits on the outflow velocities more carefully, we compared the measured Lyman-alpha intensities with those calculated from a series of coronal models (see Figure 3). The intensity of the scattered Lyman-alpha radiation depends on the width of the coronal scattering profile, the number of neutral hydrogen atoms in the line of sight (which can be calculated from the electron density and the electron temperature which determines N_{HI}/N_e) and the solar wind velocity. The width of the scattering profile was measured and the electron densities were determined from measurements of the polarization and brightness of the white light corona. The electron temperature at $r = 1.7\ R_\odot$ was determined from the observations as discussed earlier and for other heights was assumed to vary as $r^{-2/7}$ (*e.g.* the same as in Figure 2). Use of a model with an isothermal electron temperature yields similar results due to the insensitivity of the Lyman-alpha intensity to variations in the electron temperature. For the radial variation of the solar wind velocity V we assumed a constant outward particle flux NVr^2. The upper curve in Figure 3 is for a static atmosphere. The other curves show the predicted Lyman-alpha intensities for models with different outward particle fluxes parameterized by the velocity at $r = 4\ R_\odot$. At low heights where the density is high and solar

wind velocity is low there is little Doppler dimming. However, due to the predicted steady increase in flow velocity with increasing height, the amount of Doppler dimming increases with height causing the intensity to diverge from that calculated for the static model. A comparison of the calculated intensities with those measured confirms that the amount of Doppler dimming over the observed range of heights is small, corresponding to flow velocities at r = 4 $R_\odot$ less than about 150 km/sec. Given that the sound speed for a corona with T_e = 1 to 1.5 x 10^6 K is 130 to 160 km/sec, the observations suggest that the solar wind flow in the observed plasma was subsonic for r < 4 $R_\odot$ and thus that the critical point was at r $\lesssim$ 4 $R_\odot$. We are developing a more detailed inhomogeneous model from ground-based synoptic coronal data, 1980 eclipse measurements and data from the rocket coronagraphs. Results from application of this model will be reported in a subsequent paper.

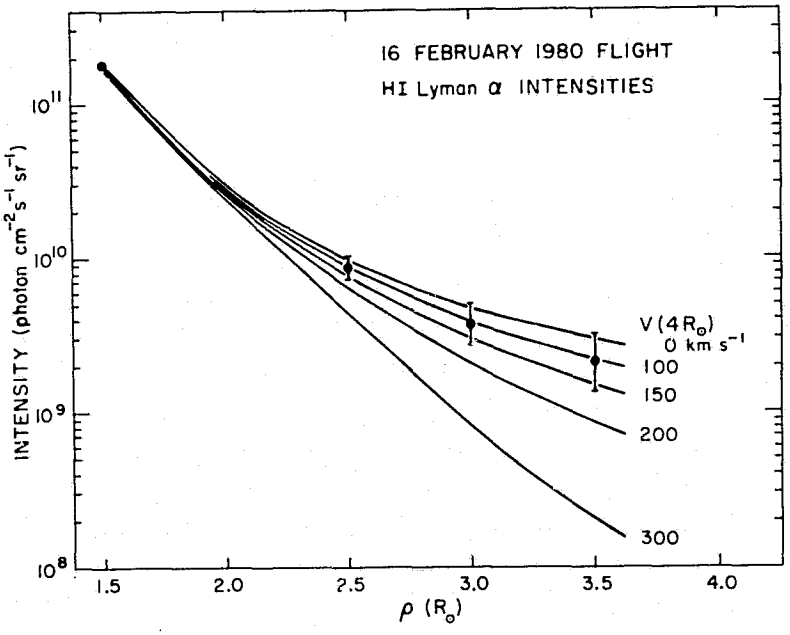

Figure 3. Lyman-alpha intensity as a function of radius. Observed values (points). Solid lines give values calculated for models with different solar wind particle fluxes parameterized here by the wind velocity at 4 $R_\odot$. The estimated uncertainty in the model fits is given by the error bars on the points.

In order to provide tighter constraints on the magnitude of the solar wind flow velocities within a few solar radii where subsonic flows have been observed on the two flights of the rocket coronagraphs, the UV coronagraph is being modified to measure the O VI resonance lines at λ1032 and λ1037. These lines are much more sensitive to low speed flows (30 $\lesssim$ V $\lesssim$ 100 km/sec) than the Lyman-alpha line (see Kohl and Withbroe 1982). The first flight of the modified coronagraphic instrument is scheduled for the spring of 1982.

5. SUMMARY

For the polar region observed at solar maximum in February 1980 we obtained the following empirical constraints on theoretical models for the solar wind acceleration region:

- nearly Gaussian H I Lyman-alpha profiles
- nearly constant hydrogen kinetic temperature with T_{HI} (kinetic) $\gtrsim 10^6$ K for $1.5 \lesssim r \lesssim 4\ R_\odot$
- subsonic flow for $r < 4\ R_\odot$ (critical point at $r \gtrsim 4\ R_\odot$)
- an upper limit of 130 km/sec for the rms velocity of waves capable of broadening the Lyman-alpha line for $1.5 \lesssim r \lesssim 4.0\ R_\odot$
- some evidence for extended proton heating or a non-thermal contribution to the motions of H I atoms in the observed region.

Future observations with the rocket coronagraphs are expected to provide additional information about the physical conditions in the solar wind acceleration region and thereby provide additional empirical constraints on solar/stellar wind theory.

Acknowledgements

This work was supported by NASA under grant NSG 5128 to the Harvard College, under Order No. W-13,998 to the High Altitude Observatory and by the Langley-Abbot program of the Smithsonian Institution.

REFERENCES

Beckers, J. M. and Chipman, E. 1974, Solar Phys., 34,151.
Gabriel, A. H. 1971, Solar Phys., 21, 392.
Hartle, R. E. and Sturrock, P. A. 1968, Ap. J., 151, 1155.
Hollweg, J. V. 1978, Rev. Geophys. Space Phys., 16, 689.
Hollweg, J. V. 1981, The Sun as a Star, NASA SP-450, ed. S. Jordan, p.355.
Holzer, J. 1977, Rev. Geophys. Space Phys., 15, 467.
Kohl, J. L., Weiser, H., Withbroe, G. L., Noyes, R. W., Parkinson, W. H., Reeves, E. M., Munro, R. H. and MacQueen, R. M. 1980, Ap. J., 241, L117.
Kohl, J. L. and Withbroe, G. L. 1982, Ap. J., in press.
Nerney, S. and Barnes, A. 1977, Rev. Geophys. Space Phys., 15, 467.
Withbroe, G. L., Kohl, J. L., Weiser, H. and Munro, R. H. 1981, submitted to Solar Phys.
Withbroe, G. L., Kohl, J. L., Weiser, H., Noci, G. and Munro, R. H. 1982, Ap. J., in press.
Zirker, J. B. 1981, The Sun as a Star, NASA SP-450, ed. S. Jordan, p.131.

D11

THE IONIZATION STATE IN A GAS WITH A NON-MAXWELLIAN ELECTRON DISTRIBUTION

S.P. Owocki and J.D. Scudder

High Altitude Observatory and Goddard Spaceflight Center

The inferred degree of ionization of a gas is often used in astrophysics as a diagnostic of the gas temperature. In the solar transition region and corona, in the outer atmospheres of cool stars, and in some portions of the interstellar medium), photoionization can be neglected, and the ionization state is fixed by the balance between ion-electron collisional ionization and dielectronic and/or radiative recombination. Under these conditions, higher degrees of ionization result from higher energy ion-electron collisions which are common in a high temperature gas, and the degree of ionization is thus a reasonable temperature diagnostic.

Actually, ionization occurs through collisions with electrons that have kinetic energies greater than the ionization potential of the given ion, and so the ionization rate depends on to the number of such high-energy electrons in the tail of the electron velocity distribution (Roussel-Dupre 1979). High-velocity electrons move across large distances between effective coulomb collisions, and, in a strong temperature or density gradient, the tail can be overpopulated relative to Maxwell-Boltzmann distribution of equivalent energy density (Scudder and Olbert 1979, 1981; Shoub 1981). Under these circumstances, the ionization rate can also be greatly increased. We illustrate these effects for a parameterized form of the electron distribution function with an enhanced high-velocity tail, namely the "kappa distribution".

Ionization in the Kappa Parameterization

Scudder and Olbert (1981) have shown that expected variations in the non-equilibrium properties of the electron distribution function f can often be well represented by changes in a generalized Lorentz function with a single parameter κ, i.e.

$$f_\kappa = \frac{A_\kappa}{\pi^{3/2} v_p^3}\left[1+\frac{1}{\kappa}\frac{v^2}{v_p^2}\right]^{-(\kappa+1)} , \qquad (1)$$

where v_p is the most probable speed and A_κ is a normalization constant given by,

$$A_\kappa = \frac{\Gamma(\kappa+1)}{\kappa^{3/2}\Gamma(\kappa-\frac{1}{2})} , \qquad (2)$$

and where $\Gamma(\kappa+1)\equiv\kappa!$ is the gamma (factorial) function (cf. Abramowitz and Stegun 1972, p. 255). This normalized "kappa " distribution is plotted in fig. 1 for various values of the parameter κ; note that for $v \lesssim \sqrt{\kappa} v_p$ the number of particles can be closely fit by a Maxwellian distribution, whereas for $v \gg \sqrt{\kappa} v_p$ the distribution declines as a velocity power law of index $\alpha=2\kappa+2$. The prominence of the power law tail diminishes with increasing κ, and it can be shown that, as $\kappa\to\infty$, the distribution approaches a Maxwellian.

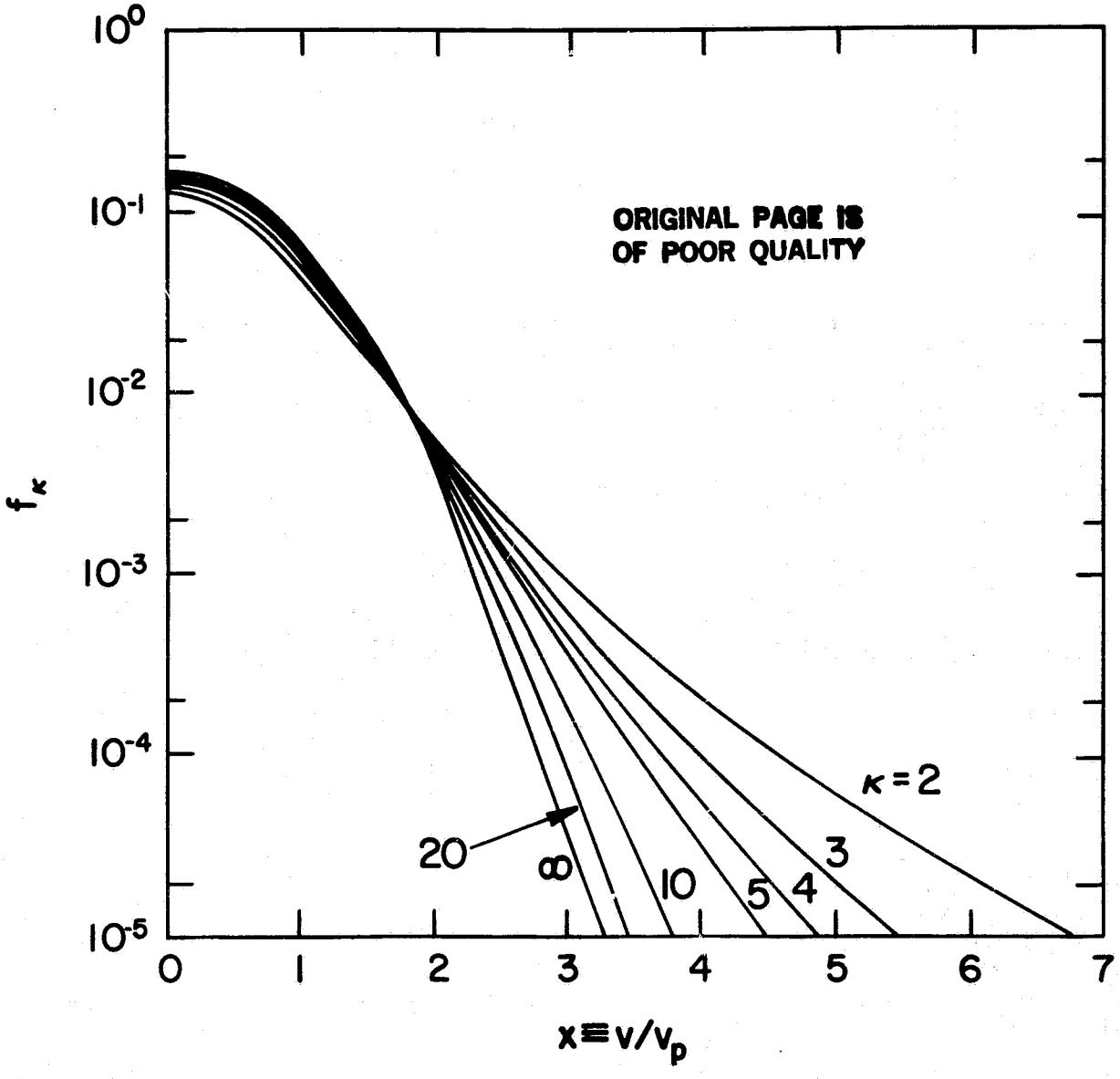

Fig. 1. Kappa electron velocity distribution function f_κ vs. electron speed v in units of the most probable speed v_p.

The electron-impact collisional-ionization rate in a given distribution of electrons can be generally written in the form $n_e \langle \sigma v \rangle$, where n_e is the overall number density of electrons, the angular brackets denote an average over the electron distribution in particle speed v, and the ionization cross section σ

varies with speed as $\sigma(v)\sim\frac{\ln(v/v_o)}{v^2}$, where v_o is the ionization threshold speed (see e.g. Lotz 1967). We can then define the rate enhancement β in a given isotropic, but non-equilibrium velocity distribution f relative to the rate in a Maxwellian distribution $f_m=(m_e/2\pi kT)^{3/2}\exp^{-(m_e v^2/2kT)}$ at a temperature T,

$$\beta \equiv \frac{\langle \sigma v\rangle_{non-th}}{\langle \sigma v\rangle_{th}} = \frac{\int_{v_o}^{\infty} v\ ln(v/v_o) f dv}{\int_{v_o}^{\infty} v\ ln(v/v_o) f_m dv}$$

$$=4\pi\frac{\sqrt{2\pi kT/m_e}}{E_1(\varepsilon_o)}\int_{v_o}^{\infty} v\ ln(v/v_o) f dv \quad , \tag{3}$$

where k is Boltzmann's constant, E_1 is the first exponential integral (cf. Abramowitz and Stegun 1972, p.228), and $\varepsilon_o\equiv\chi/kT$ is the ratio of ionization potential to thermal energy of the Maxwellian.

Performing the integral in eqn. (3) for a kappa distribution with a temperature T (defined in terms of the second velocity moment of the distribution), we find,

$$\beta_\kappa = A_\kappa\frac{x_o}{\sqrt{\varepsilon_o}}\left[\frac{\kappa}{x_o^2}\right]^\kappa\frac{{}_1F_2(\kappa,\kappa;\kappa+1;-\kappa/x_o^2)}{\kappa\, E_1(\varepsilon_o)} \quad , \tag{4}$$

where ${}_1F_2$ is the Gauss hypergeometric function (cf. Abramowitz and Stegun 1972; p. 556), and $x_o\equiv v_o/v_p$ is the ratio of ionization threshold speed to the most probable speed of the kappa distribution. For integer kappa, the definite integral represented by the hypergeometric function is most easily evaluated as a finite series through repeated integration by parts (cf. Gradshteyn and Ryzhik 1979; eqn. 2.111.3, p. 58).

In fig. 2 the kappa distribution rate enhancement $\beta_\kappa(T)$ relative to a Maxwellian with the same kinetic temperature T is plotted versus the ratio of ionization potential to thermal energy $\varepsilon_o\equiv\chi/kT$. Note that the enhancements can be very large for high ionization potentials (i.e. $\beta_\kappa\gg1$ when $\varepsilon_o\gg1$), but that there can also be rate reductions for moderate ionization potentials (i.e. $\beta_\kappa<1$ when $\varepsilon_o\approx1$). This rate reduction reflects the fact that the electrons in the enhanced high-velocity tail far above threshold are actually less effective at ionization than those of lower energy closer to the distribution core.

Effect on Specific Ionization Temperature Diagnostics

We thus see that ionization rates in a plasma with a non-equilibrium electron distribution can be substantially higher than in an equilibrium plasma with same density and temperature, and this implies that the possibly non-equilibrium nature of the plasma should be taken into account when using information on the ionization state to infer the gas temperature. As a specific example, we consider here the errors in inferred ionization temperatures that can occur for the balances $O^{+6}\leftrightarrow O^{+7}$ and $Fe^{+11}\leftrightarrow Fe^{+12}$ under conditions representative of those in the solar corona. Although the lower level of each exchange is the most abundant stage in an equilibrium balance at a typical coronal temperature of $1.5\times10^6\ ^\circ K$ (Jordan 1969, 1970), the oxygen ionization threshold energy $\chi_{O+6}=739eV$ is actually more than twice that of iron $\chi_{Fe+11}=331eV$.

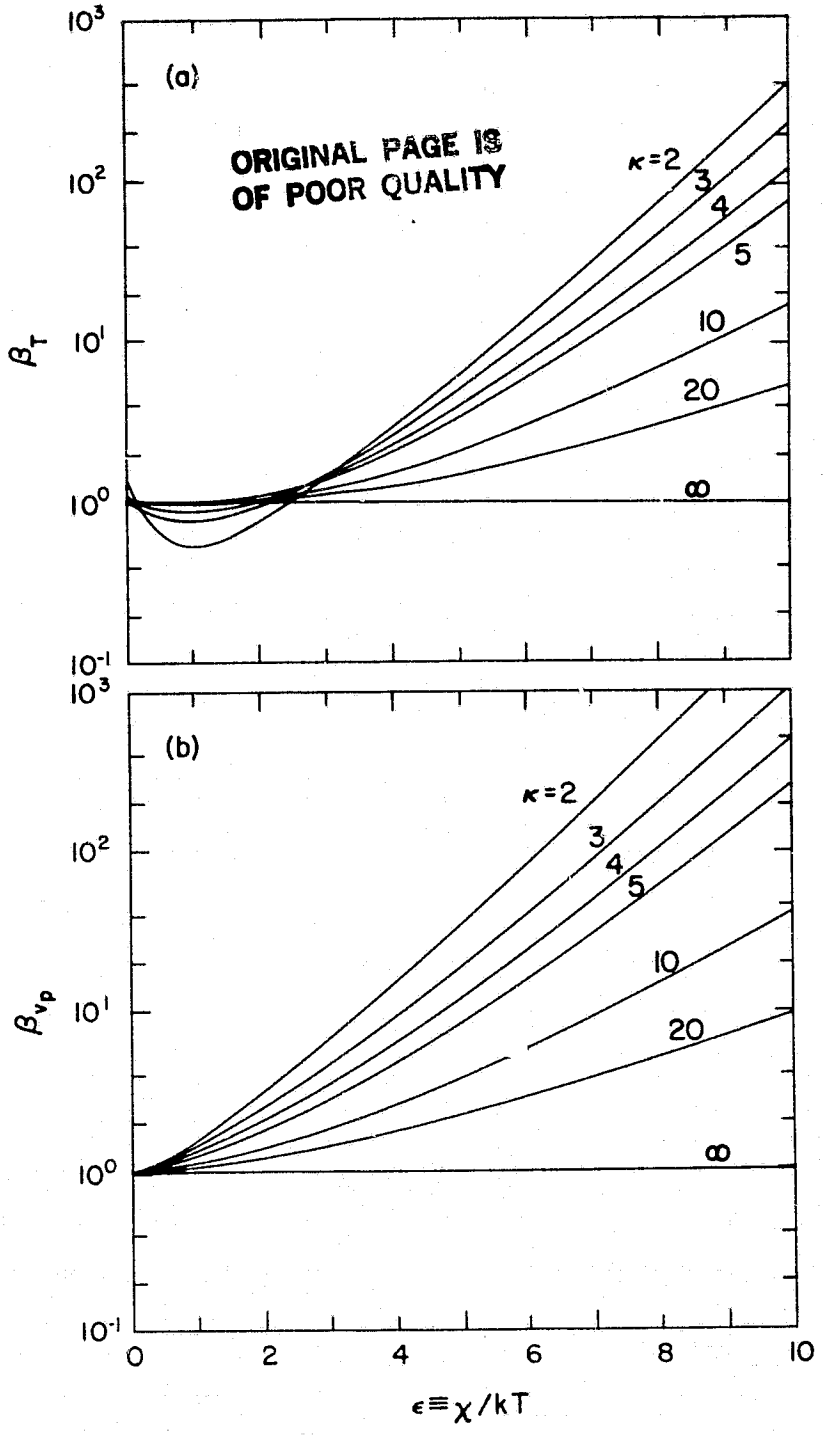

Fig. 2. a. Ionization rate enhancement $\beta_\kappa(T)$ of a kappa distribution relative to a Maxwellian with the same temperature T. b. Ionization rate enhancement $\beta_\kappa(v_p)$ of a kappa distribution relative to a Maxwellian with the same most probable speed v_p.

In table 1 are given the errors ΔT in inferring the true kinetic temperature $T=1.5\times10^6$ °K of a kappa distribution from the oxygen and iron ionization state if the non-equilibrium character of the distribution is neglected. Because of its higher threshold potential, the ionization of oxygen is much more sensitive to the high-velocity electrons and thus shows generally much larger temperature errors. In calculating the ionization temperature error ΔT, we have included any changes in recombination rate, although these changes were never large because recombination is most sensitive to low-energy electrons in the relatively unaltered distribution core. These results indicate that the oxygen ionization state is not as good a temperature diagnostic as that of iron for plasmas of coronal temperatures.

Table 1: Ionization Temperature Errors for Kappa Distribution at 1.5×10^6 °K

Kappa	*Temperature Error* ΔT $(10^{6}$° $K)$ $Fe^{+11} \leftrightarrow Fe^{+12}$	$O^{+6} \leftrightarrow O^{+7}$
2	*-0.19*	*0.75*
3	*-0.08*	*0.80*
4	*-0.02*	*0.65*
5	*0.00*	*0.53*
10	*0.02*	*0.29*
20	*0.01*	*0.16*
∞	*0.00*	*0.00*

Summary

Since collisional ionization in a plasma occurs through ion-electron collisions at energies above a given ionization threshold potential, ionization rates can be greatly increased by an enhancement in the number of electrons in the high-velocity tail of the electron velocity distribution. In astrophysical plasmas with strong gradients in temperature and/or density, such high-velocity tail enhancements may be common, and so ionization by non-equilibrium electrons may be important to interpreting properly the inferred ionization state in many astrophysical contexts. Specifically, the ionization rate in a non-equilibrium "kappa distribution" can be enhanced by as much as a factor of 10^{+3} relative to a Maxwell-Boltzmann distribution of equivalent energy density, and errors in inferred ionization temperatures can be as large as a factor of two. The relative importance of the high-velocity tail to a given ionization balance depends on the relative magnitude of the appropriate ionization potential and the mean thermal energy of electrons. In particular, the rather high ionization threshold for the oxygen balance $O^{+6} \leftrightarrow O^{+7}$ implies that the oxygen ionization in the solar corona is more sensitive to a non-equilibrium electron distribution than the ionization state of other elements (e.g. iron) with lower ionization potentials. A comparison of the ionization state of species with different ionization potentials (e.g. oxygen and iron) could therefore yield information on the form of the electron distribution function in plasmas at coronal temperatures.

REFERENCES

Abramowitz, M. and I.A. Stegun 1972, *Handbook of Mathematical Functions*, Tenth Printing, U.S. Government Printing Office, Washington

Gradshteyn, I.S. and I.M. Ryzhik 1979, *Table of Integrals, Series, and Products*, Twelfth Printing, Academic Press, New York

Jordan, C. 1969, The ionization equilibrium of elements between carbon and nickel, *M.N.R.A.S.*, **142**, 501

Jordan, C. 1970, Ionization equilibria for high ions of Fe and Ni, *M.N.R.A.S.* **148**, 17

Lotz, W. 1967, Electron impact ionization cross-sections and ionization rate coefficients for atoms and ions, *Astrophys. J. Suppl.*, **14**, 207

Roussel-Dupre, R. 1979, Ph. D. Thesis, Univ. of Colo., Boulder

Scudder, J.D. and S. Olbert 1979, A theory of local and global processes which affect solar wind electrons: I. The origin of typical 1 AU velocity distribution functions -- steady state theory, *J. Geophys. Res.*, **84**, 2755

Scudder, J.D. and Olbert, S. 1981, submitted to *Astrophys. J.*

Shoub, E.C. 1981, Electrons in a temperature gradient: I. Breakdown of LTE in the solar transition region and chromosphere, submitted to *Astrophys. J.*

D/2

MODIFICATION OF AVERAGE CORONAL PROPERTIES IN THE PRESENCE OF PERIODIC TEMPERATURE AND DENSITY VARIATIONS NEAR THE BASE

STEVEN T. SUESS*

Time-dependent flow in the solar corona has been modeled using an implicit time-differencing solution to the equations of motion for single-fluid, spherically symmetric, radial flow. No ad hoc extended energy or momentum addition is invoked in the present study. Instead, collisional thermal conduction is included (Spitzer, 1967) allowing local dynamic modifications to or by the temperature field low in the corona to also have effects on the flow field in the mid- and outer corona due to the very rapid propagation speed of a thermal pulse. The solution algorithm (Beam and Warming, 1976), new to solar wind studies (Suess, 1982), is an efficient method for including the effects of thermal conduction in a time-dependent model.

In the case of a transient motion in the corona, it is usually (but not always) the case that thermal conduction allows energy to be transported away from compression regions and into rarefaction regions. Thus, a simple compression (rarefaction) propagating upwards through the lower boundary of the computation mesh would generally carry with it a local temperature excess (deficit). Energy is, in the form of heat, conducted out of (into) the compression (rarefaction), tending to diminish the local amplitude of the propagating disturbance. This effect is here called conductive damping of the motion. Conductive damping, and the consequences on the average flow field of conductively re-distributed energy are the topics of the present study.

A particular example has been treated here. First, a steady solution for solar wind flow is found for a given set of steady boundary conditions, between 1.4 and 28 solar radii. These boundary conditions are that the density is 1.6xE06 cm-3 and the temperature is 1.6xE06 degrees. The flow profiles for this initial state are those shown at t=0 in the figures. Then, at t=0, periodic, in phase, sinusoidal variations in temperature and density are initiated and continued indefinitely. The amplitudes of the variations are 5 percent and 7.5 percent for the temperature and density respectively, imposed at 1.4 solar radii. The variations have a period of 1 hour -- shorter than a coronal transit time, but sufficiently long for the disturbances to propagate for small distances (2-3 solar radii). These oscillations are like those that might occur for acoustic oscillations, although no explanation is offered here as to how an acoustic oscillation might extend to this radius in the first place. The present example suffices to demonstrate conductive damping and alteration of average coronal properties that existed prior to the periodic variations in temperature and density that are imposed at the boundary.

The presence of oscillatory accoustic wave-like motions low in the corona represents an energy input to the solar wind. Thus, the average solar wind energy flux in the outer corona must also increase. What is found here is the relative distribution of this energy in its various forms. Specifically, due to conductive damping, essentially none of the input energy flux

remains in the form of oscillatory motion beyond 4-5 solar radii. Instead, average properties of the flow are modified. At 14.5 solar radii, the average solar wind flow speed is increased by about 5 percent, from ∿ 290 km/s to ∿ 305 km/s, and the average temperature is increased by about 10 percent, from ∿ 1.13xE06 deg to ∿ 1.25xE06 deg. This is in the presence of a pressure variation of ∿ 13 percent and an average flow speed of 22 km/s at 1.4 solar radii. Due to the large propagation speed of a thermal pulse under the present assumptions, the temperature variation is communicated to all radii in a very short time. However, it takes ∿ 15 hours for a new flow state to be established at 15 solar radii.

Figure 1 shows results of the modeling as plotted versus radius. The top panel shows the temperature at t=0, 10, and 20 hours, by which time the new, but now time-dependent, flow state has been established. The curves at t=10 and t=20 hours have been offset upwards by 100,000 and 200,000 deg respectively in order to avoid confusing overlap at small radii. The middle panel shows a similar plot of the velocity at t=0, 10, and 20 hours, with offsets of 50 and 100 km/s respectively at t=10 and 20 hours. The bottom panel shows a plot of the relative density variation versus radius at 20 hours. The relative density is defined as the difference between the density at 20 hours and 0 hours, divided by the density at 0 hours. The plot is done in this manner because the density variations never exceed 25 percent, whereas the absolute density changes by three orders of magnitude between 1.4 and 10 solar radii. The overall density variation is shown in figure 2, with curves plotted again for t=0, 10, and 20 hours.

In considering the results shown in figures 1 and 2, it is important to realize that the t=10 and 20 hour curves are plotted at the same phase with respect to the boundary condition oscillation at 1.4 solar radii, and so the variation with radius is subject to a stroboscope effect. Figure 3 circumvents this difficulty by showing the temporal variations of the flow parameters at several radii. The three panels show the variation over the interval from t=0 to t=20 hours of the temperature, velocity, and density, respectively in the top, middle, and bottom panels. The five curves in each panel correspond to the variations at the base - 1.4 solar radii, at 2.1, 3.7, 7.0, and 14.5 solar radii with the curves at these radii labeled as shown in the legend.

Figures 1 and 2 demonstrate the increase in average temperature and flow speed beyond 5 solar radii at the expense of the wave motion, but with negligible modification to the density beyond 5 solar radii. Figure 3 also illustrates this effect in the relatively large upward drift in the average temperature at 7.0 and 14.5 solar radii between t=0 and t=10 hours, and a smaller but similar drift in the average velocity. Close examination of the temperature variations also shows the large, but finite propagation speed of the thermal pulses. Each oscillation of the temperature can be followed outward in radius, but with a small phase shift to the right. The decreasing amplitude of the temperature oscillations demonstrates the conversion of energy in the thermal oscillations into kinetic energy.

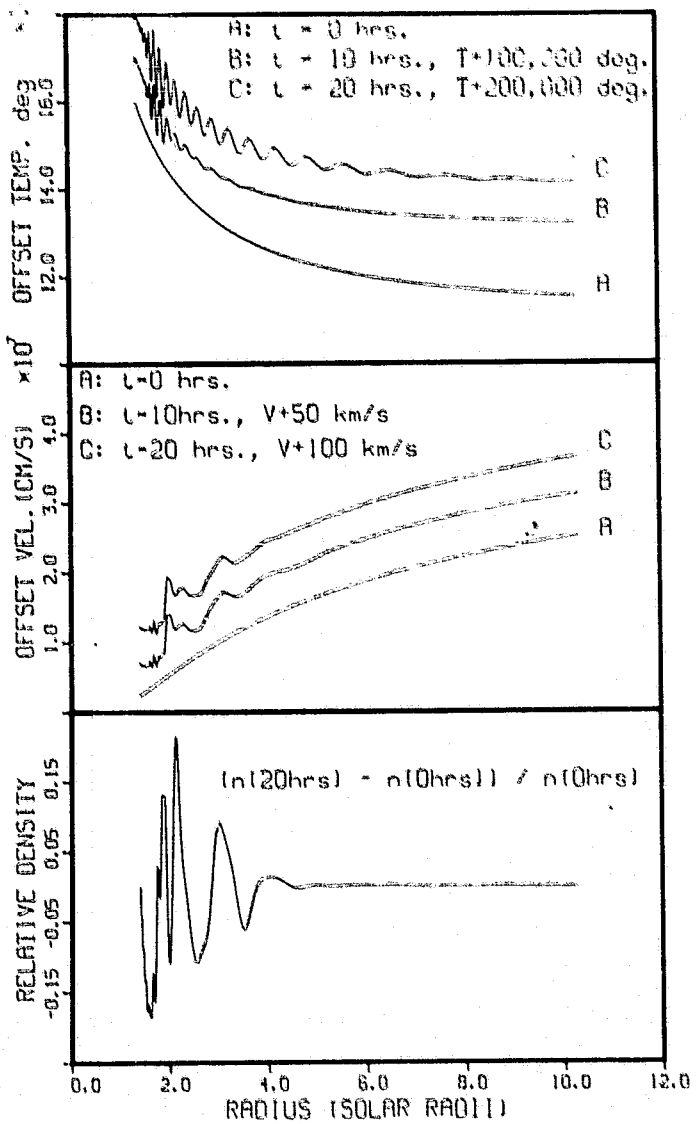

Figure 1. Radial variation of the flow field variables. Top panel; temperature at t=0, 10 and 20 hours with 10 and 20 hour curves offset upwards by 100,000 and 200,000 degrees respectively to avoid confusing overlap at small radii. Middle panel; velocity at t=0, 10 and 20 hours with 10 and 20 hour curves offset upwards by 50 km/s and 100 km/s respectively. Bottom panel; variation of the density at 20 hours relative to the density at t=0 hours, normalized to the t=0 density.

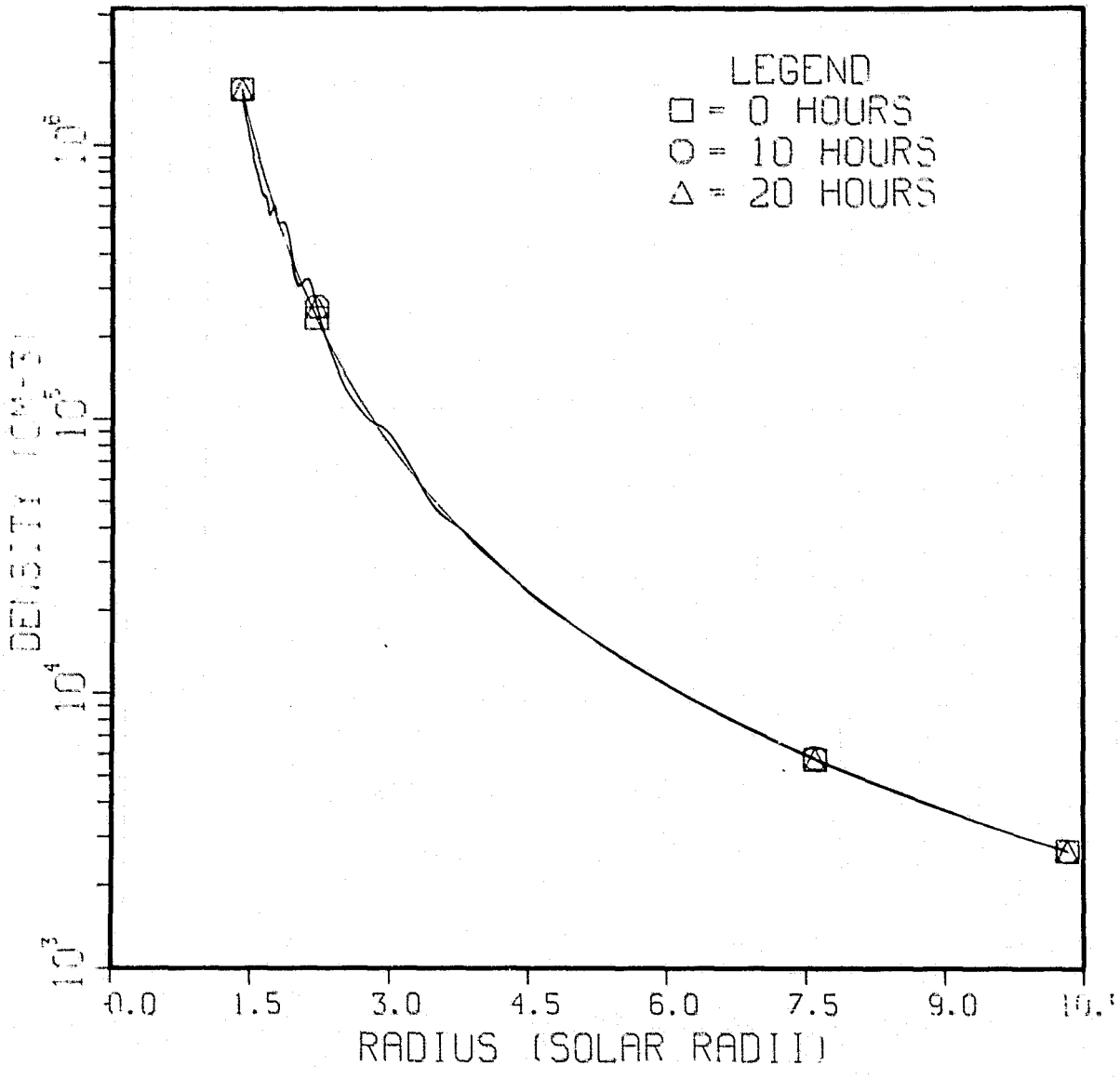

Figure 2. Radial variation of the absolute density at t=0, 10 and 20 hours. The curves, although nearly indistinguishable, are labeled individually as shown in the legend. This figure demonstrates the standard fall-off of the density with radius, upon which the oscillations are superimposed.

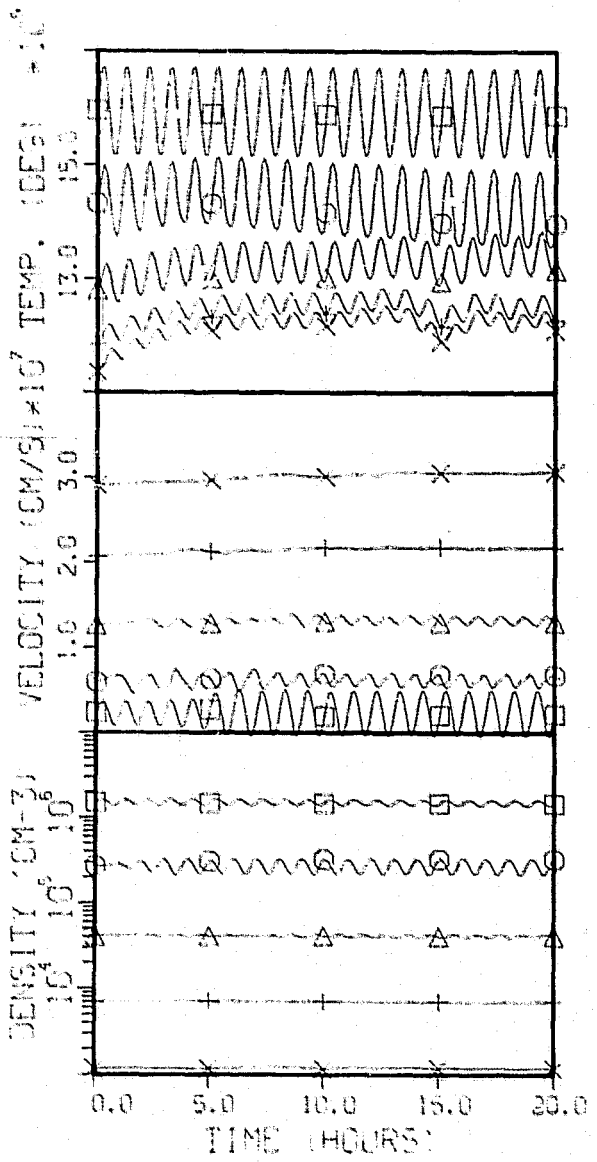

Figure 3. Temporal variations of the flow field variables at 1.4, 2.1, 3.7, 7.0 and 14.5 solar radii -- labeled as indicated in the legend. Top panel; temperature versus time. Middle panel: velocity versus time. Bottom panel; density versus time.

The velocity oscillations show steepening with distance between 1.4 and 2.1 solar radii. However, by 3.7 solar radii the velocity oscillations have been so strongly damped that steepening no longer exists and the oscillations have essentially disappeared by 7.0 solar radii -- as one would expect by the modification to average flow parameters at these larger distances. One interesting feature of the velocity variations at 1.4 solar radii is that at the minimum temperature and density, which corresponds in phase to the minimum in velocity, the velocity is actually momentarily negative. This momentary return toward the surface shows that a 13 percent pressure variation at 1 hour period corresponds to a rather strong acoustic oscillation.

The density oscillations appear to grow in amplitude between 1.4 and 2.1 solar radii, as seen in the bottom panel of figure 3. Again, this growth is arrested by conductive damping to result in only very small oscillations at 3.7 solar radii, and essentially none by 7.0 solar radii.

DISCUSSION

The obvious motivation for the just-described modeling exercise is as a preliminary investigation of the energetics of coronal expansion using a new numerical tool for the study of wave effects. As such, the model suffers from several deficiencies such as (i) starting at a too-large radius, (ii) use of a collisional description of thermal conduction at radii far larger than is justified, (iii) invoking acoustic waves at radii larger than such waves are generally thought to exist, and (iv) the magnetic field is neglected. On the other hand, it is also generally believed that energy deposition in the outer corona is necessary to produce at least the high-speed portion of the solar wind (Suess et al., 1977; Hundhausen, 1977). This energy deposition is an unresolved problem. Holzer (1979), in assuming the possibility that magneto-acoustic waves are responsible, suggests that conversion of wave into flow field energy could involve a two-step process, in which the wave flux is converted into a thermal conduction flux that in turn is converted into a bulk flow energy flux. Holzer also suggested the alternative to this is a direct conversion into kinetic energy with the thermal conduction flux always being a small fraction of the total energy flux. Both of these possibilities are slightly different than the description given by Kopp (1977) of the classical hypothesis that wave motion is converted to bulk flow energy either through viscous dissipation or through wave pressure. In the present model, wave pressure is explicitly accounted for through solution of the complete equations of motion. However, viscous dissipation is not an explicit part of the model.

What the present model does do is to show that any waves with a compressive component (i.e. magnetoacoustic waves) will be conductively damped or, in the words of Holzer, energy conversion will tend to take place in a two-step process via the thermal conduction energy flux and into bulk flow energy. This conversion would tend to take place in the range of 1.5-5.0 solar radii for waves with periods comparable to one hour. This is not to say that such a mechanism would necessary be the dominant mode of damping for magnetoacoustic waves -- but it is an effective mode in the absence of more efficient mechanisms.

Although extended studies are necessary, and have not yet even been initiated, it can be suggested that longer period oscillations or perturbations will be yet more effective in flow acceleration. In a separate description of the algorithm used to solve the equations in this model (Suess, 1982), an example was given invoking a single transient in the corona, caused by an instantaneous increase in the base temperature. In that example, it was possible, for relatively low base densities and starting at 1.0 solar radii, to raise the temperature in front of the transient to values equal to the base temperature of 2.0xE06 degrees. Conversely, behind the transient the temperature was reduced to less than 1.5xE06 degrees. This was the result of a "refrigerator-like" action of the passing transient. Compression low in the corona resulted in enhanced temperatures which, in turn caused a thermal pulse to propagate into the outer corona. The resultant energy loss from the low corona then temporarily produced the diminished temperatures until conduction could fill in the deficit from lower yet in the corona. A similar process is occurring in the present model, except that it is going on continuously in the presence of the train of waves coming up from the base of the computation mesh.

Even in the absence of thermal conduction, a polytropic model produces an analagous phenomenon of increased termperature in the compression region and a reduction in temperature behind the compresssion, in the rarefaction (Wu et al., 1975). However, the energy transfer to radii outside the compression region does not exist, and hence energy transfer from conduction to kinetic occurs over a longer time scale.

The present model was begun at 1.4 solar radii because of the negative velocities being produced at the bottom of each pressure oscillation. In principle, it is necessary to alter the manner in which the boundary condition is treated at the base, in the presence of negative velocities. The extremely short duration of the negative values in the present example, however, allows them to be tolerated with negligible effect on the accuracy of the overall computation. To lower the base of the computation to near 1.0 solar radii will probably require re-writing the analysis to utilize boundary conditions on the velocity and either temperature or density, rather than the temperature and density, to avoid the possibility of negative flows. Alternatively, it would be necessary to set up a switching condition that altered the computation mode in the presence of negative flows -- and the mathematical approach to this method is not necessarily well defined. Both of these approaches will be examined in a more comprehensive analysis.

A simpler extension to deal with is the introduction of alternate forms of the thermal conduction energy flux to account for the non-collisional nature of the plasma beyond a few solar radii. It is possible to utilize several alternative hypotheses for treating the flux within the framework of the numerical model. It is obvious that desirable consequences will almost always result because conduction of thermal energy to the outer corona and then a confinement from effective escape further into the interplanetary medium will improve the efficiency with which the solar wind flow speed is increased in most cases.

I would like to thank Prof. John Wilcox for a generous invitation to visit the Institute for Plasma Research for the 1980-81 academic year. This year was used to develop the numerical techniques used in the present examples. This work was supported in part by the National Aeronautics and Space Administration under Grant NGR 05-020-599 and Contract NA55-24420, by the Division of Atmospheric Sciences, Solar-Terrestrial Research Program of the National Science Foundation under Grant ATM77-20580, by the Max C. Fleischmann Foundation, and by the National Center for Atmospheric Research, which is sponsored by the National Science Foundation, for computer time used in this research.

*Institute for Plasma Research
Via Crespi
Stanford University
Stanford, California 94303

*Department of Commerce
NOAA/ERL/Space Environment
Laboratory
Boulder, Colorado 80303

REFERENCES

Beam, R. M., and Warming, R. F. 1976, J. Comput. Phys., 22, 87.

Holzer, T. E. 1979, Solar System Plasma Physics, vol. 1, Solar and Solar Wind Plasma Physics, E. N. Parker, C. F. Kennel and L. J. Lanzerotti (eds.), North-Holland, Amsterdam, ch.3, section 3.1.5.

Hundhausen, A. J. 1977, Coronal Holes and High Speed Wind Streams, J. B. Zirker (ed.), Colorado Associated Univ. Press, ch. 7, sect. 4.

Kopp, R. A. 1977, Coronal Holes and High Speed Wind Streams, J. B. Zirker (ed.), Colorado Associated Univ. Press, ch. 6, sec. 4.

Spitzer, L., Jr. 1967, Physics of Fully Ionized Gases, Interscience, New York.

Suess, S. T. 1982, submitted to Astrophys. J..

Suess, S. T., Richter, A. K., Winge, C. R., and Nerney, S. F. 1977, Astrophys. J., 217, 296.

Wu, S. T., Dryer, M, McIntosh, P. S., and Reichmann, E. 1975, Solar Phys., 44, 117.

D13

Dependence of Open Stellar Coronal Regions on Coronal Heating

Reiner Hammer

Joint Institute for Laboratory Astrophysics
University of Colorado and National Bureau of Standards
Boulder, CO 80309

Abstract

Models of open regions in hot stellar coronae are presented. For a given star these regions depend on the total amount ϕ_{Mo} of coronal heating and on the characteristic length L over which this energy is dissipated. The height of the temperature maximum is mainly determined by L. The coronal temperature, the mass loss rate, and the relative fraction of wind energy losses increase strongly with L as long as L is much smaller than the stellar radius. For large L, however, these quantities are only weak functions of L, while they still increase with increasing ϕ_{Mo}. Thus, if the heating occurs close to the stellar surface, the open coronal regions are cool, and most of the energy is used for radiation. Extended coronal heating, on the other hand, leads to hot coronal regions with small base pressure and predominating energy losses due to stellar wind (for large ϕ_{Mo}) and/or outward thermal conduction (for small ϕ_{Mo}).

I. Methods

Hot, solar-like coronae are known to exist around main-sequence stars of spectral type later than early F, giants of not too late type, and possibly helium-rich white dwarfs. By analogy to the Sun these coronae are expected to consist of both magnetically closed, loop-like structures and open coronal regions. In open regions thermally driven stellar wind contributes to the coronal energy losses in addition to radiation and thermal conduction. For a given star the relative importance of these terms is obviously controlled by the total amount and by the spatial distribution of coronal heating.

In order to investigate this dependence, I computed a series of theoretical models of open coronal regions. For simplicity possible effects of magnetic fields, nonspherical symmetry, and external momentum sources were neglected. The energy equation included the terms due to stellar wind, optically thin radiation, classical thermal conduction, and mechanical heating. As the detailed physics of the heating of stellar coronae is presently not

known, the absorption of mechanical energy flux ϕ_M was described by the equation

$$\phi_M = \phi_{Mo} \exp\left(-\frac{r-R}{L}\right) \quad , \qquad (1)$$

where L is the damping length, r is the radial distance, and ϕ_{Mo} is the total amount of mechanical energy flux that enters the transition region and corona at their base r = R. This heating law has often been used in the literature (e.g., Lamers and Kuperus 1974; Kuperus and Chiuderi 1976; Kopp and Orrall 1976). Tests showed that more sophisticated heating laws yield qualitatively the same results (Hammer 1981, 1982b).

The boundary conditions were those proposed by Couturier, Mangeney, and Souffrin (1979); namely, both the temperature and the conductive flux at the base of the transition region are assumed to be small compared to their maximum values in the inner corona, the solutions go through the Parker critical point, and they have vanishing temperature at infinity. The numerical method to solve this boundary value problem is described elsewhere (Hammer 1982a), along with an investigation of the influence of the boundary conditions.

Models of this type depend on four parameters; namely, the stellar mass and radius, the total amount ϕ_{Mo} of coronal heating, and the damping length L which describes where the energy is deposited. As the details of coronal heating are not known, both parameters ϕ_{Mo} and L have been varied over two orders of magnitude. The following results refer to solar mass and radius; however, there exists a variable transformation which allows us to apply them to arbitrary stars by simply scaling the axes of the figures (Hammer 1981; 1982c).

II. Results and Discussion

The dependence of the coronal temperature on the damping length is illustrated in Figure 1. It shows the temperature vs. height for three models in which the same mechanical energy flux ϕ_{Mo} is dissipated with different values of the damping length L. With increasing L the coronal temperature is seen to be larger, and the temperature maximum (indicated by a circle) lies at greater heights. This can be explained as follows. In the lower part of the transition region the temperature is lowest, therefore the density is highest, and radiation is efficiently produced. Further, some energy is required to heat up the outflowing stellar wind material. These energy losses due to radiation and enthalpy can not be balanced by local mechanical heating, because the lower transition region is very thin compared to the damping length L over which the energy dissipation occurs. Therefore, they have to be supplied by thermal conduction from above. Only at heights which are comparable to the damping length can mechanical heating become efficient and balance the down-

ward conductive flux, thus producing the temperature maximum. As up to this point the temperature continues to rise, this explains why both the height of the temperature maximum and the coronal temperature increase with increasing damping length (cf. Endler, Hammer and Ulmschneider 1979).

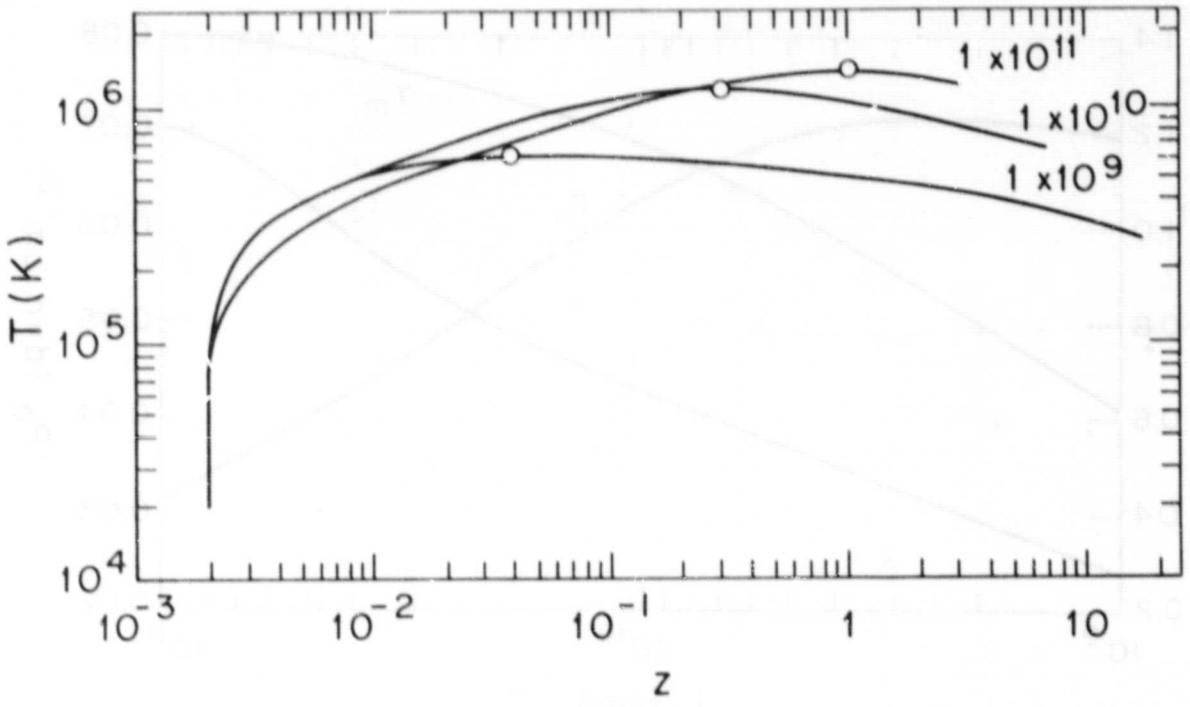

Fig. 1. Temperature T as function of height z (in units of the stellar radius; the reference level z = 0 has been chosen at 2×10^{-3} below the base of the transition region). The models have the same amount of mechanical energy flux $\phi_{Mo} = 1 \times 10^5$ ergs cm^{-2} s^{-1}, but different values of the damping length L (in cm). The temperature maxima are indicated by circles.

This behavior is more clearly shown in Figure 2. Both the maximum temperature T_m and the temperature T_c at the critical point increase monotonically with L. However, while for small L the increase of T_m is rather strong, it is much weaker when L is comparable to the stellar radius (i.e., 7×10^{10} cm in the present case). It can be shown (Hammer 1981) that there are two reasons for this saturation. Firstly, for large L the energy losses occurring below the temperature maximum, like radiation of the transition region, decrease in favor of the energy losses which occur above the temperature maximum, like the outward thermal conduction losses and part of the wind losses (see below). Therefore, less conductive flux has to be transported inward to

balance the energy losses of the lower atmosphere. Secondly, as soon as L (and thus the height of the temperature maximum) is comparable to the stellar radius, this inward conductive flux is geometrically diluted. Both effects reduce the temperature gradient and thus also the temperature at that height where the heating suffices to produce the temperature maximum.

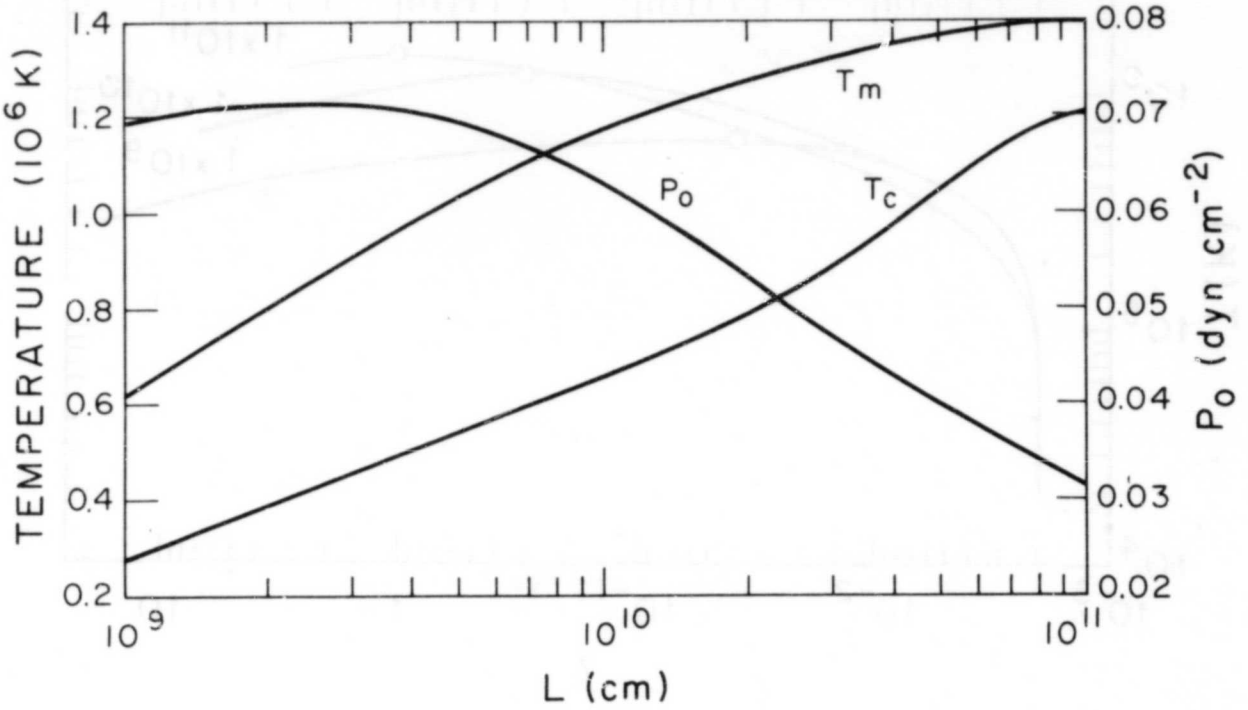

Fig. 2. Maximum coronal temperature T_m, temperature T_c at the critical point, and pressure p_o at the base of the transition region as functions of L for constant $\phi_{Mo} = 1 \times 10^5$ ergs cm^{-2} s^{-1}.

In addition to the coronal temperature, Figure 2 shows also the pressure p_o at the base of the transition region. It has a flat maximum for relatively small damping lengths.

The global coronal energy balance is illustrated in Figure 3 which shows, as a function of the damping length, the relative fractions of the total mechanical energy that are used for radiation, outward thermal conduction, and stellar wind.

The outward heat conduction at the critical point increases with L. This is mainly caused by (Hammer 1981) the increase of the temperature at the critical point (cf. Fig. 2) and thus of the thermal conductivity.

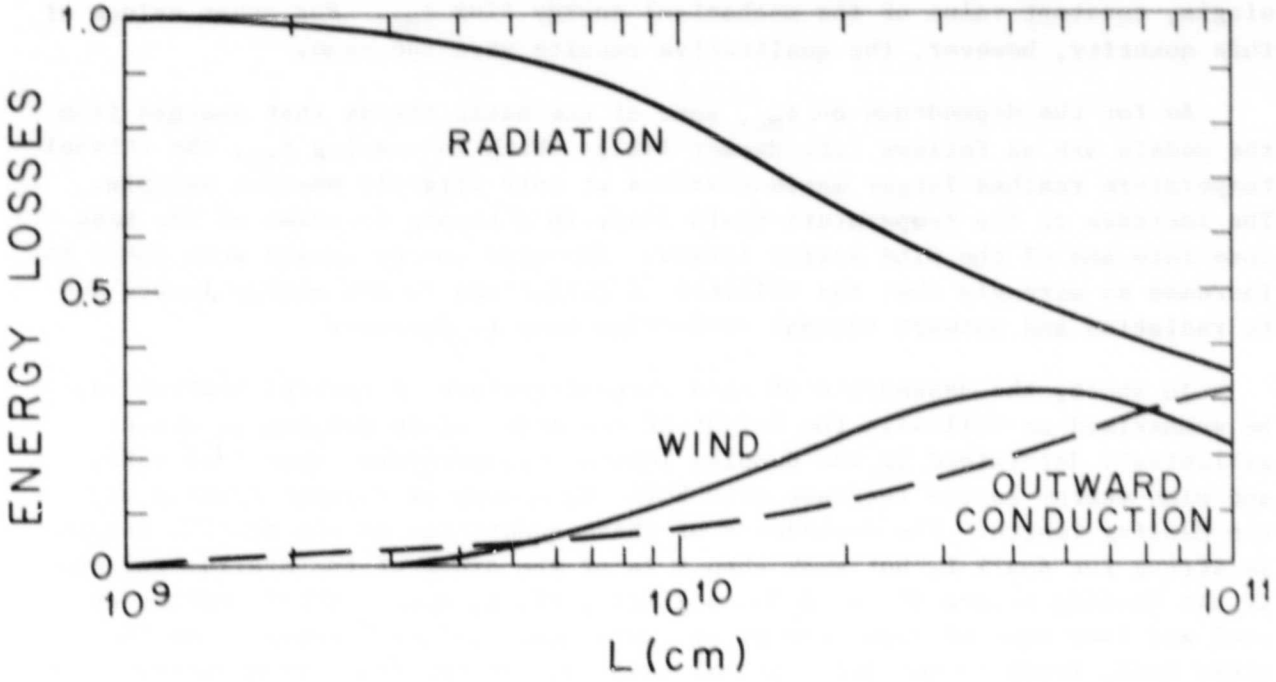

Fig. 3. Radiation and wind energy losses between the base of the transition region and the critical point and outward conductive energy losses at the critical point. All energy losses are normalized to the constant value $\phi_{Mo} = 1 \times 10^5$ ergs cm^{-2} s^{-1} of the mechanical energy flux.

The wind losses increase very strongly with L as long as L is small, while for large L they are only weakly dependent on the damping length. Incidentally, the same behavior was found for the mass loss rate. Therefore, the mass loss rate and the contribution of the wind energy losses depend in the same way on the damping length as the coronal temperature shown in Figure 2. This strong correlation between coronal temperature and stellar wind, however, is no surprise, it has already been explained by Parker (1958).

The increase of the sum of outward conductive and stellar wind energy losses, finally, explains the monotonic decrease of the radiative losses. As the radiative losses, in turn, depend strongly on the density and thus on the pressure, this explains also the decrease of p_o towards large L in Figure 2.

When comparing Figures 2 and 3, one should, therefore, notice the correlation between, firstly, the pressure and the radiative losses; secondly, the average coronal temperature and the wind losses; and thirdly, the temperature at the critical point and the outward thermal conductive losses.

So far we have only discussed the influence of the damping length L for a single, constant value of the mechanical energy flux ϕ_{Mo}. For other values of this quantity, however, the qualitative results were the same.

As for the dependence on ϕ_{Mo}, some of the basic trends that emerged from the models are as follows (cf. Hammer 1981): With increasing ϕ_{Mo}, the coronal temperature reaches larger maximum values at only slightly smaller heights. The increase of the temperature again leads to a strong increase of the mass loss rate and of the wind energy losses. The wind energy losses were found to increase so strongly that the relative contributions to the energy losses due to radiation and outward thermal conduction have to decrease.

In short, the dependence of open coronal regions on coronal heating can be summarized as follows. The height of the temperature maximum is almost exclusively determined by the damping length. Temperature, mass loss rate, and wind energy losses increase with both the amount of coronal heating and the damping length. The dependence of these quantities on the damping length is strong for small L, but weak when L is of the order of the stellar radius. If the heating occurs close to the stellar surface, open coronal regions are cool and lose most of their energy by radiation. Extended heating, on the other hand, leads to hot open coronal regions, and the dominating energy losses are stellar wind (if the total amount ϕ_{Mo} of heating is large) and/or outward thermal conduction (if ϕ_{Mo} is small).

References

Couturier, P., Mangeney, A., and Souffrin, P. 1979, Astr. Ap. 74, 9.
Endler, F., Hammer, R., and Ulmschneider, P. 1979, Astr. Ap. 73, 190.
Hammer, R. 1981, Ph.D. Thesis, University of Würzburg.
Hammer, R. 1982a, Ap. J. (submitted).
Hammer, R. 1982b, Ap. J. (submitted).
Hammer, R. 1982c, in preparation.
Kopp, R. A., and Orrall, F. Q. 1976, Ap. J. 53, 363.
Kuperus, M., and Chiuderi, C. 1976, in IAU Colloq. No. 36, The Energy Balance and Hydrodynamics of the Solar Chromosphere and Corona, ed. R. M. Bonnet, and Ph. Delache (Clermont-Ferrand: G. de Bussac), p. 223.
Lamers, H. J. G. L. M., and Kuperus, M. 1974, in Ph.D. Thesis H. J. G. L. M. Lamers, University of Leiden, p. 169.
Parker, E. N. 1958, Ap. J. 128, 664.

PREDICTIONS OF WAVE-DRIVEN WIND MODELS

L. Hartmann and E. Avrett, Harvard-Smithsonian Center for Astrophysics

There is a great deal of observational evidence that large-scale "turbulent" motions exist in the outer atmospheres of cool, low-gravity stars (cf. Wilson 1960; Smith 1980). This evidence led Hartmann and MacGregor (1980) to look for ways in which the energy in such turbulent motions could be tapped to produce low-temperature winds, since other theories had their difficulties. At the same time, IUE observations showed that stars could posess both cold winds and hot gas, the latter at temperatures characteristic of the solar transition region (Hartmann, Dupree, and Raymond 1980). This suggested a closer link between cool flows and solar activity. A combination of these and other considerations caused us to investigate the possibility of using magnetic fields to carry the turbulent energy outward, creating Alfven-wave acceleration of cold CS shells analogous to the solar wind mechanisms studied by Belcher (1971), Hollweg (1973), and Jacques (1978).

Assuming radial flow and several other simplifying appoximations, the equation of motion can be put into the form

$$v\frac{dv}{dr} + \frac{1}{\rho}\frac{d}{dr}\left(P_g + \frac{\langle \delta B^2 \rangle}{8\pi}\right) = \frac{-GM}{r^2} \qquad (1)$$

which explicitly displays the effect of the waves. The magnetic turbulent pressure gradient replaces the gas pressure in the canonical thermally driven wind in order to drive low-temperature flow.

This equation of motion exhibits multiple critical points (cf. Holzer 1977); multiple solutions are therefore possible, although generally the solutions through the innermost critical point exhibit by far the largest mass fluxes and so are of greatest interest (Holzer and Leer 1981).

At the critical point of a cold wind, the turbulent magnetic pressure gradient must essentially balance gravity. However, since for an Alfven wave $(\delta B/B) = (\delta v/A)$, where A is the Alfven speed, this requirement can be phrased in terms of the wave velocity amplitude. The result is that δv must be of the order of the escape velocity at the critical point; this means that the theory predicts the presence of large "turbulent" velocities.

The amount of mass loss obtainable clearly depends upon the field strength. One knows essentially nothing about possible surface magnetic fields and wave amplitudes. Therefore, all that can be done at the moment is to find the parameter range in which mass loss rates are compatible with

observational estimates. Typically, the calculations result in

$$\dot{M} \sim 6 \times 10^{-9} \left(\frac{R}{100R_\odot}\right)^{2.5} \left(\frac{M}{5M_\odot}\right)^{-0.5} \left(\frac{B_o}{3G}\right)^2 M_\odot \text{ yr}^{-1} \quad . \qquad (2)$$

Thus magnetic fields of a few gauss are sufficient to generate acceptably large mass loss rates. One may alternatively consider the energy flux requirements; for B = 3G, the wave flux is of order a few x 10^5 erg cm^{-2} s^{-1}. This appears reasonable in view of chromospheric radiative loss estimates which indicate the dissipation of a similar amount of mechanical energy (cf. Basri and Linsky 1979).

A further important property of the theory is that it requires wave heating which accompanies the momentum deposition. It was found that unless the waves are damped on scales comparable to the stellar radius, the calculated wind velocities are much higher than observed (Hartmann and MacGregor 1980).

Although this damping is not understood in physical terms, by fixing the damping length to yield the proper velocities a further prediction is made. With an estimate of the radiative cooling law, for which the low-temperature properties are taken from PANDORA calculations of stellar chromospheres (cf. Vernazza, Avrett, and Loeser 1981), the heating rate can be used to define wind temperatures. The balance between wave heating and radiative cooling determines the wind temperature maxima in this theory.

The consequences of such heating are displayed in Fig. 1, where winds for a variety of stars in the HR diagram have been computed, assuming B_o = 3G. One can see clearly that wind velocities and temperatures increase with increasing stellar gravity. At sufficiently high gravities winds with temperatures in excess of 10^5K appear, as radiative cooling becomes less efficient. At present the computations cannot handle winds with higher temperatures. However, these results suffice to show roughly where low-temperature winds are expected to occur.

A comparison with Reimers' (1974) survey indicates that this simple-minded calculation agrees with many of the features of the observed distribution of CS shells in the HR diagram. The calculated wind velocities are systematically too high by a factor $\sim$ 1.5 - 2; however, this problem may be alleviated by considering complications such as non-radial magnetic field geometries (Hartmann and MacGregor 1981). Furthermore, the mass loss rates indicated by (1) are adequate, and the position of the boundary of cool winds is not too far off from the observations.

A more direct test of the theory is to observe the wave heating effects on the wind temperature distribution. Extended chromospheres are produced over typical height scales of a few R_*. As an example, a wind calculated for a star with M = 1 $M_\odot$, R = 21 $R_\odot$, indicates that temperatures in the range 1 x 10^4 - 2 x 10^4K exist out to $\sim$ 1.3 R_*, where the electron densities are of order 10^8 cm^{-2}. These values compare favorably with the results of Stencel et al. (1981) from IUE observations of the density-sensitive C II lines in red giants.

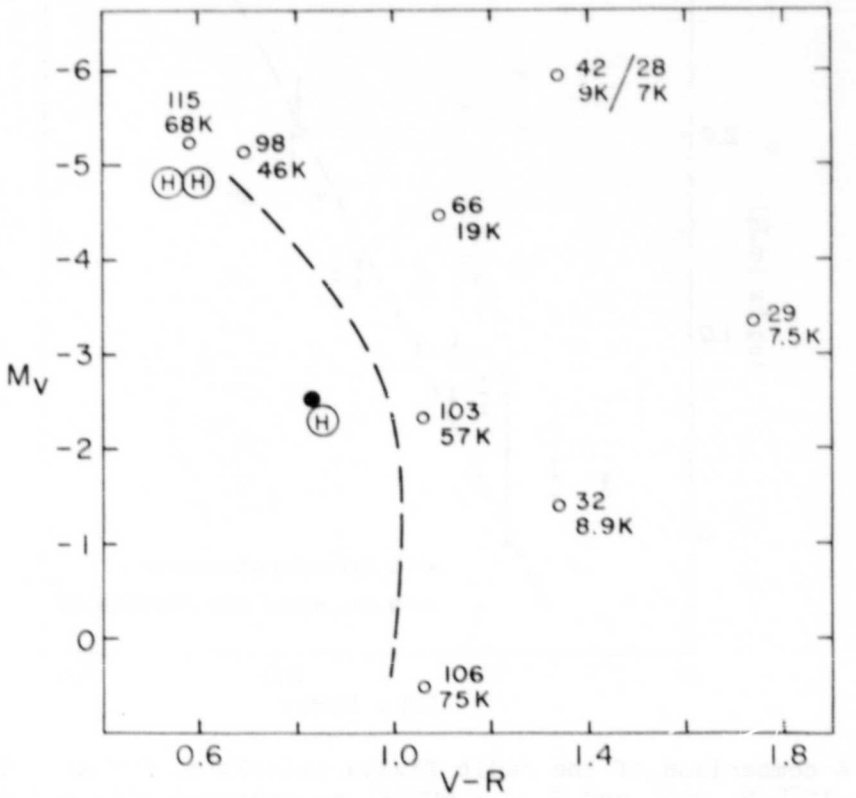

Figure 1. The variation of wind properties in the HR diagram, assuming all stars have surface magnetic fields of 3G. The models are labelled by the terminal velocity and the maximum wind temperature ($68K \equiv 6.8 \times 10^4$ K). The filled circle is a model for which no wind could be calculated, since the maximum wind temperature is in excess of 10^5 K. The dashed line roughly indicates the transition line beyond which wind models with $T_{max} < 10^5$ K are calculated. The encircled H symbols are positions of observed hybrid atmosphere stars, which exhibit both winds visible in circumstellar absorption lines and emission from ions present for $T = 1\text{-}2 \times 10^5$ K.

Models constructed for the M2I star α Ori predict wind temperatures which peak $\sim$ 6000K - 8000K at $\sim 3\ R_*$. This model has two obvious observational consequences: a) Excess radio free-free emission is produced; evidence for such an effect has been observed (Altenhoff, Oster, and Wendker 1979); b) Hα is predicted by our preliminary radiative calculations to be formed in a shell of height $\sim$ 5 - 7 R_*. This appears to be compatible with recent occultation and speckle interferometry measurements, as discussed by Goldberg (this volume).

Further observational efforts to study the chromospheric structures of red giants and supergiants are highly desirable, since the wave-driven wind theory demands extended heating regions accompanying the flow acceleration.

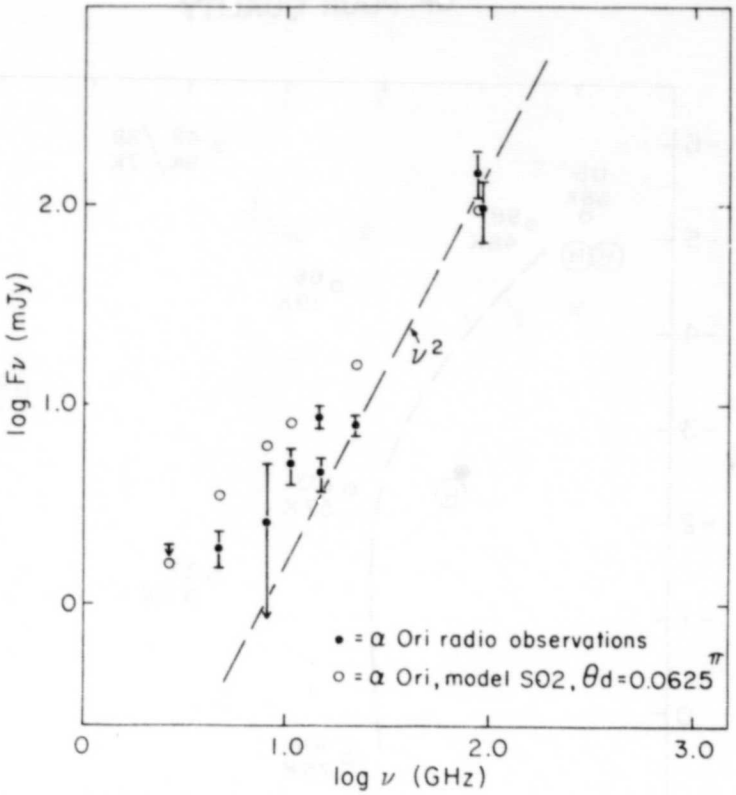

Figure 2. A comparison of the radio fluxes calculated for an α Ori wind model with $\dot{M} = 10^{-6}\ M_{\odot}\ yr^{-1}$ and $T_{max} = 6000K$, as compared with the observed radio excess (Altenhoff, Oster, and Wendker 1979). The dashed line indicates the probable photospheric contribution.

REFERENCES

Altenhoff, W. J., Oster, L., and Wendker, H. J. 1979, Astron. Ap., 73, L21.
Basri, G.S., and Linsky, J.L. 1979, Ap. J., 234, 1023.
Belcher, J.W. 1971, Ap. J., 168, 509.
Hartmann, L., and MacGregor, K.B. 1980, Ap. J., 242, 260.
_____. 1981, submitted to Ap. J.
Hartmann, L., Dupree, A.K., and Raymond, J.C. 1980, Ap. J. (Letters), 236, L143.
Hollweg, J.V. 1973, Ap. J., 181, 547.
Holzer, T.E. 1977, J. Geophys. Res., 82, 23.
Holzer, T.E., and Leer, E. 1981, in preparation.
Jacques, S.A. 1978, Ap. J., 226, 632.
Reimers, D. 1974, Mem. Soc. Roy. Liege, 6th Ser., 8, 369.
Smith, M.A. 1980, in Stellar Turbulence, I.A.U. Colloquium 51, ed. D.F. Gray and J.L. Linsky (Springer-Verlag; Heidelberg), p. 126.
Stencel, R.E., Linsky, J.L., Brown, A., Jordan, C., Carpenter, K.G., Wing, R.F., and Czyzak, S. 1981, M.N.R.A.S., 196, 47P.
Vernazza, J.E., Avrett, E.H., and Loeser, R. 1981, Ap. J. (Suppl.), 45, 635.
Wilson, O.C. 1960, in Stellar Atmospheres, ed. J.L. Greenstein (Chicago: Univ. Press), p. 436.

SPECKLE INTERFEROMETRY OF α ORI: PRELIMINARY RESULTS

L. Goldberg
Kitt Peak National Observatory

and

E. K. Hege,* E. N. Hubbard,* P. A. Strittmatter,* and W. J. Cocke
Steward Observatory, University of Arizona

OBSERVATIONS

The Steward Observatory intensified video speckle camera (Hubbard et al. 1979, Hege et al. 1980) was used at the Steward 2.3m telescope on 24 November 1980 and at the KPNO 4m telescope on 2 and 3 February 1981 for observations of Alpha Orionis. We have preliminary reductions, using procedures described in Hege et al. (1981), for three of these observations.

Date	Bandpass	Detector Scale	Resolution	Comments
24 Nov 80	6563Å/2.4Å	0".0109/pixel	0".058	Very windy. Seeing ~ 1".5
3 Feb 81	6563Å/2.4Å	0.0143	0.033	Scattered cirrus. Seeing $\lesssim$ 1".0
3 Feb 81	6500Å/20Å	0.0143	0.033	Scattered cirrus. Seeing $\lesssim$ 1".0

For the H-alpha line observations at the 2.3m telescope, 15ms shuttered exposures were reduced using photoelectron event detection procedures to produce speckle image autocorrelation functions (ACF) for both α Ori and γ Ori using a 2.4Å interference filter manufactured by Omega Optical of Brattleboro, Vermont. In order to facilitate the intercomparison of results obtained at the 4m telescope, a set of observations was made in similar fashion with the addition of a 16% transmission neutral attenator to allow reductions using event-detection procedures. Otherwise, the same observing set-up and data reduction procedures were used for both observations. Seeing-corrected autocorrelation functions (ACF_S) were produced for both stars (Hege et al. 1981). The seeing correction is produced from the long-exposure (LE) image accumulated from the same data sets. A correlation function (XC), defined as the Fourier transform (FT) of the square modulus of the Fourier transform of the long-exposure,

$$XC = FT(|FT(LE)|^2),$$

*Visiting Astronomer at Kitt Peak National Observatory, which is operated by the Association of Universities for Research in Astronomy, Inc., under contract with the National Science Foundation.

is used to estimate the seeing. The seeing-corrected autocorrelation function is

$$ACF_s = ACF - n(XC),$$

where n is a normalization determined by the average value of the quotient of the two functions at radii at which seeing effects predominate in the ACF.

$$n = \left|\langle ACF/XC \rangle\right|_{seeing}.$$

Although this seeing-corrected ACF_s is known to have significant residual contribution due to seeing effects and to contain the excess width due to the telescope aperture point-spread function (PSF), it is nevertheless useful, especially when compared with an ACF_s for an unresolved source observed and reduced in the same way.

Hα RESULTS

The H-alpha line measurements at both telescopes show evidence for structure at large scale when ACF_s (α Ori) is compared with ACF_s (γ Ori). In both measurements, the ACF_s (α Ori) signal showed large intensities at image scales well resolved but near the telescope diffraction limit. However, they also contained significant intensity at distances which could not be attributed to errors in seeing corrections since correspondingly extended intensity distributions were not seen in ACF_s (γ Ori). We are confident that this structure is real since the same effects were seen in observations made on different dates at different detector image scales using different telescopes.

In attempting to establish a characteristic diameter for the Hα envelope we adopted the following procedures. First the ACF of a uniform disk was fitted to the extended part of the ACF_s derived from the observation in order to provide a first estimate of the disk diameter D. This gave D = 0.23 ($\pm$ 0.02) arc sec and 0.22 ($\pm$ 0.05) for the 2.3m and 4m data, respectively. The "goodness of fit" between model and observation was satisfactory but by no means perfect. Furthermore, the power in the extended envelope ACF seems rather too high compared to that which would be expected from an optically thin Hα emitting envelope on the basis of the emission intensity in the observed Hα spectrum. We are therefore led to suggest that the principal component observed in the extended ACF represents the cross-correlation between the just resolved photospheric contribution (the ACF of which provides a strong central peak in the total ACF_s) and that of the extended emission. In this picture the ACF of the extended envelope would be too weak to be clearly detectable at the observed signal-to-noise ratio. In this interpretation the extended ACF component consists of an image (and its reflection) of the envelope emission convolved with the energy distribution of the central star. The measurements given above for the diameter would then represent more closely the radius of the envelope while the radial dependence in the observed ACF represents the radial intensity distribution in the envelope. The observations would thus imply that the Hα envelope is not well represented by a uniform disk but declines towards larger radius as might be expected in a wind flow. It is not possible to

specify a radius for such a distribution but it is clear that a significant contribution from the envelope has been detected out to a radius of $\sim$ 0.27 arcsecs in both the 2.3m and 4m data.

The signals are not radially symmetric. There is evidence for elongation in both sets of observations. In order to suppress as far as possible any residual asymmetries due to seeing or the data acquisition and reduction techniques, the power spectra (PS), obtained by PS = FT(ACF) using the raw, uncorrected speckle ACF, for both α Ori and γ Ori were corrected for detector noise bias (Hege et al. 1981) and the quotient power spectrum.

$$\text{Deconvolved PS} = \left(\frac{\text{PS}(\alpha\ \text{Ori}) - \text{Bias}}{\text{PS}(\gamma\ \text{Ori}) - \text{Bias}}\right)$$

was analyzed. The deconvolved power spectra show that the image of α Ori (in Hα light) is elongated. The results for 24 November 1980 show the extension to be at P.A. $157^\circ \pm 5^\circ$ (mod 180°) while those of 3 February 1981 indicate a PA at $176 \pm 5^\circ$ (mod 180°).

CONTINUUM RESULTS

For the higher intensity signals obtained with the wider (20Å) continuum filter, analogue detection procedures were used to produce power spectra (PS) for both α Ori and γ Ori. The reduction methods produce seeing corrected ACF_s in which no evidence for any extended structure with surface brightness greater than a few percent of that of the photosphere was detected. However a position angle asymmetry at 28° (mod 180°) was clearly evident in ACF_s (α Ori); the diameter of the major axis was measured to be 63 ± 2 mas and that of the minor axis 59 ± 2 mas, the major uncertainty arising from uncertainty in image scale, not from random errors.

Image phases accumulated in the course of the analogue reductions (Cocke 1980) were used, together with the debiased, deconvolved PS, to initialize image reconstruction by the Fienup (1978) method. The resultant image shows that the asymmetry is due largely to an unresolved feature at position angle 208°.

The excess brightness of this feature, compared to the brightness of neighboring image pixels, is of order 25%. Since the mean diameter in the continuum is about 60 arc-milliseconds and the measurement resolution is about 30 arc milliseconds, there are about $\sim$ 3 resolution elements in the resolved image. Thus the hot spot will contribute an excess of order 25 ($\pm$15)/3 percent or $\delta m = 0.08\ (\pm 0.05)$ to the integrated brightness of α Ori.

DISCUSSION

To summarize, the reconstructed image of α Ori in 6500Å continuum radiation on the night of 3 February 1981, has a mean diameter of about 60 mas, and shows an unresolved bright feature near the SW limb at position angle 208°. The contribution of this feature to the integrated brightness of the star is $0^m.08 \pm 0.05$. Narrow band Hα observations on 24 November 1980 and

3 February 1981 both show significant emission at relatively large distances, (radii exceeding 0".25). Moreover, the data clearly indicate that this Hα envelope is elongated, the 24 November observations yielding an extension at position angle 157° (mod 180°) and those of 3 February at position angle 176° (mod 180°). We shall postpone a detailed disucssion of these observations to a later paper, after a full image reconstruction has been attempted. It is, however, worthwhile at this stage to note some possible implications of the above results.

The continuum results are clearly important in relation to the well-known variations in both brightness and linear polarization, which α Ori is known to undergo on time scales of a few months. The brightness variations are irregular and amount to about a factor of 2, whereas the polarization varies in an orderly fashion over periods of several months. As shown in a classical paper by Stebbins (1931; see also Sanford 1933) the short-term brightness fluctuations modulate a regular, cyclic variation with a period of nearly six years. The visual magnitude and B-V color of α Ori have recently been observed by Krisciunas (1981), on 19 nights spread over the period from 1979 October to 1981 April. The brightness varied over the range $V = 0^m.78$ to $V = 0^m.29$ but B-V remained constant at $1^m.85$. Observations during the 1980-1981 season began at the end of December at which time the star had brightened to $V = 0^m.30 \pm 0.01$. The last previous observation was on 22 March 1980 when the magnitude was $0^m.73 \pm 0.02$. Between 5 January 1981 and 26 February 1981, the brightness decreased steadily from 0.29 ± 0.01 to 0.57 ± 0.01. By 17 March 1981, a second brightening occurred, to $V = 0^m.44 \pm 0.05$, after which the brightness again declined, to $0^m.61 \pm 0.03$ on 6 April 1981. It is entirely possible that the increased brightness at the beginning of 1981 was the result of the bright limb feature we observed on 3 February. On 1 February, the visual magnitude was $0^m.44 \pm 0.01$, which is not out of line with our estimate of $0^m.08 \pm 0.05$ as the excess brightness of this feature.

The observations of time-dependent intrinsic polarization at visual wavelengths in many late-type giants (c.f. Serkowski 1966; Dyck and Jennings 1971) also provides evidence for some form of nonsphericity in the structures of these stars. If the polarization arises from scattering, then either the scattering medium or the star's brightness distribution must depart from spherical symmetry (Woolf 1972). Such asymmetries may be caused by convective cells which, in red supergiants, may extend over an appreciable fraction of the stellar radius (Schwarzschild 1975). The scattering itself could be due to dust (Dyck and Jennings 1971), atomic or molecular hydrogen (Kruszewski et al. 1968) and/or electrons.

Of significance in the present context is the recent discovery of ordered changes in the linear polarization of visible light from the red supergiants α Ori and α Sco (Haynes 1980,1981; Tinbergen et al. 1981). The star α Ori was observed by Haynes on 66 nights during 1979-1980 and on 62 nights during 1980-1981. In 1979-1980, the position angle of the plane of polarization first decreased in ordered fashion for three months beginning in September 1979, from about 157° to 115°, and then increased to about 170°, while the amount of polarization decreased more or less regularly from about 0.8% to 0.4%. Most of the variation occurred during the first four months of the observing season, with very little change occurring during the period 1 February - 17 April. In October 1980, the polarization resumed its variation, the angle increasing from 0° to about 125° and the amount of polarization from about 0.2% to 0.85%.

Haynes (1980) has suggested that the changes in polarization arise from changes in the lower atmosphere and finds them consistent with the growth of a surface feature followed by progressive changes in its orientation. The speckle and brightness observations quoted here lend general support to this model and permit a certain amount of further elaboration. We conjecture that in September - October 1980, a bright feature developed on or near the stellar limb at position angle 208° and grew in luminosity until about the end of December 1980. As shown by the photometry (Krisciunas 1981), the feature then began a steady decline in integrated brightness. The secondary maximum in the visual light curve may well have been caused by another brightening elsewhere on the stellar disk. The progressive increase in the angle of the plane of polarization before and after 3 February implies either that the bright feature was moving around the limb, which seems unlikely, or that light from the surface feature was being scattered by material in motion above the limb and changing its orientation with respect to the active region. It may be significant that, on 1 February 1981, two nights before the bright feature was observed at position angle 208°, the angle of the plane of polarization was 113°, or within 5° of being at right angles to the direction of the bright spot -- as would be expected in the Hayes model.

Further information concerning the surface structure and envelope of α Ori can be derived from high angular resolution observations at other wavelengths. The present results, however, clearly illustrate the power of the speckle interferometry technique especially when the results can be combined with accurate photometric and polarimetric data.

This work has been supported by the AFGL through contract No. F19628-78-C-0058 and by the AFOSR through contract No. 82-0020. We wish to acknowledge helpful discussions with J. Beckers, J. Drummond and N. Woolf.

REFERENCES

Cocke, W.J. 1980, Proc. S.P.I.E. 243.
Dyck, H.M. and Jennings, M.C. 1971, Astron. J. 76, 431.
Fienup, J.R. 1978, Opt. Lett. 3, 27.
Haynes, D.P. 1980, Astrophys. J. (Lett.) 241, L165.
_____. 1981, Astrophys. J. (Lett.) in press.
Hege, E.K., Hubbard, E.N., and Strittmatter, P.A. 1980, Proc. S.P.I.E. 264, 29.
Hege, E.K., Hubbard, E.N., Strittmatter, P.A., and Worden, S.P. 1981, Proc. IAU Colloquium 62, Flagstaff (ed. R.S. Harrington).
Hubbard, E.N., Hege, E.K., Reed, M.A., Strittmatter, P.A., and Worden, S.P. 1979, Astron. J. 84, 1437.
Krisciunas, K. 1981, preprint.
Kruszewski, A., Gehrels, T., and Serkowski, K. 1968, Astron. J. 73, 677.
Sanford, R.F. 1933, Astrophys. J. 77, 110.
Schwarzschild, M. 1975, Astrophys. J. 195, 137.
Serkowski, K. 1966, Astrophys. J. 144, 857; IAU Information Bulletin Variable Stars No. 141.
Stebbins, J. 1931, Publ. Washburn Observatory, University of Wisconsin 15, 177.
Tinbergen, J., Greenberg, J.M., and de Jager, C. 1981, Astron. Astrophys. 95, 215.
Woolf, N.J. 1972, Mem. Soc. Roy. Sci. Liege, 6th Ser. 3, 209.

EVIDENCE FOR EXTENDED CHROMOSPHERES SURROUNDING RED GIANT STARS

Robert E. Stencel

Joint Institute for Laboratory Astrophysics
University of Colorado and National Bureau of Standards

There is now an increasing amount of both observational evidence and theoretical arguments that regions of partially ionized hydrogen extending several stellar radii are an important feature of red giant and supergiant stars. The purpose of this paper is to summarize this evidence and to examine the implications of the existence of extended chromospheres in terms of the nature of the outer atmospheres of, and mass loss from, cool stars.

1. Spectroscopic Evidence

1.1. Emission measure in the mid-UV lines of C^+

A marvelous marriage between observational astrophysics and theoretical atomic physics recently occurred when the density-sensitive variation of line ratios within the five-lined 2325 Å multiplet (UV 0.01) of C II was studied in the spectra of red giants (Stencel et al. 1981). The sensitivity of the boron isoelectronic sequence to the electron density of lines in the $2s^2 2p^2 P - 2s2p^2\ ^4P$ multiplet has been known for some years. Previous work has concentrated on N III, O IV and higher sequence members in the context of the solar atmosphere. The C II features are sensitive to densities in the 10^7-10^9 cm^{-3} regime, inappropriate for the dense solar chromosphere, but valuable in measuring densities in low gravity cool stars. Observations of the C II 2325 Å multiplet in the Sun and in the planetary nebula NGC 6572 fix the high and low density ratios for three pairs of lines. By iteratively adjusting collision strengths and A-values, Stencel et al. achieved an optimum fit to the density extremes, reducing the spread in N_e as derived from three line ratios for individual red giants. The line ratios are relatively insensitive to changes in T_e over the 7000-20,000 K range. More accurate collision strength calculations are needed, however, and observations of objects nearer the low and high density limits are being requested, but such observations require long exposures even with the IUE satellite. The implied electron densities for α Boo and α Tau are $2\text{-}3 \times 10^8$ cm^{-3}, in reasonable agreement with upper chromospheric values in models by Kelch et al. (1978) and Ayres and Linsky (1975).

In addition to the valuable density diagnostic, the ratio of total flux in the 2325 Å multiplet to that in the 1335 Å resonance line multiplet pro-

vides an independent measurement of T_e. This information combined with ionization equilibrium estimates and abundances can lead to estimates of the hydrogen column density, $\int N_H dh$, which is $\sim 6 \times 10^{20}$ cm^{-2} for α Boo. Then assuming the carbon ionization fractions and the value of N_e/N_H, we derive a lower limit to the (C II) chromospheric thickness for α Boo of $\sim 2 \times 10^{12}$ cm, which is at minimum comparable to the stellar radius. More precise calculations for the hydrogen and carbon ionization equilibria and line formation, including collisional excitation would be valuable. Preliminary calculations assuming a two-level C^+ ion and optically thin line, and the observed values, suggest that chromospheric thicknesses range from about $6R_*$ in α Boo to 10-15 R_* in M giants and supergiants, like β Peg and α Ori. It is encouraging that this same technique predicts a very thin (0.01 R_*) chromosphere for the Sun. Recent C II observations of the K0 III star β Gem indicate $N_e \sim 10^{9.1}$ and a chromospheric thickness of 0.06 R_*. This result is encouraging, because β Gem exhibits soft X-ray emission transition region emission lines, indicative of an outer atmospheric structure similar to the Sun, including a geometrically thin chromosphere. It seems physically appealing that among the red giants which show no evidence for hot coronae, the chromosphere occupies a volume homologous to that of coronae in warmer, higher gravity stars.

1.2. Other estimates of chromospheric extent and inner CS radius

The coolest and most luminous red giants are known to be surrounded by an extensive, cold circumstellar (CS) gas and dust envelope, extending possibly hundreds of stellar radii (for α Ori several arc-minutes in apparent extent -- Honeycutt et al. 1980). The radius of the inner edge of this CS shell is referred to as R_{min} and its value is important in estimating mass loss rates, but it also provides an outer limit to the extent of warm, chromospheric material near the star. Sutton et al. (1977) employed optical heterodyne interferometry on the 10 μm silicate feature in α Ori and α Sco, and found that dust emission ceases within 12 R_*, implying an extended warm interior region. Less direct techniques have inferred R_{min} for α Ori to lie in the 8-12 R_* range, cf. Bernat and Lambert (1975), Knapp et al. (1980), van der Hucht et al. (1980), Castor (1981). The radio spectrum reported by Altenhoff et al. (1979) is consistent with free-free emission from a 2-3 R_* warm region around α Ori.

1.3. Variable He I 10830 Å emission

The appearance of variable He I 10830 Å emission and absorption among red giant stars (O'Brien 1980; Zirin 1976) for which upper limits on coronal X-ray emissions are very small (Ayres et al. 1981a) poses the difficult problem of line formation that perhaps can be resolved by recognizing that the chromospheres of these stars are probably extended. The existence of emission in 10830 Å is easier to understand if it is formed over a region large compared to the photosphere. This is in contrast to thin chromosphere dwarfs where

10830 Å appears consistently in absorption. More importantly, the nature of the 10830 Å variations themselves has been used by O'Brien to argue for moving prominence-like material at large distances from red giants. The nature of these events is far from established, but they strongly imply the existence of chromospheric material at large distances above the stellar photosphere. Evidence for episodic mass ejections among red giants has also been found by Bernat (1981).

1.4. Atmospheric structure in 32 Cyg

High resolution ultraviolet spectra obtained during the recent eclipse of 32 Cyg by Stencel et al. (1982) provide direct measurement of the chromospheric temperature rise with height above the supergiant's photosphere as a result of the different lines of sight through the K5Ib stellar atmosphere to the partially eclipsed B5V companion star. Preliminary analysis using Fe I and Fe II curve of growth indicates an excitation temperature that appears to plateau at 7200 K above approximately 2 R_K.

1.5. Ionization anomalies

Ramsey (1981) has reported on the ionization balance in G5-M2 giants and supergiants, using Ca I 6573 Å and [Ca I] 7324 Å lines. He found an increasing discrepancy between observed and LTE line strengths for $T_{eff} < 4250$ K, which he interpreted in terms of increased overionization. This effect highlights the inadequacy of radiative equilibrium, LTE atmospheres for such stars, which could be due in part to a lack of collisional deexcitation in low density and extended material, or subtle filling of the line core by chromospheric emission. The NLTE effect and core filling both could have substantial impact on attempts to perform abundance analyses of these objects (see below).

1.6. Ca II K and Mg II k

Chromospheric temperatures and velocity fields can be derived from profiles of the emission cores of the resonance doublets of Ca^+ and Mg^+. Reimers (1977) has delineated that portion of the HR diagram where cool stars typically show CS (K_4) features in their K line cores, thus indicating the presence of outflowing 3000-7000 K material well above the low chromosphere. Stencel (1978) and Stencel and Mullan (1980a,b) have studied the statistics of asymmetries in the doubly reversed emission cores. They find that the Ca II K line changes from a solar-like ($K_2V > K_2R$) asymmetry to an outflow ($K_2V < K_2R$) type of asymmetry along a locus in the H-R diagram similar to that proposed by Reimers for the presence of K4 features, whereas the Mg II k line undergoes a similar asymmetry change several spectral subtypes earlier, nearly coincident with the division between stars with and without detected soft X-ray emission (Ayres et al. 1981a). Effects of interstellar Mg II absorption can affect the

apparent asymmetry (Bohm-Vitense 1981) although to first order, the impact can be judged by comparing the stellar radial velocity against the "expected" asymmetry for the stars' location in the H-R diagram.

Several bona-fide "discrepant asymmetry" (Ca II K ≠ Mg II k) stars have been isolated by Mullan and Stencel (1982), including α Boo (K2 III), α Tuc (K3 III), σ Oph (K_3 II), π Her (K_3 II), 56 Peg (K_0 II + wd). Several others are suspected of having discrepant asymmetries (e.g., 56 UMa, G8 II), although interstellar Mg II absorption may interfere. In contrast, the G giants and M giants tend to have asymmetry agreement. It is significant that when the discrepancy is found, it is always in the sense that Ca II shows V > R while Mg II k shows the opposite asymmetry. This "preferred parity" must be physically meaningful, unless a reliable counter example can be found.

At the time of this writing there is no definitive explanation for this phenomenon, although several hypotheses have been advanced. Our attempts to simulate discrepant asymmetries numerically using plane parallel, hydrostatic equilibrium (HSE) model atmospheres and comoving frame multilevel NLTE calculations including PRD have not been successful; the formation regions of Ca II K and Mg II k overlap to a great extent (cf. Fig. 1 of Vernazza et al. 1981) and unphysically steep velocity gradients would be required to produce the discrepant asymmetries. There is no reason to believe that the high pressure chromosphere models of Baliunas et al. (1979) would do any better. There are two possible solutions: we could adopt very nonsolar Ca/Mg abundance ratios to separate the Ca II and Mg II formation regions; or we could assume that the chromosphere is extended and inhomogeneous. The latter option seems preferable. Spectral synthesis calculations are needed for the following models: (1) one component, geometrically extended chromospheres (T_{max} ~ 8000 K); (2) extended chromospheres, including stellar prominences (T_{max} ~ 10,000 K), and (3) "double valued" chromospheres (T_{max} initially rising to 10^5 K, then dropping back to ~8000 K). None of these models can assume HSE, a point we'll return to later.

For a one-component chromosphere without a high temperature corona at its upper bounds the Mg II k formation region will extend well above that of Ca II K, such that it should be possible to produce discrepant asymmetries, with plausible radial velocity gradients. In the stellar prominence model an upward moving layer, which is optically thick in Mg II k but thin in Ca II K, overlies a static chromosphere, and adds absorption and emission components to the symmetric underlying profile in any desired proportions. Such models are highly nonunique however. Finally, the model based on temperature distributions proposed for other reasons by Hartmann and MacGregor (1980) may have merit in the present case. Above an initial chromospheric rise is a high temperature (10^5 K) transition region (TR) above which lies an extended, cooler chromosphere. For this model the Ca II K core emission could be primarily formed in an interior deceleration zone, while most of the Mg II k

could be formed exterior to the TR, in an expansion zone. Again, radiative transfer calculations in spherical geometry need to be carried out to demonstrate the feasibility of this appealing idea. This model does predict that TR emission lines would exist in proportion to T_{max}, and the TR thickness. Stringent limits to the emission measure of TR features must be borne in mind (e.g., α Boo), despite the existence of "hybrids" and their possible TR line variability. Actual differences in the amount of TR material in K giants and bright giants may relate to intrinsic age and evolutionary differences, much as may be the case for the G-type giants whose range of X-ray luminosities suggests this possibility (Simon et al. 1982). Finally, it should be remembered that a complete statistical sample based on simultaneous observations is far from complete, although the suggestion of discrepant asymmetries must mean either extreme variability or unique physical circumstances for such chromospheres.

1.7. Additional spectroscopic indicators

Subordinate emission lines, such as those appearing in the wings of the Ca II H and K lines (Stencel 1977) and those in the mid-UV spectra of many red giants (Stencel et al. 1980), tend to lack counterparts in warmer, high gravity, coronal-type stars. In part this could be a matter of contrast with the photospheric continuum distribution, but their appearance in stars only above the asymmetry dividing line for Ca II K (Stencel 1978; Hagen et al., this volume) suggests that they maybe useful in studying extended chromospheres.

2. Direct Evidence

2.1. Narrow-band speckle spectroscopy

A very significant advance in the study of red giants and supergiants occurred with the discovery of a large increase in the apparent diameter of α Ori when viewed in the light of Hα (see Hege et al., this volume). They report that the diameter increases from about 50 milliarsec (mas) in continuum light to over 250 mas in the Hα $\pm$ 3 Å core, suggesting chromospheric emission extending to at least 5 R_*, consistent with the previous discussion. In principle, it should be possible to resolve time-dependent chromospheric structures and possibly stellar rotation. Several groups are busy planning how best to exploit this technique; narrow band observations are being planned for a variety of strong lines. The results are guaranteed to be exciting and fundamental.

2.2. Narrow band observations of occultations

Similar efforts involving narrow band occultation observations have also indicated extended chromospheric emission among red giants. White et al.

(1981) found that 119 Tau (M2 Ib) is at least twice its continuum diameter in Hα light. Similarly, Radick and Africano (1981) found suggestions of a small increase in angular diameter of α Tau (K5 III) when viewed in a 7 Å FWHM filter that had the Ca II 8542 Å line near one edge of the bandpass. Estimates that correct for light loss, etc., suggest a larger angular diameter would be found with the filter centered on the chromospheric line. White et al. suggest that several bright cool stars, and all M supergiants with $I(104) < 2^m$, may be suitable targets for such observations.

3. Discussion

3.1. Failure of hydrostatic equilibrium (HSE)

Dimensional arguments indicate that extended chromospheres are orders of magnitude larger than their isothermal pressure scale heights ($RT/\mu g$). The average chromospheric densities implied by the C II diagnostics for α Boo and α Ori are 10^8 and 10^7 cm^{-3} respectively. The isothermal pressure scale heights in 10^4 K chromospheres are 10^{11} and 10^{12} cm. These are 50 and 250 times smaller than the dimensions implied by 5 R_* chromospheres for these stars. It appears that hydrostatic pressure alone is incapable of supporting these chromospheric extents.

Another source of pressure in red giant atmospheres is due to turbulent and expansion velocities. The averaged pressure, P_{chr}, implied by $\rho g R_{chr}$ is sufficiently large that rms turbulent velocities of 70 and 50 km s^{-1} would be required for α Boo and α Ori, respectively, to support it. While for α Boo, 70 km s^{-1} is consistent with the transient Ca II K_4 feature displacements reported by Reimers (1977) for similar stars, 50 km s^{-1} seems a factor of 3 or more above chromospheric or expansion velocities derived for α Ori (Bernat 1981). A plausible alternative to hypersonic velocites would be the support due to a modest magnetic field energy density ($B^2/8\pi$). Assuming an r^2 divergence, the surface (1 R_*) field required is only 9 and 2 gauss, respectively. These field strengths are comparable to those assumed by Hartmann and MacGregor (1980) in their Alfvén wave heating model for red giants. However, the magnetodynamic support arises in the tangential component of the field ($\underline{B} \times \nabla \times \underline{B}$), and if small Alfvénic perturbations on a stronger, fixed radial field are required, the total energy in the support field over large dimensions must be enormous. The Alfvén wave heating theory is probably appropriate to describe the stellar wind in the far-field limit, but an alternative may be necessary in the near-field. Mullan (1981) has discussed the stability of emerging flux loops in stellar atmospheres, and argues from analogy with solar helmet streamers that below a certain mass-to-radius ratio (i.e. log g ~ 2), such loops will not find stable configurations, and must evolve to open topology. Reconnection near the base may pinch off magnetically confined

plasma bullets which are propelled upwards, in effect driving the mass loss (see comments by Mariska and Boris in this volume). The idea is appealing in that it explains the observed episodic nature of mass loss, but it has not yet been supported by realistic calculations (Pneuman 1981).

3.2. Energy balance and the hybrid stars.

It has been noted by R. Hammer (private communication) that the intensity distribution across the extended chromospheres will be indicative of radiative loss and hence of the heating mechanism. Although the details of the dissipation remain preliminary, compressional wave heating modes (e.g. acoustic and slow mode with field equipartition) are much more closely tied to the density distribution than the noncompressional wave heating modes (e.g. Alfven-waves). The radiative loss rate as a function of radius then indicates the heating mode, assuming an exponential density falloff. Considering that if the number of isothermal pressure scale heights involved is large, the radiative losses in Hα then appear essentially insensitive to density, as there is detectable signal from the extended material. This points toward noncompressional wave heating as the important mechanism, although the details of its dissipation await further clarification. The spatial variation of chromospheric line emission provides an important clue, and needs more careful measurement.

If Alfvénic wave heating is an appropriate description of the outer atmospheres of noncoronal stars, the thickness and density of their transition regions determine the visibility of their 10^5 K emission features in the far ultraviolet. Again, the statistics are incomplete, but perhaps as many as one in four of the K giants and bright giants so far sampled are hybrid (Reimers, this volume; Simon et al. 1982). It is particularly dangerous to draw premature conclusions for this region of the H-R diagram because it is also occupied by the Ba II stars, many of which are thought to have white dwarf companions and thereby enhanced transition region emission (Schindler et al. this volume). If the transition regions of such stars are also extended (2-3 R_* in the MacGregor-Hartmann models), they might be spatially resolved near the star in speckle spectroscopy of helium or other lines. The suggestions of variability in TR emission lines (e.g. comparing the Iota Aur and Theta Her at different epochs) indicate changes in the energy input responsible for the TR formation, and the mass loss. This may be important in the formation of the variable He I 10830 Å absorption and emission seen among such stars.

3.3. Future prospects.

The concept of a geometrically thick chromosphere surrounding noncoronal type stars is appealing in that a wide range of observed properties of red giant stars can be more easily understood. One characteristic of extended chromospheres that distinguishes them from the thin chromospheres of the Sun and G giants, is the fluorescent line pumping that can occur: e.g. O I (pumped

by Ly-β, Haisch et al. 1977), numerous lines of S I (Brown and Jordan 1980) and CO (Ayres et al. 1981b). Note that these fluorescent features can be confused with important TR lines due to wavelength coincidences, and any hybrid candidate must be carefully scrutinized with respect to this possibility. Further, abundance estimates may be suspect if the filling in of line cores by chromospheric emission, which reduces line equivalent widths, is overlooked (e.g. O I and metal lines, Sneden et al. 1979).

Among the high priority observations in the next few years should be simultaneous X-ray (EXOSAT), far ultraviolet and Mg II (IUE), Ca II, Hα and He I 10830 Å observations of red giants, as well as a thorough exploration of the immense potential of speckle spectroscopy (section 2.1 above) of such objects. In terms of calculations, models for line formation and radiative losses in extended, spherical chromospheres should receive first attention. Any attempts to comprehensively interpret the outer atmospheres of red giant stars must take into account the evidence for the extended chromospheres, their variability and large scale asymmetries (as suggested by the speckle data — Hege et al. this volume — and by linear polarization work — Hayes 1980).

I am pleased to acknowledge useful conversations with Leo Goldberg, Reiner Hammer, Jeffrey Linsky and Dermott Mullan. Unparalleled editorial assistance was cheerfully provided by Lorraine Volsky, Leslie Haas, and Gwendy Romey. This research was supported in part by NASA grants to the University of Colorado, for which I am grateful.

References

Altenhoff, W., Oster, L. and Wendker, H. 1979, Astr. Ap., 73, L21.
Ayres, T. and Linsky, J. 1975, Ap. J. 200, 660.
Ayres, T., Linsky, J., Vaiana, G., Golub, L. and Rosner, R. 1981a, Ap. J. (in press).
Ayres, T., Moos, W., Linsky, J. 1981b, Ap. J. 248, L137.
Baliunas, S., Avrett, E., Hartmann, L. and Dupree, A. 1979, Ap. J. 233, L129.
Bernat, A. 1981, Ap. J. 246, 184.
Bernat, A. and Lambert, D. 1975, Ap. J. 201, L153.
Bohm-Vitense, E. 1981, Ap. J. 244, 504.
Brown, A., and Jordan, C. 1980, M. N. 191, 37P.
Castor, J. I. 1981, in Proceedings of the Erice Conference: Physical Processes in Red Giants, eds. I. Iben and A. Renzini (Dordrecht: Reidel).
Haisch, B., Linsky, J., Weinstein, A. and Shine, R. 1977, Ap. J. 214, 785.
Hartmann, L. and MacGregor, K. 1980, Ap. J. 242, 260.
Hayes, D. P. 1980, Ap. J. 241, L165.
Honeycutt, R., Bernat, A., Kephart, J., Gow, E., Sandford, M. and Lambert, D. 1980, Ap. J. 239, 565.

Kelch, W., Linsky, J., Basri, G., Chiu, H-Y., Chang, S.-H. Maran, S. and Furenlid, I. 1978, Ap. J. 220, 967.
Knapp, G. R., Phillips, T., and Huggins, P. 1980, Ap. J. 242, L25.
Mullan, D. 1981, in Proceedings of the Erice Conference: Physical Processes in Red Giants, eds. I. Iben and A. Renzini (Dordrecht; Reidel).
Mullan, D. and Stencel, R. 1982, B.A.A.S. 13 (Boulder meeting — in press) and Ap. J. (in press — Feb. 15).
O'Brien, G. 1980, Dissertation, University of Texas.
Pneuman, G. 1981, preprint.
Radick, R. and Africano, J. 1981, A. J. (in press).
Ramsey, L. 1981, Ap. J. 245, 984.
Reimers, D. 1977, Astr. Ap. 57, 395.
Simon, T., Linsky, J. and Stencel, R. 1982, Ap. J. (in press).
Sneden, C., Lambert, D. and Whitaker, R. 1979, Ap. J. 234, 964.
Stencel, R. 1977, Ap. J. 215, 176.
Stencel, R. 1978, Ap. J. 223, L37.
Stencel, R. and Mullan, D. 1980a, Ap. J. 238, 221.
Stencel, R. and Mullan, D. 1980b, Ap. J. 240, 718.
Stencel, R., Mullan, D., Linsky, J., Basri, G. and Worden, S. P. 1980, Ap. J. Suppl. 44, 383.
Stencel, R., Linsky, J., Jordan, C., Brown, A., Carpenter, K., Wing, R. and Czyzak, S. 1981, M.N.R.A.S. 196, 47.
Stencel, R., Chapman, R., Kondo, Y. and Wing, R. 1982, Ap. J. Suppl. (in preparation).
Sutton, E., Storey, J., Betz, A., Townes, C., and Spears, D. 1977, Ap. J. 217, L97.
van der Hucht, K., Bernat, A., Kondo, Y. 1980, Astr. Ap. 82, 14.
Vernazza, J., Avrett, E. and Loeser, R. 1981, Ap. J. Suppl. 45, 635.
White, N., Kreidel, T. and Goldberg, L. 1981, Ap. J. (in press).
Zirin, H. 1976, Ap. J. 208, 414.

SHOCK WAVES, ATMOSPHERIC STRUCTURE, AND MASS LOSS IN MIRAS

L.A. Willson

Iowa State University, Ames, IA 50011

and

J.N. Pierce

Mankato State University, Mankato, MN 56001

Introduction

Large amplitude shock waves are observed to be present in the atmospheres of the Mira variables: spectral line doubling with $\Delta v \geq 30$ km/s is present in infrared spectra (Hinkle et al. 1981) and even the visible spectra contain some evidence for such shocks (Willson, Wallerstein, and Pilachowski 1982). These shocks are sufficiently large to clearly dominate the energy balance of the atmosphere. Mira variables also show symptoms of substantial mass loss rates: they are strong maser and infrared continuum sources and have strong circumstellar absorption features (Gehrz and Woolf 1971; Knapp et al. 1981; Wallerstein 1979). The pulsation induced shocks which are seen to be present are obvious suspects for causing or enhancing the mass loss from these stars. The Miras thus present an ideal case for the study of dynamical effects on atmospheric structure, since both the dynamics and the results are clearly observable.

The motivation for the present study of the structure of the shocks in the atmosphere was the determination by Willson and Hill (1979 = WH) that the shocks alone could be sufficient to cause the observed mass loss. In the lower atmosphere the shock heated material is expected to cool efficiently, and hence the conditions for isothermal shocks are satisfied. As the density decreases, however, the cooling length becomes comparable to the scale height and/or the separation between shocks; at this point the isothermal shock approximation breaks down. If the isothermal shock equations are replaced by adiabatic conditions at this point, the overlying atmospheric layers will be driven off, producing mass loss rates comparable to or even larger than those observed. Obviously the transition from isothermal to adiabatic shocks will not occur discontinuously; a coupled study of the shock structure and the atmospheric structure is clearly needed to determine what will, in fact, occur. Such calculations are not yet available. Published studies have either assumed isothermal and/or adiabatic shocks and studied the resultant atmospheric structure or have calculated cooling behind arbitrarily selected shocks. In this paper we present the results of calculations of the thermalization and cooling of the material passing through shock fronts whose properties were selected to be consistent with both the isothermal models and the spectroscopic observations.

The input to the present calculations was a set of shock amplitude-density combinations selected from the models presented in Hill and Willson (1979) as likely to occur in the Mira atmosphere. For each combination of amplitude and density the relaxation behavior of the gas behind the shock front was followed for a time interval equal to the period of the star; the procedure was iterated until the conditions reached at t = P were identical with the pre-shock conditions assumed. Cooling mechanisms included were metallic line radiation and radiative recombination of ions and molecules for atomic and molecular species from H (log N = 12) through B (log N = 3). For details of the assumptions, parameters, and procedures used see Pierce (1980). The amplitude-density-altitude relation used for most of the calculations is sketched in Figure 1.

Results

The shock relaxation behavior defines four physically different zones in the Mira atmosphere. In the lowest zone, (A), the isothermal shock approximation is probably satisfactory, although the complexity introduced by $H + H \leftrightarrows H_2$ together with large optical depth in the shock rendered the solution beyond the present effort. In the next atmospheric zone, (B), where the shock is sufficiently optically thin for transfer effects to be negligible in the relaxation calculation, the shocks are isothermal; however, for the periodic solution the minimum temperature reached between shocks increases gradually with altitude in the atmosphere. In the third region, (C), the shocks are no longer isothermal; the temperature is still decreasing at the time of the arrival of the next shock. Through this region the minimum temperature reached increases even more rapidly than in the second zone. In the fourth region, (D), the thermalization time also becomes comparable to the time between shocks; here, no single temperature suffices, and the processes of ionization and excitation are decoupled. Details of the behavior of the material in this zone were also outside the scope of the present study. These four zones together comprise the atmosphere for the Mira from $R_* \sim 1$ AU, $\log \rho_o = -10.5$, to $R = 2\text{-}3\ R_*$, $\log \rho_o = -15$.

The temperature structure of individual shocks is shown in Figure 3; the atmospheric temperature structure, defined as the minimum temperature reached between shocks, is shown as a function of pre-shock density (or distance) in Figure 2. This latter plot may be compared directly with an observational constraint on the temperature structure of the Mira atmosphere: the requirement for the collisional excitation of the v=2 and v=3 levels in SiO which give rise to observed maser features is T = 3000-5000 K in the region where $\log \rho_o \sim (-12)$ (Elitzur 1981). This is quite consistent with Figure 2, suggesting that the most important cooling processes have been included in our calculations.

Thus: shock waves in the atmospheres of the Mira variables drastically alter the atmospheric stucture, producing a steady increase in temperature outward through most of the atmosphere. The shock waves are isothermal in the lower atmosphere, but the cooling time exceeds the time between shocks in the region with $-13.5 > \log \rho_o > -15$, and in the regions with $\log \rho_o < -15$ the

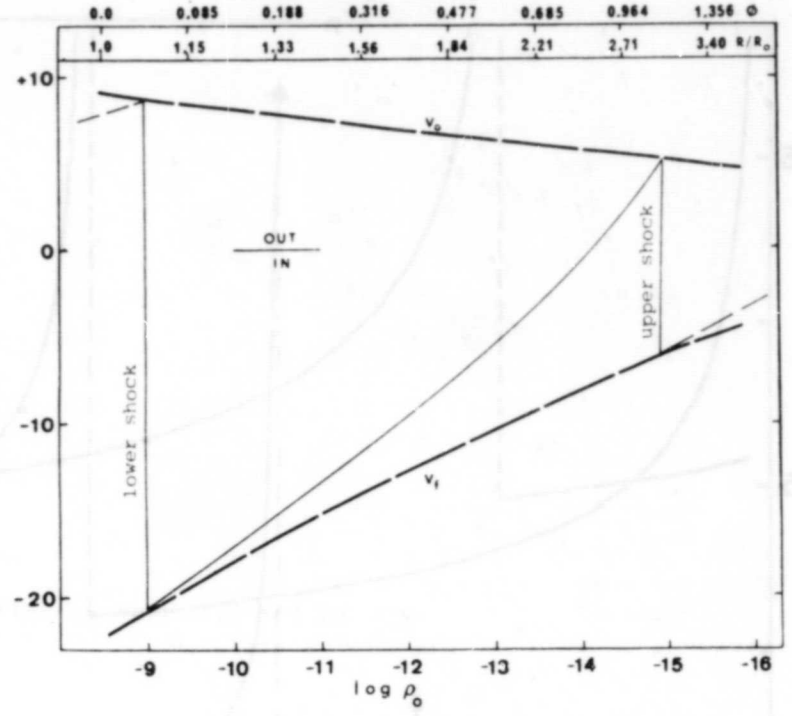

Figure 1. Shock velocity and amplitude as a function of density based on the models of Hill and Willson (1979) and used as input for the shock relaxation calculations. Distance and phase of arrival of shock front at a given layer are also indicated for Pierce (1980) case A: 1.2 M_o, 332^d, 225 R_o "fundamental mode" Mira.

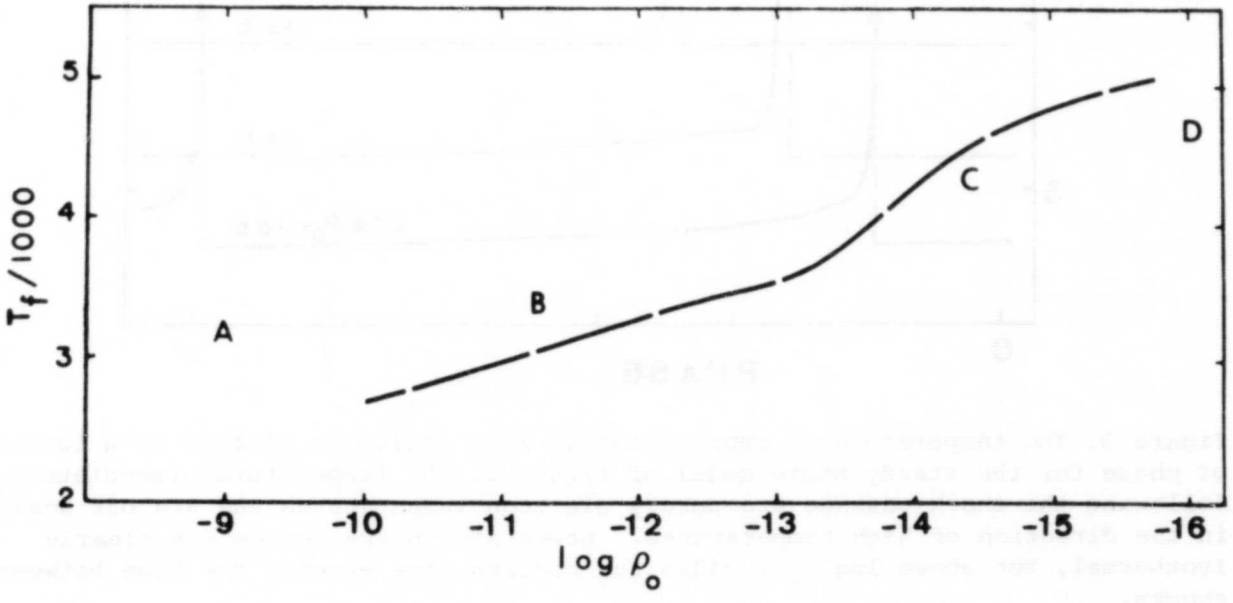

Figure 2. The minimum temperature reached in each cycle in a steady state with repeated shock passage is plotted as a function of pre-shock density for the model of Figure 1; the values are substantially the same for other models calculated as a function of density but not as a function of R.

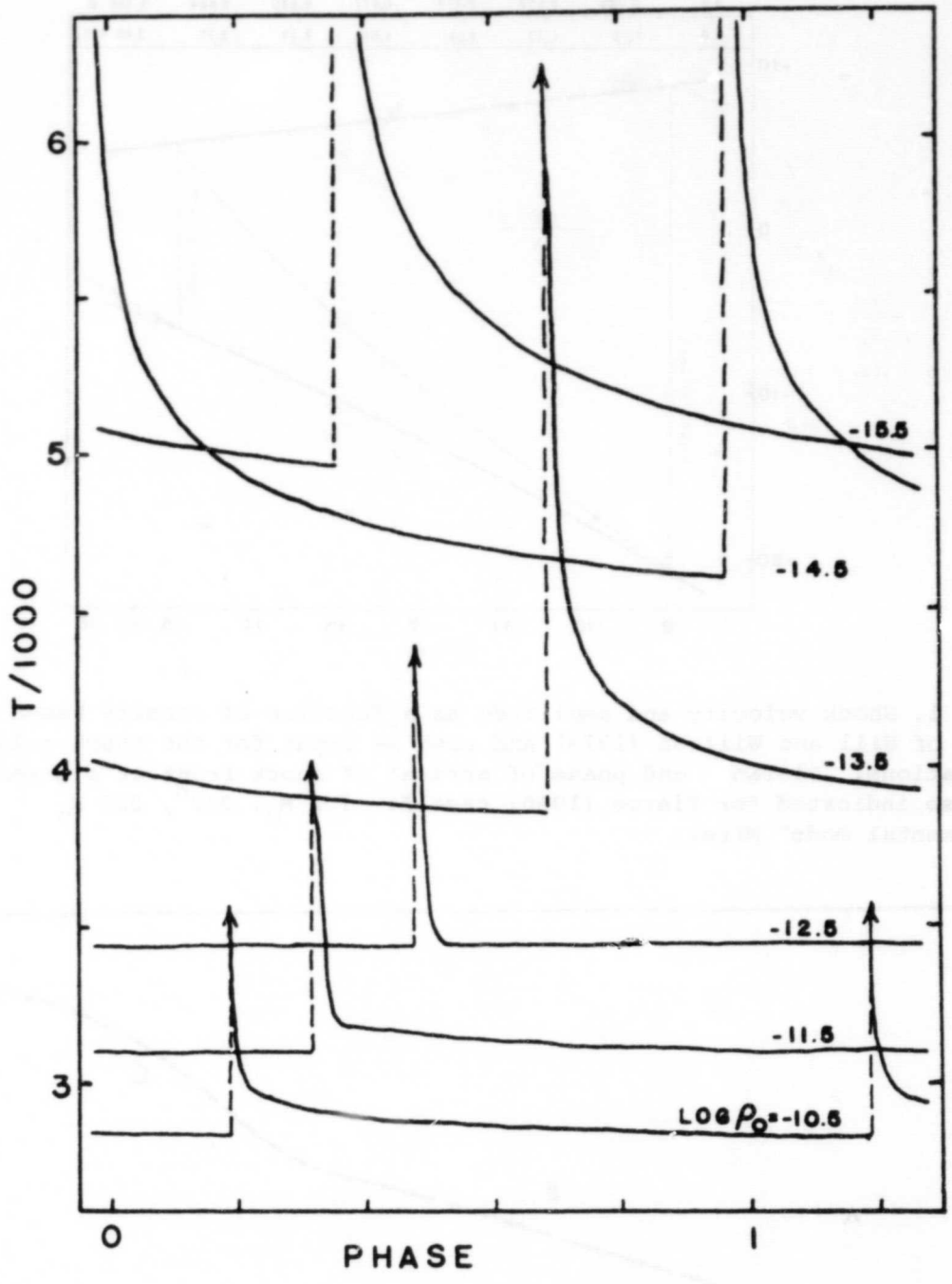

Figure 3. The temperature of representative mass shells is plotted as a function of phase for the steady state model of Figure 2. The temperatures immediately following the shock passage are purely electron temperatures and are off scale in the direction of high temperatures. Lower atmosphere shocks are clearly isothermal, but above log ρ_o = -13.5 the cooling time exceeds the time between shocks.

thermalization time exceeds the period, and a single temperature no longer describes the gas.

Implications

From these calculations of shock relaxation we can conclude that the conversion from isothermal to adiabatic shocks discussed by WH in their mass loss calculation is supported by more detailed shock structure calculations. In the WH calculation the minimum temperature reached was assumed constant throughout the atmosphere; the adiabatic shocks assumed in the upper atmosphere sufficed to eject that portion of the atmosphere. In Wood's (1979) study of mass loss from coupled shocks and dust the temperature was assumed to decrease monotonically through the atmosphere; dust was assumed to form when the temperature became low enough, and this also resulted in substantial mass loss. However the present study raises doubts about the assumed decrease in temperature through the atmosphere, and hence leaves uncertain the location where dust forms around these stars. Clearly any detailed understanding of the mass loss processes in Miras must await further coupled calculations of the overall structure of the atmosphere with the detailed structure of the shocks.

Bibliography

Elitzur, M. 1981, Physical Processes in Red Giants, Iben, I. and Renzini, A. (eds.), p. 363.

Gehrz, R. D. and Woolf, N. J. 1971, Ap. J., 165, 285.

Hill, S. J. and Willson, L. A. 1979, Ap. J., 229, 1029.

Hinkle, K., Hall, D. N. B., and Ridgway, S. T. 1981, Ap. J. (to appear).

Knapp, G., Phillips, T. G., Leighton, R. B., Lo, K. Y., Wannier, P. G., and Wootten, H. A., 1981 (preprint).

Pierce, J. N. 1980, Ph.D. Thesis, Iowa State University.

Wallerstein, G. 1979, Proceedings of IAU Colloquium #46 Changing Trends in Variable Star Research (Reidel).

Willson, L. A. and Hill, S. J. 1979, Ap. J. 228, 854.

Willson, L. A., Wallerstein, G., and Pilachowski, C. 1982, MNRAS 198 (to appear).

Wood, P. R. 1979, Ap. J. 227, 220.

III. MAGNETIC FIELDS

MAGNETIC FIELDS ON THE SUN

Robert Howard

Mount Wilson and Las Campanas Observatories
Carnegie Institution of Washington

ABSTRACT

Synoptic observations of solar magnetic fields are discussed. Seen in long-term averages, the magnetic fields of the sun show distinctive behavior. The active-region latitudes are characterized by magnetic fields of preceding polarity. The flow of following polarity fields to make up the polar fields is episodic, not continuous. This field motion is a directed poleward flow and is not due to diffusion. The total magnetic flux on the solar surface, which is related linearly to the calcium emission in integrated sunlight, varies from activity minimum to maximum by a factor of 2 or 3. Nearly all this flux is seen at active-region latitudes—only about 1% is at the poles. The total flux of the sun disappears from the surface at a very rapid rate and is replaced by new flux. All the field and flux patterns that we see originate in active-region latitudes.

The polar magnetic fields of the sun were observed to change polarity recently. The north polar field changed from positive to negative in the late spring of 1980, and the south polar field changed from negative to positive in the autumn of 1980.

A large-scale velocity feature is found to be associated with the active-region latitudes. This consists of latitude zones with slightly slower than average and slightly faster than average rotation rates. These are formed in a pattern of travelling waves that originate at the poles in both hemispheres and drift to the equator in a period of 22 years. At any one latitude, this torsional oscillation has a period of 11 years. The active-region latitudes are centered about one shear zone of the torsional wave at the lower latitudes.

The variations of the full-disk solar flux are shown to lead to the proper rotation rate of the sun, but the phase of the variations is constant for only a year or two at most.

1. Introduction

Synoptic solar observations of various sorts have been made at the Mount Wilson Observatory for decades. Since 1967, full-disk longitudinal magnetic and line-of-sight velocity observations have been recorded digitally at the

150-foot solar tower telescope magnetograph on a daily basis. This paper is a review of recent published research from Mount Wilson concerning the large-scale latitude distribution of magnetic fields and the large-scale association of solar activity and rotation. In addition, results concerning the torsional inclination of field lines and the persistence of solar-active longitudes are discussed.

All these results have come about as a result of the accumulation of many years of fundamental, synoptic data of the sun. Such observing programs are necessary if we are to address the problems of long-term solar variability and large-scale atmospheric circulation.

For all these observations, the line Fe I 5250.2 Å was used. The square aperture was changed in 1975 from 17.5 arcseconds to 12.5 arcseconds. With this smaller aperture, we obtain a full-disk observation with about 24,000 data points. The instrument and the observations have been described (Howard 1976).

2. Magnetic Fields Over the Solar Cycle

A recent study of the accumulated magnetic field data (Howard and LaBonte 1981) has led to new results concerning the large-scale magnetic field and flux distributions. These results refer to data averaged over several rotations, so there is no longitude discrimination in the analysis. The results may be summarized as follows:

a) The sunspot latitudes (which vary during the cycle) are characterized by the presence of preceding polarity magnetic fields.

b) Following polarity fields migrate poleward from the active-region latitudes in several discrete flows that result from directed motion—not diffusion. These flows increase in velocity as the cycle progresses, averaging about 10 ms^{-1}.

c) The polar magnetic fields of the sun appear to be built up only from such flows of magnetic fields from lower latitudes. The flows of the new cycle reverse the sign of the polar fields around or shortly following maximum. Most recently, the polar fields reversed in the spring of 1980 in the north and in the autumn of 1980 in the south.

d) The weak (<2 Gauss) fields show basically the same patterns as the stronger fields. For both the strong and the weak fields, all organized large-scale field patterns originate in the active-region latitudes.

e) The magnetic field strength at the poles of the sun is no more than a few Gauss.

f) The variation of total magnetic flux ($F_T = |F_+| + |F_-|$) on the sun is only about a factor 3 from spot minimum (1976) to a very active maximum (1979).

g) Magnetic flux is highly concentrated toward the solar equator. The flux in the polar fields is a small fraction (~1%) of the total flux on the sun.

h) Magnetic flux can spread rapidly (50-100 m s^{-1}) over the solar surface from outbreaks of active regions without segregating into separate unipolar latitude zones. This is presumed to be due to diffusion by the supergranular network.

i) Horizontal (non-radial) magnetic fields are not an important factor in the large-scale field patterns in the photosphere.

j) The rate at which magnetic flux appears at the solar surface is sufficient to replace the total flux present in about 10 days.

k) Nearly all the magnetic flux seen on the sun emerges and subsequently disappears at the activity latitudes.

3. Solar Cycle

Recent results (Howard and LaBonte 1980; LaBonte and Howard 1981) have demonstrated a significant connection between a large-scale velocity pattern and the activity cycle. This pattern, seen in Figure 1, consists of latitude zones of slower than average or faster than average rotation. These zones originate at the polar latitudes and drift equatorward, requiring about 22 years to drift from pole to equator. There are two sets of slow and fast zones in each hemisphere at any one time. The central latitude of active-region flux eruption occurs at the shear zone (at low latitudes) between a fast and poleward slow zone. The amplitude of the effect is about 3 m s^{-1}.

The high latitude portion of this travelling torsional wave is clearly the most interesting part, both observationally and theoretically. It would be very difficult to prove that the low-latitude wave was not the result of some small latitude-dependent bias in active-region velocity fields, but the extension of the same wave to high latitudes makes this explanation appear very unlikely. In order to examine the possibility that the high-latitude wave is caused by some mathematical artifact from an existing low-latitude pattern, LaBonte and Howard (1982) have repeated their reduction procedures with a simulated torsional pattern at low latitudes only. This analysis demonstrates that the pattern seen at high latitudes is not created artificially by the low-latitude pattern.

All the evidence, then, suggests that the torsional oscillations are a true solar velocity field. Consequently, an important question arises: Is the torsional wave direct evidence of a large-scale subsurface oscillation that provides in some way a mechanism to cause the activity cycle, or is this surface velocity field an indirect consequence of some subsurface dynamo effect? Yoshimura (1981) has suggested the latter explanation. He proposes that the torsional oscillation is a Lorentz force wave, caused by the motion

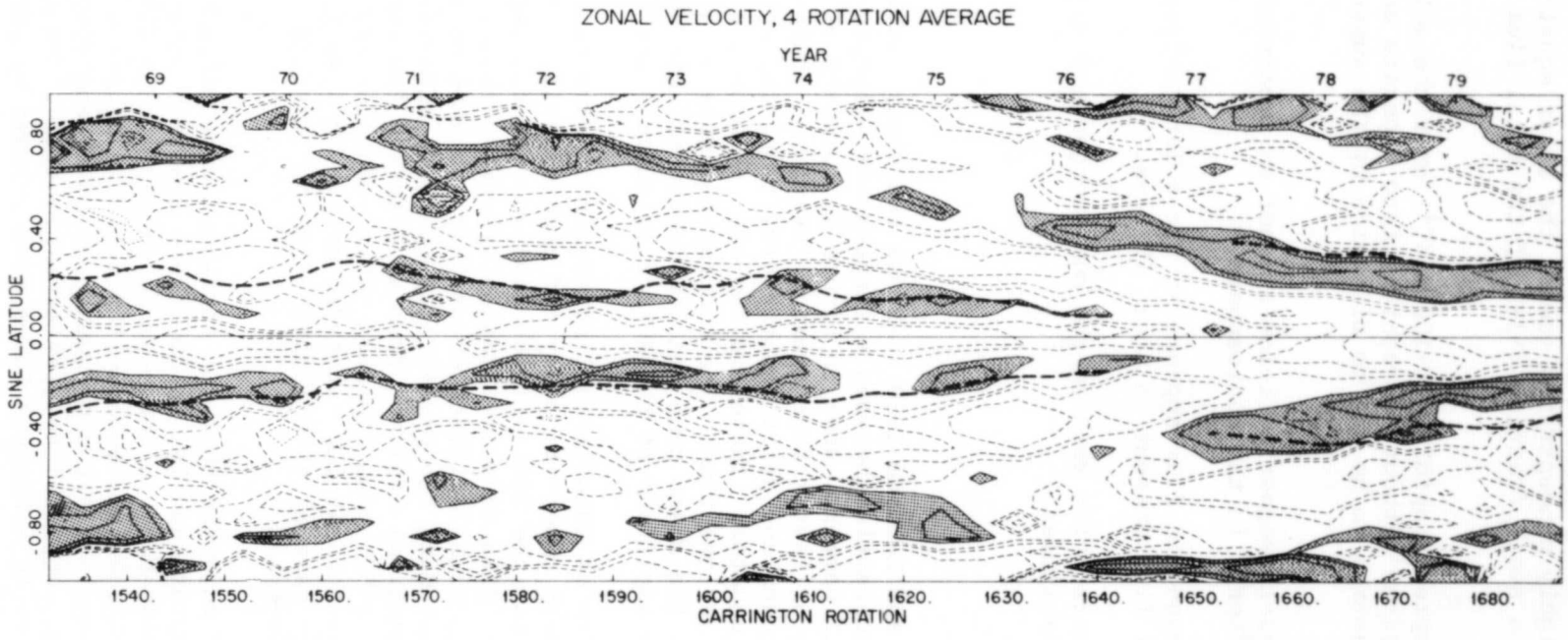

Figure 1. Contour plot of the zonal-excess rotation velocity. The zonal excess is the zonal rotation velocity minus a smooth curve fitted to all zones. There are 34 equal zones of equal width in sine latitude. The daily values have been averaged over 4 Carrington rotations (109.1012 days). Contour levels are 1.5, 3, and 6 ms^{-1}. Solid contour and cross hatching represent westward (faster-than-average) motion. Dashed contours represent eastward motions. The heavy-dashed lines represent the central latitudes of the magnetic flux distribution in each hemisphere. There are 2670 full-disk observations included in this plot.

of the subsurface flux tubes predicted by contemporary dynamo theory. A similar suggestion has been made by Schüssler (1981). But the observed torsional velocity pattern is incompatible with this explanation because: 1) Such a Lorentz-force wave approximates the behavior of the observed torsional wave at low latitudes, but it cannot account for the high latitude portion of the pattern; 2) the amplitude of the observed torsional shear does not decrease with time as one would expect in the case of a Lorentz-force wave, and, indeed, as the calculations of Yoshimura and Schüssler predict; and 3) one would expect the Lorentz-force wave to disappear before it reaches the solar equator because the resulting flux eruption dies out before it reaches the equator, but the torsional wave proceeds with little or no decrease in amplitude right down to the equator.

Several attempts have been made to accommodate the torsional oscillation with the heuristic model of Babcock (Moore 1981; Giovanelli 1981). These efforts give promise of providing an important start toward a theoretical understanding of the solar cycle. At any rate, the α-ω dynamo, which in recent years has received much attention from theoreticians, appears not to operate in the sun, or at least not on a scale that can be important as a mechanism for the solar cycle.

From time to time, it has been suggested that a torsional oscillation of the sun is responsible for the activity cycle. Most recently, Layzer et al. (1979) have suggested that torsional oscillations of a primordial magnetic field might be responsible for the cycle, but no detailed models have been calculated.

4. The Orientation of Magnetic Field Lines

The magnetic field lines in the solar photosphere are oriented very nearly in the meridional plane (Howard 1974). The small toroidal inclination that is observed is such as to trail the solar rotation slightly. Foukal and Duvall (1980) have suggested that this is due to the Reynolds stresses of supergranular convective motions, not to the drag caused by the loss of angular momentum to the solar wind.

Figure 2 shows a plot of east-minus-west magnetic fluxes which suggests a tilt of a few tenths of a degree—preceding polarity fields trailing the rotation, and following polarity fields leading the rotation. This effect is seen only at the active-region latitudes.

5. The Sun as a Star

The measured total magnetic flux of the sun is a good indicator of the level of solar activity, and it is related in a simple way to the "S" parameter of stellar chromospheric Ca emission (LaBonte 1982). From a study of this solar-flux parameter from the Mount Wilson data, LaBonte (1982) has shown that the phase of the rotational (27-day) variation of the full-disk flux can stay

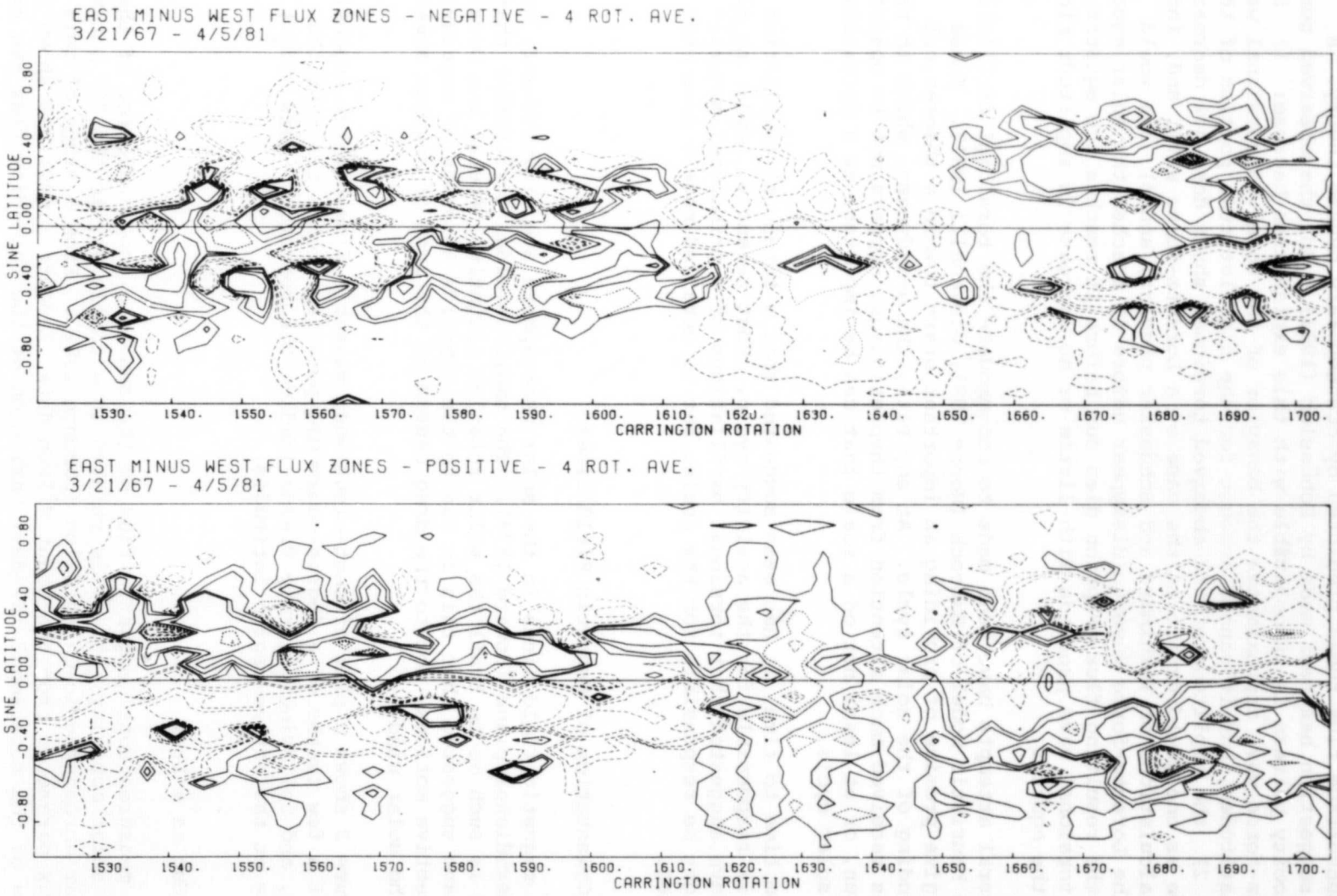

Figure 2. East-minus-west magnetic flux values for negative (top) and positive (bottom) flux measurements. These represent disk-longitude zones (13° in width) at 40° east or west of the central meridian. These data are from March 1967 to April 1981. Solid contours are positive, and dashed contours are negative. Contour levels are $\pm 5 \times 10^{18}$, $\pm 1 \times 10^{19}$, $\pm 2 \times 10^{19}$, $\pm 4 \times 10^{19}$, Maxwells.

fairly constant for several years.

This effect is illustrated also in Figures 3 and 4, which show autocorrelations of the measured full-disk total flux for one-year intervals and superposed-epoch plots of this quantity for multiple-year intervals. The superposed-epoch plots have been constructed with the Carrington synodic period (27.2753 days). This period has been shown to be a fair approximation to the true period of rotation of the sun at the active-region latitudes where nearly all the magnetic flux is found (Bumba and Howard 1969), but certainly some smearing occurs in the superposed-epoch plots over intervals of several years.

Support for this work has come from the National Aeronautics and Space Administration (Grant NGR 09-140-015), the Office of Naval Research (Contract N00014-81-C-0065), and the National Science Foundation (Grant AST-80-20445). Dr. Barry J. LaBonte has been a collaborator on much of this work. Mr. John E. Boyden has done much of the computer programming.

REFERENCES

Bumba, V. and Howard, R. 1969, Solar Physics, 7, 28.

Foukal, P. and Duvall, T. L. 1980, Solar Physics, 67, 9.

Giovanelli, R. G. 1981, preprint.

Howard, R. 1974, Solar Physics, 39, 275.

Howard, R. 1976, Solar Physics, 48, 411.

Howard, R. and LaBonte, B. J. 1980, Ap. J. (Letters), 239, L33.

Howard, R. and LaBonte, B. J. 1981, Solar Physics, in press.

LaBonte, B. J. 1982, in preparation.

LaBonte, B. J. and Howard, R. 1981, Solar Physics, in press.

LaBonte, B. J. and Howard, R. 1982, Solar Physics, submitted.

Layzer, D., Rosner, R., and Doyle, H. T. 1979, Ap. J., 229, 1126.

Moore, R. L. 1981, B.A.A.S., 12, 893.

Schüssler, M. 1981, Astron. Astrophys., 94, L17.

Yoshimura, H. 1981, Ap. J., 247, 1102.

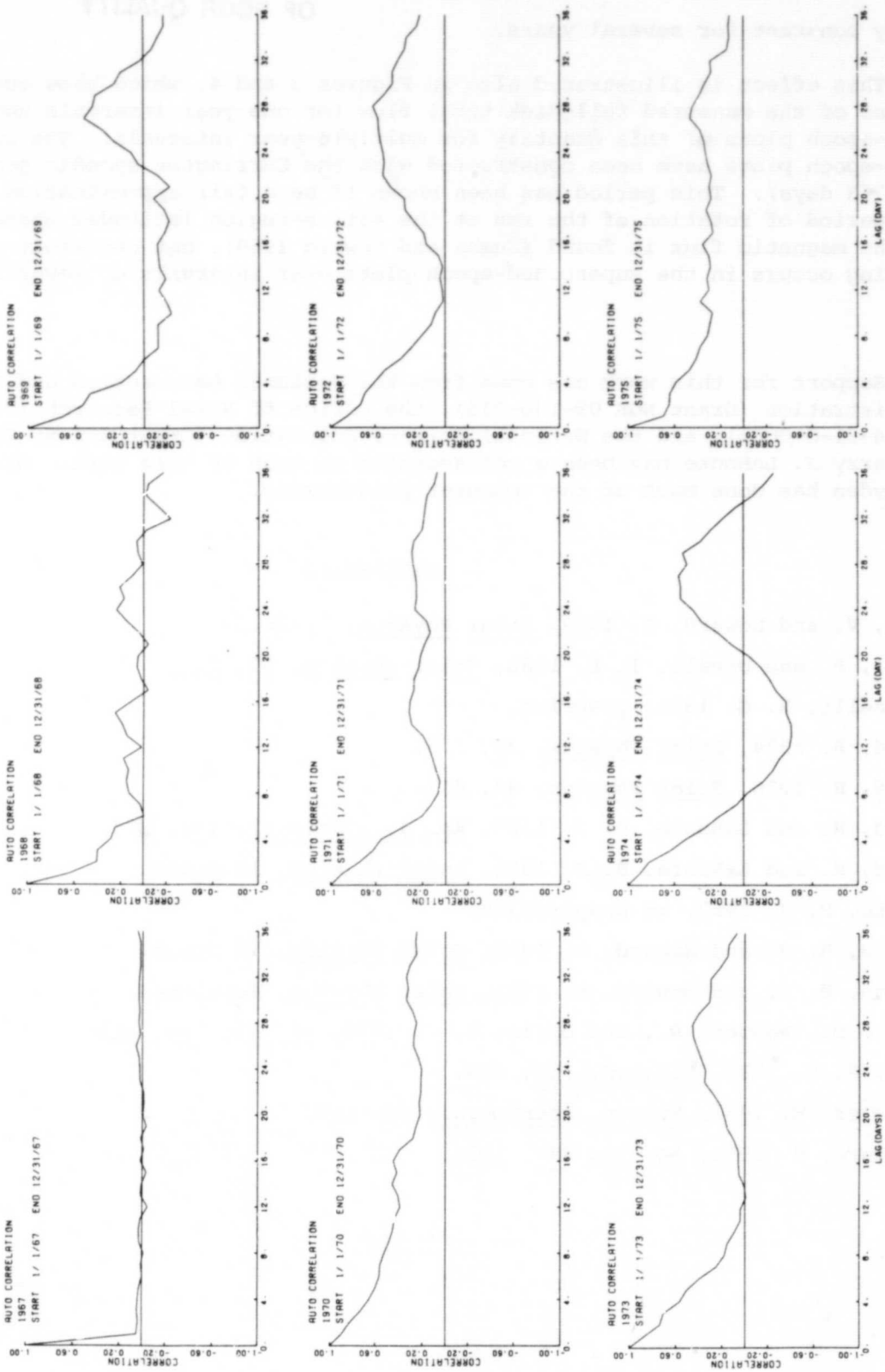

Figure 3. Autocorrelations of the total full-disk magnetic flux of the sun for the years shown.

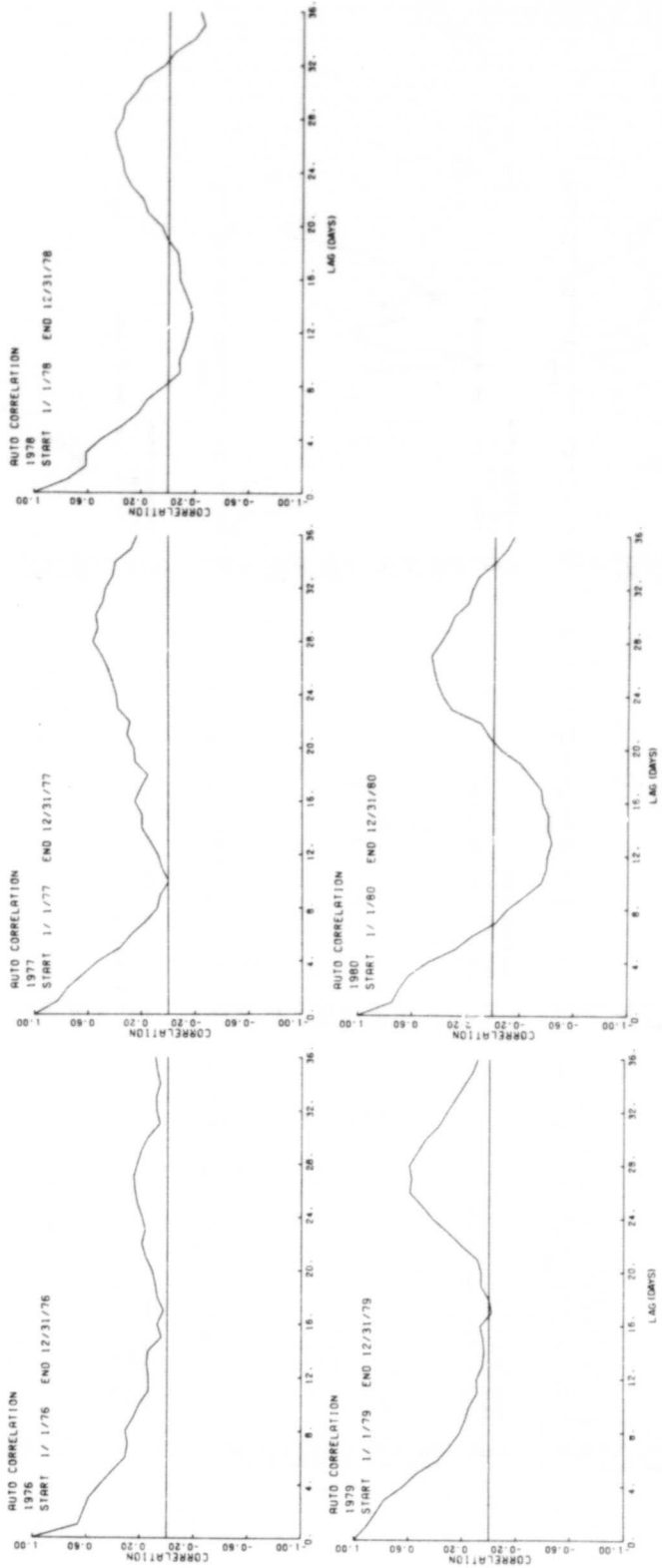

Figure 3. Continued.

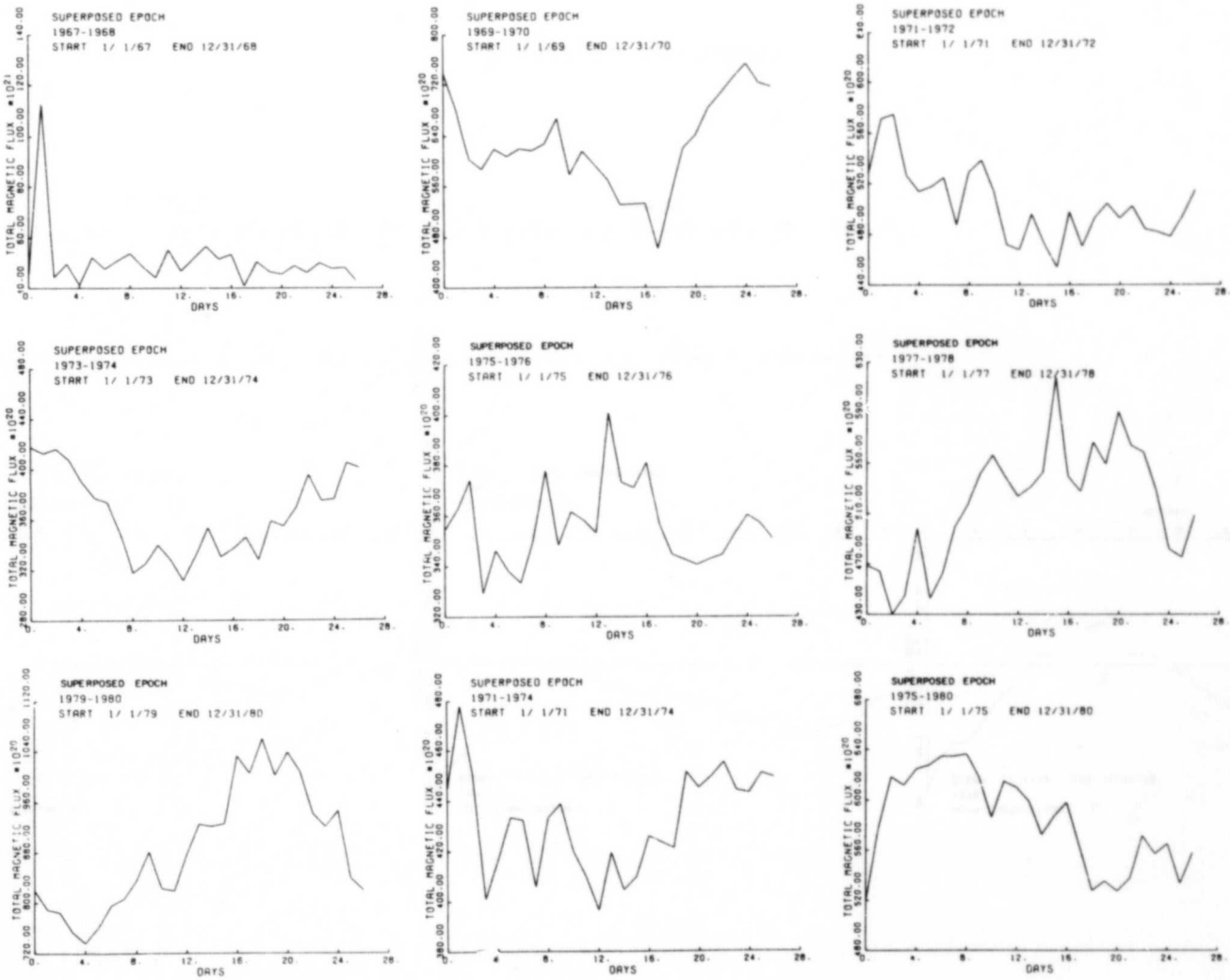

Figure 4. Superposed-epoch plots of the total full-disk magnetic flux of the sun for the intervals shown. The period is 27.2753 days.

CONVECTIVE DYNAMOS FOR ROTATING STARS

Peter A. Gilman

High Altitude Observatory,
National Center for Atmospheric Research*

I. Introduction

Let me first set some bounds on my topic, since I have only thirty minutes. First, I feel it appropriate to focus primarily on the global stellar dynamo problem, as opposed to the problem of how individual magnetic flux tubes are formed and behave. One reason I do this is that we are now confronted with rather clear evidence that some stars have field reversing dynamos, and others do not. I believe global dynamo theory is currently better able to provide clues as to why this occurs. I do not mean to imply that flux tube dynamics is not important for stellar dynamo theory; on the contrary, it may be crucial. However, no one has yet attempted to incorporate flux tube dynamics into dynamo models beyond very crude parameterizations. This problem is difficult enough for the sun, for which at least we can see some of the properties of flux tubes at the top of the convection zone. Clearly the uncertainties rise significantly for other stars.

The second reason I choose to focus on the global dynamo problem is that I feel I know more about it, and it gives me the (selfish) excuse to say something about my own recent work!

My current view is that convectively driven dynamos are the most likely source of magnetic fields in stars that have convection zones. Dynamo theory applied to the sun and stars still has numerous serious difficulties yet to be cleared up, and it could, in the end, still fail, but on balance I find the case for dynamo origin of fields much more convincing than any other explanation. Certainly dynamo origin has been explored much more extensively and carefully. Competing "theories," if we can call them that, usually involve torsional or some other kind of oscillations acting on a perhaps primordial field buried under the convection zone. Such oscillations can always be postulated, but rotation observations made at the surface, e.g., Howard and LaBonte, (1980); LaBonte and Howard, (1981), indicate perturbations on the differential rotation of less than 0.5%. As we will illustrate later in more detail, differential rotation plays a central role in stellar dynamo theory, because of its ability to induce toroidal magnetic fields from poloidal ones. It's very hard for me to see how such weak oscillations can compete in inducing fields. The same argument applies to acoustic oscillations in a star competing with convection to generate and maintain either differential rotation or magnetic fields, and yet such effects have been proposed.

Even more extreme is the notion that fields in the solar or a stellar convection zone are primordial, having never been dissipated, as has been argued principally by Piddington (see, e.g., Piddington, 1978, and earlier references cited therein). I feel the crucial point that has been missed here is that, however large the electrical conductivity, turbulence is quite capable of cascading magnetic energy down to length scales on which ohmic dissipation takes place, on a time scale which is essentially the eddy turnover time for the energy containing eddies. Frisch (1977) has made this argument by analogy with ordinary turbulence, and I find it quite convincing. I believe the

*The National Center for Atmospheric Research is sponsored by the National Science Foundation.

difficulty with stellar dynamo theory is not that there is no induction of fields (which would have to be the case if the fields were primordial, since they are not growing without limit) but that the theory predicts too much induction. As I will argue later, we are currently probably underestimating the magnitude of processes which bound the field.

Tidal forcing from the planets (principally Jupiter in the solar system) has also been proposed numerous times (particularly in the Soviet literature) to explain the solar cycle. I have not attempted a calculation of the tidal flows expected in the sun, but, again, they seem very unlikely to be able to compete with convection and differential rotation. So far, all we have here is the apparent near coincidence of solar cycle and Jupiter orbital periods. But of course the true magnetic period of the sun is 22 years, not 11. The planetary tidal hypothesis is amusing to contemplate in one respect, in that, if it held for stars generally, then we should expect that stars observed to have CaII, and therefore magnetic, cycles also have planetary systems whose major planets have orbital periods somewhere near a decade, while stars with non-cyclic CaII emission apparently do not. I leave it to others, if they wish, to ponder that possibility further.

II. Brief sketch of solar dynamo theory

Dynamo theory as it is currently applied to the sun and stars has its roots principally in the work of Parker (1955). Parker demonstrated that the combination of a) differential rotation b) "cyclonic" or helical motions, and c) turbulent diffusion of magnetic fields, could give rise to amplification of large scale toroidal and poloidal magnetic fields, as well as migratory dynamo waves which could explain the migration of the sunspot zones toward the equator. New toroidal fields are produced from the poloidal field by the shearing of differential rotation; new poloidal fields are generated from the toroidal field by the lifting and twisting of the helical motions; and turbulent diffusion allows coalescence of small scale magnetic structures into a net global pattern.

Important papers by Babcock (1961) and Leighton (1964, 1969) followed, which were closer to the solar dynamo problem in a phenomenological sense, but were mathematically and physically less rigorous, more *ad hoc*. But all involve an oscillating feedback between poloidal and toroidal fields, and a dissipation mechanism to keep the fields from growing without bounds.

Greater rigor and formality returned to the dynamo problem with the development, principally by Steenbeck, Krause, and Radler, of "mean field electrodynamics" in the late 1960's (for reviews, see Krause 1976, Radler, 1976). This theory attempts to predict the behavior of a global scale average field from the action of small scale fluid motions on small scale magnetic fields. In mathematical terms, the induction equation for this mean field $\vec{B}$ takes the form

$$\frac{\partial \vec{B}}{\partial t} = \nabla \times (\vec{V} \times \vec{B} + \alpha \vec{B}) - \lambda \nabla \times \nabla \times \vec{B}. \qquad (1)$$

In equation (1) $\vec{V}$ represents the global motion present, larger in scale than the averaging element (which in practical terms is a volume element larger than an individual eddy but smaller than the dimensions of the fluid body, or perhaps an axisymmetric ring of fluid of small cross-section). The parameter α incorporates Parker's

cyclonic motions, and in the theory is proportional to the helicity $H = v \cdot \nabla \times \vec{v}$ of the fluid flow $\vec{v}$ in the form

$$\alpha = -\frac{1}{3}\overline{v \cdot \nabla \times v}\tau \qquad (2)$$

in which τ is a correlation time which measures the persistence of the small scale motion and the overbar denotes an ensemble or volume element average. λ is a turbulent diffusivity for magnetic flux. α and λ are usually taken to be scalars although in general we should expect them to be tensors.

When $\vec{V}$ is taken to be an axisymmetric differential rotation $\omega(r, \phi)$, where r is radius and ϕ latitude, and $\alpha/r\omega << 1$, then the α effect is ignored in generation of toroidal fields, and we have the so-called $\alpha - \omega$ dynamos, which are a more formal and general version of Parker's migratory dynamo. $\alpha - \omega$ dynamos have been applied most extensively to the sun, because they generally give field reversing solutions with migratory toroidal and poloidal fields. The long series of dynamo models by Yoshimura (see, e.g., Yoshimura 1975a) are also of this type. However, Yoshimura has identified α (his "regeneration action") with global or "giant cell" convection on the sun, while most other solar dynamo modelers have been less specific about the scale of motion principally responsible for α.

In simple $\alpha - \omega$ dynamo models, the frequency of field reversals is proportional to the square root of the product of α and the angular velocity gradient, so the larger the helicity, or shear in the differential rotation, the shorter the dynamo period. With "tuning" of the parameters ω, α, and λ, $\alpha - \omega$ dynamos can simulate many features of the solar cycle. Results from a particularly simple example from Stix (1976) are illustrated in Figure 1. This model has angular velocity increasing with depth in a step function, and an $\alpha \sim \cos\phi$. An 11 year period is seen in the migration of toroidal and poloidal fields toward the equator.

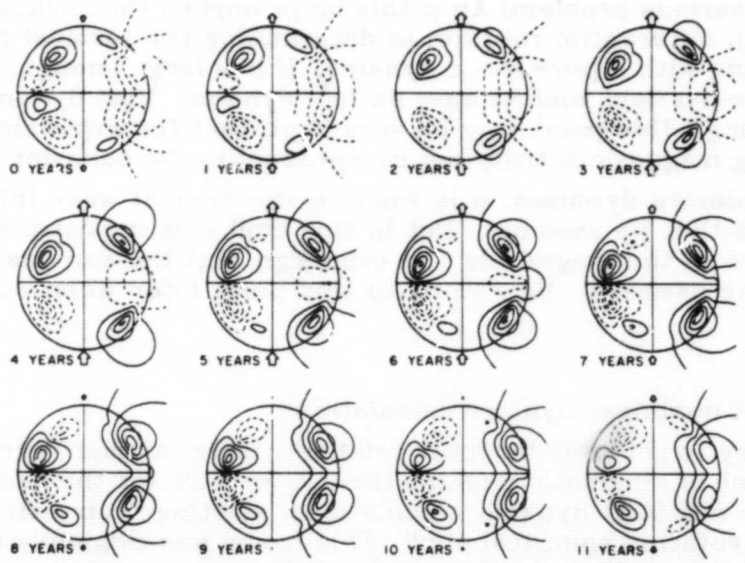

Figure 1. α–ω dynamo solution from Stix (1976) showing evolution for one complete "solar cycle." Closed contours on left in each cross section are toroidal field magnitudes (solid and dashed opposite signs); Poloidal field lines are on the right. Reprinted by permission of the publisher.

Dipole symmetry of the fields, such as is reflected in Hale's sunspot polarity law and polar fields, is slightly favored in dynamo models where α and ω gradients are concentrated in low latitudes, but it is not really understood why. More highly tuned models involving more complex functions for α and ω, such as that of Yoshimura (1975a), can give poleward migration of poloidal fields near the poles. Still further elaborations involving introduction of *ad hoc* nonlinear feed backs with time delays (e.g. Yoshimura 1978a,b) allow generation of successive solar cycles of varying amplitude and period.

Yoshimura (1975b) demonstrated that in $\alpha - \omega$ dynamos the migration of toroidal field with time is along isorotation surfaces. Which direction the field propagates is determined by the sign of the product of the helicity or α and the sign of the angular velocity gradients. Propagation toward the equator with the right phase relation between toroidal and poloidal fields requires the angular velocity increase with depth, as well as $\alpha>0$ (helicity left handed or negative) in the northern hemisphere, $\alpha < 0$ in the southern hemisphere. We will illustrate in more detail how helicity and differential rotation interact to produce migration of the toroidal field when we sketch some of our own recent results below.

A large part of the "success" of $\alpha - \omega$ dynamos in simulating solar cycle behavior is clearly due to the number of free parameters that can be tuned. In addition, with few exceptions, only the kinematic dynamo problem is being solved. That is, the motions are assumed, not calculated, and feedbacks from the induced electromagnetic body forces are ignored. But even in the kinematic dynamo context there are serious difficulties. The turbulent diffusivity λ is a considerable oversimplification of what must really be happening; it is undoubtedly a time varying tensor, perhaps even changing sign, and is dependent in some nonlinear fashion on the scale and magnitude of motions included. The angular velocity gradient with depth in the sun is not known beyond inferences from the difference between sunspots and doppler rotations that it increases inward in the outermost 10 - 20 x 10^3 Km. But perhaps most important, mixing length arguments (Kohler, 1973) and consistent global convection models such as our own predict helicity and α which are 2 - 3 orders of magnitude too large to give the correct solar cycle period. (The sign of α does not appear to be a serious problem) An α this large implies that helicity is competing on equal terms with differential rotation in determining the toroidal field, so that we no longer are dealing with a pure $\alpha - \omega$ dynamo. If α is large enough, it determines both poloidal and toroidal field, and we have an "α^2" dynamo. Most dynamos of this type are not field reversing! This point may be very important for explaining the existence of stars with strong magnetic activity but no apparent cyclic behavior.

In the Yoshimura dynamos, α is small in the limit of weak influence of rotation upon convection that he assumes. But in this limit it is impossible to maintain a differential rotation of the magnitude and even sign that the sun has with convection of the amplitude he assumes. We return to this point later when considering our own model results.

III. Some current nonlinear dynamo calculations.

In part to try to get away from the relatively large number of free parameters and functions present in kinematic dynamo theory, we have for the past three years been doing nonlinear full MHD dynamo calculations, starting from a nonlinear model for convection in a rotating spherical shell. This model was originally developed to study what amplitude and profile of differential rotation is generated by global convection, as a function of such basic input parameters as the rotation rate of the system and

the amount of heating at the bottom of the shell. The mathematical structure of this model has been described in detail in a number of previous publications, e.g. Gilman 1975, 1977; Gilman and Miller, 1981. In brief, it represents a stratified but incompressible shell of fluid heated uniformly from inside and rotated at a specified rate. Stress free boundary conditions confine the angular momentum to the shell in the absence of magnetic stresses acting across a boundary. The fluid is assumed to have constant diffusivities for momentum and temperature. Solutions are found for the three dimensional nonaxisymmetric velocity, temperature and pressure patterns using a Fourier expansion in longitude, and a grid in the meridian plane. Typically between 16 and 25 longitudinal wave numbers are included. The nonlinear interactions among all these modes are explicitly calculated.

We have used this model primarily to determine the conditions under which differential rotation similar in profile and magnitude to that of the sun are obtained, when solar values are used for most of the physical parameters of the model. In general, we have found that large amplitude, broad equatorial acceleration occurs only when the convection zone is relatively deep, say 1/3 of the radius or more, and the influence of rotation upon the convection is strong (the opposite limit to that used by Yoshimura, 1972). Under these circumstances the amplitude or kinetic energy of the convection is comparable to that of the differential rotation, the precise ratio depending sensitively upon such parameters as the eddy viscosity of the fluid.

We have generalized the hydrodynamic code to a full MHD code using the same solution procedures (see Gilman and Miller, 1981) to find a number of dynamo solutions, mostly for the case when the model differential rotation surface profile is at least initially similar to that of the sun. In these calculations, we are, as with the $\alpha-\omega$ dynamos, forced to use a turbulent diffusivity for magnetic field, but there is no assumed α as in equation (1). The full induction effects of the convection and differential rotation are instead explicitly calculated, and the full feedback of the electromagnetic body force arising from the dynamo generated fields is retained. Under certain circumstances, its effects can be quite important, as we shall see.

Usually, we find a dynamo solution by first allowing the hydrodynamic solution for convection and differential rotation to become fully established, through a time integration of the equations starting from an initial random temperature field. Then we add a toroidal magnetic field and follow its subsequent development or decay. In some cases, we use as initial conditions for a new calculation the end solution for a previous case with somewhat different parameter values, partly in order to speed convergence, but particularly to find certain finite amplitude dynamo solutions for conditions under which a small amplitude magnetic field would decay.

Although our model is not an $\alpha-\omega$ dynamo in the sense that we do not lump induction effects into a parameter α, our solutions behave in many ways similar to such dynamos, and it is useful to describe their behavior in terms of the separate effects of differential rotation and helicity. Let me take you through a series of schematic drawings that describe the induction process going on in this model, which repeats many of the arguments given in Parker (1955) made specific to the properties of convection and differential rotation we find in the model.

Figure 2 gives a schematic of the global convection pattern found in the model and the differential rotation it drives. I call your attention particularly to the structure of the convection. The horizontal velocity vectors are tilted relative to the east-west direction, and the whole flow pattern has a spiral structure. The first feature implies angular momentum transport by the convection toward the equator, which is responsible for maintaining the equatorial acceleration. The second feature indicates

the flow has helicity, which together with the differential rotation, drives the dynamo. Both of these properties of the convection arise due to the influence of coriolis forces. This particular drawing of the convection is for a case of moderate influence of rotation upon the convection, for which the axis of the convective roll bends toward the pole with latitude. With stronger influence, the axis cuts the outer surface at a finite latitude, as the roll attempts to align with the axis of rotation. The convection pattern seen in Figure 2 illustrates how closely linked the mechanism for differential rotation maintenance (angular momentum transport) and dynamo action (helicity) are. The physics of the system really does not allow them to be varied independently, as has been done in kinematic dynamo calculations.

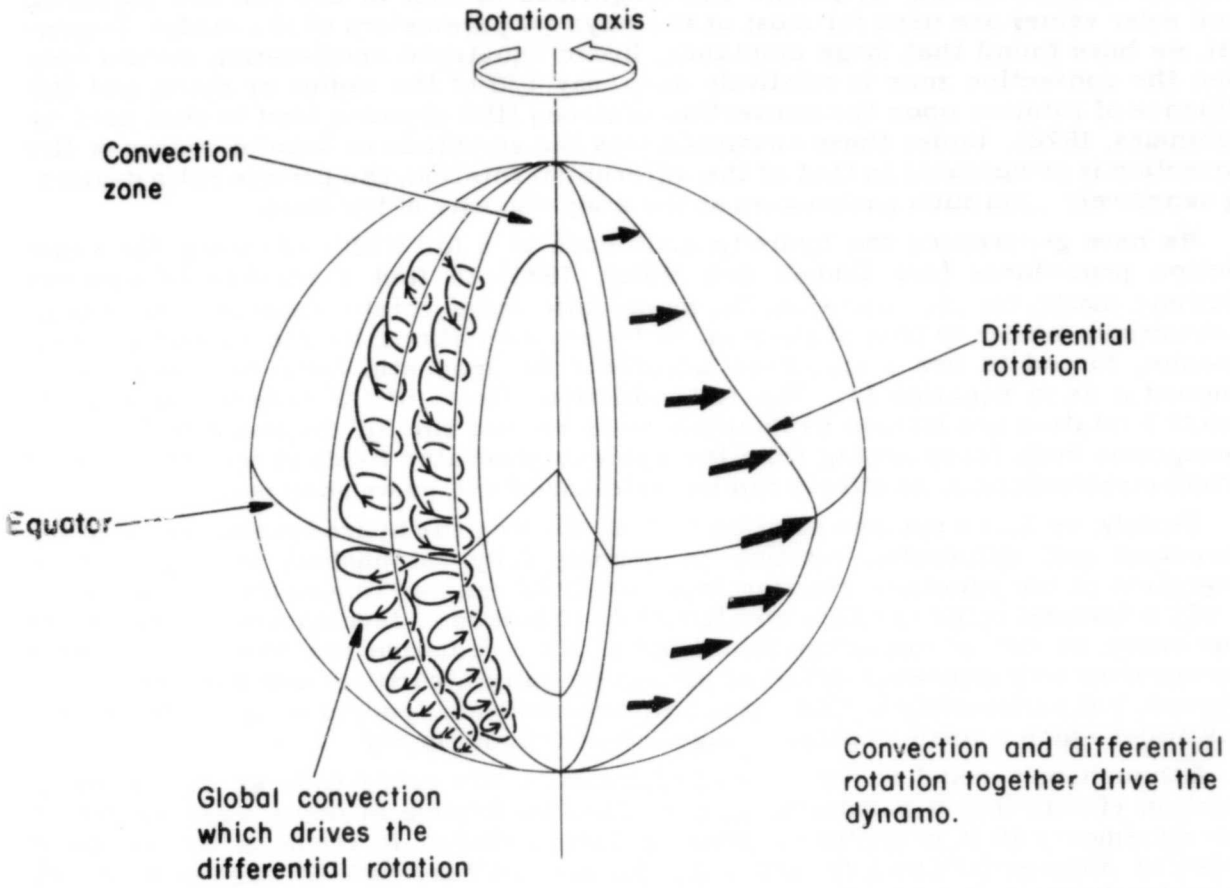

Figure 2. Schematic of global convection patterns which drive the differential rotation in a spherical shell convection model.

Figure 3 shows typical meridional cross sections of differential rotation and helicity found in solutions with strong influence of rotation upon the convection. The angular velocity Ω is constant on cylinders concentric with the axis of rotation, and therefore Ω decreases with radius as well as latitude. Outside the tangent cylinder to the inner boundary (dashed line) the helicity is negative (left-handed) in the northern hemisphere, positive in the southern hemisphere. (The shell is cut off at 60 degrees N and S to avoid computational instability due to convergence of the meridians.)

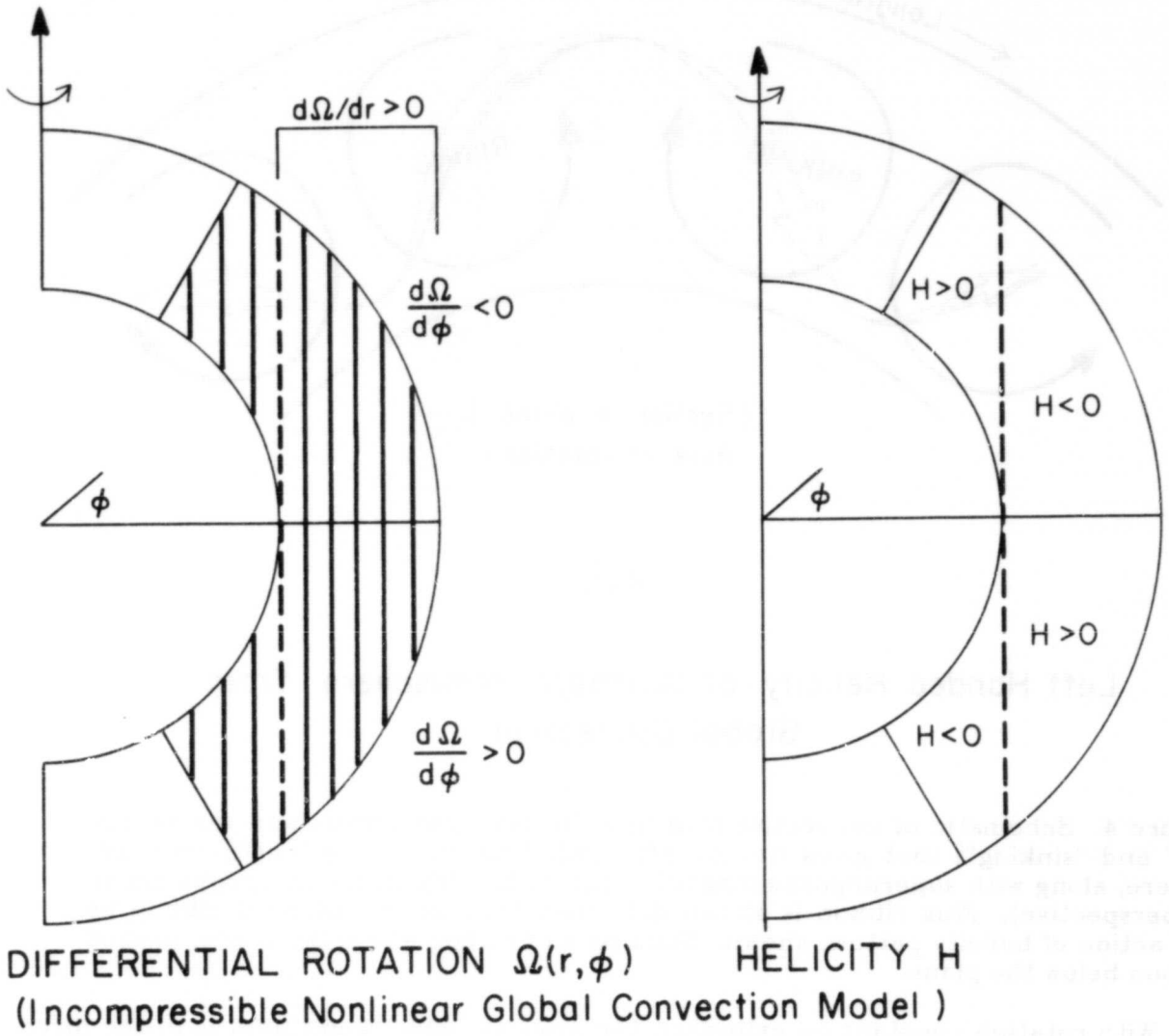

Figure 3. Schematic distribution of angular velocity (left) and helicity (right) generated in global convection model when influence of rotation upon the convection is strong. Helicity $H = \vec{v} \cdot \nabla \times \vec{v}$, where $\vec{v}$ is the convective velocity vector.

In our dynamo calculations, we have found that it is the helicity outside the tangent cylinder that is primarily responsible for the dynamo action (the model clearly does not handle high latitude helicity and dynamo action as well, either, something which needs further study). What that helicity does to a toroidal flux tube or ribbon is shown in Figure 4, which is a cross-section of the shell at a northern hemisphere low latitude in the plane perpendicular to the axis of rotation. Clockwise flow is associated with fluid, rising out of the plane, counterclockwise with sinking fluid. An initially straight toroidal flux ribbon will be lifted in a direction parallel to the rotation axis and pushed out toward the outer boundary, sunk and pushed toward the inner boundary, taking on the structure shown. (The solid line part of the ribbon lies above the plane, the dashed part below the plane.) The end result of this lifting and twisting process is schematically shown for one loop in Figure 5 A new loop in the meridian plane has been formed from the original toroidal field.

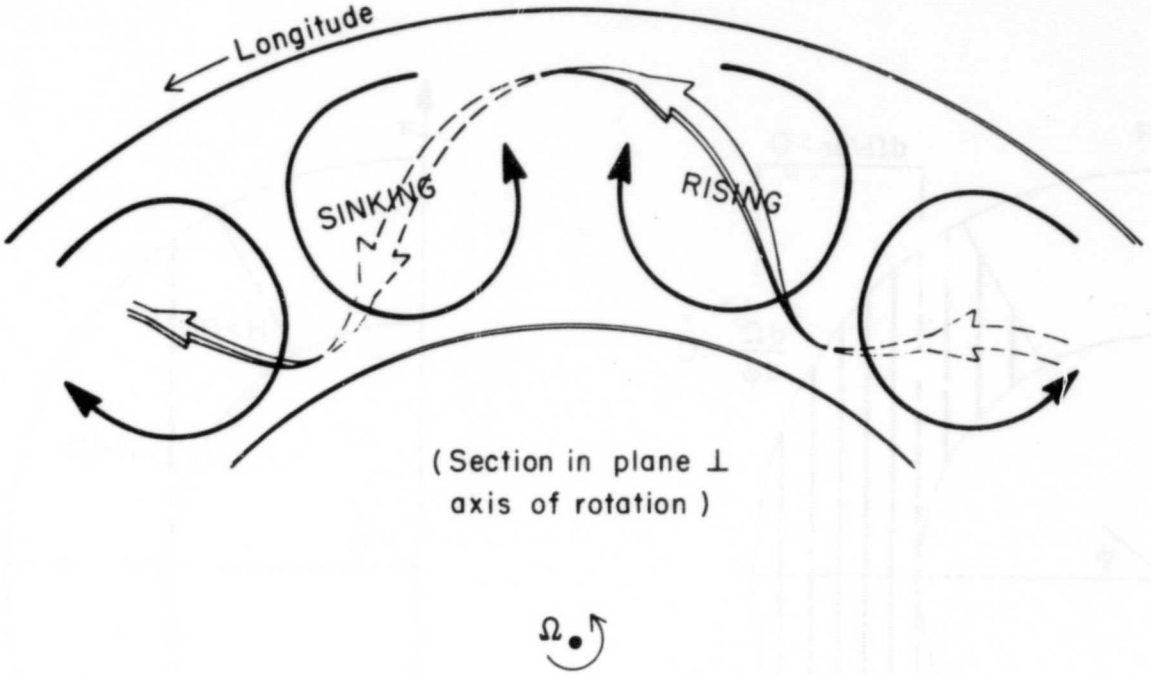

Left Handed Helicity of Northern Hemisphere from Global Convection

Figure 4. Schematic of convective flow field (heavy solid arrows and words "rising" and "sinking") that gives rise to left-handed helicity in the northern hemisphere, along with superimposed magnetic flux ribbon (light, broad, arrows drawn in perspective). Flux ribbon is shown deformed from purely toroidal ribbon by the action of helicity pattern shown. Solid part of ribbon above the plane, dashed ribbon below the plane.

With rotation constant on cylinders, the angular velocity gradient is in the direction perpendicular to the axis of rotation (z direction in Figure 5). This gradient then shears the meridional flux loop again out into the toroidal direction. With angular velocity increasing outward, the outer part of the loop will be pushed forward in longitude, the inner part backward. This results in new toroidal field near the top of the loop of the same sign as original, and toroidal field of the opposite sign near the bottom. The net effect is to move the pattern of toroidal field upward, and therefore poleward, roughly parallel to the rotation axis. In the southern hemisphere, due to the change of sign in helicity, the toroidal field pattern would move downward. This propagation direction is opposite to what we want for the sun, and we return to this point below.

What we have illustrated is what a single convective mode whose structure looks like that in Figure 2 would do. In reality in the model, there is always present a whole spectrum of convective modes of different longitudinal wave numbers, different amplitudes, and somewhat different structures. But their net effect is similar to what we have shown.

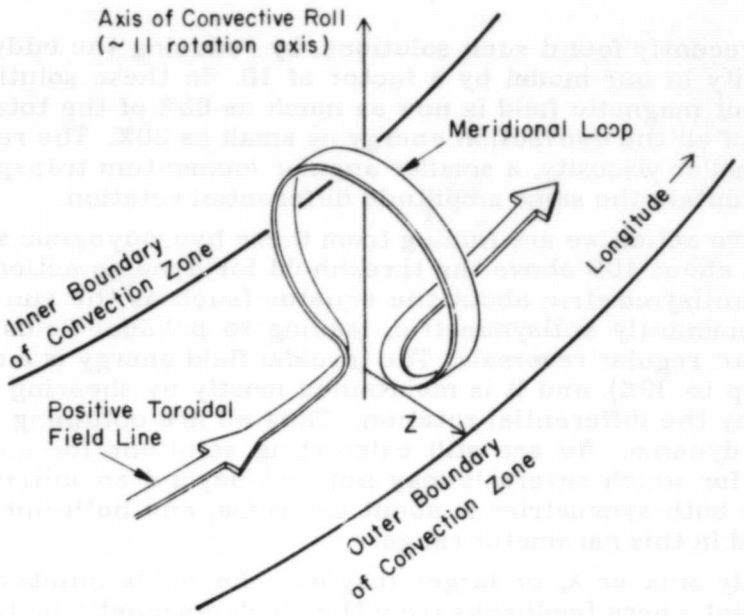

Schematic of Deformed Field Line to be Acted Upon by Differential Rotation

Figure 5. Schematic of flux ribbon twisted up into meridional plane by helicity, about to be acted upon by differential rotation.

IV. Nonlinear dynamo results

For a given hydrodynamic solution, whether we get dynamo action (growing magnetic fields sustained at finite amplitude) or not depends upon what magnitude we assume for the turbulent diffusivity λ. Obviously, the smaller is λ, the more dynamo action we should get. In every case, there is a threshhold value of λ above which (magnetic Reynolds number below which) an initial perturbation field decays, below which it grows. This behavior is similar to that for the kinematic dynamo problem. But the kind of dynamo action we get depends sensitively on the relative amplitudes of differential rotation and convection. We find it convenient to measure these amplitudes by the total kinetic energies integrated over the whole volume of convecting fluid.

The first dynamo calculations we performed (Gilman and Miller, 1981) were for flow patterns for which the kinetic energy of the convection was 2/3 or more of the total, the differential rotation 1/3 or less. We found what I would call "random" dynamo action, in which amplified fields were maintained, but no clear pattern of field reversals emerged, nor was any dominant symmetry in the magnetic field about the equator established even if one was assumed initially. The toroidal field was a small percentage of the total magnetic field energy (~ 5 - 10%), and its maintenance was primarily by the helicity of the convection, not by differential rotation. Thus, in this case our dynamo was more of the α^2 type than the $\alpha - \omega$ type. Initially, this was a discouraging result, but it seemed clear we needed to find other hydrodynamic solutions for the same amplitude differential rotation (since that is constrained by observations) but smaller convection amplitude, in order to reduce the relative role of convection in maintaining toroidal field. A second reason for doing this is that the convection spectrum significantly exceeded the upper limits estimated for the sun by LaBonte, Howard and Gilman (1981).

We have recently found such solutions, by reducing the eddy viscosity and thermal conductivity in our model by a factor of 10. In these solutions, the differential rotation without magnetic field is now as much as 80% of the total energy of the system, the sum of all the convection energy as small as 20%. The reason this is possible is that with smaller viscosity, a smaller angular momentum transport rate by the convection can maintain the same amplitude differential rotation.

The dynamo action we are finding from these hydrodynamic solutions is quite different. Within about 10% above the threshhold for dynamo action to occur, an initial toroidal field antisymmetric about the equator (such as the sun is believed to have) remains predominantly antisymmetric, leading to poloidal fields of dipole type, and undergoes clear, regular reversals. The toroidal field energy is a much larger fraction of the total (up to 30%), and it is maintained mostly by shearing of the axisymmetric poloidal field by the differential rotation. Thus we are obtaining solutions very much like an $\alpha - \omega$ dynamo. We are still calculating solutions for an initially symmetric toroidal field, for which reversals may not last beyond an initial transient. But the threshhold for both symmetries is about the same, and both initial symmetries seem to be preserved in this parameter range.

For slightly smaller λ, or larger magnetic Reynolds number, we find the fields grow to the point where feedbacks from the electromagnetic body force cause fundamental changes in the dynamo itself. In particular, the convection is relatively unaffected, but the differential rotation can be severely reduced. For an antisymmetric dynamo only 15% or so above the threshhold, the feedback is strong enough to reduce the differential rotation kinetic energy by more than a factor of 2. At 60% above the dynamo threshhold, the differential rotation kinetic energy reduction is a factor of 5. In the latter case, the field reversals appear to cease, (more like the "α^2" dynamo again) and the dominant symmetry changes from antisymmetric to symmetric. In the former case, the solutions are tetering on the edge of the same behavior. Presumably in solutions still further above the dynamo threshhold, the differential rotation would be damped even more.

The preferential suppression of differential rotation compared to convection is, we believe, a rather general result. The reason it occurs is that, even when the differential rotation is substantially larger in amplitude than the convection, the work it does against the viscous force is much less, because it is a much larger scale flow pattern and its velocity gradients are weaker. Consequently, a given electromagnetic body force is, compared to the viscous force, a larger brake on the differential rotation than on the convection. With the convection undiminished, the angular momentum transport by it remains the same, but the differential rotation drops in magnitude until the sum of work done against the viscous force and the electro-magnetic body force roughly equals the work against viscosity alone in the absence of a magnetic field.

Presumably, if we calculate dynamos for even smaller turbulent magnetic diffusivity λ, we would generate fields of such magnitude that the convection itself would start to be suppressed. This would provide the final upper limit on dynamo field strength since the strength of the entire induction process would be bounded by its own feedbacks.

Even though the differential rotation is damped, the average magnetic energy sustained is higher in the solutions we have studied. We appear, therefore, to have found at least two distinctly different classes of solutions: field reversing dynamos with somewhat lower levels of magnetic fields, and non-reversing dynamos with a higher level of field. We suggest these two types of solutions might provide an explanation for the two types of variability seen in calcium emission, e.g., Vaughan and

Preston, (1980). The strong, irregular emitters have generated a strong enough field to greatly reduce their differential rotation, while the weaker emmitters have not. It is not clear how a change in rotation rate in the model would affect when field reversals occur and what the field amplitude is, because it would be felt in both the differential rotation maintenance and in the helicity. We would need to do a lot more calculations to sort this out, but it may be that for higher rotation rates, the range of parameter values over which the dynamo action suppresses differential rotation is expanded, making it more likely to occur in a sample population of stars.

Durney, Mihalas and Robinson (1981) have also proposed that the strong, noncyclic CaII emitters are dynamos operating further above the dynamo threshhold. They argue that as a result several different dynamo modes are excited which interact and interfere, obscuring a simple cyclic variability. In a nonlinear dynamo model such as ours it is not possible to separate out different dynamo "modes" but it is clear that when differential rotation is suppressed, more of the magnetic energy goes into smaller scale, and the field does take on a less global character, as they suggest. Our mechanism is different from theirs, however, in that it employs a nonlinear feedback from the induced fields to suppress the global, reversing component of the total pattern - it is not just obscured, it is not present.

Returning to the solar case, when we do get field reversals in our model, the period is too short for the sun by about a factor of 10. Our reversing toroidal field is quite broad in spatial scale compared to what may be the case on the sun as evidenced by sunspots. I continue to suspect the short period occurs because the model does not capture the true small scale interaction between an intermittent solar field and global convection. The solar field may "escape" a lot of the helicity if, for example, the field is continually pushed into the corners of giant convection cells, contrary to the idealized picture we drew in Figures 4 and 5. Indeed, Childress (1979) has illustrated with a very simple model how this might happen. Alternatively, or perhaps as well, the global convection on the sun may be even smaller in amplitude than even in our present model calculations.

V. Role of compressibility

An additional difficulty is that when field reversals occur, the migration of the toroidal fields is toward the poles (along the isorotation surfaces) rather than toward the equator. Currently, the only way we see around this difficulty is through the addition of several scale heights of density variation with radius in our model convection zone, something we obviously need to add anyway. The reason compressibility may help is that we have early indications (Glatzmaier and Gilman, 1981a) that global convection modes that extend all the way from top to bottom in a rotating compressible convection zone will generate a differential rotation nearly constant on cylinders with equatorial acceleration only near the bottom of the zone where the scale height is large. The rotation will decrease with height in the outer part. The helicity profile will remain similar to that in Figure 3 at all levels (Glatzmaier and Gilman, 1981b). Figure 6 shows a schematic differential rotation profile we might expect from a full nonlinear compressible calculation (not yet attempted), showing a maximum angular velocity somewhere in the middle of the layer.

Given such a profile, the migration of the toroidal field with time would be toward high latitudes and toward the outer boundary deep in the convection zone until the field reaches the level of angular velocity gradient reversal. Thereafter migration would be back toward the equator. Thus a new magnetic cycle would be thought of as starting near the equator deep down, where synchronization of the two hemispheres would be a natural consequence. Toroidal field, i.e., sunspots, of a new cycle would be seen first in a mid latitude, as observed. This scheme is consistent with an informal

suggestion made by Raymond Hide more than a decade ago, that the latitude where new cycle spots first appear may be a measure of the depth of the convection zone. This assumes whatever dynamo action maintains them is operating primarily outside the tangent cylinder to the inner convection zone boundary due to rotational effects, as is the case with our dynamo.

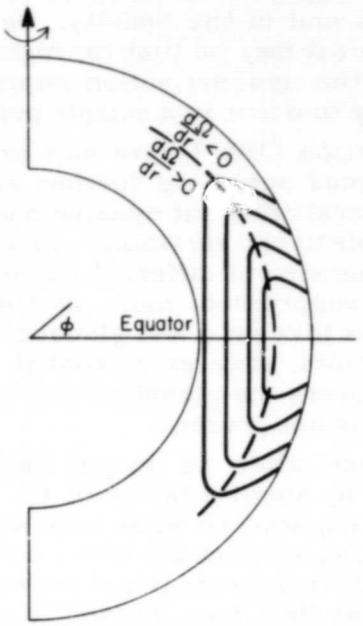

DIFFERENTIAL ROTATION $\Omega(r,\phi)$
(Compressible Model - Glatzmaier & Gilman Initial Tendency Calculation)

Figure 6. Contours of differential rotation predicted to be produced by compressible global convection when individual convection cells reach from bottom to top of the convection zone, as calculated by Glatzmaier and Gilman (1981a).

This picture is rather different from present $\alpha - \omega$ dynamo models applied to the sun. It should be regarded as an hypothesis to be tested with a full compressible dynamo model, certainly not as a result already obtained. We should remark that in a compressible dynamo model, magnetic buoyancy will also be present, and we expect this effect to be particularly important in the top part of the convection zone where a field of given strength results in a much larger buoyancy force than near the bottom.

VI. Other feedback effects.

In addition to the feedback effects already described, there are two others also worth mentioning. The first is that even if the induced magnetic field is weak, say having magnetic energy no more than 10^{-3} or 10^{-4} of the kinetic energy of the system, the cumulative effect can still be significant. In particular, the fluid flow is instable to small perturbations, so that the time histories of two solutions, one with no magnetic field and one with a small field, diverge away from each other after a few thousand timesteps. At the same elapsed time in the two cases, the same convective modes, i.e.,

the same longitudinal wave numbers, will have different amplitudes and phases. The two solutions eventually become uncorrelated with each other. This limits the predictability of such flows, and argues against any deterministic feedback with a long, but essentially fixed, time delay, such has been invoked by Yoshimura (1978 a,b) to explain the amplitude meanderings in the envelope of the solar cycle.

Another, quite different form of feedback we have encountered is one which gives rise to a finite amplitude dynamo instability. For a certain range of magnetic turbulent diffusivity λ a small amplitude magnetic field decays, but a large amplitude field, which has already partially suppressed the differential rotation, is sustained, and has field reversals. The mechanism is that, for a small field, further decay does not amplify the differential rotation, so the decay continues. But a drop in a finite amplitude field results in some resurgence of the differential rotation, which prevents further decay. In this case we have essentially a servomechanism which keeps the field within a certain range. How important this mechanism might be in stars is unknown, as is the range of λ for which it is true. Presumably, if λ is large enough, the field will decay no matter how much differential rotation growth there is. And, as we have already mentioned, if λ is small enough, a large amplitude field is maintained even though the differential rotation is almost completely suppressed. We are continuing to study these kinds of nonlinear dynamos.

VII. Questions concerning application of dynamo theory to the sun and stars

Let me close by summarizing some of the uncertainties and difficulties involved in applying dynamo theory to the sun and stars.

(1) We do not know the profile of angular velocity with depth on the sun, and we know virtually nothing about differential rotation for any other star. There is some hope we can infer rotation with depth for the sun from frequency shifts in the 5 minute oscillations (see, e.g., Rhodes, Deubner and Ulrich, 1979). Measuring differential rotation in stars is an extremely difficult problem, likely to elude us for a long time yet, although Bruning (1981) may have pointed the way as to what to look for.

(2) The form and magnitude of the helicity of the motions cannot be measured, and theoretical predictions of this quantity generally give values much too large when used in dynamo models applied to the sun.

(3) Since global convection has not been measured even on the sun, we cannot pin down the ratio of differential rotation to convection. Our model, and kinematic dynamo theory before it, indicates this ratio is very important for determining what kind of dynamo a star will have.

(4) The theory of turbulent diffusion as applied to stars, particularly diffusion of magnetic flux, is very uncertain.

(5) The relative importance of magnetic buoyancy and convection in stellar dynamos is unclear, and probably can be assessed only in theoretical models which allow both to exist.

(6) The "filling factor" for the magnetic field, that is, what fraction of the volume contains strong fields, is known for the surface of the sun, but not below; only a few very qualitative inferences have been made for other stars. How intermittent the field is will strongly affect the behavior of the dynamo, both induction processes and feedbacks.

(7) Convection zone depth is somewhat uncertain for stars. It is an important parameter for dynamos, because it puts limits on the spatial scale of the largest convective elements, the turnover time for these elements, and it helps determine the

profile of differential rotation. Shallow convection zones are bound to have different differential rotation profiles than deep zones (Gilman, 1980). Convection zone depth will also affect the tendency of stars to form more complex differential rotation profiles, such as illustrated in Figure 8. Also, the region just under the bottom of the convection zone might be the seat of more regular motions favorable for dynamo action, as has been suggested by Galloway and Weiss (1980).

A final remark I wish to make is that even stars without convection zones might conceivably be acting as dynamos. This is most likely to be the case for rapidly rotating stars, where the violation of Von Zeipel's theorem would be greatest. In such stars, Eddington - Sweet circulations should be set up, due to nearly spherical pressure and temperature surfaces not coinciding with more rotationally distorted potential surfaces. However, Busse (1981) has recently argued that the end result of these circulations would instead be primarily a differential rotation, in the form of a baroclinic thermal wind. He demonstrates that such differential rotation profiles are likely to be unstable to non-axisymmetric disturbances in the form of baroclinic waves similar in many respects to those which occur in the terrestrial and other planetary atmospheres. In such a rapidly rotating system, there is no doubt such disturbances would contain helicity, so that the resulting mix of reduced differential rotation and finite amplitude waves could easily act as a dynamo. Baroclinic instability in stars is virtually unexplored at present, but may prove to be important, and is worth further study. It may also occur above convective cores, and possibly beneath convective envelopes.

Acknowledgement

I wish to thank Ron Gilliland for reviewing the manuscript, and Betsy Alves and Bobbie Morse for typing it.

REFERENCES

Babcock, H. W. 1961, *Astrophys. J. 133*, 572.

Bruning, D. H. 1981, *Astrophys. J., 248*, 274.

Busse, F. H. 1981, *Geophys. Astrophys. Fluid Dyn. 17*, 215.

Childress, S. 1979, Phys. Earth Planet. Interiors *20*, 172.

Durney, B. R., Mihalas, D. and Robinson, R. D. 1981, *Pub. Astron. Soc. Pac.* (in press).

Frisch, V. 1977, in Proc. IAU-Colloqu. *38*, "Problems of Stellar Convection" Spiegel, R. A. and Zahn J.-P., Eds. (Springer-Verlag Lecture notes in Physics #71) New York p. 325.

Galloway, D. J. and Weiss, N. O. 1980, *Astrophys, J. 243*, 945.

Gilman, P. A. 1975, *J. Atmos. Sci. 32*, 1331.

Gilman, P. A. 1977, *Geophys. Astrophys. Fluid Dyn. 8*, 93.

Gilman, P. A. 1980, in Proc. IAU Collqu. 51, "Stellar Turbulence," Gray, D. F. and Linsky, J. L., Eds., (Springer-Verlag - Lecture Notes in Physics #114), New York, p. 19.

Gilman, P. A. and Miller, J. 1981, *Astrophys. J.* (Suppl.) *46*, 211.

Glatzmaier, G. A. and Gilman, P. A. 1981a, *Astrophys. J.* (submitted).

Glatzmaier, G. A. and Gilman, P. A. 1981b, *Astrophys. J.* (Suppl.) *45*, 351.

Howard, R. and La Bonte, B. J. 1980, *Astrophys. J. 239*, L33.

Kohler, H. 1973, *Astron. Astrophys. 25*, 467.

Krause, F. 1976, in Proc. IAU Symp. 71, "Basic Mechanisms of Solar Activity," Bumba, V. and Kleczek, J., Eds., (Reidel, Boston), p. 305.

La Bonte, B. J. and Howard, R. 1981: *Solar Phys.* (in press).

La Bonte, B. J., Howard, R., Gilman, P. A. 1981: *Astrophys. J.* (in press).

Leighton, R. B. 1964, *Astrophys. J. 140*, 1559.

Leighton, R. B. 1969, *Astrophys. J. 156*, 1.

Parker, E. N. 1955, *Astrophys. J. 122*, 293.

Piddington, J. H. 1978, *Astrophys. Space Sci. 55*, 401.

Radler, K.-H. 1976, in Proc. IAU Symp. 71, "Basic Mechanisms of Solar Activity," Bumba, V. and Kleczek, J., Eds., (Reidel, Boston), p. 323.

Rhodes, E. J., Deubner, F.-L., Ulrich, R. K. 1979, *Astrophys. J. 227*, 629.

Stix, M. 1976, in Proc. IAU Sump. 71, "Basic Mechnisms of Solar Activity," Bumba, V. and Kleczek, J., Eds., (Reidel, Boston), p. 367.

Vaughan, A. H. and Preston, G. W. 1980, *Publ. Astron. Soc. Pac. 92*, 385.

Yoshimura, H. 1972, *Astrophys. J. 178*, 863.

Yoshimura, H. 1975 a, *Astrophys. J.* (Suppl.) *29*, 467.

Yoshimura, H. 1975 b, *Astrophys. J. 201*, 740.

Yoshimura, H. 1978 a, *Astrophys. J. 220*, 692.

Yoshimura, H. 1978 b, *Astrophys. J. 226*, 706.

C-3

SOLAR PLAGES AND THE INTERPRETATION OF STELLAR Ca II H AND K LINE VARIATIONS IN LATE TYPE DWARFS

J. W. Cook

E. O. Hulburt Center for Space Research, Naval Research Laboratory

Approximately a dozen late type dwarf stars have been observed by Wilson (1978) to undergo cyclic variability in Ca II H and K line emission which seems analogous to the solar activity cycle. What might be learned about these stars from solar analogies? We first estimate the Ca II K index variation of the Sun viewed as a star, and compare with the observed range of Wilson's stellar observations. We suggest trends of increasing relative variation H-K(max)/H-K(min) with later spectral type, due to decreasing dilutional contribution of residual photospheric flux to a 1 Å band at line center, and of increasing relative variation with decreasing relative time of rise to maximum τ_{rise}/τ, reminiscent of the observed solar correlation of a quick rise to sunspot maximum with a strong cycle.

I. INTRODUCTION

Two long term observational programs illustrate the growing interaction between solar physics and stellar astronomy suggested by the phrase "the Sun as a star." Wilson (1978) has recently summarized results from monitoring Ca II H and K line emission core fluxes in 1 Å bands from 91 late type dwarfs (F V - K V) over more than a decade. He has convincingly demonstrated that about a dozen of these have completed a cycle of variation which appears analogous to the solar activity cycle. White and Livingston (1978) have reported results from a program to monitor the solar Ca II H and K line full disk flux. They found an increase in the full disk K index with the onset of activity in the current solar cycle 21. The quiet disk center K index remained constant, leading White and Livingston (1978) to conclude that the full disk K index increase is due to an increasing flux contribution by plages and does not represent a more global brightening.

Because the Sun is the only late type dwarf for which we can obtain spatially resolved observations of inhomogeneous surface structure, modeling of stellar atmospheres must rest heavily upon solar analogies. In this paper we first consider the Sun as a star and estimate the K index variation expected over a solar cycle viewing the Sun as a point source, and compare with observations of Livingston and White. The range of stellar variations observed by Wilson (1978) are then examined. We also estimate the modulation of the amplitue of variation for different lines of sight to the stellar rotational axis if stellar "plages" were confined to low stellar latitudes, as is seen on the Sun. We argue that relatively small extensions of properties already observed on the Sun will match the stellar observations.

II. THE SUN AS A STAR

We make use of the observed solar plage-to-quiet region contrast, the observed latitude distribution of solar plages, and an estimate of the fractional flat disk area covered by plages versus sunspot number. We assume that solar Ca II K line flux variability arises from a changing fraction of the surface covered by plages having an average contrast C to the quiet background. Sheeley (1967) used this approach to estimate a ratio of 1.40 for the Ca II K flux at solar maximum to that at solar minimum, using C = 3 from observations of the Ca II K line in quiet and plage regions and a value of 0.20 for the maximum fractional flat disk area f covered by plage from planimetry of Mt. Wilson Ca II K_2 spectroheliograms.

Cook, Brueckner, and VanHoosier (1980) used a contrast model to examine flux variability in the far UV over the solar cycle. They determined an approximate calibration of f (viewed in the solar equatorial plane) with sunspot number R_Z, based on Sheeley's (1967) measurements, which gave $f = 6.25 \times 10^{-4} R_Z$. They also examined the importance of center-to-limb variation (basically arising from the different sampling of $\mu = \cos\theta$ over lines of constant heliocentric latitude versus radial lines), and showed that the straightforward formula $\text{Flux}(R_Z) = \text{Flux}(R_Z=0)[Cf + (1-f)]$ is adequate for the flux variability viewed in the equatorial plane.

Wilson's (1978) stellar H and K indices are proportional to the equivalent widths over 1 Å intervals centered on the Ca II H and K emission cores. A 1 Å band at line center is somewhat wider than optimal for sampling the solar chromospheric emission core (see Figure 1 in White and Livingston, 1978). The observed variation over an activity cycle is diluted by inclusion of a residual photospheric contribution from the line wing and core. We estimated the solar plage K index contrast from Sheeley's (1967) observations of quiet and plage Ca II K profiles by integrating the flux over a 1 Å interval at line center. We also determined the K(0.5Å) contrast over a 0.5 Å band at line center, and the K_3 contrast in intensity at line center. This gives a range C = 1.67-2.33 for the Wilson K index contrast, and we adopt C = 2.0. Similarly, the K(0.5 Å) contrast is 3.0, and the K_3 contrast 3.5.

Figure 1, from Cook, Brueckner, and VanHoosier (1980), shows a fit to solar Ca II K line measurements of the flux in a 0.5 Å band at line center furnished by Livingston and White (1979, private communication) for the period up to the end of 1978, well into the rise of the current sunspot cycle, which are well reproduced by a contrast factor C = 3 and a value for f from the calibration with R_Z. Figure 2 shows more recent observations (Livingston and White 1980, private communication) toward the peak of the current cycle of the K_3 index, fit using C=3.5. Both sets of observations are in good agreement with a contrast model estimate of $K(R_Z) = K(R_Z=0)[Cf+(1-f)]$ using the appropriate C, with no free parameters.

The latitudinal flux anisotropy arising from the predominant occurrence of plages at low heliocentric latitudes was estimated by Cook et al. (1980) at several wavelengths in the 1400-2100 Å continuum, and for Lα. They

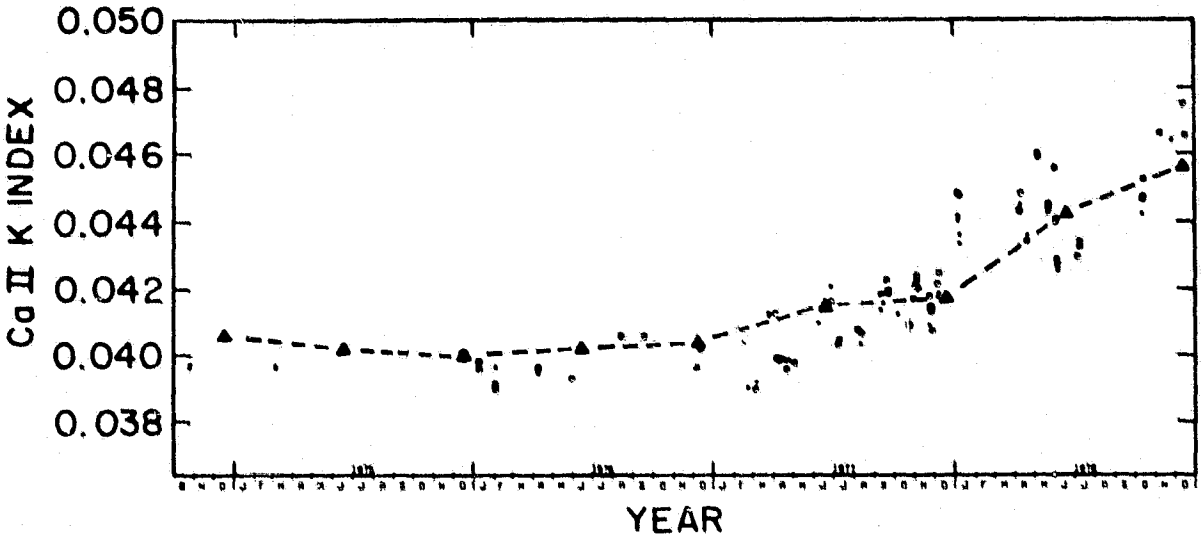

Figure 1. Solar full disk Ca II K (0.5 Å width) measurements furnished by Livingston and White (private communication). These measurements have been fit by a contrast model with C=3.0 using monthly average sunspot numbers for June and December of the years shown. From Cook, Brueckner, and VanHoosier 1980.

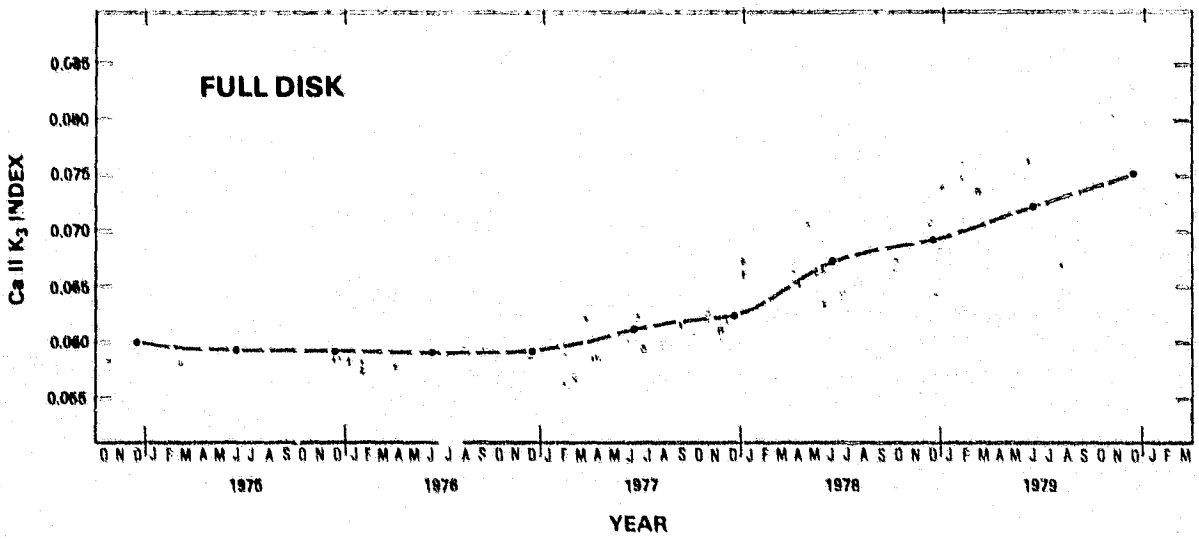

Figure 2. Solar full disk Ca II K_3 measurements furnished by Livingston and White (private communication). These measurements have been fit by a contrast model with C=3.5 using monthly average sunspot numbers for June and December of the years shown.

assumed that plages are confined within zones of approximate latitude $\pm(5°-35°)$. The projected fractional flat disk area F of two zones ranging from $\pm(\theta_1-\theta_2)$ in heliocentric latitude, viewed at angle α to the solar equatorial plane, is approximately $F(\alpha) = F_\perp + (F_{//}-F_\perp)\cos^2\alpha$, where $F_{//} \equiv F(\alpha=0) = (1/\pi)\,[2(\theta_2-\theta_1)+(\sin 2\theta_2 - \sin 2\theta_1)]$ and $F_\perp \equiv F(\alpha=\pm\pi/2) = \cos^2\theta_1 - \cos^2\theta_2$. Cook et al. (1980) assumed that plages are distributed within these zones in such a way that $f(\alpha)/f_{//} = F(\alpha)/F_{//}$, where $f_{//}$(= previous "f") is known for given R_Z. If we ignore center-to-limb variation we have $\text{Flux}(R_Z,\alpha) = \text{Flux}(R_Z=0)\{(C-1)f_{//}\,[F(\alpha)/F_{//}] + 1\}$. For low heliocentric latitudes the ratio $F_\perp/F_{//}$ is relatively independent of the width of the assumed plage zone and depends essentially on the central latitude $\theta_o = (\theta_1+\theta_2)/2$. Typical values for $F_\perp/F_{//}$ at central latitude θ_o, in the form $\theta_o(F_\perp/F_{//})$, are 5°(0.14), 10°(0.27), 15°(0.42), and 20°(0.57). We assume a solar value of $\theta_o = 20°$. Thus we estimate the solar K index as a function of sunspot number R_Z and line of sight α to be $K(R_Z,\alpha) = K(R_Z=0)\{(C-1)f_{//}[F(\alpha)/F_{//}] + 1\}$, where $f_{//} = 6.25 \times 10^{-4}\, R_Z$. For a plage zone ranging from $\pm(5°-35°)$ $F_{//} = 0.577$, $F_\perp = 0.321$, and $F(\alpha) = F_\perp + (F_{//}-F_\perp)\cos^2\alpha$. $K(R_Z=0)$ is independent of α.

If $f_{//} = 0.20$ (very active days at the peak of a strong cycle) the solar fractional increase in the Wilson K index is 1.20 in the equatorial plane and approximately 1.11 over the poles. The average over a longer period such as a month, at a cycle peak with monthly average sunspot number $\langle R_Z\rangle = 200$, would be approximately 1.13 in the equatorial plane.

III. EXTENSION TO STELLAR OBSERVATIONS

Using the framework developed for the Sun we can estimate the range of fractional variability generated by relatively small changes in the plage contrast, plage area, and plage latitude dependence, illustrated in Table 1. We consider contrasts of 2, 3, and 5; values for f_{max} from 0.10 to 0.30; and central plage zone latitudes of 10°, 15°, and 20°. We give relative fractional flux variability in the equatorial plane $K_{//}/K_{//}(\text{quiet})$ and the pole-to-equatorial plane anisotropy $K_\perp/K_{//}$ for different value of θ_o. How do these ranges of variability compare with Wilson's observations of G and K dwarfs with cyclic flux variation?

Wilson (1978) plots nightly mean, and tabulates seasonal average, values of mean H-K fluxes. We assume that the contrast in both lines is identical, and will directly compare our estimated changes in the K index with the H-K index observations from Wilson (1978). These observations are not absolutely calibrated in flux, and our use of them involves only relative variations. In Table 2 we list the 13 stars considered by Wilson (1978) to have completed a cycle of activity; they show a range in H-K(max)/H-K(min) of 1.15-1.45. Examination of Table 1 shows that these values are easily matched by several combinations of available parameters. In fact a choice of parameters near the observed solar values is grossly consistent with the observed stellar variations.

Figure 3 shows a plot of H-K(max)/H-K(min) versus spectral type for the 13 dwarfs. Also shown is our estimated range of fractional variation of the solar K index on active days at sunspot maximum for viewing angles ranging

TABLE 1

VARIABILITY OF CA II K INDEX

f_{max}	C	K_{II}/K_{*}(quiet) $=f(C-1)+1$	θ_o $F_\perp/F_{II}$	$K_\perp/K_{II}$ 10° 0.27	15° 0.42	20° 0.57
0.10	2	1.10		0.93	0.95	0.96
	3	1.20		0.88	0.90	0.93
	5	1.40		0.79	0.83	0.88
0.20	2	1.20		0.88	0.90	0.93
	3	1.40		0.79	0.83	0.88
	5	1.80		0.68	0.74	0.81
0.30	2	1.30		0.83	0.87	0.90
	3	1.60		0.73	0.78	0.84
	5	2.20		0.60	0.68	0.77

TABLE 2

VARIATIONAL AMPLITUDE OF CYCLIC DWARFS

Star (HD number)	Spectral Type	Period (years)	H-K index Min	Max	H-K(max) / H-K(min)	τ_{rise}/τ
81809	G2	10	0.154	0.194	1.26	0.45
103095	G8	7	0.164	0.189	1.15	0.50
3651	K0	10	0.184	0.229	1.24	>0.45
149661	K0	8	0.317	0.404	1.27	0.31
165341A	K0	10	0.317	0.459	1.45	0.20
10476	K1	9	0.187	0.249	1.33	0.44
155886	K1	8	0.366	0.442	1.21	0.50
219834B	K2	8	0.196	0.241	1.23	0.44
160346	K3	8	0.246	0.353*	1.43	0.31
4628	K4	9	0.205	0.272	1.33	0.44
131156B	K4	10	0.864	1.138	1.32	0.35(?)
201091	K5	7	0.440	0.618	1.40	0.36
201092	K7	8(?)	0.630*	0.820*	1.30	0.63(?)

*Value estimated from Figures 1-5 in Wilson (1978) rather than taken from tabulated average seasonal max or min.

from the equatorial plane to the pole. This gives an idea of the possible range of corrections that might be applied to the other plotted points for reduction to a common viewing angle.

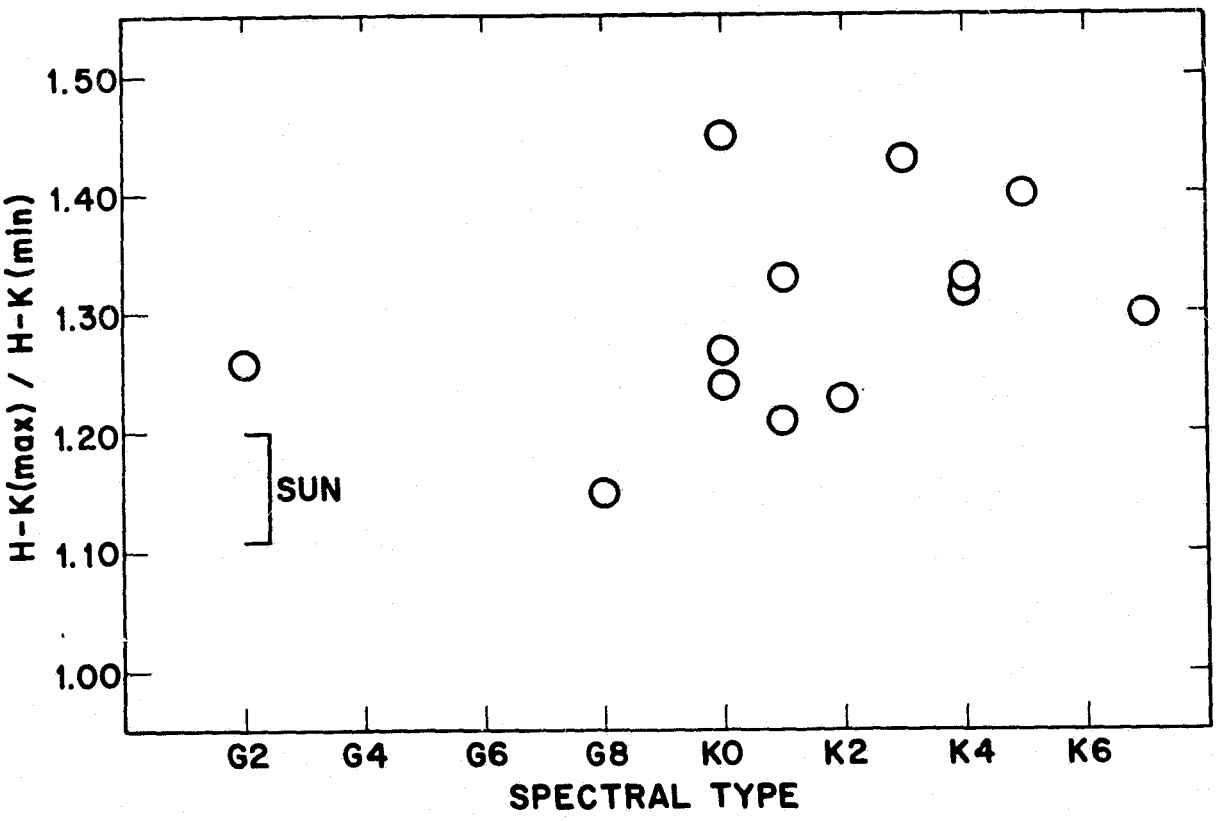

Figure 3. Amplitude of variation H-K(max)/H-K(min) versus spectral type. The estimated range of solar variability is shown for viewing angles ranging from the solar equatorial plane (top) to the poles (bottom).

There appears to be a general trend toward increasing fractional variation in later spectral type. G dwarfs are poorly represented in Figure 1. Some further support for the suggested trend is offered by consideration of 12 stars which Wilson (1978) believed to possibly be undergoing cyclical variation. He observes that the 3 candidates in the spectral range F7-G3 "are uncertain because of very small measured amplitudes, whereas in the later groups [9 stars of type G8 and later] the uncertainty is more often due to an insufficient time of observation." A possible explanation for this trend lies in the lessening of photospheric dilution of the K index with later spectral type. We recall that the average solar plage contrast in the K line over a 0.5 Å band at line center is approximately 3, which

is diluted to approximately 2 over a 1 Å band. Observations of the Ca II K line profiles from 43 stars of spectral types F0-M2 reported by Linsky et al. (1979) illustrate the quick rise of chromospheric emission over photospheric residual background, arising from decreasing T_{eff}, for late type dwarfs beyond approximately G8-K0. The increase in fractional variation seen in Figure 1 is at least consistent with a rise in contrast over a 1 Å band from C = 2 at G2 (giving H-K(max)/H-K(min) = 1.20 for f = 0.20 in the stellar equational plane) to an undiluted solar value of C = 3 in later K types (giving H-K(max)/H-K(min) = 1.40 for f = 0.20).

In Figure 4 we show the fractional variation H-K(max)/H-K(min) versus the fractional time of rise to maximum τ_{rise}/τ, also listed in Table 2. Notice that the star with greatest fractional variation, HD 165341A, shows the steepest rise to maximum of the 13 cyclic dwarfs (approximately 20% of the period). We have determined a value for each star using Wilson's (1978) suggested total period τ and an estimate from his plots of the time of rise from minimum to maximum flux. These quantities are not well determined from the observations, and have a large possible error. Nevertheless a general trend of increasing fractional amplitude with decreasing fractional time of rise to maximum is apparent. Part of this would be expected from the argument of increasing contrast factor C with later spectral type if quick rise time stars were predominantly K types. For this reason we label each point with the stellar spectral type, in order to demonstrate that within a single spectral type or small range of types the trend is still evident. The suggested stellar trend is reminiscent of the solar correlation (Bray and Loughhead 1965) of a quick rise to sunspot maximum with a strong cycle (high peak sunspot number).

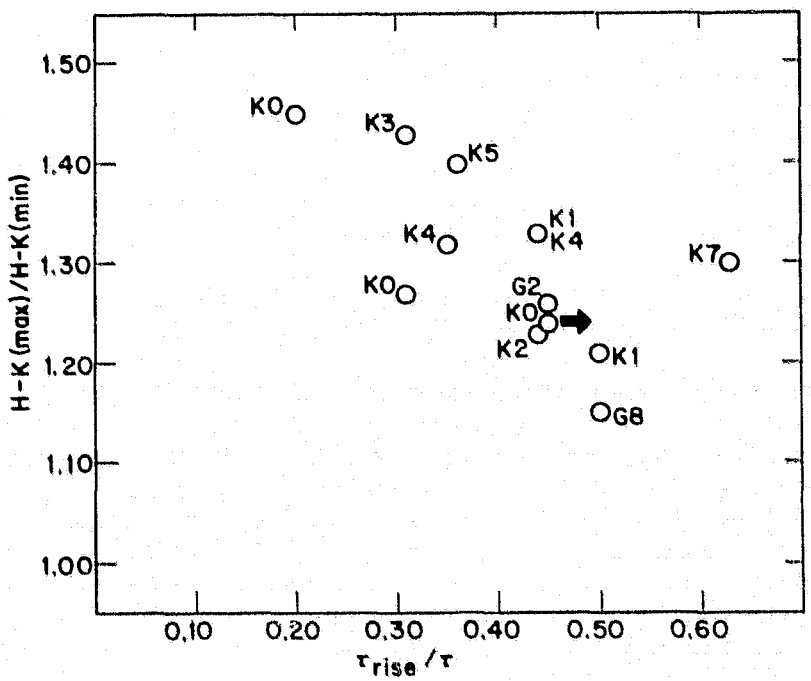

Figure 4. Amplitude of variation H-K(max)/H-K(min) versus fractional time of rise to maximum.

For an average line of sight angle to the stellar rotational axis of 45°, $F(\alpha=45°)/F_{\parallel} = 0.78$ for a plage zone centered at ±20° stellar latitude. For the typical example of HD 103095 (G8 V) the observed value of H-K(max)/H-K(min) is (0.189/0.164) = 1.15. If $\alpha = 45°$ this would correspond to a value in the equatorial plane of 1.21 using C = 2, with about 21% of the flat disk covered by plage at cycle maximum, or 16% of the surface area.

IV. DISCUSSION

We suggest that approximately solar values for contrast and plage area can reproduce the stellar variational amplitudes observed by Wilson (1978) for the subset of his program stars which underwent a cycle of flux variation over approximately a decade, and might be expected to be most similar to the Sun. This does not mean that chromospheric heating rates per unit surface area do not vary greatly in different stars at any given spectral type; a range of activity can be observed. Kelch, Linsky, and Worden (1979) have estimated chromospheric heating rates in eight late type dwarfs from observations of Ca II K profiles. Using radiative equilibrium models for each star they determined the temperature enhancements above the radiative equilibrium values necessary to produce the observed profiles, and so obtained the upper photospheric, temperature minimum, and chromospheric non-radiative heating. They found a typical range of total Ca II K line chromospheric energy losses of approximately a factor of 5 from quiet chromosphere to active chromosphere G and K dwarfs; at spectral type G2 this is equivalent to the ratio of chromospheric losses from plages versus quiet regions. We suggest that this is the approximate range of normal quiet, or global, stellar activity, while variation in the basic level of activity arises from stellar "plages". The variational range, at any given quiet activity level, is consistent (though not uniquely so) with approximately solar values for the maximum fractional surface area covered by stellar "plages" and a relative contrast in Ca II K_{1R}-K_{1V} emission flux between stellar "plage" and "quiet" regions of approximately 3, the observed solar contrast, throughout the G V - K V range. This contrast would be diluted over a 1 Å band at line center to approximately 2 by a residual photospheric contribution at spectral type G2, and rise to an undiluted value of 3 in latter K types. Modulation of the variational amplitude by the line of sight to the polar axis could amount to 40% in extreme cases of stellar contrast, plage area, and plage latitudinal dependence. Of course consistency does not guarantee correctness, but solar analogies should be considered first in interpreting the stellar observations.

Wilson's (1978) observations give us some information on a single cycle from a number of stars; for the Sun we know the past behavior of a number of cycles in a single star. The stellar observations allow the possibility of determining which of the observed regularities in the solar cycle are of more universal significance and which are not. As an example, we have suggested that quick rise to maximum and strength of the cycle are correlated in other stars, as with the Sun. We have found no correlations involving the cycle period. Also, the amplitude of variation does not appear to be correlated with the actual minimum value of the H-K index, which for dwarfs of the same spectral type is a measure of the basic (quiet) level of activity. That is, amplitude of variation does not appear to be correlated with quiet level of chromospheric heating.

Because of the small number of stars and the scatter of plotted correlations we can only suggest trends which we believe are plausible because of their comprehensibility in terms of solar analogs. We hope that this paper at least suggests types of analysis which could be performed on a larger base of observations.

REFERENCES

Bray, R. J., and Loughhead, R. E. 1965, Sunspots (New York: John Wiley), pages 240-241.
Cook, J. W., Brueckner, G. E., and VanHoosier, M. E. 1980, J. Geophys. Res., 85, 2257.
Cook, J. W., Meier, R. R., Brueckner, G. E., and VanHoosier, M. E. 1980, Astron. Ap., 97, 394.
Kelch, W. L., Linsky, J. L., and Worden, S. P. 1979, Ap. J., 229, 700.
Linsky, J. L., Worden, S. P., McClintock, W., and Robertson, R. M. 1979, Ap. J. Suppl., 41, 47.
Livingston, W., and White, O. R. 1979, 1980, private communication.
Sheeley, N. R. 1967, Ap. J., 147, 1106.
White, O. R., and Livingston, W. 1978, Ap. J., 226, 679.
Wilson, O. C. 1978, Ap. J., 226, 379.

HIGH-SENSITIVITY CIRCULAR POLARIMETRY OF THE SUN, 0.5 — 1.7 μ

James C. Kemp

Department of Physics, University of Oregon

ABSTRACT

Using an isometric (symmetrical) photoelastic-modulator polarimeter and a Cassegrain telescope, I have obtained broadband polarization measures of the Sun, with unprecedented sensitivity. With an instrumental background of $<3 \times 10^{-6}$, differential effects $\Delta q = V/I$ of 1×10^{-7} were detectable. Some results: (1) The λ dependence of broadband circular polarization in spots was observed out to 1.7 μ, extending the visible-light measurements of Illing, Landman, and Mickey. The q drops to of the order of 1×10^{-5} at 1.2 μ (in a strong spot), then rises at 1.6 μ. While molecules or other special mechanisms must play a role in the visible-light polarization, at $\lambda > 1.5$ μ the q values seem consistent with gray magneto-opacity. (2) By surveying inactive regions I have set upper limits to broadband polarization due to global or deep-seated magnetic fields. For a double-toroidal pattern I find a differential measure $q_D = (q_{NE} + q_{SW} - q_{NW} - q_{SE})/4$, at 1.7 μ, of $(+1.2 \pm 0.7) \times 10^{-7}$, a mean from three series in 1981. Based on a simple estimate by L. Biermann this would correspond to deep-down toroidal fields of ≤ 2000 gauss. Extensions of this work are discussed.

I. BACKGROUND

Magnetic fields in the sun, known as sunspots but presumably also permeating the entire sphere, are closely connected with short-term and long-term changes in the sun's external behavior. All approaches to the study of the solar magnetic fields should be developed. The classic approach involves the Zeeman splitting of spectral lines, particularly through the magnetograph method, in which unresolved Zeeman splittings are sensed by differential circular polarization as between the red and blue wings of a line. A less well-known approach involves measuring the broad-band circular polarization, using pass bands much wider than the line widths. While red- and blue-wing polarizations of an atomic line are approximately equal and opposite, and tend to cancel out over a broad band, it was pointed out by the writer (Kemp 1970) that at least a residual non-cancellation always exists, owing to a gray magneto-emission or magneto-opacity effect. Illing, Landman, and Mickey (1974a,b; 1975) studied the broadband circular polarization in sunspots, and found that the polarization levels were 10-100 times larger than those expected from the gray magneto-opacity, in the mid visible. Two extra mechanisms were proposed. One was a differential-velocity effect (Illing et al. 1975); the other involves the special properties of electronic transitions in molecules, in which net or non-cancelling circular polarization may occur over appreciable spectral intervals (Illing 1981). Detailed circular polarization spectra in sunspots had

been reported by Harvey (1973), in which molecular transitions of CN around 1.1 μ has shown a net polarization. Thus at least three mechanisms are recognized for broadband magnetic circular polarization; the first of these is always present.

While the broadband effects here are quite small, they may have a special importance. Zeeman splittings of atomic lines are formed high in the photosphere, or more precisely, the effective depths probed by magnetographic observations are quite small, probably $\tau \sim 0.2$. This is due both to the line opacities and perhaps to the fact that the line widths are greater at larger depths; there the line-wing polarizations, which are inversely proportional to the line widths, would be diluted. Continuum and other broadband effects, on the other hand, may reflect deeper-lying magnetic-field geometries. For the continuum polarization, line blocking and broadening are obviously inoperative. A further point is that the continuum magneto-opacity extends into the infrared, where the density of spectral lines falls off. Thus, the opacity minimum in the solar photosphere near 1.6 μ can be taken advantage of in broadband polarimetry, to probe as deeply as possible.

With photoelastic-modulator polarimeters (Kemp, Wolstencroft, and Swedlund 1972; Kemp 1981) the instrumental circular polarization can be as small as 10^{-6}, at least if linear-to-circular conversion is unimportant. The linear polarization of the sun well away from the limb in inactive regions is $\lesssim 2 \times 10^{-5}$ at wavelengths 0.5 - 1.7 μ, as verified by my own measurements in the course of this project. A linear-circular conversion factor of <0.01 is typical for photoelastic modulators, thus it was anticipated that circular polarizations of 10^{-6} would be accessible assuming zero instrumental circular polarization in the telescope. Cassegrain telescopes are ideal in this connection, having no oblique reflections.

II. OBSERVATIONS

Measurements with a PEM polarimeter were carried out during June-August 1981 using the 81-cm Cassegrain stellar telescope at Pine Mountain, Oregon. The telescope was fitted with a screen passing 2% of the sun's light, the screen consisting of an opaque plate with an array of 1-cm holes, covering the top of the telescope tube. Because of the essential symmetry the screen should not have introduced polarization artifacts, and this presumption was verified by tests in which the screen was rotated to various positions. The detector used was a germanium photodiode, which is effective over the band 0.4 - 1.7 μ. An 84-kHz photoelastic modulator of the isometric type (Kemp 1981) was used. In the first tests on the sun, I found what seemed to be an instrumental circular polarization of $\sim 5 \times 10^{-6}$ at 1.6 μ, smaller in the visible. (I should note that nothing other than the sun itself could be used as an unpolarized standard, at least not at 1.6 μ.) It was known that a spurious signal at this level could arise due to a modulated reflectance in the PEM optical element, an effect which is more severe in the i.e., due to the increased strain amplitude required at long wavelengths. This limiting effect could be cancelled in principle by a precise orienting of the analyzer ("decoder") polarizer, such that the polarizer axis is precisely 45° rotated from the PEM eigenaxis (see

Kemp 1981). An optimum alignment was made in the lab, and tests on the telescope were also made with the aid of a spinning depolarizer wave plate added above the polarimeter. A residual apparently instrumental polarization of about 2×10^{-6} seemed to remain, at 1.6 μ (the worst case). This was seen as a uniform background over the sun's disk and did not, for example, change with horizon distance nor from day to day. Thus an instrumental residue at this level was arrived at, but this was nominally constant. Differentially, as between different regions on the sun, the detection limit was at least as low as 0.5×10^{-7}. With later developments of this instrumentation I feel that absolute solar polarimetry at levels down to 10^{-8} will be quite feasible.

Photon-statistical errors were not a limitation. These errors were negligible in broad filter bands such as the 1.66 μ band ($\Delta\lambda = 0.15$ μ), for integration times of 5 - 10 minutes with the large apertures used, ~1 arcminute diameter.

The 1.6 μ filter band was emphasized because this corresponds to the opacity minimum in the solar photosphere, as noted above, thus we see most deeply into the sun at this wavelength.

Detections were easily made of broadband circular polarization in sunspots, as shown in Figure 1. On the two dates shown, comparison was made with nearly simultaneous magnetographic pictures made at Big Bear Solar Observatory (Cal Tech), by A. Patterson (Patterson and Zirin 1981). Generally I used a 1.6 arcminute-diameter aperture, which was usually larger than individual active regions. Comparisons with a 45 arcsec-diameter aperture on one or two large spots indicated that the dilution of polarized flux by unpolarized light outside the umbra was by a factor not much more than 2.

In Figure 1, the predominant magnetograph polarities (N,S) are compared with the circular polarization signs. Here the actual sense of circulation of the electric vectors, as seen on a stationary plane above the solar disk, is indicated by circular arrows. In the axial-vector convention (Kemp 1970, 1977), $q = V/I$ is called positive if the E vector rotates counterclockwise on such a stationary plane. Uniformly in Figure 1, positive broadband q is found with south magnetograph polarity, and vice versa. This correlation agrees with the signs observed in mid-visible filter bands by Illing et al. (1974a,b; 1975), if account is taken of an apparently opposite sign convention used by them for V, I (Mickey 1981). My measures in other bands at 0.5 μ, 0.86 μ, and 1.2 μ all had the same signs as the 1.6 μ sign, for a given spot.

In Figure 2 is shown a 4-filter sequence on one strong spot. The large q value at 0.55 μ is in rough agreement with the sizeable polarizations in green and yellow bands for strong sunspots reported by Illing et al. The monotonic sign in Figure 2 is noteworthy, but I cannot rule out sign changes in the gaps between bands.

Observations were made of inactive regions, with a view to finding overall patterns — poloidal or toroidal. The measuring scheme of Figure 3 was used, in which a 1.5 arcmin-diameter aperture was placed sequentially in NE, NW, SE, and SW quadrants, also in N and S regions. Obvious active features were avoided. The sampling positions were varied somewhat during measuring sequences, so as to achieve a crude averaging over the regions indicated.

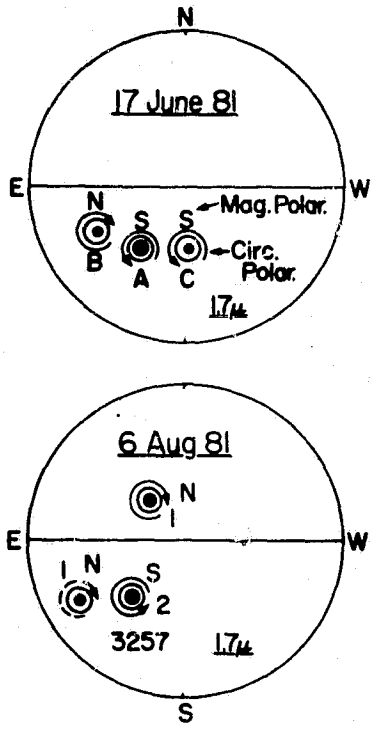

Figure 1. Sketches of sunspot configurations studied on two dates. Circular arrows indicate senses of broadband circular polarization (E vector rotation senses in a stationary plane above the spots). Letters N,S indicate magnetograph polarities.

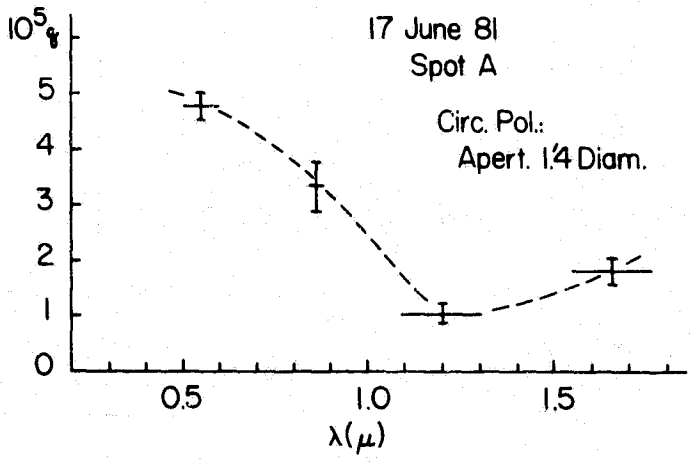

Figure 2. Circular polarizations in four interference-filter bands, for the strong sunspot A of Figure 1. Horizontal bars indicate the approximate band passes (FWHM).

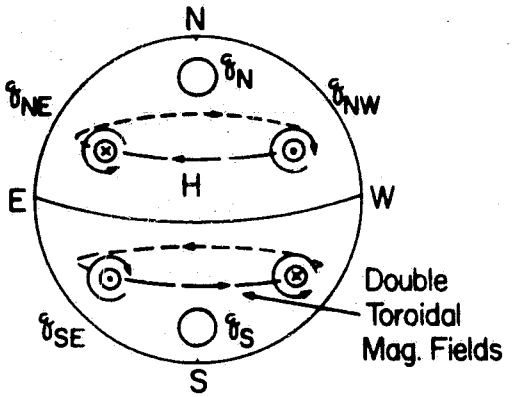

Figure 3. Scheme for observations searching for sector (quadrant) and hemispheric broadband circular polarizations. Hypothetical, internal double-toroidal magnetic fields are also sketched, including expected senses of emergent circular polarization. The most probable observed sign of the differential quantity q_B (see text) is consistent with the pattern shown.

For these measures, I define certain differential polarizations $q_{NS} = (q_N - q_S)/2$; and $q_B = (q_{NE} + q_{SW} - q_{NW} - q_{SE})/4$. The latter would be a measure of double-toroidal magnetic fields with opposite directions, discussed in the next section. My measures for these quantities in the 1.6 μ band are listed in Table 1. Here the errors were computed from the fluctuations among integration sequences spanning up to several hours. Greater interest attached to the q_B measures and much more time was spent on these; the NS measurements were relatively brief and had larger errors.

Table 1.
Differential circular polarizations from sectors, 1.6 μ band.

Date 1981	10^7 q_{NS} ("poloidal")	10^7 q_B ("double toroidal")
28 May	-11 ± 30	+1.0 ± 3.0
14 June	-33 ± 30	-
6 Aug.	-3.7 ± 5.0	-
12 Aug.	-3.4 ± 3.0	+1.4 ± 1.0
20 Aug.	+2.7 ± 5.0	+1.2 ± 0.7

III. DISCUSSION

The probable role of molecular effects in the broadband circular polarization of sunspots has been discussed by Illing (1981). I believe that the underlying gray magneto-opacity circular polarization (Kemp 1970, 1977; Lamb and Sutherland (1974) is also evident, notably in the infrared. The estimate for

gray, free-free magneto-opacity is $q \simeq 2\ eB/(mc\omega)$, where ω is the optical angular frequency. For B = 4000 gauss and $\omega = 2\pi\ c/\lambda = 2\pi\ c/(1.6\ \mu)$, we find $q \simeq 1 \times 10^{-4}$. If we take into account a twofold dilution of the polarized umbral flux in our measuring apertures, corrections due to radiative transfer, and dilution due to slightly weaker polarization due to bound-bound and bound-free magneto-opacities, the 1.66 μ q value is not out of keeping with this estimate. The polarization does have the correct sign for absorptive, electronic magneto-opacity: A North-polarity spot, with outward B field (see Figure 1) should and does have negative q. At wavelengths beyond 1.5 μ, most of the molecular bands would be of the vibrational-rotational type, which would not be significantly Zeeman-active. Thus it appears that the underlying gray magneto-opacity is visible in the 1.66 μ circular polarization.

In the sector polarizations of Figure 3 and Table 1, no clear detections are claimed. As for the North-South poloidal effect, relatively brief samples give the upper limit $q_{NS} \lesssim 4 \times 10^{-7}$ at 1.6 μ.

As pertains double-toroidal fields, previous evidence was given by Duvall, Scherrer, Svalgaard, and Wilcox (1979), based on Zeeman measures using the Fe I 5250 Å line. They indicated fields of the order of 0.1 — 0.2 gauss for such fields. Since these fields are essentially "buried," considerably stronger fields of this type might be observed deeper into the photosphere.

Internal double-toroidal magnetic fields ought to produce a finite differential measure of the type q_B, defined above, in the broadband circular polarization. In Table 1, I indicate $|q_B| \lesssim 1 \times 10^{-7}$, at 1.6 μ. From the gray magneto-opacity formula for the free-free case referred to above, for 1.6 this corresponds to B $\lesssim$ 2 gauss. For q_B positive, the toroidal circulation would be precisely as drawn in Figure 3, with the field directed inward in the NE. An effective observing optical depth $\tau \sim 1{,}0$ at 1.66 μ means a geometrical depth of about 500 km. From equation (11) of Biermann and Schluter (1951) we can make an estimate for the double-toroidal field at a small depth h into the surface, at latitude ~45°, namely B $\lesssim$ 2000 h/R, in gauss, where here $R = 0.7 \times 10^6$ km, the sun's radius. At h = 500 km this would give about 2 gauss. (The interior field would be in the kilogauss range.) Thus, in this crude framework our upper limit for q_B could be a marginal detection, but I do not claim this here.

If sunspot pairs are produced by the convection or tearing upward of internal toroidal fields of this sort, then the present polarities of spot pairs (South-polarity spots "leading" in the Northern hemisphere) are consistent with the senses of toroidal circulation drawn in Figure 3. The polarities are also consistent with the measured most-probable sign of the differential circular-polarization measure q_B, namely positive. I propose a long-term program of yet more accurate measurements of the broadband circular polarization to determine, first, whether a real effect of the "q_B" type is really present; and if it is, whether the sign of q_B changes over the activity cycle. (We might hope to see a reversal — or lack of reversal — at the next predicted minimum in 1987 (Waldmeier 1981).)

A problem with the double-toroidal magnetic fields as generated by the Biermann mechanism is that the senses of circulation of the fields are dictated only by the differential-rotation function $\omega(z)$. The canonical view is that the differential rotation pattern is invariant, as measured either by spot rotations or by sectoral radial velocities (Scherrer, Wilcox, and Svalgaard 1980): The equatorial angular velocity ω is larger than the angular velocities at large latitudes (plus or minus). However, at this Workshop, Howard (1981) has summarized data which suggest systematic, although complex, changes in the differential angular-velocity pattern over the 22-year solar cycle. For the Biermann mechanism to explain the double-toroidal fields and the 11-year reversal of the spot polarities, it would be necessary for the deep-down differential-velocity pattern $\omega(z)$ to be periodically reversed. Might it be possible that there is a deep-down reversal, which is somehow obscured by purely surface observations? The proposed reversal suggests a kind of internal torsional oscillation, only dimply perceived at the surface — apart from the manifest reversal of the sunspot-pair polarities!

I am grateful to various persons who encouraged this project and exchanged information about related work. These were especially J.W. Harvey, Rainer Illing, D.L. Mickey, J.M. Wilcox, and P.H. Scherrer. I thank Hal Zirin and Alan Patterson for generously supplying magnetograms as well as whole-disk photographs of the sun, taken at Big Bear Observatory on certain dates.

REFERENCES

Biermann, L., and Schluter, A. 1951, Phys. Rev., 82, 863.
Duvall, T.L., Scherrer, P.H., Svalgaard, L., and Wilcox, J.M. 1979, Solar Phys., 61, 233.
Harvey, J.W. 1973, Solar Phys., 28, 43.
Howard, R.F. 1981, review paper, this volume.
Illing, R.M.E., Landman, D.A., and Mickey, D.L. 1974a, Astron. & Ap., 35, 327.
Illing, R.M.E., Landman, D.A., and Mickey, D.L. 1974b, Astron. & Ap., 37, 97.
Illing, R.M.E., Landman, D.A., and Mickey, D.L. 1975, Astron. & Ap., 41, 183.
Illing, R.M.E. 1981, Ap.J., 248, 358.
Kemp, J.C. 1981, paper given at San Diego SPIE Meeting, 28 August; and to appear in Proc. SPIE, vol. 307, Sec. on "Polarizers and Applications."
Kemp, J.C. 1970, Ap.J., 162, 169.
Kemp, J.C. 1977, Ap.J., 213, 794.
Kemp, J.C., Wolstencroft, R.D., and Swedlund, J.B. 1972, Ap.J., 177, 177.
Lamb, F.K., and Sutherland, P.G. 1974, in Physics of Dense Matter, ed. C.J. Hansen, p. 265. I.A.U. Symposium volume.
Mickey, D.L. 1981, private communication.
Patterson, A., and Zirin, H. 1981, private communication.
Scherrer, P.H., Wilcox, R.M., and Svalgaard, L. 1980, Ap.J., 241, 811.
Waldmeier, M. 1981, Solar Phys., 73, 207.

IV. CONTRIBUTED PAPERS ON RELATED TOPICS

STELLAR CONTRIBUTIONS TO THE DIFFUSE SOFT X-RAY BACKGROUND

Jay Bookbinder, Y. Avni*, L. Golub, R. Rosner** and G. Vaiana

Harvard-Smithsonian Center for Astrophysics

I. INTRODUCTION

One of the results of the EINSTEIN/C.f.A. x-ray stellar survey was a determination of the contribution of the disk stellar population to the galactic component of the diffuse soft (0.28 - 1.0 keV) x-ray background. Our analysis employed both binned and unbinned nonparametric statistical methods that have been developed by Avni et al. (1980). These methods permitted us to make use of the information contained in both the 22 detections and 4 upper bounds on the luminosities of 26 dM stars in order to derive their luminosity function. We have not as yet developed luminosity functions for earlier stellar types, which leads us to use a delta-function approximation for their true luminosity functions. For these earlier stellar types, we have used the median luminosities as determined by Vaiana et al. (1981), which underestimates their contribution to the background. We find that it is the M dwarfs that dominate the disk population stellar contribution to this background.

To calculate the contribution of the stellar sources to the background, we have made use of simple models both for the spatial distribution of the stars and for the properties of the intervening interstellar medium. We choose a model in which all stellar classes have the same functional form for their spatial distribution: an exponentially decreasing distribution above the galactic equatorial plane, and a uniform distribution within the galactic plane for a region of several kiloparsecs centered on the sun. In the same spirit of keeping our model simple, we assume that it is sufficient to choose a uniform interstellar medium, characterized by a single relevant parameter, r_o, which is the energy weighted mean free path of an x-ray photon. This quantity is regarded as a free parameter, and our calculations span the range of $r_o \sim 200$ pc to $r_o \sim 10$ kpc. We believe that these values of r_o are the correct order of magnitude for ISM absorption at high galactic latitudes ($|b| > 30^o$), and since they cover the range from strong absorption to essentially free propagation, we will be able to estimate the effect of interstellar absorption on the stellar component of the x-ray

---

*

** Also from Weizmann Institute, Rehovot, Israel
EINSTEIN Observatory Guest Observer

background. Since we assume a uniform ISM that is characterized by average quantities, whereas the real ISM is both quite inhomogeneous and has an exponential density profile perpendicular to the galactic plane, our model can be compared only with the average properties of the soft x-ray background, such as observed with a wide field of view.

II. DISCUSSION

We present our first result, the integral x-ray luminosity function for dM stars, in Figure 1. Among these M dwarfs, the ratio of their x-ray to visual luminosity, f_x/f_v, varies from 10^3 to 10^{-1} (Rosner and Vaiana 1980). As we will see below, probably only in the case of dM stars is it necessary at present to construct a detailed x-ray luminosity function; and for this purpose we have used the data from the Einstein Observatory/CfA Stellar Survey of nearby stars. Stars that were included in the pointed survey for a priori reasons of noted activity (i.e. flare stars) were not included in the construction of the luminosity function, as they would tend to bias the function towards the high luminosity tail. The stars that are included in the construction are all members of the survey of dM stars within a 6 pc radius, selected solely by the distance criterion.

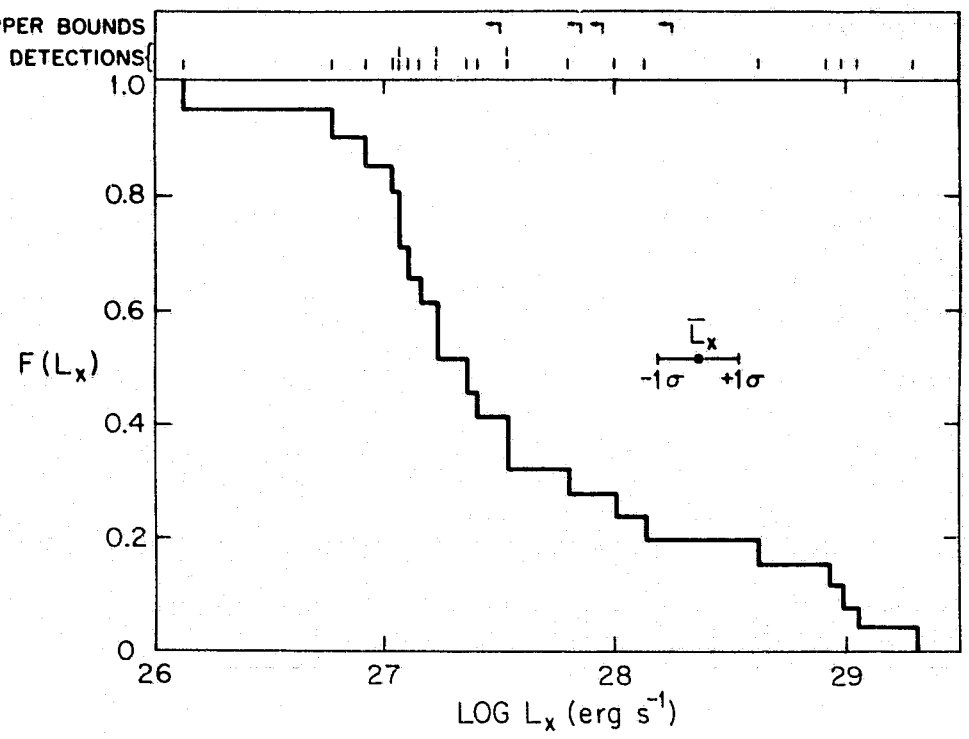

Figure 1. Integral x-ray luminosity function for dwarf M stars. Also indicated are the values of x-ray luminosity detections and upper bounds (top of the figure), and the mean x-ray luminosity for dM stars.

To reduce the information contained in the survey to a luminosity function, we use a non-parametric statistical approach developed by Avni et al. (1980) that can, as a special case, be applied to volume-limited samples. This method is quite different from the standard procedures, which involve observations of 'complete' samples. The complete samples are most often flux-limited, and one traditionally develops the luminosity function based solely on those objects whose fluxes are higher than the sample threshold. This paper uses a method which permits the use of objects which have been observed down to a limiting-flux level, whether they have been positively detected or not; the flux limit may also be different for each object. The maximum-likliehood technique that is employed allows us to combine data sets that were acquired with quite different sensitivities. Moreover, this method does not waste the information that can be obtained by considering those objects whose fluxes fall below the observational thresholds.

From the integral luminosity function we obtain a mean x-ray luminosity for dwarf M stars: $\bar{L} = 2.3\ (+1.1\ -0.7) \times 10^{28}$ ergs s^{-1}. The two-σ error bars are (+2.6,-1.2). We are now able to calculate the integrated stellar flux $f_i(|b|)$ (in the range of 0.28 - 1.0 keV) as a function of galactic latitude:

$$f_i(|b|) = n_i(0)\ \bar{L}_i/4\pi\gamma_i \quad \text{ergs cm}^{-2}\ \text{s}^{-1}\ \text{sr}^{-1}$$

where $\bar{L}_i$ is the mean x-ray luminosity of the ith source class and $\gamma_i = r_o^{-1} + \sin|b|/\beta_i$ is the effective inverse scale height. The stellar parameters given in Table I are used to generate Figure 2, where we show results using an interstellar absorption parameter of $r_o = 200$ pc (solid curve) and $r_o = 10$ kpc (dashed curve). We note that the integrated flux has a considerable dependence on the ISM absorption. Because most of the flux is due to distant sources, the result of decreasing r_o is to decrease the flux by a factor of nearly three. Several other aspects of this plot are of interest as well. First, concurrent with the decrease in the flux as the absorption is increased, comes a decrease in the latitude dependence of the flux. Examination of the figure shows essentially no latitude dependence of the flux when $r_o = 200$ pc and $|\beta| > 30^o$. Secondly, M dwarfs dominate the x-ray background in this bandpass. The next most important contributors are dF stars, whose contribution to the soft x-ray flux is a factor of five less than that of the dM stars.

We are now able to compare our model's predictions with the observations of Tanaka and Bleeker (1977), whose total average soft x-ray background flux in the M-band is:

$$f_{obs}(0.28 - 1.0\ \text{keV}) \sim (0.4 - 2.6) \times 10^{-8}\ \text{ergs cm}^{-2}\ \text{s}^{-1}\ \text{sr}^{-1}$$

These integrated energy flux values are indicated for both the low-flux and high-flux regions (excluding known point sources), though it is important to note that the high- and low-flux regions in different energy bands are not

Table I

	Log L_x (1)	n(o)[pc^{-3}] (2)	b(pc) (2)
dF	29.0	0.003	190
dG	27.8	0.006	340
dK	27.8	0.01	350
dM	28.36	0.065	350

1. Estimated median L_x (ergs s^{-1}) from Vaiana et al. 1981, for spectral classes dF, dG and dK. The mean L_x for dM stars is derived from the integral luminosity function that is shown in Figure (1).

2. Stellar space densities and the galactic scale height are the values given by Allen (1973).

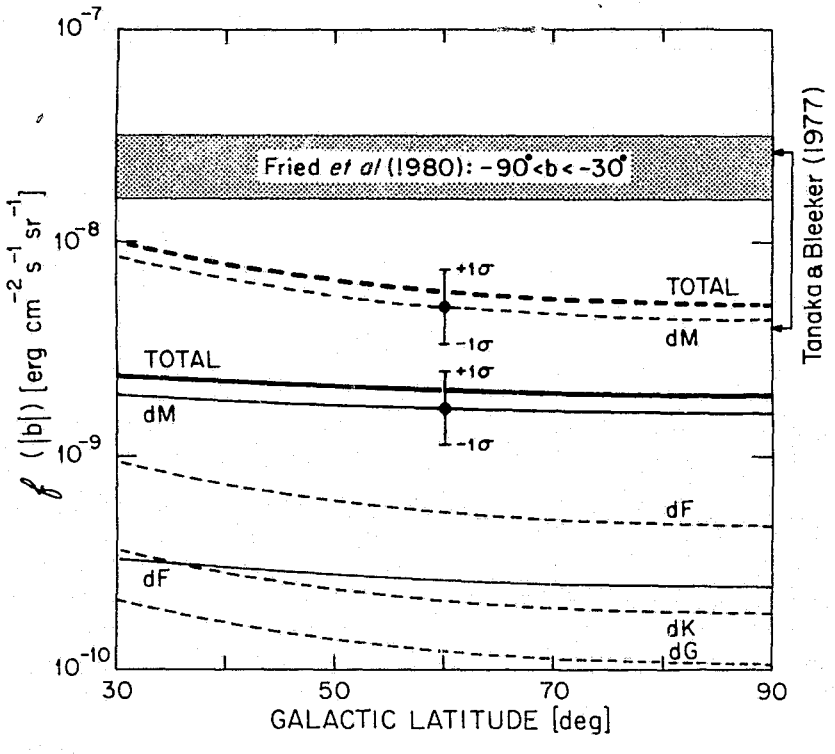

Figure 2. Predicted contribution to the diffuse soft x-ray background (0.28 - 1.0 keV) from stars [solid: r_o = 200 pc; dashed: r_o = 10 kpc]. Also shown is the range of observed background fluxes obtained from the results of Fried et al. (1980) for the (0.28 - 1.0 keV) band for $-90^o < b < -30^o$, and the corresponding flux range quoted by Tanaka and Bleeker (1977). The 1-σ error bounds on the M dwarf contribution (which dominates by far) are also indicated.

always coincident. For a choice of model parameters $|b| = 30^{o}$ and $r_{o} = 200$ pc, we predict a total stellar contribution to the M-band flux of 2.5 (+1.1 -0.8) x 10^{-9} ergs cm^{-2} s^{-1} sr^{-1}, or 7% to 14% of the maximum observed flux. The error bars, here as elsewhere, reflect only the uncertainty in the x-ray luminosity function, but not in the assumed stellar distribution or ISM absorption properties. If we observe an area of the sky that is characterized by a low value of interstellar absorption, then the stellar contribution rises to 1.0 (+0.5 -0.3) x 10^{-8} ergs cm^{-2} s^{-1} sr^{-1}, corresponding to between 27% and 58% of the maximum M-band flux.

We can perform the same comparisons with the more recent Wisconsin results (Fried et al. 1980). Because of the strong possibility that the North Polar Spur is an (independent) x-ray source, we will confine our attention to the Southern Galactic hemisphere, at latitudes $|b| > 30^{o}$. Note that the range of the Wisconsin data is comparable with, and overlaps, that quoted by Tanaka and Bleeker (1977). For the same stellar parameters that we used above, the comparison suggests that the stellar contribution may account for 11% to 24% of the minimum flux and 6% to 12% of the maximum observed flux. Again, for region of low absorption, the contribution rises to 23% to 48% of the maximum observed flux.

References

Allen, C.W. 1973 Astrophysical Quantities; London; Althone Press
Avni, Y., Soltan, A., Tananbaum, H. and Zamorani, G. 1980 Ap.J., 238,800
Fried, P.M., Nousek, J.A., Sanders, W.T. and Kraushaar, W.L. 1980, Ap.J., 242, 987
Rosner, R. and Vaiana, G. 1980 Proc. Erice Summer School in High Energy Astronomy. ed. G Setti and R. Giacconi
Tanaka, Y. and Bleeker, J.A.M., 1977, Space Sci. Rev., 20,815
Vaiana, G.S. et al. 1981, Ap.J., 244,163

Observations of FK Comae Stars

Bernard W. Bopp
University of Toledo

I. Introduction

Since 1975 I've been obtaining observations of three puzzling objects (FK Comae, HD 199178, UZ Librae) that, I now believe, comprise a new and potentially very important class of variable. My acquaintance with the stars goes back several years. During a cloudy night on Kitt Peak, while reading an old issue of PASP, I ran across an article by Merrill (1948) describing the spectrum of a remarkable object, HD 117555. The star was intriguing in that it was a rapidly rotating ($v \sin i$ ~ 100 km s^{-1}) G-giant with Ca II emission and a very broad (~20 Å) Hα emission line. I was surprised to learn that little else was known of the object, and apparently no follow-up spectroscopy had been performed. At about the same time (1974) an article by Wisniewski (1973) appeared, describing some photometry of a K-star with Ca II emission. The star, UZ Lib, varied by ~0.3 mag with a period of ~9.5 days. Though Wisniewski called the object a β Lyrae variable, I believed the variability was due to surface activity (starspots) and thought UZ Lib was a BY Draconis-type variable. Spectrograms I obtained in 1974 showed this idea was wrong; UZ Lib instead showed rotationally broadened lines and Hα emission and was apparently a giant. UZ Lib and FK Com were clearly related.

For the next few years I concentrated on obtaining more data, especially spectroscopic, of these objects. It turned out that Greenstein, Herbig, Aller and Popper had made some rather extensive observations of FK Com during the years 1955-70, but nothing had been published. I borrowed and measured some of these spectra, in addition to obtaining more data on my own. At that time, I assumed FK Com and UZ Lib were binary star systems of one sort or another; this would after all, explain the rotational speeds (the result of tidal synchronism) and might vaguely hint at the origin of the Hα emission (gas streams?). However, after measuring a few dozen spectrograms, I could not be firmly convinced that the velocities of these two stars showed any large periodic variations. I also started a small program to search for additional variables like FK Com by obtaining Hα spectrograms of giants with Ca II emission, and turned up a new member of the class, HD 199178. [Unknown to me, Herbig (1958) had obtained a spectrogram of HD 199178 years earlier, and had noted the similarities with FK Com.]

The late spectral type and rapid rotation certainly suggested that these stars should have strong UV emission features from a highly active chromosphere, and this is indeed the case. Bopp and Stencel (1981) report IUE observations that show FK Com and HD 199178 to exceed the RS CVn's by up to an order of magnitude in the flux from emission lines such as

O I λ1300, Si II λ1530, and C II λ1335.

While the importance of these FK Com stars to the rotation-activity connection is clearly important, I believe the evolutionary status of these objects is even more significant. The FK Com stars may represent the further evolution of W UMa (contact) binaries into a coalesced configuration, a scenario that had been posed by Webbink (1976) years earlier. In this paper I intend to describe the observational data I've accumulated, and relate FK Com, UZ Lib and HD 199178 as a group of stars. At the same time, I will note the crucial observational tests of the proposed evolutionary status of these stars that need to be performed.

II. Observations

a) Spectral Type

The existence of a G-giant like FK Com with a rotational velocity ≥ 100 km/sec was, initially at least, so outlandish to me that I suspected an incorrect classification. However, luminosity discriminants, such as λ4077 Sr II, are strong in FK Com. Harlan (1974) gives FK Com a spectral type G0 pn III, and Keenan and McNeil (1976) classify it G2 IIIa. Perhaps abundance anomalies could affect these classifications, and as a check I obtained IR observations of the three stars while at the University of Wyoming in 1974 and 1980. All the FK Com stars have 2 - 10μ energy distributions that are characteristic of giants, and none show an IR excess. The IR data for FK Com are given in Table 1. Finally, Slettebak (1975) classifies UZ Lib as KO-1 III, and Nassau and van Albada (1947) give a spectral type of G5 IV for HD 199178.

Table 1.
IR Observations of FK Comae.

Date UT	2.3μ	3.6μ	4.8μ	8.7μ	11.4μ
29/30 Apr. 1975	+6.06	+5.95	+5.96	+6.05	>5.29
16 March 1981	+5.99	+5.88	+5.91	---	---

Color Indices

	V-R	V-K	V-L	V-M
G5 III	+0.69	+2.08	+2.18	+2.02
G8 III	+0.70	+2.16	+2.27	+2.09
FK Com	+0.75	+2.19	+2.30	+2.29
G2 V	+0.53	+1.44	+1.61	+1.44
G5 V	+0.54	+1.49	+1.67	---

b) Photometry

All the FK Com stars are photometrically variable by 0.1 - 0.3 mag, with periods of a few days. Chugainov (1976) first reported FK Com to be variable by 0.1 mag in V, with a period of 2.412 days. (Apparently others had doubts about FK Com--the GCVS classifies it as an ellipsoidal variable, with double Chugainov's period.) Wisniewski's (1973) rather extensive photometry of UZ Lib yielded a period of ~9.5 days, with a V amplitude of ~0.3 mag; little or no color change was seen. However, Wisniewski chose to interpret UZ Lib as a β Lyrae eclipsing binary, clearly untenable in view of the spectral type. We suggested (Evans and Bopp 1974) that the correct period of UZ Lib was 4.75 days, which is also the one used by Hoffmann (1980). Hoffmann's data show that amplitude to have decreased to ~0.25 mag and the shape of the light curve to have changed significantly since Wisniewski's observations five years earlier. There are additionally some puzzling photographic observations by Parenago (1931) which resulted in a classification of the star as an RR Lyrae variable with a period of 0.4413 days(!).

The available photometry of HD 199178 is meagre, but definitely establishes it as variable. Differential photometry with high precision was obtained at my request by W. H. Sandmann at McDonald Observatory in 1975. His differential observations (Figure 1) show HD 199178 to vary by ~0.03 mag in V, and a period of 3-4 days is suggested by the data. Additional observations from KPNO in 1976 confirm the variability, but because different comparisons were used, they are not suitable for improving the period.

Note that the nature of the photometric variability of these stars is consistent with a starspot model. The periods, amplitudes, and sense of color change argue that cool spots are responsible for the variability, an interpretation very consistent with the stars' late spectral types and rapid rotations. Rucinski (1981) has modeled his photometric data on FK Com by assuming 10% of the stellar surface is covered by spots 600 - 1000 K cooler than the surrounding photosphere. Parenago's early data on UZ Lib might even be interpreted as the product of intense, rapid, flarelike activity. Short-duration brightenings, possibly flare-related, have been reported in FK Com by Chugainov (1976) and Rucinski (1981).

c) Emission Lines

Ca II is a strong emission feature in all the objects. The H + K region in FK Com is shown in Figure 2. The Ca II emission is rotationally broadened, apparently to the same extent as the photospheric absorption features. The Ca II lines are symmetric, and show no signs of structure. They do vary in intensity, however. At times the intensities of the lines are about up to the surrounding continuum, but sometimes only 50% as high. I don't have adequate data to determine if the Ca II emission variability is periodic, or phased with the photometric periods.

The Hα emission in these stars, especially in FK Com, is perhaps their most bizarre aspect. I illustrate two profiles from FK Com in Figures 3 and 4; note particularly the extreme width of the feature (~1000 km/sec full

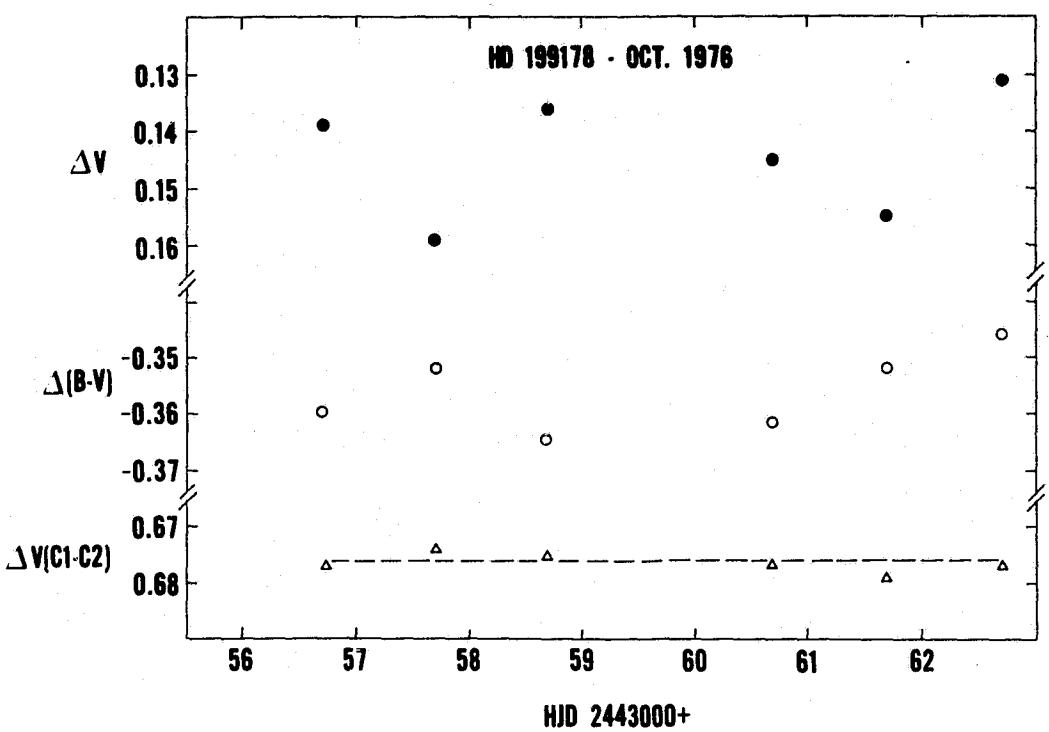

Figure 1. Photometric variability of HD 199178. Differential magnitudes with respect to HD 199547 are plotted (the scatter in the measures can be judged from the lower C1 - C2 curve). An amplitude for HD 199178 of ~0.03 mag is indicated, with a period near four days.

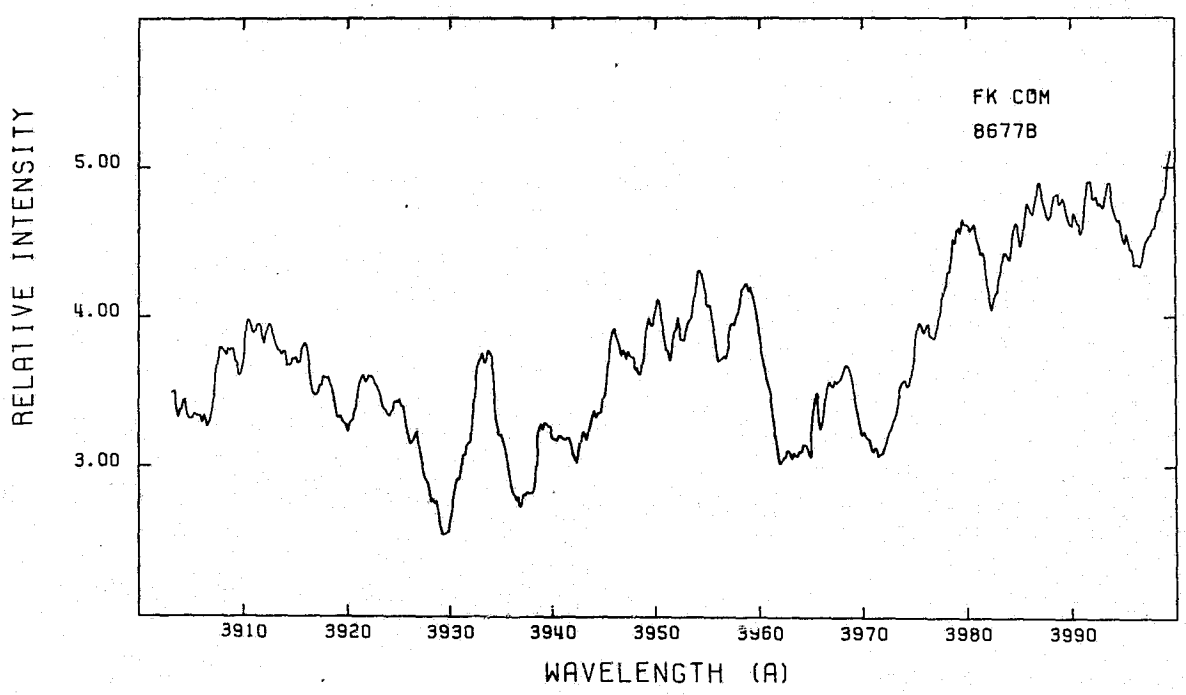

Figure 2. The Ca II H+K region in FK Com, from a KPNO coudé spectrogram. Note the extremely broad Ca II reversals.

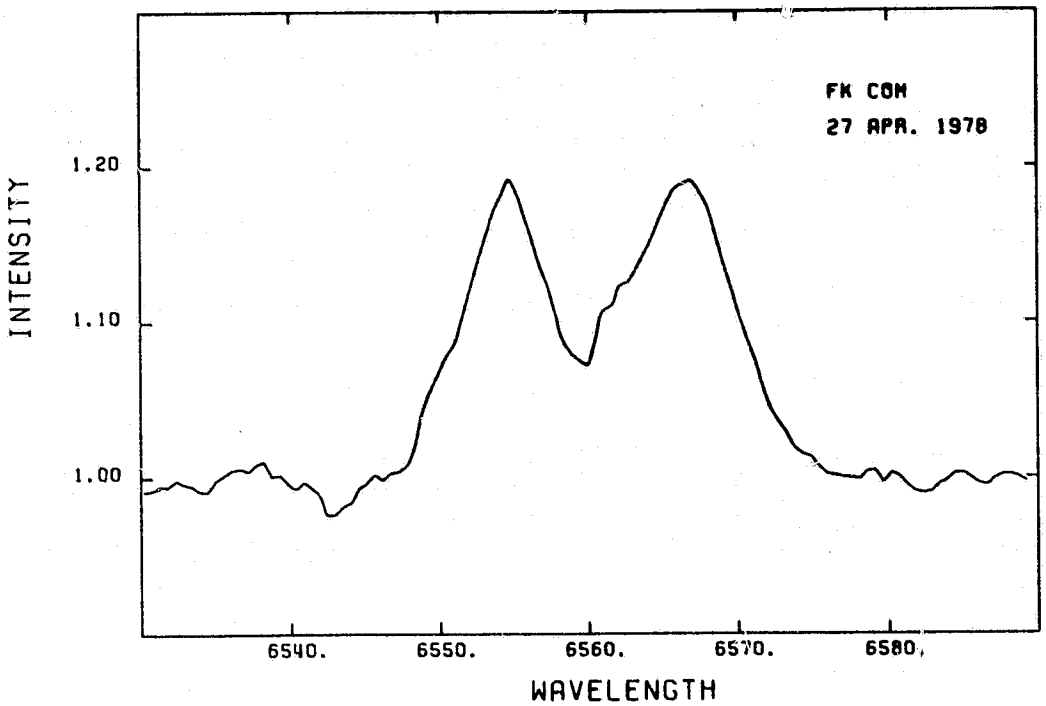

Figure 3. The Hα profile of FK Com from a Ritter Observatory spectrogram.

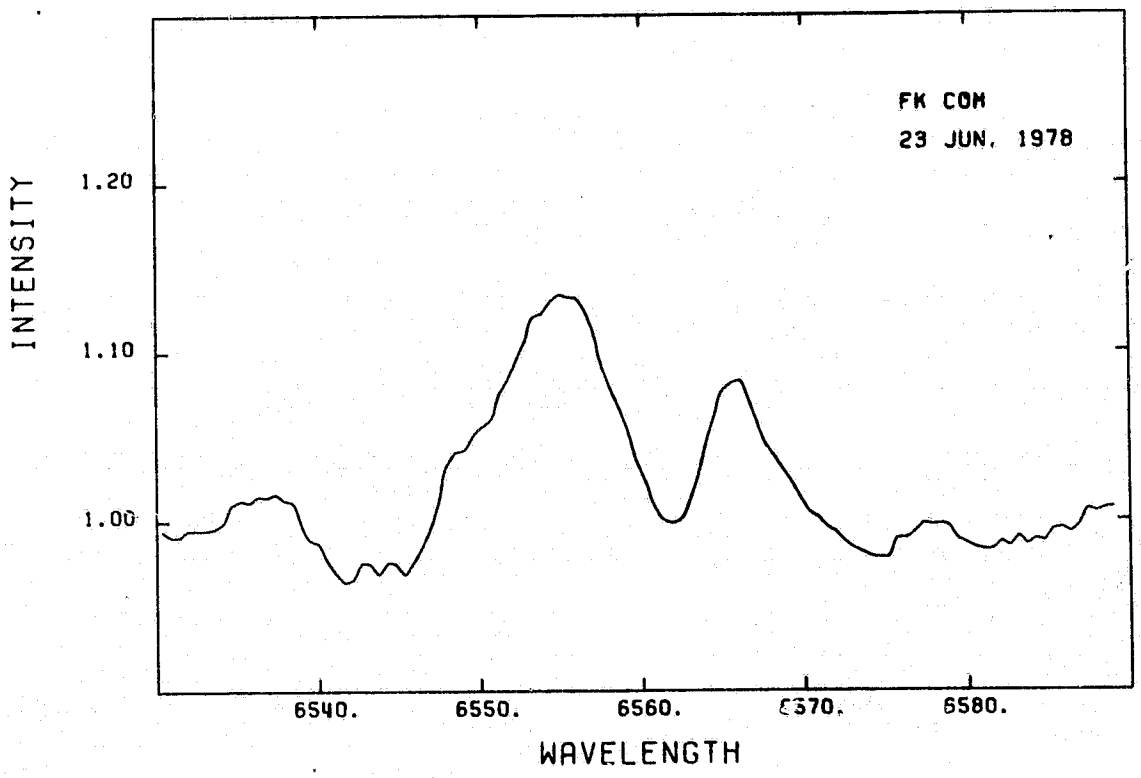

Figure 4. Same as Figure 3, but note the change in overall emission intensity and V/R ratio.

width at the continuum) and the changes in profile (V/R ratio). I will restrict my remarks on the Hα profile of FK Com, since both Walter and Basri (1981) and Ramsey (1981) have more homogeneous, better data sets. However, the feature is variable in profile and intensity on at least a night-to-night timescale. I certainly do not doubt the periodicities in Hα profile and V/R ratio that Walter and Ramsey find, but a 2.4 day periodicity is not clearly apparent in FK Com Hα data obtained by Herbig in 1958 and 1967 (private communication). Perhaps the lower resolution and S/N of the earlier data are to blame, but another possibility, much more likely I believe, is that stochastic Hα variations (flare related?) may at times overwhelm any periodic changes. Such effects are well known in other surface-active stars like HR 1099.

For UZ Lib, the Hα data are limited but the profile (Figure 5) is qualitatively similar to that of FK Com, though the total width is "only" 10 Å. My initial spectroscopic observations of HD 199178 were disappointing, in that they showed a weak absorption feature at Hα. However, further observations showed the line to have a blue-shifted emission peak at times (Figure 6).

d) Radial Velocities

Up to this point, all the characteristics of the FK Com stars (with the possible exception of the unusually broad Hα emission) might be explained by assuming them to be binaries--"super RS CVn's", if you wish. I almost wish it could be this easy, but the velocity data argue strongly against this interpretation.

HD 199178 has the best velocity data, extending over a four year baseline, and with internal errors of about 2 km/sec (Table 2). No variability significantly in excess of the internal error is indicated, but the Ca II velocities are offset by +10 - 15 km/sec from the absorption velocities. (This latter behavior is not seen in the RS CVn's). Even going back more than 50 years, Adams et al. (1929) give a radial velocity of -22.0 ± 1.0 km/sec from three plates, not significantly different from the Table 2 data, especially considering the different dispersions employed. For UZ Lib, we have only a few coudé plates, but no large absorption line velocity variations are seen, and the Ca II emission is again offset by about +15 km/sec.

I actually obtained, or had access to, the largest amount of spectroscopic data on FK Com itself, but these data turn out to be the most ambiguous. FK Com is rotating at the fastest rate of the three, and the absorption line profiles are a mess. In addition to being shallow and dish-shaped, the lines are severely affected by blending, making measurement of plates difficult even on Grant-type comparators. As a result, only a few lines could be measured with any reliability, and the internal errors are about ± 10 km/sec. About all that can be said is that I see no large variations in radial velocity (and certainly no trace of line doubling, or variable line widths). There is stronger evidence for velocity variation

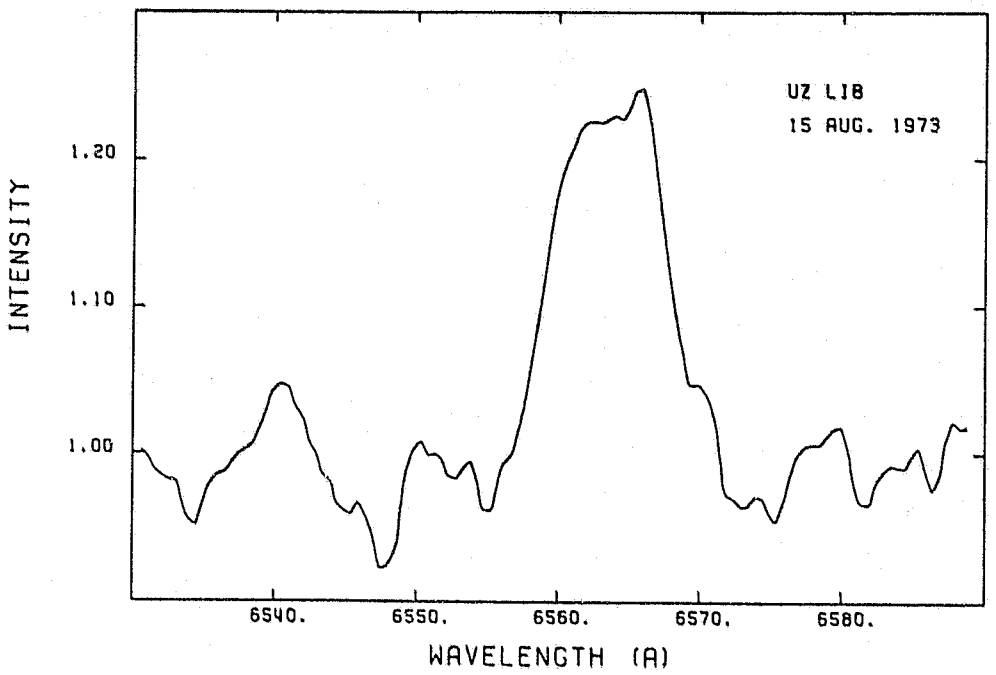

Figure 5. The Hα profile of UZ Lib, from a Lick coudé spectrogram loaned by George Herbig.

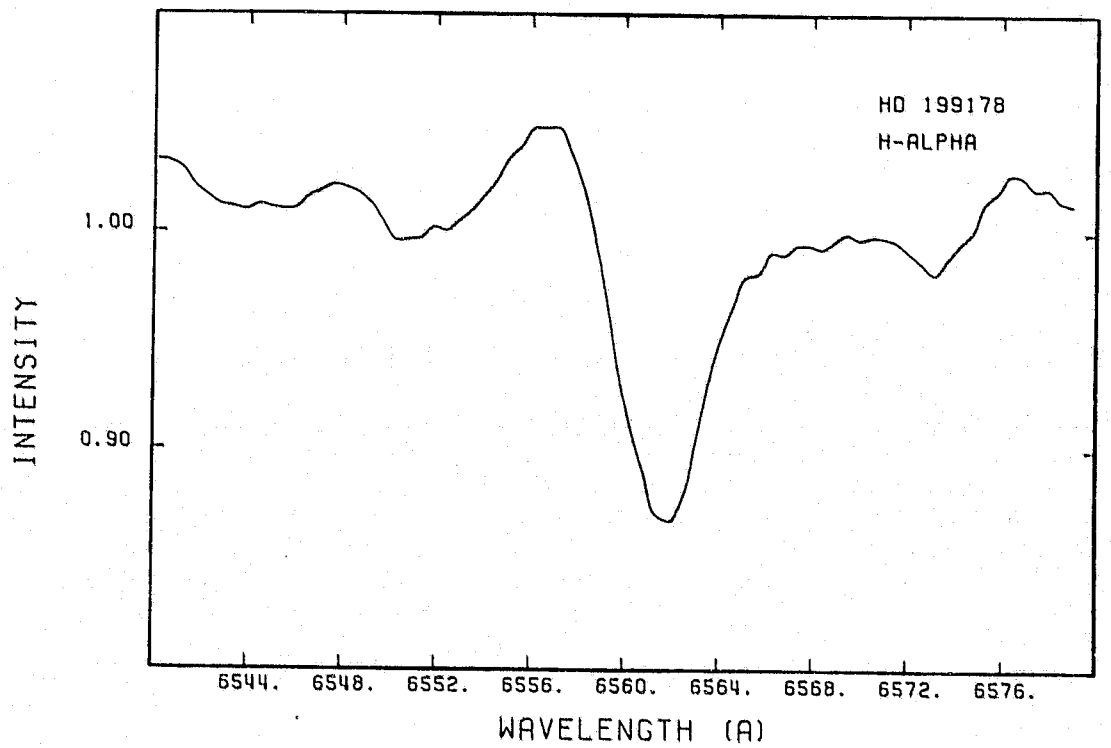

Figure 6. The Hα profile of HD 199178 from a Ritter spectrogram. Note the shallow absorption feature and blue-shifted emission wing.

in the H+K emission lines, which seem to vary erratically by 60 km/sec or so, and again are displaced to the red of the absorption lines by 20 - 30 km/sec. For completeness, I mention that Heard (1956) did claim FK Com to be variable in velocity. Needless to say I've subjected all the velocity data to standard period finding programs, with null results.

Table 2.
Velocity Observations of HD 199178.

HJD	Velocity (km s^{-1})		Disperson (Å mm^{-1})
2440000+	Ca II	Abs. (m.e.)	
2692.575	-13.9	-23.6 (1.5)	30
2708.630	-20.0	-32.6 (2.1)	30
2712.572	-19.0	-28.1 (1.9)	30
2715.628	-23.3	-35.2 (1.9)	30
2716.596	- 9.1	-33.4 (3.7)	30
2731.528	-32.6	-30.9 (2.0)	30
4507.737	-26.2	-39.6 (0.9)	16
4509.768	-15.2	-39.9 (1.8)	16
4511.745	-26.1	-31.6 (2.2)	16
4512.732	-23.6	-36.3 (1.5)	16

III. Evolution

Though there are differences in the Hα profile among the three FK Com stars, I believe there are enough similarities to merit the creation of a group of objects. The FK Com stars, then, are rapidly rotating G-K giants with strong chromospheric activity and no strong evidence for periodic velocity variations. They are certainly not RS CVn's in the conventional sense, nor do they resemble any of the stars in the "long-period group" (like λ And, for example). Instead it has been proposed (Bopp and Rucinski 1981, Bopp and Stencel 1981) that the FK Com stars are the descendants of the W UMa binaries, having evolved according to a scenario described by Webbink (1976). In Webbink's model, the mass ratio (secondary/primary) decreases on an evolutionary time scale until the secondary is completely dissipated, during the primary's initial ascent of the giant branch. Webbink predicts that a contact system, initially with 1.1 and 0.7 $M_\odot$ on

the main sequence will evolve to the following configuration when the primary is at the base of the giant branch (spectral type G9 III): the mass ratio will have decreased to ~0.09, the period will have increased to 2.41 days, and the rotational velocity of the primary will be 108 km s^{-1}. Of course the secondary, or rather its remnant, will be much too faint to detect in the combined visual spectrum. The orbital velocity variation of the primary would amount to only ± 16 km s^{-1}.

The resemblence to FK Com is so striking (though I confess the observed and predicted agreement of period is probably fortuitous!) that I believe it presents us with an origin for these objects. FK Com is the most rapid rotator of the three, and thus may represent a system of extreme mass ratio, on the way to complete coalescence. Conversely, the further evolution of Webbink's contact systems results in the dynamical instability of the secondary, and it is completely swallowed by the primary. Angular momentum is lost in this stage by the development of an "excretion disk" around the system. Perhaps the bizarre Hα profile has its origin in such a mechanism. The larger period objects HD 199178 and UZ Lib have then evolved beyond FK Com itself. The rotation should be slower (as is observed); the stars should be completely coalesced, and the Hα may then be a pure active-chromosphere phenomenon, induced by the rapid rotation. I note that the Hα profile of UZ Lib is not terribly different from that observed in HR 1099. Regarding HD 199178, filled-in Hα absorption is a universal characteristic of long- and short-period RS CVn's, and even blue shifted emission peaks have on occasion been seen in HK Lac and SZ Psc.

IV. Future Observations

The high space density of W UMa binaries implies that the FK Com stars, their descendants, should be common. Future research on these objects should concentrate on finding more of them. I have been very encouraged by the discovery of two new bright FK Com stars in the southern hemisphere by A. C. Collier (preprint). Again these stars have all the characteristics of the three stars I have described: they are rapidly rotating, chromospherically active G-K giants with photometric (rotational) periods of a few days. Most importantly, Collier has good-quality radial velocity data on both stars which limit their velocity variations to $\leq \pm 3$ km s^{-1}. The two new objects confirm the existence of a group of stars, and support their interpretation as evolved contact systems. Collier presents space density arguments which indicate support for a scenario where the FK Com stars evolve from W UMa predecessors.

The most fruitful way of finding additional FK Com stars appears to be high-resolution observations of Ca II emission objects that are found from objective prism surveys (see e.g., Weiler and Stencel 1979). Of course, most of the stars found in surveys of this sort will be chromospherically active RS CVn's or BY Dra variables, so a high-resolution spectrum to detect extreme rotational broadening is necessary. Low-resolution objective prism surveys at Hα do not appear to turn up new FK Com objects. Certainly objects with little or no emission above continuum, like HD 199178, will be

missed. But I have examined nearly two dozen F-G-K Hα emission objects from, for example, Henize's lists and the AS catalog, without turning up any FK Com (or even RS CVn) objects. Instead these surveys pick put rather intense Hα emitters which upon examination turn out to be T Tauri stars, RV Tauri variables, F supergiants, or heavily reddened Be stars. By way of contrast, the Ca II emission surveys effectively select out the RS CVn-like stars--Collier's southern hemisphere FK Com's were found as part of a high-resolution survey of the Ca II emitters in Bidelman and MacConnell's (1973) list.

Finally, let me briefly list the important optical observations that need to be obtained for the FK Com stars:

1. Improved velocities. In the case of FK Com itself, velocities with precisions of about ± 5 km s^{-1} could decide if the star is evolving toward coalescence or already coalesced. With modern digital detectors and cross-correlation techniques, such observations are readily feasible.

2. Synoptic photometry. While the photometric periods of FK Com and UZ Lib have been reasonably well determined at a single epoch, photometry over a baseline of several seasons could do much to determine the timescale of spot formation and infer the existence of differential rotation. Alternatively, if the light variations arise from a mass-transfer mechanism, as Walter and Basri (1981) suggest, then stability of photometric period is to be expected, rather than the period and phase changes so characteristic of the appearance and disappearance of spots.

3. Line profiles. For the photospheric absorption spectra, detailed fits of the profiles, employing model atmospheres, should be attempted. Possibly other atmospheric peculiarities of the FK Com stars could be identified in this way.

Even more intriguing is the idea that the absorption features in the FK Com stars could be prone to variable asymmetries as the spot rotated into and out of view. Such an effect has been seen in high resolution/high signal to noise spectra of some of the more rapidly rotating RS CVn stars by Vogt and Fekel (private communication). Their data show the absorption contribution of the spot, and suitable deconvolution of the line profiles will yield important information on temperatures and geometries. Of course this technique works best in stars where the rotational profile is clearly resolved, and where the effects of a binary companion are minimized. Clearly the FK Com stars are ideal for this sort of observation.

Acknowledgements

A great many people have helped me while I muddled through, looking for a solution to the FK Com puzzle. In particular I thank George Herbig, Jesse Greenstein, Lawrence Aller and Dan Popper for the loan of many spectrograms; Phil Keenan and Arne Slettebak for their insight on spectral classification; Bob Gehrz and John Hackwell for obtaining IR measurements; Jay Gallagher and Ron Webbink for help in theoretical matters; Paul Noah for his

programming expertise and assistance in data reduction; Kathleen Mulligan for her help in making many velocity measurements. Finally, I thank my good friend Slavek Rucinski for his help and constant encouragement. This research was supported by grants from NSF (AST 77-09450) and NASA (NAG 5-67, NAGW 229).

References

Adams, W. S., Joy, A. H., Sanford, R. F., and Stromberg, G. 1929, Ap.J. 70, 207.
Bidelman, W. P. and MacConnell, D. J. 1973, A.J. 78, 687.
Bopp, B. W. and Rucinski S. 1981, in "Fundamental Problems in the Theory of Stellar Evolution" (IAU Symposium No. 93).
Bopp, B. W. and Stencel, R. E. 1981, Ap.J. (Lett.) 247, L131.
Chugainov, P. F. 1976, Izv. Krymskoj. Astrof. Obs. 54, 89.
Evans, D. S. and Bopp, B. W. 1974, Observatory 94, 90.
Harlan, E. A. 1974, A.J. 79, 682.
Heard, J. F. 1956, P.D.D.O. Vol. II, No. 4, p. 107.
Herbig, G. H. 1958, in Etoiles a Raies d'Emission, Pub. U. Liege, p. 251.
Hoffman, M. 1980, Inf. Bull. Var. Stars, No. 1878.
Keenan, P. and McNeil, R. 1976, An Atlas of the Spectra of the Cooler Stars (Columbus: Ohio State University Press).
Merrill, P. W. 1948, P.A.S.P. 60, 382.
Nassau, J. J. and van Albada, G. B. 1947, Ap.J. 106, 20.
Parenago, P. 1931, Variable Stars (Russian) 3, 99.
Ramsey, L. 1981, this meeting.
Rucinski, S. 1981, Astr. Ap., in press
Slettebak, A. 1975, private communication.
Walter, F. and Basri, G. 1981, this meeting.
Webbink, R. F. 1976, Ap.J. 209, 829.
Weiler, E. J. and Stencel, R. E. 1979, A.J. 84, 1372.
Wisniewski, W. Z. 1973, M.N.R.A.S. 161, 331.

ON THE ENIGMA OF FK COMAE

F. Walter

Joint Institute for Laboratory Astrophysics
University of Colorado and National Bureau of Standards

and

G. Basri

Space Sciences Laboratory
University of California, Berkeley, California

I. INTRODUCTION

Stellar chromospheric and coronal activity appears ubiquitous among late-type stars to the left of the TR-wind boundary line (Linsky and Haisch 1979). The level of activity as measured by the X-ray surface flux is linearly proportional to the stellar angular velocity, with the exception of slowly rotating dwarfs (Walter 1981, 1982; Walter and Bowyer 1981). The peculiar rapidly rotating G giant FK Comae (Merrill 1948) appears to fit into this pattern. Line widths indicate V sin i = 120 ± 20 km s^{-1} (Bopp and Stencel 1981); photometry indicates a 2.4 rotational period (Rucinski 1982). FK Com has strong Ca II H and K and Hα emission, strong transition region UV lines (Bopp and Stencel 1981), and an X-ray surface flux in good agreement with its rapid rotation (Walter 1981).

Yet, FK Comae is an enigmatic star. It is a rapid rotator, but it is not clear why it is a rapid rotator. There is no direct evidence for duplicity; indeed, the upper limit of 20 km s^{-1} on the K velocity puts tight constraints on any binary configuration, especially if sin i ~1, as indicated by the large V sin i. An upper main sequence star conserving angular momentum as it evolves across the Hertzsprung gap may give rise to a rapidly rotating G giant. However, the luminosity of FK Comae makes it unlikely that its progenitor was earlier than ~A5, which makes this scenario doubtful. Bopp and Stencel (1981) have suggested that FK Comae is an example of a coalesced W UMa system (Webbink 1976), wherein the orbital angular momentum has become rotational angular momentum of the coalesced star.

Equally peculiar is the Hα emission line profile, as displayed in Figure 1. The line profile varies markedly from night to night and the Hα emission equivalent width varies between 2 and 10 Å. Because of the extreme width of

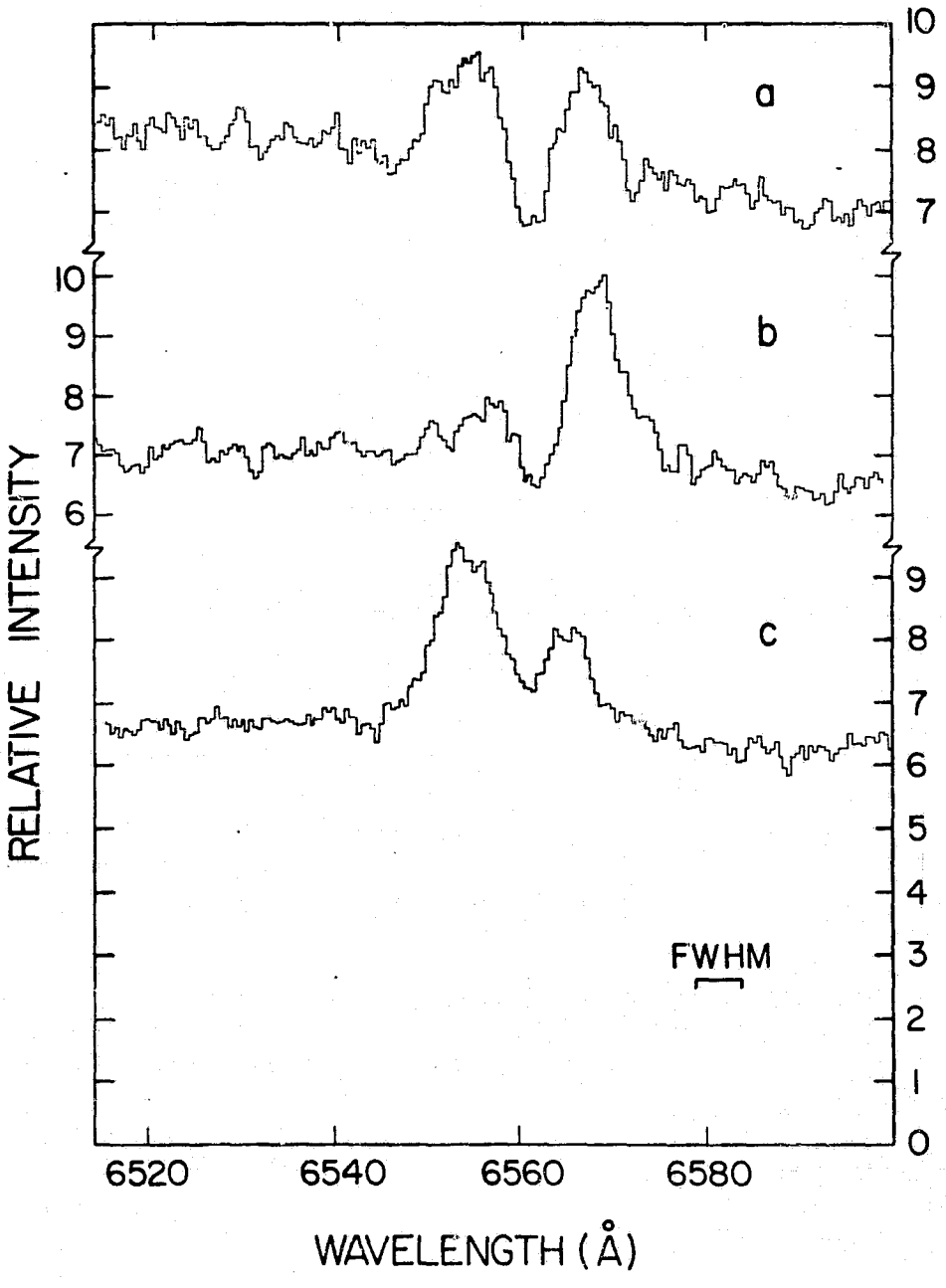

Figure 1. Three representative Hα profiles of FK Comae obtained in second order with the IDS scanner on the 40" Nickel Telescope. The ~5 channel instrumental full width is indicated. These data are plotted in counts per second, uncorrected for the instrumental response function. The profiles were obtained at the following days (JD-24,440,000.0): a) 655.781; b) 735.757; c) 734.699.

the line (~20 Å), it is unlikely that the line could be formed in a chromosphere, for if it were all the metallic lines would also be in emission (Walter and Basri 1982), as in the extreme T Tauri stars. Furthermore, Hβ is not in emission above the continuum, indicating that Hα likely arises in a low density atmosphere.

II. OBSERVATIONS

In the spring of 1981 we obtained 95 Hα line profiles in 16 nights using the 40" Nickel reflector and the IDS scanner of the Lick Observatory. The data were reduced by fitting each Hα profile as a sum of two Gaussian lines. Because the central absorption often fell below the continuum level, it is likely to be true absorption and not merely a lack of emission. The data were fitted as the sum of a broad emission line and a narrow absorption line, with all parameters free to vary. The V/R ratio shows a strong modulation with the $2^d.4$ stellar rotation, as also has been shown by Ramsey et al. (1981). In Figure 2a V/R is plotted modulo the rotation period. Also plotted in Figure 2 is the radial velocity of the Hα emission centroid, measured with respect to a photospheric absorption feature. This too shows a strong modulation on the stellar rotation period, with a semi-amplitude equal to the photospheric V sin i. The wavelength of the central absorption is consistent with the Hα rest wavelength on most occasions.

These data show that the Hα emission is localized on one side of the star, near the photosphere. It cannot be corotating at any significant distance above the photosphere, else the radial velocity would show a much larger semi-amplitude. The lack of strong modulation in the Hα equivalent width argues for a large extent of the Hα emitting region. The cause of the extreme width of the Hα profile is obscure, but this width may be the clue which unravels the enigma of FK Comae.

III. A MODEL FOR FK COMAE

The data in Figure 2 are plotted with zero phase corresponding to the ephemeris of Ruciński's (1982) optical photometry. Ruciński noted that his photometry agreed well in phase with that which Chugainov (1976) obtained five years previously. Phase stability of dark spots over five years is unexpected; it is not observed in RS CVn systems since the spots migrate around the star. Phase stability over such a long term (~800 stellar rotations) implies the existence of a preferred direction, perhaps supplied by a low mass binary companion to FK Comae.

Our Hα spectroscopy was obtained 1.5 years after Ruciński's photometry. If one assumes a dark spot model, then the Hα should arise on the dark side of the star (the one with the spots and the enhanced stellar activity). Our data are exactly out of phase with this interpretation. Rather than postulate a 0.5 cycle phase shift in the photometric phase during that year and a half, we assume that the phase is indeed stable (as it was during the 40 rotations covered by our observations). The Hα emission seems to arise on the bright side of the star, with maximum blueshift near phase 0.2, as the star is becoming brighter in the visual.

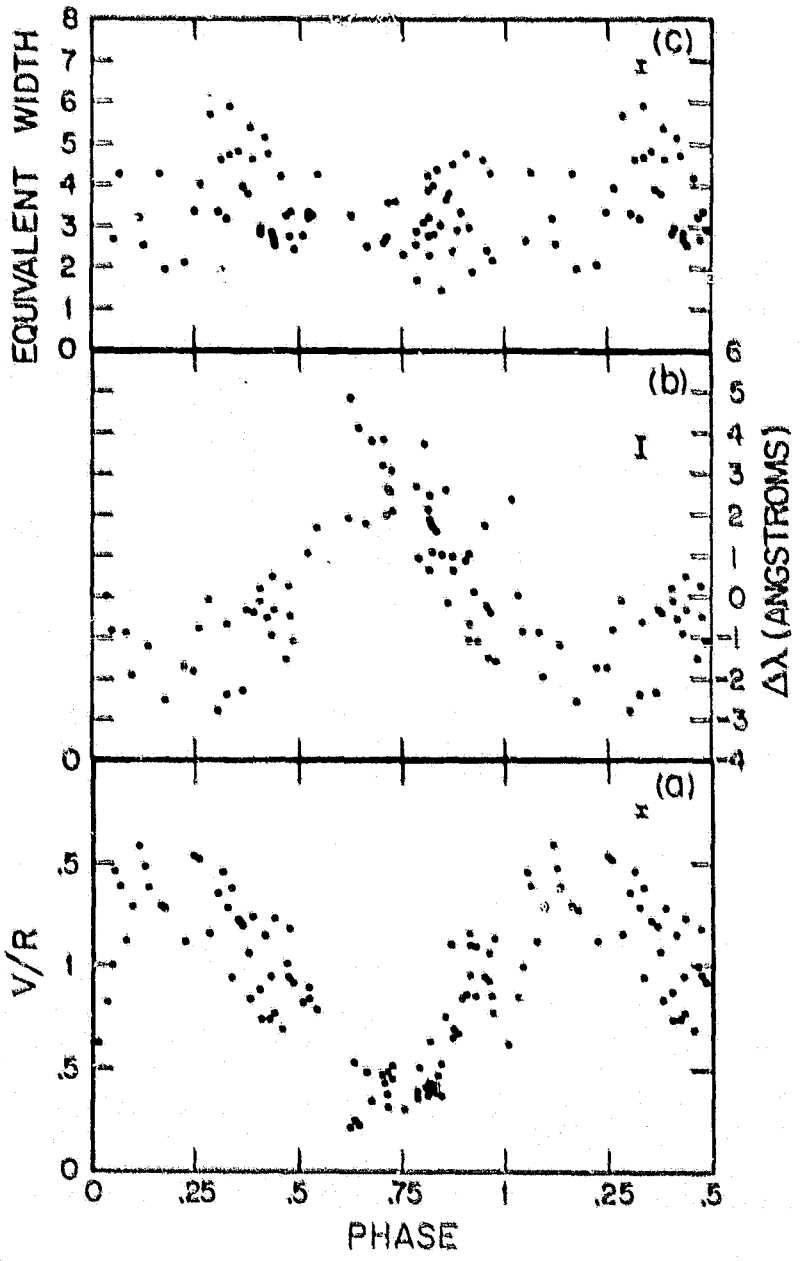

Figure 2. Properties of the Hα line of FK Comae plotted relative to the $2^{d}.4$ stellar rotational period of Chugainov (1976). V/R, in the lower panel, is the ratio of the violet to red peak intensities. We have plotted 2-R/V where V/R > 1 to achieve symmetry. The middle panel shows the redshift of the Hα emission centroid; a clear modulation of ±100 km/s from the Hα rest wavelength is seen. The equivalent width of the Hα line is plotted at the top. For clarity 1.5 cycles are plotted.

From the available data, we can obtain limits on the parameters of this binary system assuming sin i = 1. From V sin i and P, $R > 5.2\ R_\odot$. This is a lower limit on the diameter a of the system. From the upper limit to the K velocity variation, and assuming $m_2 \ll m_1$, $aq < 0.94\ R_\odot$, where $q = m_2/m_1$, and $0 < q < 0.18$. From Kepler's law, assuming rotational and orbital synchronization the mass of FK Comae is bounded by $a^3/1.18 < 424\ m_1 < a^3$, with m_1 in solar units. If we assume that the Hα width of ±400 km/s is the escape velocity from the G giant, then $m_1 = 2.2\ M_\odot$, $m_2 < 0.4\ M_\odot$, and $9.7\ R_\odot < a < 10.3\ R_\odot$.

We hypothesize that Roche lobe overflow from the secondary gives rise to an accretion stream which falls directly onto the surface of the G giant. Due to the size of the primary, no accretion disk can form in this system (Lubow and Shu 1975). The photometric variability is due to heating of the photosphere by the accretion stream; the observed $0^m.1$ variation indicates $\dot{m} \sim 10^{-8}$ $M_\odot$/yr, if no mass is lost to the system. It is likely that a shock will form in the atmosphere of the G giant where the accretion stream impacts (at an angle of ~50°); the accreting matter, with velocities on order of the escape velocity, will spread over a large fraction of the equatorial region of the G giant. Presumably the Hα emission arises from recombination in this warm, symmetric halo. The Hα emission and the photospheric heating will be centered at the impact point of the accretion stream. The chromospheric and TR lines should show a strong rotational modulation, with the atmosphere being hotter and denser above the bright side of the star. The gravitational potential is insufficient to account for the X-ray emission, which may be due naturally to dynamo action induced by the rapid stellar rotation.

In Figure 3 we plot the radial velocity of the Hα emission centroid, as predicted by this accretion model, along with the data. The predicted radial velocity curve is an intensity weighted numerical integration over the visible hemisphere. A good description of the data is obtained for a surface brightness distribution falling off linearly from the impact point, with the extent in the leading direction twice that in the trailing direction, and with the emission at a radius of 1.15 stellar radii. The expected Hα equivalent width modulation is ~50%, which is consistent with the observations.

FK Comae, by our interpretation, is not a peculiar rapidly rotating single giant, but is a synchronously rotating mass accreting G giant in a high mass ratio close binary. In evolutionary status, FK Comae could well be an evolving W UMa system which has not yet coalesced into a single star. The mass transfer, and presumably the evolution as well, is occurring on a thermal timescale.

The stellar activity on FK Comae appears to be a combination of normal rotation induced stellar activity and accretional heating, which dominates at low temperatures. By conventional standards, FK Comae is a chimera at this evolutionary stage. Replace the primary with an upper main sequence dwarf and one has an Algol system. Replace the primary with a degenerate dwarf and one has a cataclysmic variable. Perhaps further study of this system will provide insights not only into stellar activity but also into stellar evolutionary processes under large mass transfer rates.

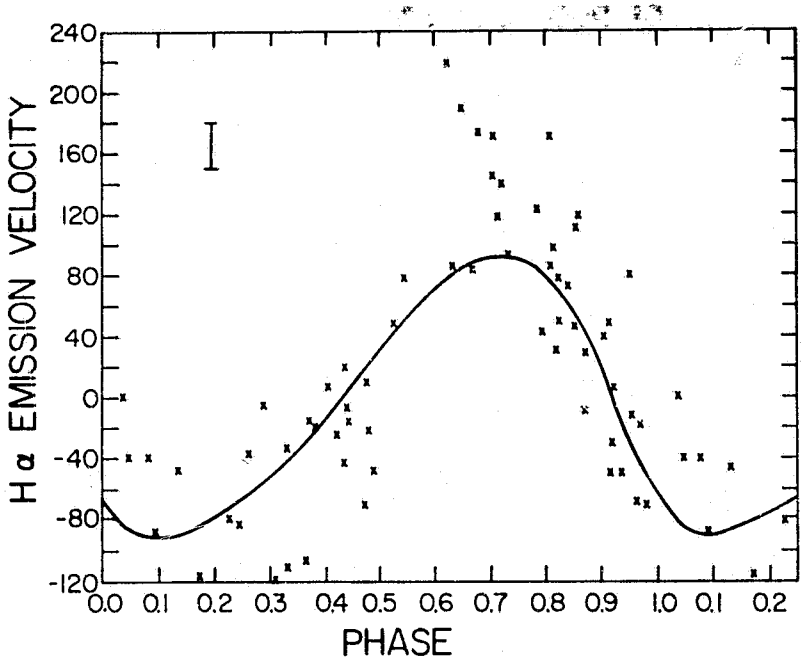

Figure 3. The radial velocity data for the Hα emission centroid (Figure 2b) are plotted along with the best model prediction. The model has emission distributed over 270° of the stellar surface in a triangular pattern with the leading edge twice the length of the trailing edge, and an effective radius for the emission centroid of 1.15 stellar radii. The error bar represents the typical measurement error of the radial velocity.

ACKNOWLEDGMENTS

We thank S. Bowyer for his insightful comments on earlier drafts of this work. This work was done at the Space Sciences Lab, University of California Berkeley, and was supported by NSF grant AST80-05874 to Professor Bowyer.

REFERENCES

Bopp, B., and Stencel, B. 1981, Ap. J. (Letters), 247, L131.
Chugainov, P. F. 1976, Izv. Krymskoj Astrof. Obs., 54, 89.
Linsky, J. L., and Haisch, B. M. 1979, Ap. J. (Letters), 229, L27.
Lubow, S., and Shu, F. 1975, Ap. J., 198, 383.
Merrill, P. 1948, Pub. A.S.P., 60, 387.
Ramsey, L., Nations, H., and Barden, S. 1981, preprint.
Rucinski, S. 1982, Astr. Ap., in press.
Walter, F. 1981, Ap. J., 245, 677.
Walter, F. 1982, Ap. J., in press.
Walter, F., and Basri, G. 1982, Ap. J., submitted.
Walter, F., and Bowyer, S. 1981, Ap. J., 245, 671.
Webbink, R. F. 1976, Ap. J., 209, 829.

A FLARE EVENT IN THE PECULIAR GIANT FK COMAE

Lawrence W. Ramsey and Harold L. Nations
The Pennsylvania State University

ABSTRACT

We present observations of a very energetic flare event in the peculiar rapidly rotating star FK Comae. During this event on June 18th 1981 the usual asymmetrical double peaked H alpha emission feature with an equivalent width (EW) of $\sim$ 3-4 Å changed to a broad emission feature with EW $\sim$ 13 Å. Sixteen spectra were obtained over 2 hours. Some changes in the emission profile are apparent on this time scale. The following night the enhanced emission persisted but at a lower level and it was substantially redshifted. This event is interpreted in terms of a model where material is injected into a disk co-rotating with the angular velocity of the stellar surface. A localized region of surface activity is conjectured to be the source of the event.

I INTRODUCTION

The rapidly rotating G giant FK Comae has lately re-emerged as an object of some interest as other papers in this volume attest. This is in no small part due to the suggestion by Bopp and his collaborators (Bopp and Rucinski 1981; Bopp and Stencel 1981) that FK Comae may represent the remnant of a coalesced contact binary system. This suggestion rests largely on the unusually high rotation (v sin i = 120 km/s) for a giant star coupled with the apparent lack of radial velocity variations indicative of a binary system. In addition Ramsey et al. (1981) discovered a regular variation in the asymmetry of the highly unusual H alpha emission line which is consistent with the observed rotational and photometric period (Chugainov 1976). In that paper it was suggested that much of the observed H alpha emission comes from a disk of material co-rotating with the same angular velocity as the surface of the star out to several stellar radii. The existence of such an "excretion" disk in coalesced binaries was suggested by Webbink (1976). The observed asymmetry variation was explained in terms of a disk density inhomogeneity concentrated near the stellar surface and associated with a region of enhanced surface activity on the star. We report here on observations of a flare event observed in the H alpha line at 6563 Å. We present evidence that this flare event appears to be originating from a localized region of the stellar surface longitude consistent with the postulated inhomogeneity.

II OBSERVATIONS

Observations were obtained on 18 June 1981 starting about 02:30 UT. A series of sixteen 300 second integrations were obtained over a period of two and a half hours on this date. In addition three 300 second integrations were done on the following night, June 19th. The SIT spectroscopy system was used on the fiber coupled spectrograph (Ramsey et al. 1980,1981) with the 1.6

meter telescope at Penn State's Black Moshannon Observatory in central Pennsylvania. The data were reduced in a standard fashion by subtracting a combination of sky plus pedestal and then ratioing to a flat field obtained from a tungsten lamp. Figure 1 shows the normalized sum of all the data for the 18th in the top spectrum. This should be compared to the "normal" spectrum of the H alpha region in FK Comae as depicted below it. It is clear that the H alpha line has greatly increased in strength from its normal equivalent width (EW) of about 3 Å to about 13 Å. The profile is also nearly symmetrical.

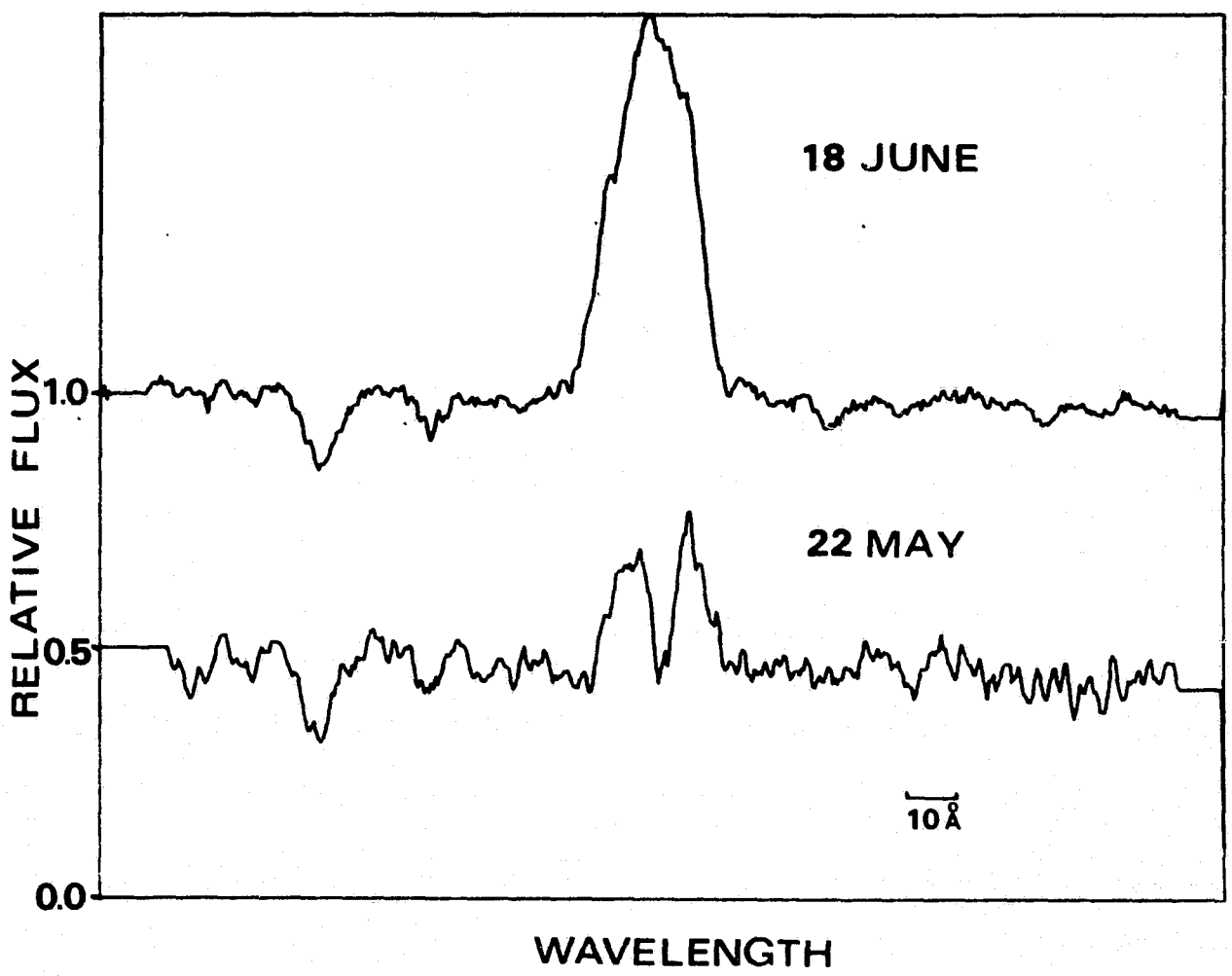

Fig. 1. The top spectrum is the summed and normalized flare spectrum for June 18, 1981. For comparison purposes the non-flare spectrum is displayed below. This second spectrum is on the same scale but offset 0.5 continuum units.

III DISCUSSION

Observations of a similar event in February 1981 by Walter (1981) indicate that the rise time of these events can be on the order of hours or less. Given this we thought it might be interesting to see what short time scale variations might be present in our sequence of spectra on the 18th. As mentioned above the integration time per spectra was 300 sec with some variation of the intervals between the spectra which were used to obtain radial velocity and flat field calibrations. We have chosen to search for variations by ratioing individual spectra with the mean flare spectrum displayed in Figure 1. The results are given in Figure 2. The position of the photospheric H alpha line center is indicated by the verticle dashed line. The fluctuations in the ratio spectra 40 to 50 Å away from line center are a good indication of the noise. Each ratio spectrum is labeled with the mean time of the exposure. These data show strong indications of changes in both the shape and intensity of the emission line profile on time scales as short as 20 minutes. Perhaps most notable in Figure 2 is the slight asymmetry change apparent in the ratio spectra. In the initial spectrum a slight blue enhancement and red deficit are indicated whereas in the later spectra this situation is reversed. In addition there is slight evidence for some weakening in the ratio spectra as time progresses. This weakening is also apparent in a comparison of the line profile sequence.

One of the most significant results of our observations comes from comparing the radial velocities of the emission features on the consecutive nights. We choose to estimate the emission coming from the flare/disk combination by subtracting off the spectrum of a normal giant star from that of FK Comae. This is done by artificially broadening the spectrum of the G8 giant HR4932 which was observed concurrently on both nights and has nearly the same radial velocity. Figure 3 illustrates this process for the 19 June data. The resultant H alpha profile is designated the Reduced Emission Profile. When this is done for the average profiles for both nights we obtain the reduced emission profiles shown in Figure 4. Again the vertical line represents the position of the photospheric H alpha line center. It is clear that the mean radial velocity of the emission feature has changed substantially from -123 km/sec on the 18th to +145 km/sec on the 19th. This strongly suggests that the source of the emission is localized relative to a fixed range of longitude on the stellar surface. Thus it might involve either a local instability in the disk or the ejection of matter from a region of activity on the star itself.

The mean phase of the 18 June spectra is 0.54. This corresponds to when the density enhancement postulated by Ramsey et al. (1981) is above the visible hemisphere of the star. Thus the blue shift is consistent with material being ejected from an active region generally associated with the disk density enhancement. On the following night (phase 0.95) the density enhancement was more nearly on the opposite side of the star. Consistent with this the emission was redshifted. Thus our radial velocity measurements indicate that the flare event involves the ejection of material from a localized region on or above the surface of the star. It is also apparent that on the second night the EW had decreased by a factor of two and the blue/red asymmetry has re-emerged. It is not entirely clear whether this represents a real decay of the flare or just an occultation effect. The high

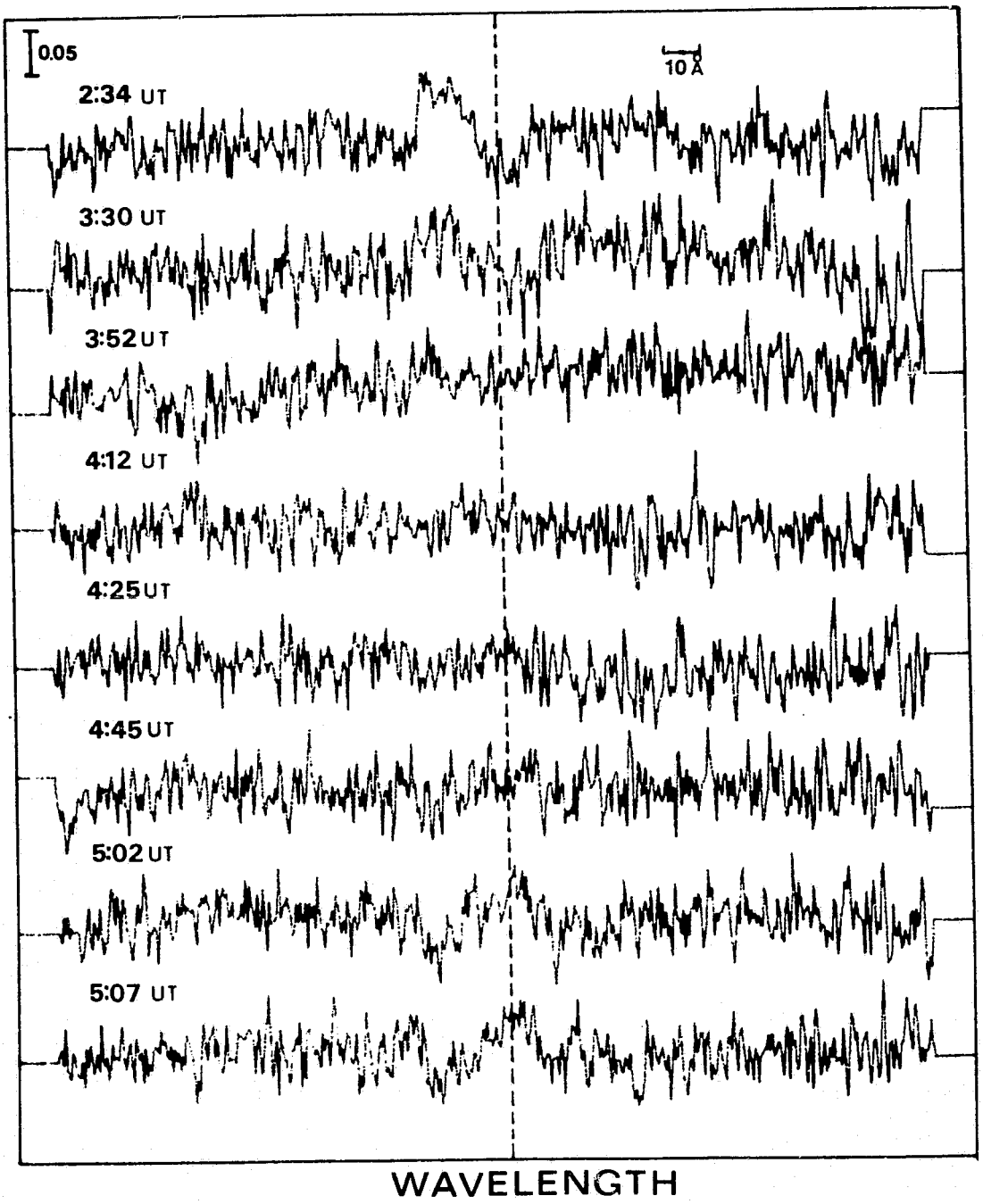

Fig. 2. Here we present the ratio of the individual flare spectra to the normalized mean spectrum in Figure 1. We show here 8 of the 16 flare spectra, basically every other spectrum. The mean time of each integration is also shown with each ratio spectrum. The vertical bar in the upper left shows the size of a 5% variation. Again all these spectra are on the same scale but offset for display purposes. The vertical dashed line indicates the position of the photospheric H alpha line.

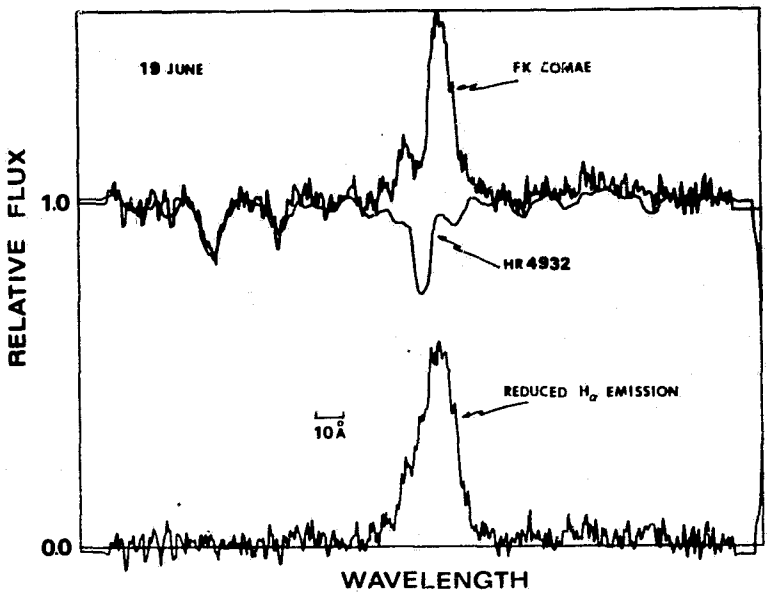

Fig. 3. We illustrate here our technique for obtaining the Reduced Emission Spectra. The spectrum of FK Comae on June 19th is shown with the broadened spectrum of HR4932 matched to it. By subtracting these we obtain the bottom Reduced Emission spectrum which represents the combination of the flare, chromospheric and disk spectra.

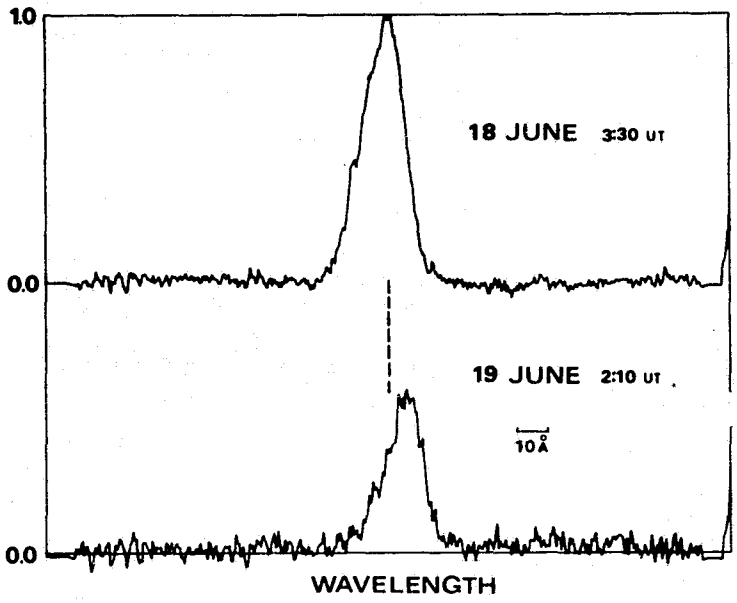

Fig. 4. The differing mean radial velocities of the reduced emission profile for the 18th (phase 0.54, top) and the 19th (phase 0.95, bottom) are illustrated here. Again the vertical line represents the photospheric H alpha position.

value of v sin i for FK Comae cited above suggests that the inclination is near 90^{o} and an emitting region near the surface of the star would be occulted. Thus material streaming away at some distance from the star is likely responsible for the very enhanced red asymmetry in the spectrum in Figure 3. On the other hand the fact that the spectrum appeared normal four days later at phase 0.62 suggests that it is reasonable to consider that some decay might have taken place from the night of the 18th to the 19th.

Our model to explain this flare event differs substantially from that proposed by Walter (1981) in which he postulates that a shell ejection mechanism may be at work. We conjecture that the flare event originates on the star itself in a surface active region. This surface active region is the same region which is the source of the magnetic loop structures hypothesized by Ramsey et al. (1981) to contain the density enhancement in the disk which is in turn responsible for the emission line profile asymmetry under normal conditions. During the flare event material is ejected radially outward from the star, possibly along magnetic field lines. The H alpha emission is assumed to be recombination radiation as the material expands into the existing disk structure. It is quite possible that the material in the disk, estimated by Ramsey et al. (1981) to be $\approx 2 \times 10^{-11}$ solar masses, is entirely due to such flare events. Scaling the numbers given in the above quoted paper the flare emission measure is about $3 - 5 \times 10^{56}$ cm^{-3}. If we assume a volume of 1 R_{*} for the flare we can estimate that up to 4×10^{-13} solar masses are ejected. Under these circumstances about 50 events/year could completely replenish the excretion disk.

We would like to acknowledge useful and stimulating discussions with Drs. Lawrence Auer, Bernard Bopp and Frederick Walter during the preparation of this paper. We also acknowledge the valuable assistance of Mr. Samuel Barden in working with the fiber spectrograph. This research has been supported in part by NSF grants AST7819317, AST8025204 and the United States Air Force (contract F19628-80-C-0036).

IV REFERENCES

Bopp, B. W. and Rucinski, S. M. 1981, in IAU Symposium 93, "Fundamental Problems in the Theory of Stellar Evolution", eds. D. Sugimoto, D. N. Schramm and D. Q. Lamb (Dordrecht: Reidel) in press.

Bopp, B. W. and Stencel, R. E. 1981, Ap. J. (Letters), 247, L131.

Chugainov, P. F. 1976, Izv. Krymsk. Astr. Obs., 54, 89.

Ramsey, L. W., Nations, H. L., and Barden, S. C. 1981, Ap. J. (Letters), 251, December 15 issue.

Ramsey, L. W., Barden, S. C., Nations, H. L., and Truax, R. J. 1980, Bull. A. A. S., 12, 836.

Walter, F. M. 1981, preprint.

Webbink, R. F. 1976, Ap. J., 209, 829.

N83 20870 D24

A Comparison of Circumstellar Gas and Dust in M Giants and Supergiants

Wendy Hagen, Wellesley College
Dale F. Dickinson, JPL
Roberta M. Humphreys, University of Minnesota
and
Robert E. Stencel, JILA

INTRODUCTION

Mass loss from M stars was first observed in 1935 by Adams and MacCormack, who observed violet-displaced absorption cores in strong resonance and low excitation potential lines in the spectrum of Alpha Orionis. In 1956 Deutsch was able to prove that the expanding matter observed was actually being lost to the system through observations of the binary system Alpha Herculis. The observed absorption lines due to the expanding circumstellar (CS) envelope of the M primary were superimposed on the spectrum of the G star companion, and such lines are never observed in a G star spectrum. In addition, the companion is itself a spectroscopic binary, and the radial velocities of the CS lines did not share the variations present in the normal G-star lines due to orbital motion. Detailed analyses of CS gas based on studies of line profiles have since been presented by Weymann (1962), Sanner (1976) and Bernat (1977).

Mass loss is also observed in the Ca II H and K lines in M giants and supergiants. The normal K3 central absorption feature is replaced by a deeper (central intensity indistinguishable from zero) K4 feature, which is generally blue-shifted with respect to line center. These H and K features can be used to establish the existence of mass loss from stars whose CS envelopes are not sufficiently extensive to be observable in the weaker lines. Unfortunately, the great strength of the transition gives rise to such large optical depths in the line that observations of the H and K profiles cannot be used to determine column densities nor mass loss rates for the stars. Reimers (1977) has studied the regions of the H-R diagram for which mass loss is observed in the H and K lines, and Boesgaard and Hagen (1979) have used observations of the K4 features to study velocity gradients in CS envelopes of M giants.

The extended envelopes of M giants and supergiants are also detected in the infrared. Dust grains surrounding the star radiate in the infrared, and an infrared excess is observed for the star. Oxygen-rich stars show an emission feature at 10 microns which is attributed to silicate grains, and carbon stars show a much smoother spectrum, with a less prominent emission

feature due to SiC at 11.5 microns (c.f. Merrill and Stein 1976). Observations of CS dust have been used to estimate the amount of CS material by Gehrz and Woolf (1971), Dyck and Simon (1975) and Hagen (1978).

The mechanism of mass loss is not yet understood. Some authors favor radiation pressure on the dust grains, which are then able to drag the gas along with them (c.f. Kwok 1975, Menietti and Fix 1978). An analogy of the solar wind may be driving the mass loss--thermal expansion of the outer atmosphere takes place after a mechanical energy deposition has heated the gas (c.f. Fusi-Pecci and Renzini 1975, Mullan 1978). Hartmann and MacGregor (1980) have suggested momentum deposition by Alfven waves as a mass loss mechanism in red giants. In the case of the Mira variables, shock waves appear to be able to drive the mass loss (Willson and Hill 1979, Wood 1979). For an excellent review of proposed mechanisms for mass loss see Castor (1981).

Previous work comparing the relative amounts of CS gas and dust by Hagen (1978) showed no correlation between the two. If the mechanism of mass loss were indeed radiation pressure on grains, one should expect to see that the dustiest stars should also show the greatest amount of CS gas, which was not observed to be the case.

In the spectra of red giants and supergiants, luminosity-sensitive weak emission features appear superposed on the broad absorption line wings of the Ca II H and K lines (Stencel 1977). Similar features are seen to occur in solar chromospheric limb spectra (Canfield 1971) and are due to singly ionized metals and rare earths. These features in stellar spectra appear to be related to the existence of an extended chromosphere surrounding red giants and supergiants and may be diagnostics for chromospheric heating. These lines have been modeled in the solar thin-chromosphere case, by Cram et al. (1980) as due to UV line wing photons from the deep photosphere pumping upper levels of multiplets UV 1 of Fe II, with the cascade in multiplet V 3 becoming visible due to the added opacity of the Ca II line wings. It is not clear that this would be the case in a thick chromosphere, where many subordinate transitions appear optically thick. Implicitly, one might think that the emission features occur then because of geometrical effects, suggesting that the wing emission lines can serve as secondary diagnostics of chromospheric heating, particularly when the K-line core is obscured by extensive CS absorption, as in stars in the present study.

This paper presents the results of a study of CS gas and dust in a larger sample of stars than that of Hagen (1978). If the gas-to-dust ratio varies considerably from star to star, does this variation correlate with any other observable properties of

the stars, such as the appearance of chromospheric diagnostics like the Ca II H and K profiles, the presence of Ca II wing emission lines, or other extended CS envelope diagnostics such as the presence of microwave maser emission?

The observations were obtained at Cerro Tololo Interamerican Observatory and Kitt Peak National Observatory. CS gas was observed with 2.5 and 5.1 A/mm echelle spectra obtained with the 4-meter telescopes. CS dust was observed through infrared photometry done with the CTIO 60" and KPNO 50" telescopes.

RESULTS

1. THE H AND K LINES. All stars observed showed the deep CS K4 component. All but the latest stars of luminosity class III showed nearly identical Ca II H and K profiles, with a relatively narrow K4 absorption, whose blue shift with respect to line center leaves the long-wavelength emission peak stronger. The H and K profiles of the latest giants and most of the supergiants showed much broader K4 absorption, and reduced or no emission. Those which did show emission had the two peaks of nearly the same intensity or the short-wavelength component stronger. Emission intensity was estimated on a scale of 0 (no emission seen) to 3 (emission intensity roughly equal to the continuum level outside the H and K wings), and the width of the K4 feature was measured off the tracings. These values appear in Table 1.

The Mira variables showed a variety of profiles, some with extremely strong emission due to shock waves in the stellar atmosphere. As the Miras were not all observed at the same phase they do not provide a uniform sample for comparison of the H and K profiles.

2. CIRCUMSTELLAR GAS. Optical observations of CS gas are hampered by the fact that the majority of the metals in the CS gas are singly ionized, but the majority of observable resonance lines arise from neutral metals. The ionization conditions within the CS envelopes are very poorly understood (see Bernat 1977, Hagen 1978) and use of the lines of neutral metals to estimate total column densities would require ionization corrections which would be both very large and very uncertain. Consequently the line of Sr II at 4077 A has been used for the estimation of the total amount of CS gas, as this line arises from the dominant stage of ionization in the envelope. However, it should be noted that there is a possibility that the abundance of strontium may not be normal in these evolved stars, which would affect the derivation of the total CS column density from the Sr line.

The column density of Sr II was derived from the degree of asymmetry in the observed line profile following Hagen (1978).

TABLE 1

Estimated emission intensities of Ca H and K and K4 absorption widths.

Star	Spectral Type	Tau (Sr)	Tau (10)	K4 Width (A)	Em Str	Loss Rate (M⊙/yr)
1. Stars with "Early Giant" H and K Profiles						
45 Ari	gM6	<0.5	<.005	0.3	2	<1.3 E-7
Delta 2 Lyr	M4 II	<0.5	<.005	0.4	3	<1.3 E-7
Eta Per	K3 Ib	<0.5	<.005	0.3	3	<1.3 E-7
Pi Aur	M3 II	<0.5	<.005	0.3	3	<1.3 E-7
R Lyr	M5 III	<0.5	<.005	0.3	3	<1.3 E-7
HR 8421	gM8	<0.5	0.01	0.3	3	6.1 E-8-1.6 E-7
18 Cep	gM5	<0.5	<.005	0.3	3	<1.3 E-7
57 Psc	gM4	<0.5	<.005	0.3	3	<1.3 E-7
Rho Per	M4 II-III	<0.5	<.005	0.3	3	<1.3 E-7
Delta 2 Gru	M3 III	<0.5	0.01	0.3	3	6.1 E-8-1.6 E-7
Psi Phe	M4 III	<0.5	0.01	0.3	3	6.1 E-8-1.6 E-7
HR 587	gM5	<0.5	0.01	0.3	3	6.1 E-8-1.6 E-7
HR 257	M4 III	<0.5	0.01	0.3	3	6.1 E-8-1.6 E-7
Lambda Vel	K5 Ib	<0.5	<.005	0.3	3	<1.3 E-7
Alpha Her	M5 II	3.7	0.01	0.5	2	7.8 E-7
2. Stars With Late-Giant/Supergiant H and K Profiles						
119 Tau	M2 Iab	4.0	<.005	0.6	2	8.0 E-7
TV Gem	M1 Iab	noisy	0.1	0.5	0	>9.2 E-8
BU Gem	M1 Ia	noisy	0.06	0.6	0	>5.5 E-8
EU Del	M6 III	<0.5	<.005	0.4	1	<1.3 E-7
W Cyg	M4e - M6	<0.5	0.015	0.6	0	9.2 E-8-1.9 E-7
TW Peg	M6 - M7	<0.5	0.1	0.8	0	6.1 E-7-7.1 E-7
KK Per	M2 Iab	44	0.02	0.9	1	8.7 E-6
SU Per	M3 Iab	50	0.1	1.2	1	1.0 E-5
AD Per	M3 Iab	7.8	0.03	0.6	2	1.7 E-6
HD 37536	M2 Iab	4.6	0.02	0.6	2	1.0 E-6
R Dor	M8 III	<0.5	0.02	0.6	0	1.2 E-7-2.2 E-7
HD 90586	M2 Iab/b	9.6	0.08	0.8	<0.5	6.8 E-6
EV Car	M3 Ia/Iab	1.8	0.3	0.8	0	5.3 E-6
V396 Cen	M4 Iab/b	5.0	0.06	0.6	1	1.3 E-6
AH Sco	M5 Ia/Iab	2.9	0.2	1.3	0	1.8 E-6
BO Car	M4 Ib	3.4	0.005	0.6	1	6.9 E-7
HD 95950	M2 Ib	>50	0.03	1.0	3	>9.9 E-6
VX Sgr	M4e Ia - M8	0.86	0.1	1.6	0	7.8 E-7
Mu Cep	M2 Ia	6.3	0.2	1.1	0	2.5 E-6
Alpha Ori	M2 Iab	12.3	0.05	0.8	2	2.7 E-6
Alpha Sco	M1 Ib	3.2	0.02	0.7	2	7.4 E-7
X Her	M6e	0.5	0.08	1.0	0	5.9 E-7
RX Boo	M7e - M8e	0.6	0.06		0	4.8 E-7
HD 207076	M7 III	0.9	0.1	1.0	0	7.9 E-7

The observed asymmetry was compared to theoretical line profiles computed with the Kunasz-Hummer code for the calculation of line profiles formed in an expanding, extended atmosphere. Due to the difficulty of measuring radial velocities on the echelle plates with their curved orders, shell expansion velocity was assumed to be 10 km/sec in all cases. Should the expansion velocity be less than this value, the CS column densities will be underestimated, and vice versa. Column densities would be underestimated by about 30% for a true expansion velocity of 7 km/sec.

No star with a Ca II K profile typical of the early giants showed detectable CS Sr II, with the exception of Alpha Her, which showed the widest K4 absorption of all stars observed to have a stronger long-wavelength emission component. Most of the stars with late giant/ supergiant H and K profiles did show detectable CS Sr II. CS absorption in Fe I and/or Al I was seen in most stars with late giant or supergiant H and K profiles, and in none of the early giants. The derived optical depths at Sr II 4077 are presented in Table 1.

Asymmetries in the sense expected for mass loss were seen in the Sr II lines of several of the Miras. However, the assumption of the 10 km/sec expansion velocity for the CS envelope would be far more dangerous. The photospheric spectrum of Miras goes through substantial radial velocity variations during a cycle, while the overlying CS spectrum would be expected to be found at a constant velocity, invalidating the assumption of a 10 km/sec displacement between the photospheric line and the CS core.

3. CIRCUMSTELLAR DUST. The quantity of CS dust was estimated from the contrast in the 10-micron silicate emission feature as described by Hagen (1978), assuming an inner shell radius of 10 R*, and that the dust falls off as the -1.5 power of the radius. Stars with early giant H and K profiles all showed very little CS dust, with tau(10 microns) never greater than 0.01. Derived optical depths are presented in Table 1.

4. WING EMISSION LINES. Virtually all of the stars observed, including the Miras and those which did not show Ca II H-K core emission, showed one or more of the H-K wing emission lines, identified on the basis of wavelength coincidence with the stellar line list by Stencel (1977; see also Rutten and Stencel 1980). The most frequently found lines were near 3932 A (Ti II), 3936 A (Fe I or Fe II?), 3938 A (Fe II) and 3967 A (Fe I?), in addition to the occasional appearance of H-epsilon emission at 3970 A. H-epsilon emission is associated with low chromospheric pressures (Ayres and Linsky 1975). The strong wing emission lines found in the Miras at 3938, 3945 and 3969 A are due to collisionally excited Fe II V3 formed in the atmospheric shocks of such stars. For the non-Miras, the widths of the wing emission are luminosity sensitive, particularly the 3936 A

feature, where $M_v \approx 40 - 18 \log$ HWHM(mA) (c. f. Hagen et al. 1981). Among the non-Mira stars in our sample with zero K-line emission strength, BU Gem, EV Car, AH Sco, VX Sgr and Mu Cep have 3936 A emission features consistent with their supergiant luminosity classifications, yielding $M_v < -6$. Improvement of this technique must await correlations based on high signal-to-noise, ultra-high-dispersion data that are presently unavailable.

DISCUSSION

The quantity of CS gas is plotted against the quantity of CS dust in Figure 1. As seen by Hagen (1978) no correlation is seen, although stars in which CS gas is below the threshold of detectability are generally the same ones in which no dust can be observed. As the sample contains stars of varying temperature and luminosity, the plot was redone for only M1-3 Iab stars, and no correlation was seen within this more uniform sample either. As concluded by Hagen (1978), that the dustier stars do not also show more CS gas indicates that the dominant mass loss mechanism is probably not radiation pressure on dust grains.

Jennings and Dyck (1972) noted an anticorrelation between the presence of CS dust and Ca II H and K emission--dustier stars show less emission. In Figure 1, the stars with emission strength 0 are shown as open circles. It can be seen that no emission is seen for some stars which are considerably less dusty than some stars which show emission. What appears to be important is the dust-to-gas ratio, the degree of condensation of grains. The more complete the condensation, the less H and K emission. However, the H-K wing emission lines appear to be insensitive to the disappearance of the H-K core emission even in the high dust-to-gas stars. This implies that either chromospheric heating is occurring although masked in the cores of H and K, or that an alternate mechanism for exciting the wing emission lines ($T_{ex} > 5000$ K) must be postulated.

Apart from this correlation of gas-to-dust ratio with K2 emission, the most striking thing about this collection of data is the lack of correlations. CS envelopes apparently contain a heterogeneous set of properties among stars in our sample.

A large K4 absorption width is indicative of velocity gradients in the shell and/or large turbulence (Boesgaard and Hagen 1979). However, if the CS absorption feature in the Sr II 4077 line is formed over a large velocity gradient, the sharpness of the CS core will be washed out and the column density underestimated. Thus an anticorrelation between K4 width and Sr II column density might be expected(especially among stars of similar spectral and luminosity class). However, plots for both the entire sample and the M1-3 Iab stars were scatter diagrams.

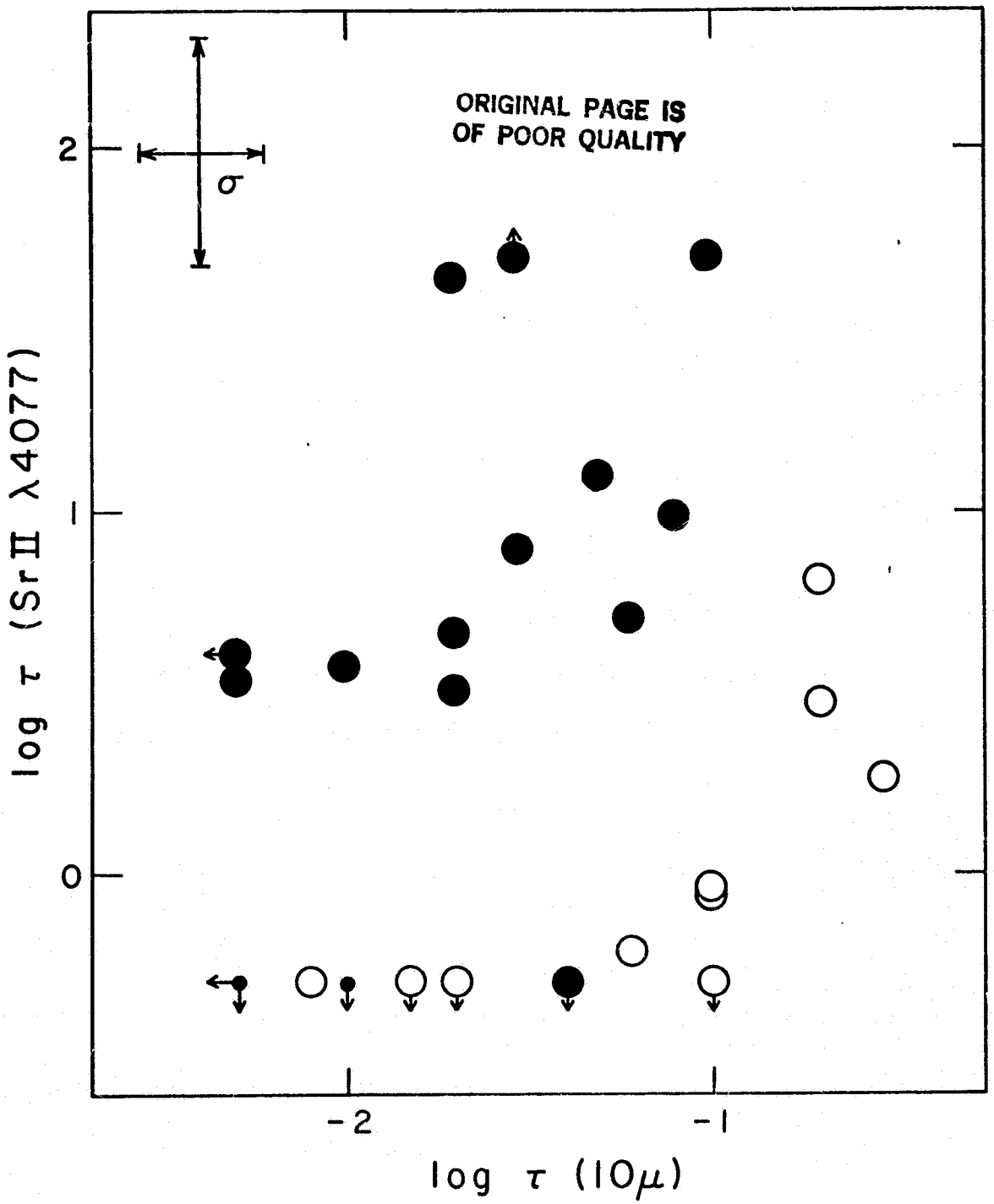

Figure 1. A comparison of quantities of gas and dust. The optical depth as derived for the Sr II 4077 line is plotted against the optical depth as derived for the 10-micron silicate feature. Open circles represent stars for which no emission was seen in the Ca II H and K lines. The small circles each represent several stars with giant H and K profiles. The filled circle in the region of the diagram populated mainly by open circles represents BM Sco, a peculiar K supergiant.

The mass loss rates quoted in Table 1 should be regarded as estimates at best, due to the number of assumptions included in their derivation. The inner shell radius enters linearly into the derivation of a mass loss rate from a column density. It has been assumed to be 10 R_* in all cases, but values ranging from star to star of a factor of 10 on either side are not out of the question. For a recent review of the inner shell radius problem see Castor (1981).

REFERENCES

Adams, W. S. and MacCormack, E. 1935, Ap. J. 81, 119.
Ayres, T. R. and Linsky, J. L. 1975, Ap. J. 201, 212.
Bernat, A. P. 1977, Ap. J. 213, 756.
Boesgaard, A. M. and Hagen, W. 1979, Ap. J. 231, 128.
Canfield, R. C. 1971, Solar Phys. 20, 275.
Castor, J. I. 1981, in Physical Processes in Red Giants, ed. I. Iben and A. Renzini (Dordrecht: Reidel), 285.
Cram, L., Rutten, R. and Lites, B. 1980, Ap. J. 241, 374.
Deutsch, A. J. 1956, Ap. J. 123, 210.
Dyck, H. M. and Simon, T, 1975, Ap. J. 195, 689.
Fusi-Pecci, F. and Renzini, A. 1975, Mem. Soc. Roy. Sci. Liege, 6e ser., tome VIII, 383.
Gehrz, R. D. and Woolf, N. J. 1971, Ap. J. 165, 285.
Hagen, W. 1978, Ap. J. Supp. 38, 1.
Hagen, W., Humphreys, R. M. and Stencel, R. E. 1981, P.A.S.P. Oct. 1981, in press.
Hartmann, L. and MacGregor, K. B. 1980, Ap. J. 242, 260.
Jennings, M. C. and Dyck, H. M. 1972, Ap. J. 177, 427.
Kwok, S. 1975, Ap. J. 198, 583.
Menietti, J. D. and Fix, J. D. 1978, Ap. J. 224, 961.
Merrill, K. M. and Stein, W. A. 1976, P.A.S.P. 88, 285.
Mullan, D. 1978, Ap. J. 226, 151.
Reimers, D. 1977, Astron. Astrophys. 57, 395.
Rutten, R. and Stencel, R. 1980, Astron. Astrophys. Supp. 39, 415.
Sanner, F. 1976, Ap. J. Supp. 32, 115.
Stencel, R. E. 1977, Ap. J. 215, 176.
Weymann, R. J. 1962, Ap. J. 136, 844.
Willson, L. A. and Hill, S. J. 1979, Ap. J. 228, 854.
Wood, P. R. 1979, Ap. J. 227, 220.

 D25

PREDICTED MAGNITUDES AND COLORS FROM COOL-STAR MODEL ATMOSPHERES

Hollis R. Johnson
Thomas Y. Steiman-Cameron
Indiana University

An intercomparison of model stellar atmospheres and observations of real stars can lead to a better understanding of the relationship between the physical properties of stars and their observed radiative flux. In this spirit we have determined wide-band and narrow-band magnitudes and colors for a subset of models of K and M giant and supergiant stars selected from the grid of 40 models by Johnson, Bernat and Krupp (1980) (hereafter referred to as JBK). The 24 models selected have effective temperatures of 4000, 3800, 3600, 3400, 3200, 3000, 2750 and 2500 K and log g = 0, 1 or 2. Emergent energy fluxes (erg/ cm^2 s A) were calculated at 9140 wavelengths for each model. These computed flux curves were folded through the transmission functions of Wing's 8-color system (Wing, 1971; White and Wing, 1978) and through Johnson's (1965) wide-band (BVRIJKLM) system. The calibration of the resultant magnitudes was made by using the absolute calibration of the flux curve of Vega by Schild et al. (1971).

By folding the models through the Wing filters, we have extended to lower temperatures the work of Piccirillo et al. (1981) in determining the relationship between effective temperature and Wing color temperature. The predicted Wing magnitudes are listed in Table 1. Color temperatures are computed by fitting a blackbody through the magnitudes predicted by those filters which represent the continuum. This usually involves fitting the magnitudes given by filters 2 and 6. Before this fit is made, corrections must be made to the magnitudes of filter 1 and 2 to account for absorption by CN. A description of the reduction method is given by White and Wing (1978). The color temperatures predicted by these models are shown in Figure 1 for the log g = 0 and log g = 2 cases. Also plotted are the empirical relations found by Ridgway et al. (1980) and model predictions by Bell et al. (1976). The color temperature-effective temperature relation for the JBK models has been previously shown by Piccirillo et al. for effective temperatures above 3200 K. As shown by these authors, the color temperatures predicted by model atmospheres with effective temperatures between 3200 and 4000 K are insensitive to gravity and are in good agreement with observations. We now find that for effective temperature below 3200 K the predicted color temperatures demonstrate a strong gravity dependence.

CN and TiO indices are determined by the depression of the flux through filters 1, 4 and 8 below that predicted by a blackbody through the continuum points. Filters 4 and 8 determine the CN index while filter 1 determines the TiO index. Predicted CN and TiO indices for the models are given in Table 1. White and Wing have calibrated the Eight-Color TiO index with spectral type.

TABLE 1.
Predicted Wing Magnitudes

Model	CN	TiO	Wing 1	Wing 2	Wing 3	Wing 4	Wing 5	Wing 6	Wing 7	Wing 8
4000/2	7	13	2.51	2.33	2.35	2.38	2.55	2.55	2.57	2.68
4000/1	11	9	2.48	2.33	2.31	2.40	2.55	2.53	2.55	2.70
4000/0	16	10	2.47	2.31	2.26	2.40	2.52	2.49	2.50	2.71
3800/2	5	36	3.03	2.62	2.73	2.64	2.75	2.74	2.75	2.84
3800/1	8	26	2.94	2.62	2.66	2.65	2.75	2.74	2.75	2.88
3800/0	12	18	2.86	2.61	2.58	2.66	2.74	2.71	2.72	2.90
3600/2	5	64	3.66	2.94	3.29	2.94	2.93	2.92	2.93	2.99
3600/1	7	55	3.59	2.95	3.19	2.96	2.96	2.96	2.96	3.05
3600/0	10	44	3.49	2.96	3.07	2.97	2.94	2.96	2.96	3.10
3400/2	7	99	4.47	3.34	4.04	3.31	3.09	3.08	3.08	3.13
3400/1	8	90	4.43	3.40	4.02	3.37	3.16	3.15	3.15	3.21
3400/0	9	86	4.39	3.39	3.90	3.37	3.21	3.19	3.19	3.28
3200/2	9	136	5.30	3.75	4.72	3.68	3.24	3.22	3.23	3.27
3200/1	10	130	5.53	4.00	4.97	3.90	3.35	3.32	3.31	3.37
3200/0	11	132	5.69	4.13	5.07	4.01	3.45	3.41	3.39	3.47
3000/2	11	162	5.93	4.07	5.21	3.95	3.38	3.35	3.35	3.42
3000/1	11	155	6.30	4.45	5.56	4.26	3.53	3.48	3.46	3.53
3000/0	12	155	6.74	4.84	5.99	4.58	3.68	3.61	3.57	3.66
2750/2	15	202	6.75	4.43	5.87	4.25	3.56	3.51	3.53	3.65
2750/1	14	181	6.98	4.82	6.11	4.57	3.72	3.65	3.64	3.75
2750/0	14	171	7.38	5.28	6.49	4.93	3.92	3.81	3.77	3.90
2500/2	23	251	7.62	4.75	6.52	4.51	3.76	3.68	3.77	4.00
2500/1	20	224	7.68	5.06	6.67	4.77	3.90	3.81	3.84	4.05
2500/0	18	142	7.41	5.56	6.71	5.19	4.13	4.01	3.98	4.16

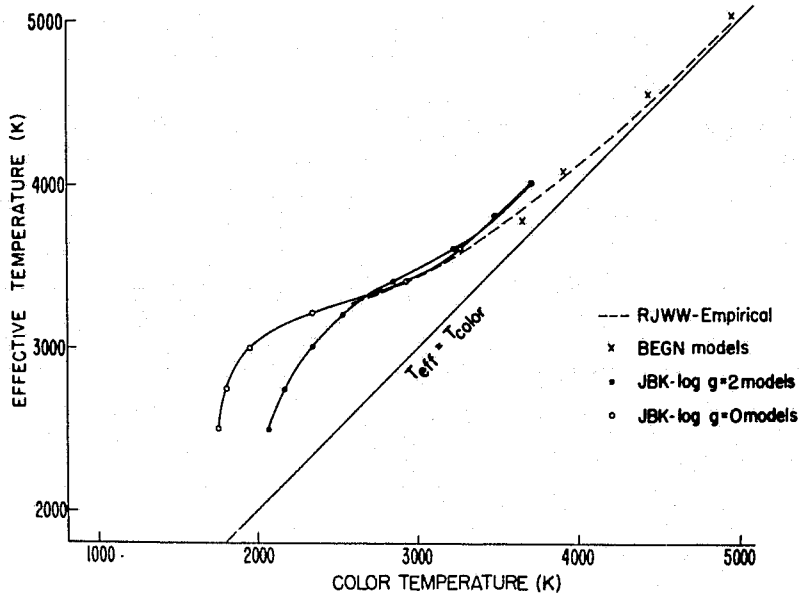

Figure 1. Color temperature vs. effective temperature for JBK log g = 0, 2 models. Also shown are relations found by Ridgway et al. (1980) and Bell et al. (1976).

The calibration was originally determined for giants but has been found to give good agreement with supergiant spectral types as well. The spectral type of each of the JBK models has been determined on the basis of the TiO index of that model and the Wing calibration. In this manner the effective temperature scale for K5 through M5 giants and supergiants has been evaluated. Table 2 gives the result of this evaluation.

In a similar way, model fluxes were folded through the B, V, R, I, J, K, L and M filters of the Johnson wide-band system. The models were not run through the U and N filters. Those color indices involving the B or V magnitudes give colors which are too blue, indicating an opacity source(s) unaccounted for in the models. Theoretical models by other workers show the same problem. The predicted wide-band colors are listed in Table 3. For completeness the V-R index is listed with the acknowledgement that this index is too blue.

Figure 2 shows a plot of R-I versus effective temperature for the JBK log g = 0, 2 cases. The relation between spectral type and TiO index found by Wing allows us to establish the relation between effective temperature and spectral type found in Table 2. Using this temperature scale, color indices for various observed spectral types can be compared with the model predictions. Lee (1970) observed R-I colors for M giants and supergiants as a function of spectral type. Using the calibration in Table 2 to convert spectral type to effective temperature, we have plotted Lee's observations in Figure 2. The comparison of observed and predicted R-I colors for M giants demonstrates an incredible correlation! The R-I observations for M2 through M5 agree almost exactly, while the agreement between theory and observation for M1 and M2 is extremely good. The comparison for the supergiants, while not quite as good as for the giants, is still excellent.

Figure 3 shows the predicted relationship between the TiO index and R-I color index for giants and supergiants. On the same diagram the TiO indices for M giants and supergiants as determined by Wing and the R-I colors as determined by Lee are plotted. Again excellent agreement is found. The location of the giants agrees extremely well with that predicted by the models. Supergiants, while not agreeing as well with the models, still exhibit a remarkably good fit except for the very coolest stars (M5).

The excellent agreement between observed and predicted quantities is very reassuring regarding use of the JKB models. Good agreement between model predictions and observations has also been found for the relation between TiO band strengths and J-K colors for M supergiants in the Galaxy, LMC, and SMC (McGregor 1981) and for the relation between TiO band strengths and near infrared colors of globular cluster giants (Johnson et al. 1982). Additional comparisons of model predictions with observations -- including triumphs and difficulties -- will be discussed in a forthcoming paper (Steiman-Cameron and Johnson 1982).

TABLE 2.
Effective Temperatures Calibrated by the TiO Index of White and Wing

Spectral Type	Effective Temperature (K) Giants (log g = 2)	Effective Temperature (K) Supergiants (log g = 0)
K5.0	3980	3850
M0.0	3900	3720
M1.0	3800	3630
M2.0	3690	3560
M3.0	3560	3460
M4.0	3400	3330
M5.0	3180	3150

TABLE 3.
Values of Wide-Band Colors Predicted by the Model

Model	V-R	R-I	R-J	R-K	R-L	R-M	J-K
4000/2	.83	.75	1.62	2.62	2.71	2.66	1.01
4000/1	.84	.73	1.60	2.59	2.69	2.63	1.00
4000/0	.85	.73	1.60	2.57	2.68	2.61	.96
3800/2	.87	.92	1.89	2.98	3.07	3.03	1.09
3800/1	.90	.86	1.82	2.92	3.02	2.96	1.10
3800/0	.93	.83	1.78	2.86	2.98	2.91	1.08
3600/2	.90	1.23	2.33	3.48	3.58	3.52	1.14
3600/1	.94	1.14	2.23	3.42	3.53	3.48	1.19
3600/0	1.00	1.05	2.13	3.33	3.45	3.40	1.20
3400/2	.96	1.61	2.92	4.06	4.16	4.08	1.14
3400/1	1.03	1.56	2.87	4.12	4.24	4.17	1.24
3400/0	1.09	1.48	2.77	4.07	4.20	4.14	1.30
3200/2	1.06	1.93	3.39	4.46	4.56	4.44	1.07
3200/1	1.19	2.00	3.61	4.83	4.96	4.83	1.22
3200/0	1.31	2.02	3.68	5.02	5.17	5.06	1.34
3000/2	1.18	2.12	3.64	4.61	4.71	4.57	.97
3000/1	1.35	2.23	3.97	5.11	5.23	5.06	1.14
3000/0	1.57	2.37	4.32	5.63	5.78	5.60	1.31
2750/2	1.38	2.33	3.87	4.71	4.88	4.73	.84
2750/1	1.56	2.40	4.15	5.17	5.29	5.11	1.01
2750/0	1.81	2.50	4.52	5.71	5.85	5.62	1.20
2500/2	1.69	2.47	3.99	4.74	5.04	4.78	.76
2500/1	1.86	2.51	4.20	5.09	5.31	5.05	.89
2500/0	2.05	2.48	4.45	5.57	5.75	5.85	1.12

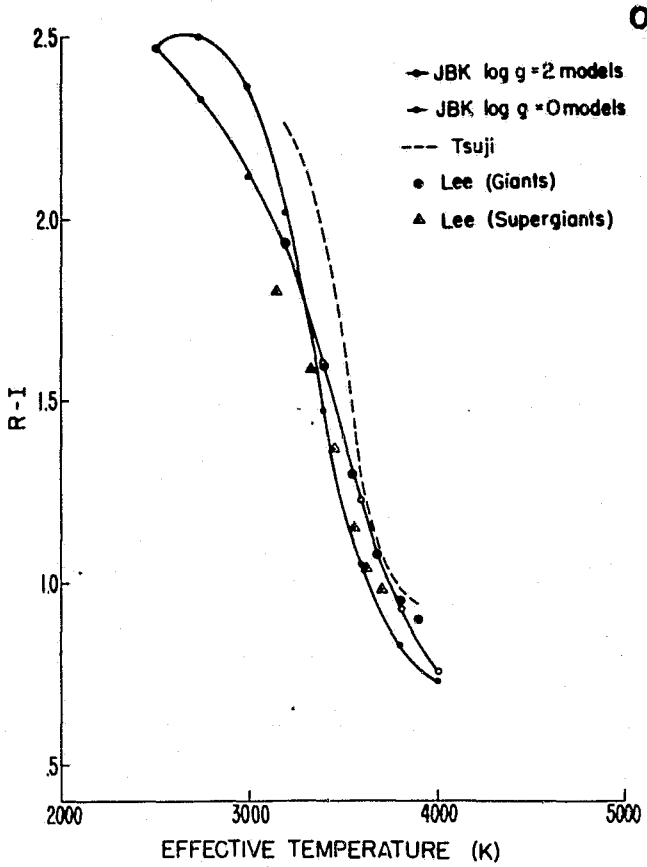

Figure 2. R-I vs. effective temperature for JBK log g = 0, 2 models, Tsuji's (1978) relationship and Lee's (1970) observations for giants and supergiants.

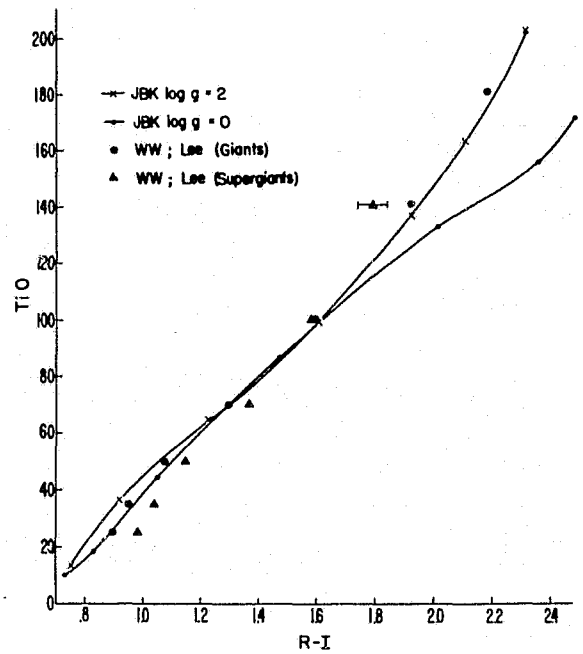

Figure 3. TiO index vs. R-I for JBK log g = 0, 2 models. Also shown are observed values for K5 - M5 giants and supergiants, with TiO index taken from White and Wing (1978) and R-I taken from Lee (1970).

Our understanding of colors and magnitudes has profited by helpful discussions with R. K. Honeycutt and J. Piccirillo. This research was supported by NSF grant AST-7913149. Much of the computing was supported by Indiana University through the Wrubel Computing Center. This support is gratefully acknowledged.

REFERENCES

Bell, R. A., Eriksson, D., Gustafsson, B. and Nordland, A. 1976, Astr. and Ap. Suppl., 23, 37.

Johnson, H. R., 1965, Ap. J., 141, 923.

Johnson, H. R., Bernat, A. P., and Krupp, B. M. 1980, Ap. J. Suppl. 42, 581.

Johnson, H. R., Mould, J., and Bernat, A. P. 1982, Ap. J., submitted.

Lee, T. A. 1970, Ap. J., 162, 217.

McGregor, P. 1981, Ph.D. Thesis, Australian National University,Canberra.

Piccirillo, J., Bernat, A. P., and Johnson, H. R. 1981, Ap. J., 235, 126.

Ridgway, S. T., Joyce, R. R., White, N. M., and Wing, R. F. 1980, Ap. J., 235, 126.

Schild, R., Peterson, D. M., and Oke, J. B. 1971, Ap. J., 166, 95.

Steinman-Cameron, T. Y., and Johnson, H. R. 1982, Ap. J., in preparation.

Tsuji, T. 1978, Astr. and Ap., 62, 29.

White, N. and Wing, R. 1978, Ap. J., 222, 209.

Wing, R. F. 1971, in Proc. Conf. Late-Type Stars, ed. G. W. Lockwood and H. M. Dyck (Kitt Peak Obs. Contrib., No. 554), p. 145.

D26

HIGH-RESOLUTION IUE OBSERVATIONS OF THE 1981 ECLIPSE OF 32 CYG

D. Reimers, A. Che, and K. Hempe
Hamburger Sternwarte, Universität Hamburg

Summary

32 Cyg shows a spectacular pure emission line spectrum during eclipse. Six weeks later, most lines, which were observed in emission during eclipse, are seen as P Cygni type profiles with strong absorption components. The lines are formed through line scattering of B star light in the extended atmosphere (wind) of the K supergiant. During eclipse, the emission parts of the P Cyg lines remain visible since the size of the line scattering "sphere" around the B star is larger than the red giant.

Other emission lines are formed in a shock front near the B star (CIV, SiIV, FeIII) and possibly in an accretion disk.

The strong FeII UV Mult. 191 λλ 1785-88 Å is shown to be formed through optical pumping via FeII UV Mult. 9 photons.

The phase dependence of the P Cyg type profiles is modelled by means of line transfer calculations in nonspherical, 3-dimensional geometry with velocity fields.

The semi-amplitude of the B star orbit has been determined as $K_B = 35 \pm 5$ km/s. This yields a mass ratio near to 2.

I Introduction

In a project to determine mass-loss rates of red supergiants through observations of circumstellar lines in the UV spectra of their hot B star companions, we have obtained high-resolution IUE spectra of the systems Boss 5481, σ Sge, 32 Cyg, 47 Cyg, and ζ Car. Qualitatively, the spectra of these stars in the UV are B star spectra upon which P Cyg type lines and broad emission lines are superimposed. These lines are formed i) through line scattering of B star light in the extended winds of the red supergiants (Stencel et al. 1979, Reimers, 1980), ii) in accretion disks and/or shock

fronts around the B stars (Reimers and Kudritzki, 1980 ; Chapman, 1981), iii) in the chromospheres of the red giants near eclipse (MgII in pure absorption, Chapman, 1981). The lines seen as P Cyg type lines out of eclipse turn into pure emission lines during eclipse in 32 Cyg (and in ζ Aur, Chapman, 1981).

In this preliminary note we present a qualitative explanation of the origin of the different types of lines observed.

II Observations and Discussion

The observations used in this note are high-resolution short- and longwavelength IUE spectra of 32 Cyg taken on August 2, 1980, March 31 and June 17, 1981. The corresponding locations of the B star in its orbit relative to the K supergiant and the observer is shown in Fig. 1.

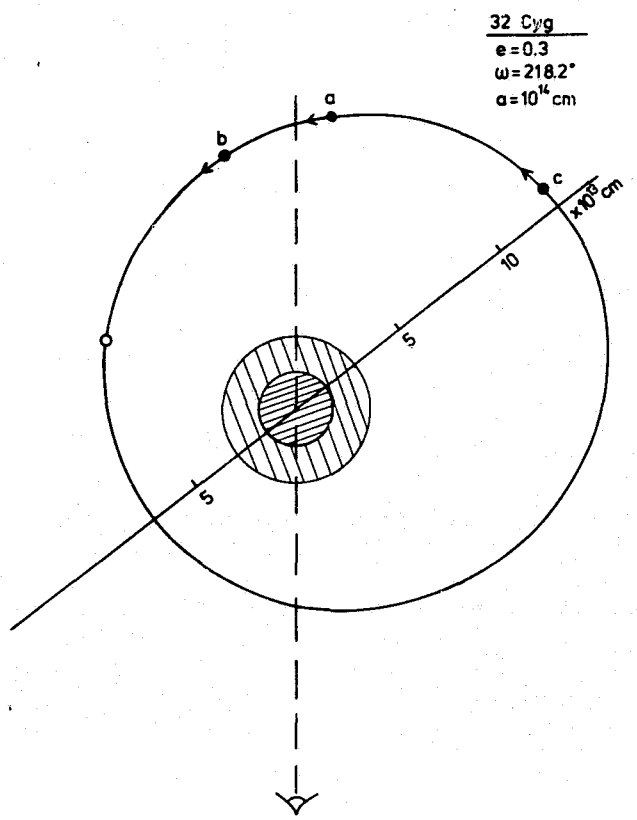

Fig. 1. Orbit of 32 Cyg with location of B star at times of observations. Black dot: B star. Small hatched circle: K supergiant. Phase a: March 31, 1981 ; b: June 17, 1981 ; c: August 2, 1980.

On March 31, the B star is totally eclipsed in the UV, and a spectacular pure emission line spectrum with hundreds of lines was observed. A similar spectrum was observed with the IUE during the eclipse of ζ Aur B (Chapman, 1980). For wavelengths $\lambda > 2600$ Å, the K giant continuum begins to emerge. Six weeks later, the B star has emerged from eclipse again, and most of the bright shell lines observed in emission on March 31 are seen as P Cyg type profiles, i.e. with strong absorption components on the violet side and reemission on the red side at the same wavelengths the emission lines had on March 31.

The observed nonstellar lines can be classified as follows

a) Scattering lines

Resonance lines and low excitation lines of abundant ions like FeII (e.g. UV Mult. 1, 2, 3, 8), SiII, MgII, AlII etc. belong to this class. In Fig. 2, as an example the line profile of SiII 2 1533.43 Å is displayed on a velocity scale with the B star radial velocity as reference zero velocity. The latter is determined from B star lines like SiIII 1298.9 Å. For the emission line phase, interstellar lines visible at all phases have been used to set up the wavelength reference scale.

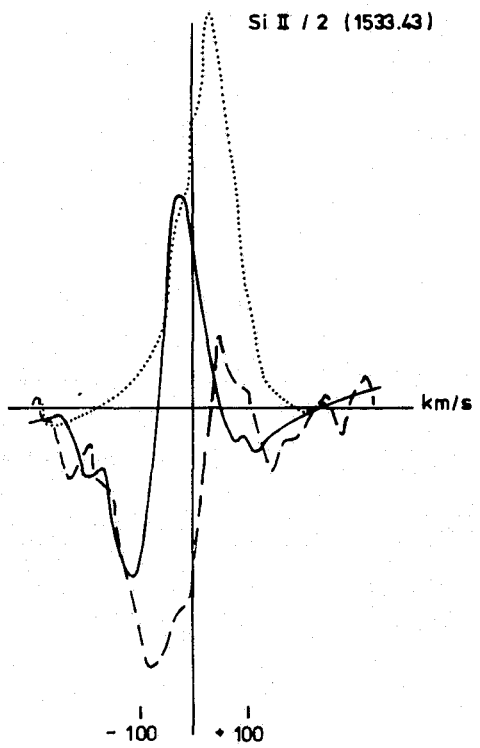

Fig. 2. Phase dependence of typical resonance lines on a velocity scale with B star at zero velocity (Phases: a: dotted line (eclipse), b: broken line, c: full line). For illustration, the zero flux niveau of the emission line at eclipse has been set up to the B star continuum flux at the other phases.

Lines belonging to this class are in emission during eclipse (phase a). The emission is slightly redshifted relative to the B star velocity since at this phase the K giant wind in the line scattering region around the B star is moving essentially away from us towards the B star. Shortly after egress from eclipse (b), we observe a particularly strong, blueshifted absorption line formed in the long absorption path close to the K giant (covering wind velocities from $-v_\infty$ to $+v_\infty$). The emission is essentially unchanged and superimposed upon the strong absorption line. At phase (c), far out of eclipse, a normal looking P Cyg profile emerges.

The wind velocity as measured from the violet edges of weaker lines of this class is nearly independent of phase and close to 60 km/s. At other phases (not shown here), multiple absorption components appear in several lines with velocities of several hundred km/s as was first noticed by Stencel et al. (1979).

It is obvious from Fig. 2 that, due to the strong phase dependence of the lines, besides density, velocity and mass loss rate, the location of the B star relative to the supergiant and to the line of sight can be inferred from the line profiles if the line transfer problem is treated properly.

For this purpose, a nonspherical, 3-dimensional line transfer code has been developed for line scattering in ζ Aur systems, i.e. with the light source outside of the density and velocity symmetry center (Hempe, 1981). The basic assumption is that the wind is expanding spherically from the K supergiant. That means that in a first approximation, we neglect disturbances of the K star wind by the close B star. Bending of stream lines due to the orbital movement of the red giant are taken into account. Entrance parameters are the orbital elements, orbital inclination, wind velocity, and the mass-loss rate. Line transfer calculations are performed with a Sobolev type approximation for the line source function plus exact integration of the formal integral for the line flux profiles (for details, see Hempe, 1981). Our first results are displayed in Fig. 3. No attempt has been made at this time to match the observed profiles in detail. As can be seen and according to our present experience with a larger set of calculated profiles, the observed variation of lines with phase is reproduced by the model calculations. We expect therefore to be able to determine mass-loss rates of the red giants in a number of these systems.

b) Lines formed by optical pumping

As mentioned above, there is complete correspondence between all the emission lines visible on March 31 and the P Cygni type lines with strong absorption parts seen on June 17 except the FeII resonance UV multiplet 9 $\lambda\lambda$ 1260 - 1276 Å . These lines are strong in absorption on June 17 while in

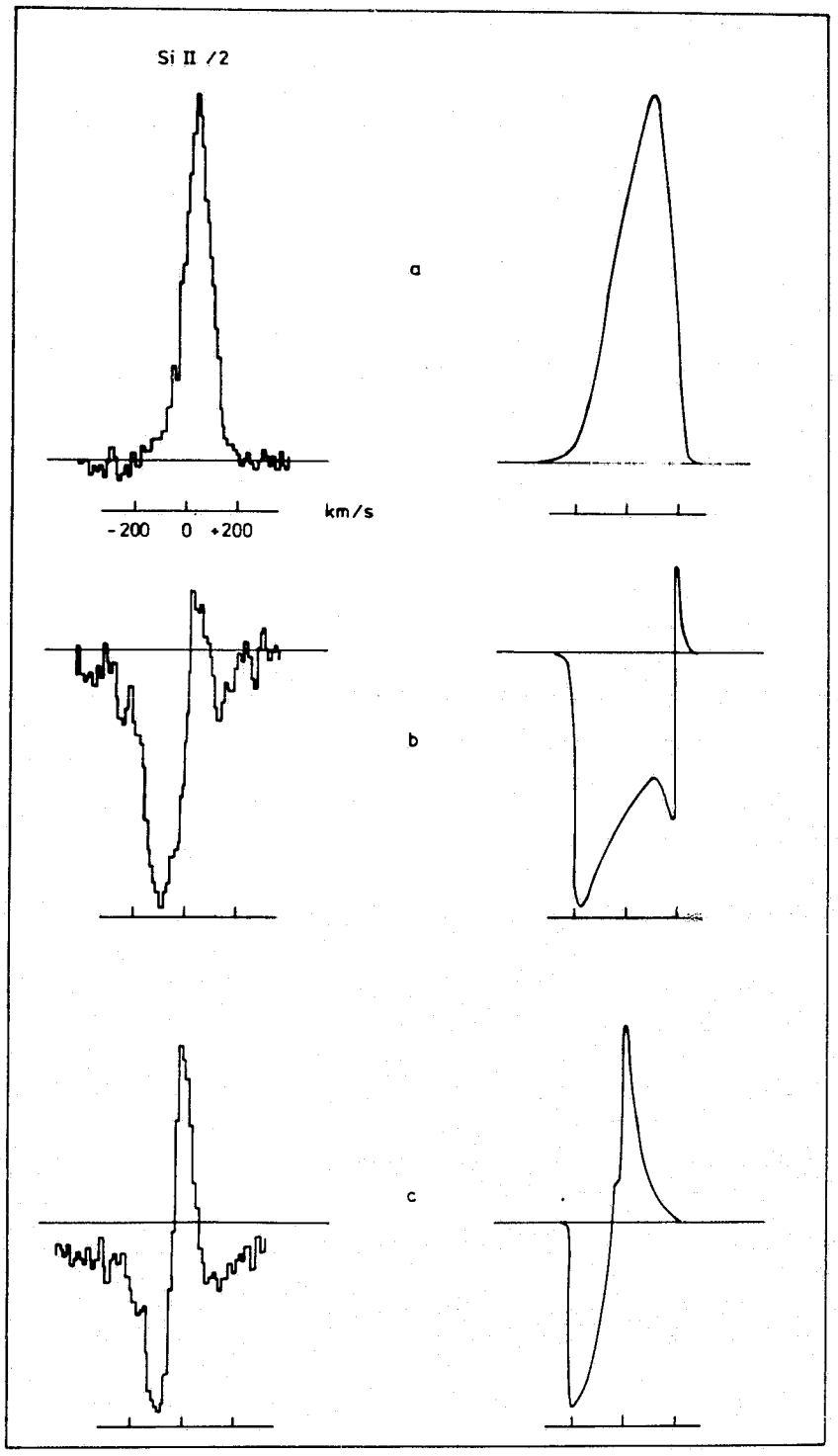

Fig. 3. Schematic comparison of observed SiII resonance line with phase dependent theoretical line profiles. Wind velocity and optical depth are not properly chosen here for a quantitative fit.

the emission line phase on March 31 none of the lines is seen (Fig. 4). This is in striking contrast to all other observable FeII resonance line multiplets (UV Mult. 1, 2, 3, 8). As an example, we show the behaviour of UV mult. 8 (Fig. 4). The disappearance of multiplet 9 is accompanied by exceptional strong FeII UV mult. 191 λλ 1785-88 emission lines (Fig. 5). The exceptional strength of this FeII multiplet is conspicuous in all systems consisting of a cool supergiant ard a hot B star.

The interpretation of this peculiar behaviour is self-evident: the FeII multiplets 9 and 191 have a common x $^6P^o$ upper level (cf. FeII energy level diagramme, Fig. 6). Since the branching ratio for downward transitions of mult. 191 to mult. 9 lines is of the order of 10^2 (the former have very large f-values, Table 1) and since there are no further allowed downward transitions from x $^6P^o$, all photons absorbed in the resonance mult. 9 are converted to mult. 191 photons. The favourable circumstances of the 32 Cyg eclipse made this pure case of optical pumping directly visible to the observer.

Collisions are not important: with typical cross sections for electron collisions of the order of 10^{-8} cm^2 and a typical electron density near the B star of 10^7 cm^{-3} , the collision rate is many orders of magnitude below the fast radiative rates (Einstein coefficients $\approx 10^8$ s^{-1}).

Remarkable is also the intensity ratio within the 1785-88 Å triplet (Fig. 5). The ratio of the f-values 1785.26 / 1786.74 / 1788.00 is 2.25 / 1.71 / 1.13 (Table 1) which is confirmed by the relative strengths of the absorption parts of the lines in the post-eclipse phase on June 17 (not shown here), while in the emission phase (and among the emission components on June 17) the central λ 1786.74 Å component is strongest. This can be understood as a direct consequence of the pumping mechanism: the 1785.26 Å line is pumped via 1260.54, 1266.69 and 1271.24 Å with a combined f-value $\Sigma f = 0.0317$, the 1786.74 Å line via 1267.44, 1272.00 and 1275.15 Å with $\Sigma f = 0.033$, and the 1788.00 Å line via 1272.00 and 1275 Å with $\Sigma f = 0.0239$ (cf. Table 1 for the transitions and f-values).

Obviously, due to the fast decay of the x $^6P^o$ state via multiplet 191 lines, the intensity ratio within this multiplet is controlled only by the pump rates. This is confirmed by the correspondence of the observed line intensity ratio 1785 / 87 / 88 with the respective pump rates represented by the Σf. The λ1785 line must be somewhat weakened by the coincidence of FeII 1260.54 with SiII 1260.42, since part of the B star photons at 1260.54 Å are removed via the SiII line (this is visible as an emission line at the position of SiII on March 31) and no longer available for pumping. Without this coincidence, the 1785.26 line could be expected to be nearly as strong as the 1786.74 Å line.

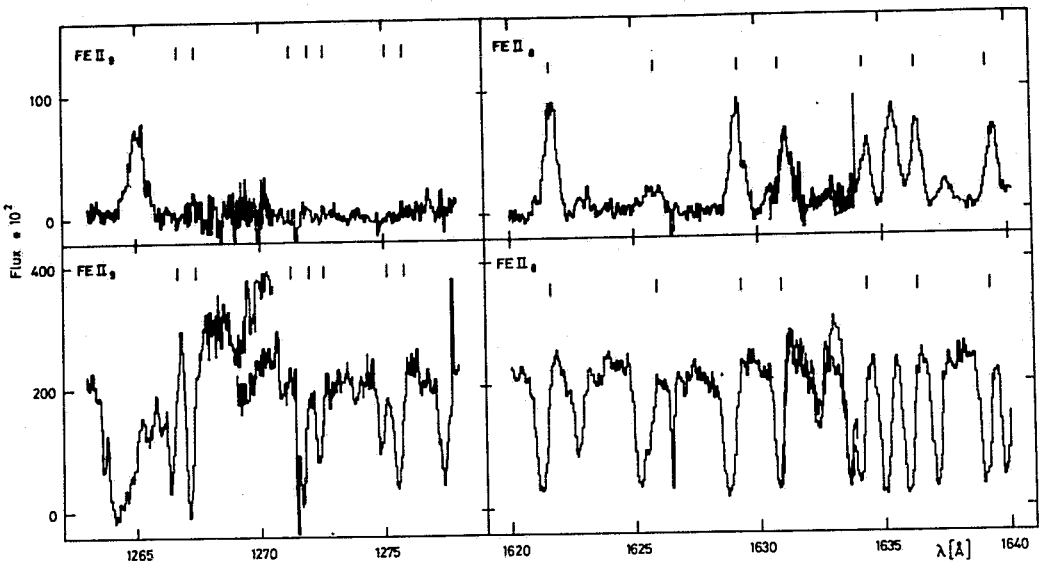

Fig. 4. Position of the pumping FeII Mult. 9 lines (vertical bars) in the emission line phase of 32 Cyg on March 31, 1981 (upper left) and in the spectrum taken shortly after eclipse on June 17 (lower left). For comparison, the normal-behaving FeII resonance Mult. 8 is shown at the same phases.

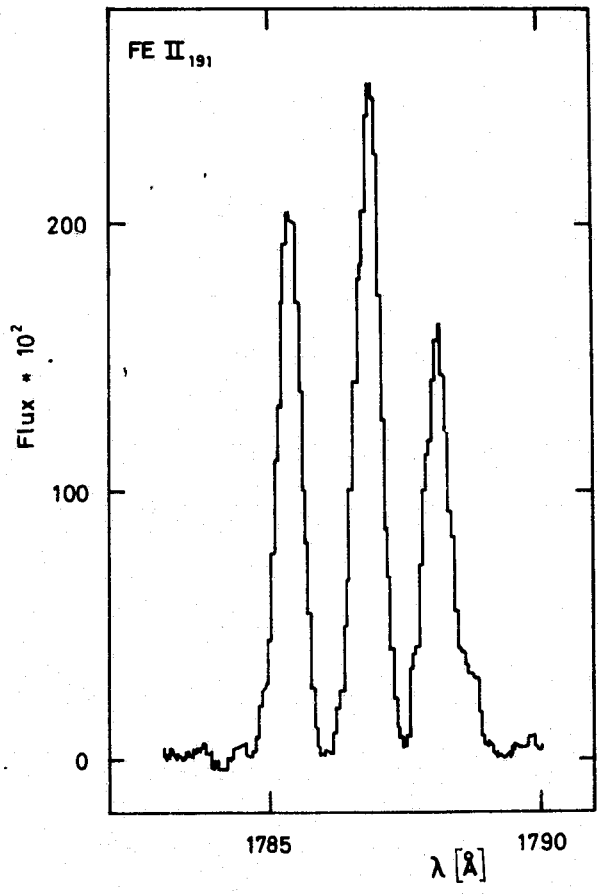

Fig. 5. FeII UV multiplet 191 lines in 32 Cyg during eclipse.

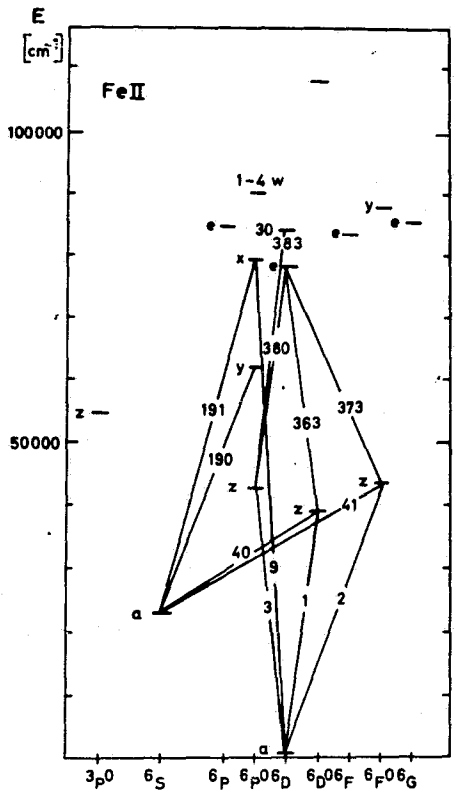

Fig. 6. Grotrian diagramme of FeII (relevant part).

Table 1. Atomic data for lines of FeII multiplets 9 a^6D - x $^6P^o$ and multiplet 191 a^6S - x $^6P^o$ (Moore, 1952 ; Kurucz and Peytreman, 1975).

Mult.	Laboratory wavelength [Å]	Angular momentum J	f - value
9	1275.15	1.5 - 2.5	0.0073
	1271.24	2.5 - 3.5	0.0017
	1275.80	1.5 - 1.5	0.0071
	1272.00	2.5 - 2.5	0.0129
	1266.69	3.5 - 3.5	0.0069
	1272.64	2.5 - 1.5	0.0068
	1267.44	3.5 - 2.5	0.0128
	1260.54	4.5 - 3.5	0.0177
191	1785.26	2.5 - 3.5	2.25
	1786.74	2.5 - 2.5	1.71
	1788.00	2.5 - 1.5	1.13

We have searched - without success - for further pumping lines, lines present as strong absorptions on June 17 without a counterpart in the emission line phase, similar to FeII mult. 9. There are two more anomalously strong emission lines, FeII multiplet 193 λ 1473.82 Å and 1465.04 Å which are probably pumped via the resonance multiplet FeII 18 ($\lambda\lambda$ 1096 to 1105). Since the lines are not observable with IUE, and since we had no f-values available to check the branching ratio, we can only suspect optical pumping.

c) Shock front and/or accretion disk lines

Lines of highly ionized metals (C IV, Si IV, Al III, and FeIII) as well as FeII UV Mult. 60, 78, 99 and a few others do not show P Cyg type profiles. Before and during eclipse (phases c, a) the lines appear in pure emission, immediately after eclipse (b) in absorption (Fig. 7a, b). There is evidence that the emission line region is partially eclipsed in phase with the B star. Since temperatures of the order of 10^5 K are required for the highest ionization stages, these are probably formed in a shock zone near to the B star.

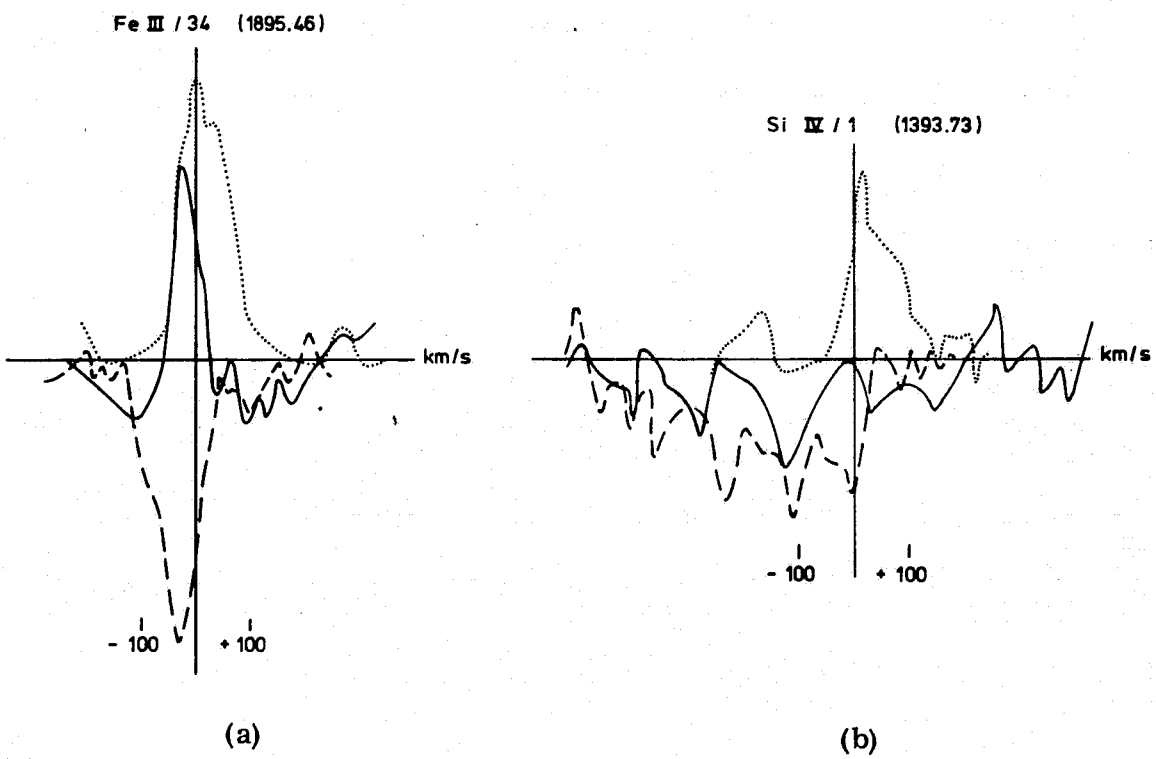

Fig. 7a, b. Same as Fig. 2 for lines formed near the B star.

The Fe II Mult. 60 and 78 lines appear in all these binary systems as emission lines, e.g. in ε Car, HR 2902, 47 Cyg, Boss 5481, VV Cep and ζ Sge. In δ Sge it could be shown that the lines must come from a rotating disk around the B star (Reimers and Kudritzki, 1980). The association of Si IV, C IV, and Fe III lines with a shock front near the B star has also been suggested in ζ Aur by Chapman (1981).

Finally, we report upon the first determination of the mass ratio in the 32 Cyg system which is not available with sufficient accuracy from optical observations (cf. Wright, 1970). Since the IUE does not permit to measure absolute radial velocities, we have determined the semi-amplitude of the B star orbit K_B [km/s] from the varying shift of the B star lines relative to sharp interstellar components in Si II, Fe II, and Mg II lines. The result of a fit of the line shifts to the known form of the radial velocity curve is $K_B = 35 \pm 5$ km/s. The accuracy cannot be improved at present, since there are only few photospheric B star lines uncontaminated by the shell. With $K_K = 17$ km/s (Wright, 1970), a mass-ratio ≈ 2 is found, close to the mass-ratios of ζ Aur and 31 Cyg.

Acknowledgements

We wish to thank the staff of VILSPA for their assistance in obtaining the data. The Deutsche Forschungsgemeinschaft supported this work with grants under Re 353/4, Re 353/6-3, Re 353/6-4, and Re 353/7.

References

Chapman, R. D. 1980, Nature 286, 580.
Chapman, R. D. 1981, Ap. J. 248, 1043.
Hempe, K. 1981, Astron. Astrophys. submitted.
Kurucz, R. L., and Peytremann, E. 1975, SAO Special Report No. 362.
Moore, Ch. E. 1952, An Ultraviolet Multiplet Table, NBS, Washington.
Reimers, D. 1980, in Proc. 2. Europ. IUE Conf., ESA SP-157, p. XXXIII.
Reimers, D., and Kudritzki, R. P. 1980, ibid. p. 229.
Stencel, R. E., Kondo, Y., Bernat, A. P., and McCluskey, G. E. 1979, Ap. J. 233, 621.
Wright, K. 1970, Vistas in Astron. 12, 147.

POLARIMETRY AND PHOTOMETRY OF TWO RS CVn STARS

Mark S. Barbour and James C. Kemp
Department of Physics, University of Oregon

I. Introduction.

We began in late 1979 a photometric and polarimetric study of two RS CVn-type stars, HR 5110 and λ Andromeda. The combined instrumentation of two telescopes at Pine Mountain Observatory, 61-cm and 81-cm telescopes equipped with photometer-polarimeters, was applied. A large quantity of high-accuracy data has been amassed, some of it as yet not synthesized. The intent is to show interesting and representative results from portions of the data.

The optical polarization studies had two general aims. One was to find the phase-locked "orbital" polarization variation, which is expected in binaries. Such an effect in HR 5110 was reported already (Barbour and Kemp 1981). The pattern and amplitude is comparable to that in Algol (Kemp et al. 1981), except that the wavelength dependence is different; other comments will be made below. Our second aim was to look at variability on other time scales, with a view toward seeing polarization effects due to either spot rotation, flaring, and/or general activity.

The photometry was directed particularly toward rapid variability, on time scales down to minutes. Indeed, such activity was immediately evident especially in λ And.

Correlated rapid photometric and polarimetric variability was also looked for, and one clear example is shown here. Much more such coordinated observation is needed. Of great interest is whether flaring and other active events are global, "spherical" in character -- or whether "directed" outbursts occur. In the latter case, the asymmetry should produce a polarized effect.

The physical parameters and other facts about λ And are summarized by Baliunas and Dupree (1979), who give key references. General references on HR 5110 are listed in Barbour and Kemp (1981).

II. Observations and Comments.

Photometry was carried out on the 81-cm telescope at Pine Mountain using semi-continuous comparisons against 25 CVn, for HR 5110, and against ψ And, for λ And. Generally 50-second integrations in the sequence object-sky-comparison were used, under a computer-controlled automatic program. Errors in the Figures were computed from the variances among series of such sequences. The polarimetry was done on the 61-cm PMO telescope using the instrumentation of Kemp and Barbour (1981).

Phase-locked polarization. In HR 5110, 18 additional nightly points were added to the U-band data of Barbour and Kemp (1981), in 1981. The basic phase curves were unchanged. Thirty nights of V-band data show similar phase curves but with much reduced amplitude.The 2nd harmonic amplitude $P_2 = (Q_2^2+U_2^2)^{1/2}$ in V band is smaller than that in U band (where it is about 0.017%) by a factor of 0.4. The rise in intrinsic polarization in the u.v. is strongly indicative of Rayleigh scattering, probably on the cool secondary, as a main polarizing mechanism. In Algol, which is a similar system to HR 5110 in some respects (see Kemp et al. 1981), the corresponding ratio of V-band to U-band polarization amplitudes is 0.7, which is consistent with a large ratio of Thomson to Rayleigh scattering in that case due to the warmer secondary.

In λ And, about 25 nights of U-band data folded on the 20.5212-day period indicate a phase-locked polarization amplitude of roughly 0.02%, while in V band the amplitude seems decidedly less than 0.01%. Our phase coverage on the 20.5-day period is still inadequate, thus we forego showing curves here.

Definite polarization variability in the two stars occurs also on time scales down to 30 minutes. While this is interesting in itself, the rapid variation is probably stochastic in nature, thus a large number of nights' averaging are called for to clarify the mean phase-locked (orbital) curves.

Rapid variability. In Figures 1 and 2 we show cases of changes within a night in the two stars. Figure 1 illustrates an apparently correlated photometric and polarization change in HR 5110. In Figure 2 we compare the light variation in λ Andromedae as between a seemingly "quiet" night, and a night showing a sharp transition. Using a number of nights of such data, we searched for signs of some sort of periodicity or quasi-periodicity in the rapid changes, without success. Of great interest will be methodical search for a systematic relationship between the light-flux and polarization changes.

A two time-scale light curve of λ And. In Figure 3 we show a real-time light curve of this star, exhibiting both changes within individual nights as well as a long-term trend. Note that the short-time errors per single point (involving a few minutes' integration) are typically 0.007 magnitude. The object is clearly "noisy": Note the enormous transition on the night JD 2444535.

As for the long-term trend in Figure 3, a roughly sinusoidal change with a period in the vicinity of 20 days is perceived. However, no claim is made here for an orbital light variation since scarcely one cycle is covered. In fact the recognized long-period light variation in λ And has an approximate to period of 50 days (Landis et al. 1978) rather than 20.5 days, and is suspected be connected with spot rotation, rather than with the orbital motion. Thus our curve here may be atypical.

Continuation. We are continuing these observations and would like to publish a synthesis in coming months, the data shown here being only samples. However, the work being unsupported, funds are not available for fuller analysis and publication at this time.

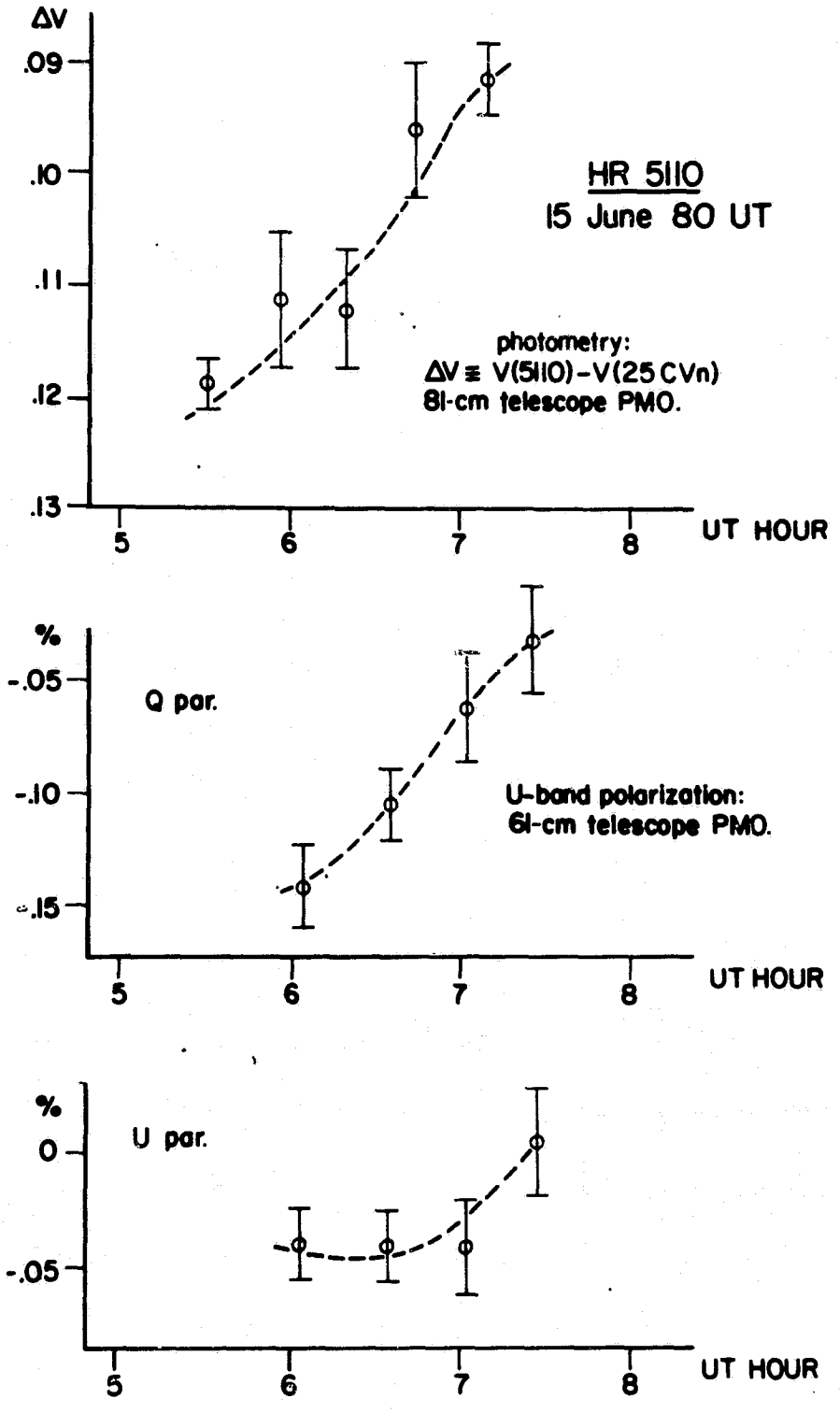

Figure 1. Example of seemingly correlated light and and polarization changes in HR 5110, on a time scale of 1-2 hours.

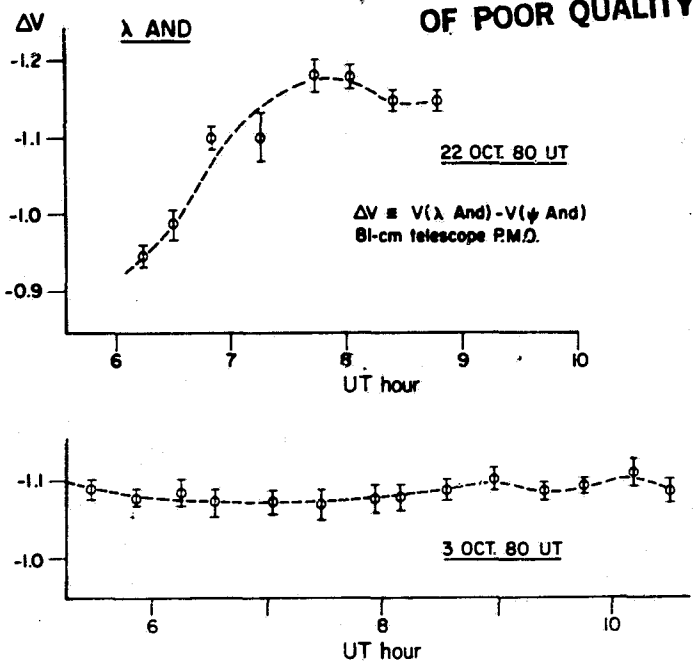

Figure 2. Some high-sensitivity rapid photometry of λ Andromedae from two nights, showing extreme cases of "quiet" and "noisy" behavior.

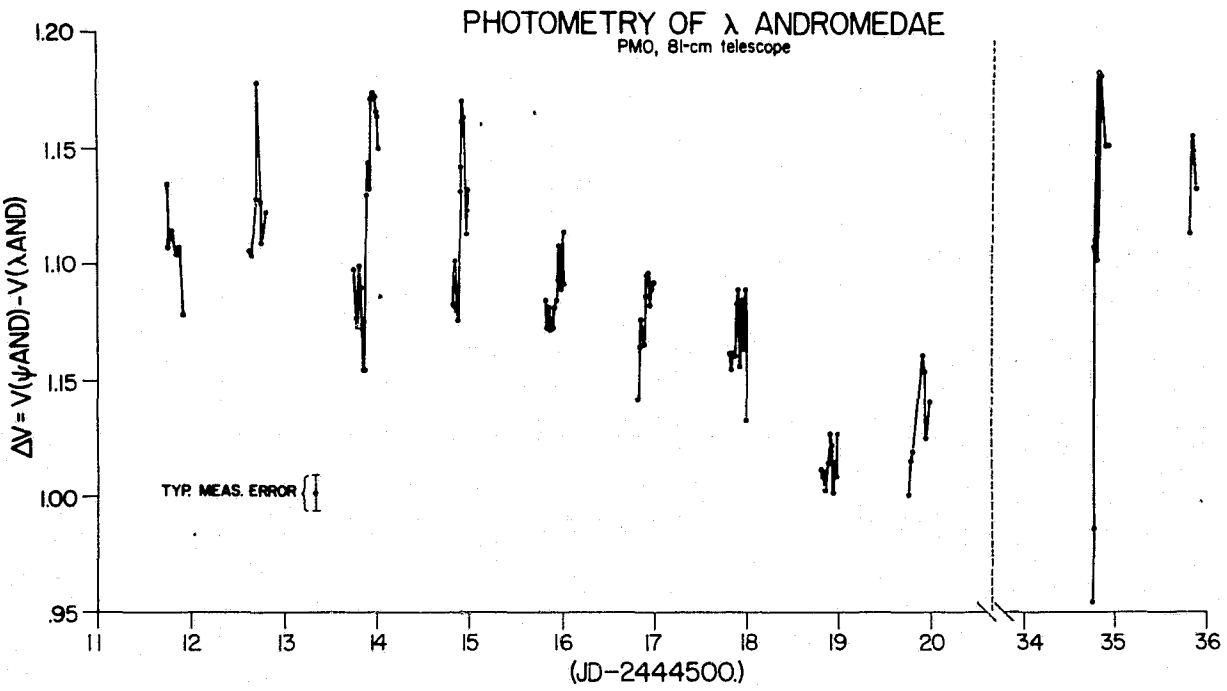

Figure 3. An almost-continuous series of nights of photometry of λ And in Septembe. October 1980, showing rapid changes within nights as well as a long-term trend.

REFERENCES

Baliunas, S.L., and Dupree, A.K. 1979, Ap.J., 227, 870.

Barbour, M.S., and Kemp, J.C. 1981, Ap.J., 246, 203.

Kemp, J.C., and Barbour, M.S. 1981, P.A.S.P., 93, 521.

Kemp, J.C., Barbour, M.S., McBirney, R.E., and Rudy, R.J. 1981, Ap.J. 243, 557.

Landis, H.J., Lovell, L.P., Hall, D.S., Henry, G.W., and Renner, T.R. 1978, A.J., 83, 176.

AUTHOR INDEX

AMERICAN INSTITUTE OF AERONAUTICS & ASTRONAUTICS, INC.
TECHNICAL INFORMATION SERVICE
555 WEST 57th STREET • NEW YORK, N.Y. 10019